Project Healios

Final Report

Unmanned Vertical Lift for Medical Equipment Distribution

TU Delft Fall 2020 DSE **Group 3**

Delft University of Technology - Faculty of Aerospace Engineering

Project Healios

Unmanned Vertical Lift for Medical Equipment Distribution

Final Report Draft

by

Design Synthesis Exercise Group 3

Name	Student Number	Email Address
Chung, Chris	4666658	
Firlefyn, Michiel V.M.	4558774	
González Martínez, Pablo	4582675	
Hinssen, Yara M.	4659023	
Lukens Ruiz, Diego S.	4648196	
Menor de Oñate, Adrián	4668901	
Rademaker, Julia T.E.	4646096	
Simonelli, Alessandro	4648285	
Szekeres, Balázs	4277295	
van Wagensveld, Dario A.	4647181	

Under the guidance of
Dr. Marilena D. Pavel (Tutor)
Ir. Ronald van Gent (Coach)
Ir. Natàlia Gomes de Paula (Coach)

Delft University of Technology
Faculty of Aerospace Engineering

January 25, 2021

TU Delft Delft University of Technology

Preface

This is the concluding report in a series of 4 documents describing the work of Group 3 as part of the Design Synthesis Exercise (DSE) conducted in the Fall of the 2020-2021 academic year. The DSE is a project performed by a group of 10 undergraduate students as their Bachelors thesis project to obtain the degree of Bachelor of Science in Aerospace Engineering at the Delft University of Technology.

All team members have dedicated themselves full time for a period of 10 weeks between November of 2020 and January of 2021 to the completion of this project. Due to the ongoing COVID-19 pandemic, communication between group members and supporting staff was conducted almost entirely online. The main goal of the project was to design an unmanned aerial vehicle (UAV) capable of delivering medical equipment and payload to remote areas and to provide emergency relief during natural disasters.

In this final report the focus is placed on the detailed design phase of the UAV. In addition to the technical design, operational, logistic, and financial considerations are also addressed.

We would like to thank the tutor, coaches, teaching assistants, and the organising committee of the DSE for their guidance, advice, and support during this project.

- Dr. Marilena D. Pavel, *Tutor*
- Ir. Ronald van Gent, *Coach*
- Ir. Natàlia Gomes de Paula, *Coach*
- Ir. J.A. Melkert, *OSSA*
- Dr. Ir. E. Mooij, *OSSA*
- Dr. Ir. C.J. Simao Ferreira, *OSSA*
- Ir. J. Sinke, *OSSA*
- Dr. Ir. W.J.C. Verhagen, *OSSA*
- R. Coenen, *Teaching Assistant*

Executive Summary

Healios is an unmanned aerial vehicle (UAV) with vertical take-off and landing (VTOL) capabilities designed for high speed, long range, deliveries of medical payloads to remote locations.

Over the last century, with the rise of global warming, there has also been an increase in frequency of natural disasters. Consequently, more flexible and easier to implement solutions are needed to provide aid to those in need of emergency relief in areas affected by natural disasters. Examples of such disasters are unfortunately present throughout history. The most recent example is that of the current COVID-19 pandemic, which serves as a harsh reminder that the primary health networks in many places of the world is ill-equipped to deal with rapid surges in the demand for medical supplies. In addition, a more resilient supply chain to deliver medical supplies to end users in locations that are difficult to access due to poorly developed or non-existent infrastructure is needed. To make the supply chain more resilient, a no-contact delivery method is needed that can also deliver vaccines to remote areas.

Currently, the disaster relief sector faces numerous issues related to the efficiency of its operations. One of the biggest issues is the lack of solutions to access's natural disaster zones, where damaged infrastructure prevents the use of traditional vehicles. This is also the case in rural and remote areas in undeveloped regions, where the infrastructure may not be there to begin with. This is known as the "last mile" problem in supply chain management, a well known phenomenon where the delivery of goods and to an end user from a central transportation hub is limited by the capability or lack thereof of covering the last mile of the trip. This difficulty in covering the last mile can be a result of a variety of factors, with the main one being poor infrastructure.

In the context of emergency delivery and disaster relief the current solution to the last mile problem is the use of helicopters. Helicopters have two main uses in disaster relief: delivering packages, and/or rescuing people from the area. The main disadvantage of the current solutions is the scarcity of helicopters, and related to this, the cost of operating a helicopter. This is where project Healios hopes to provide a more effective solution.

The Healios UAV is designed to deliver medical supplies to remote areas; however this is a very broad goal that could encompass many different activities. In addition, depending on the context of the vehicle's operations (i.e where the vehicle is operating) the necessary operations could differ significantly. Thus two distinct use cases have been identified for the vehicle. The first type of use cases is those where an immediate response is needed, such as after a natural disaster, like a tsunami or an earthquake. The second type deals with long-term responses where an immediate response is not needed, and more elaborate operations and logistics can be planned in advance. In addition to the two separate use cases, for both use cases, Healios will be designed to be able to perform two types of missions:

- **Local Delivery Mission** — Delivery of up to 50kg payload to end-users in a range of 50km. The vehicle must perform a two-way delivery mission within a minimum time span at high speed.
- **Logistics Mission** — Delivery of up to 50kg payload to logistic centres within a 200km range. The vehicle must perform a one-way trip operation within a minimum time span at high speed to safely deliver the package .

Summary of Previous Work

Three out of the four main phases of the project have been completed thus far. These are the project planning phase, the baseline phase, and the midterm phase.

During the first phase the project was organised by assigning managerial and technical roles to the various team members and performing a detailed planning of the project activities. The baseline phase then focused on a thorough identification of requirements from a series of stakeholders, and the generation of some preliminary concepts for the Healios UAV.

During the midterm phase a wide range of concepts were generated. These were categorised into three families, namely rotorcraft designs, fixed-wing designs, and blended wing body designs. From each family an

optimal design was selected. These designs were compared through the use of an extensive trade-off process which took into account the resilience, complexity, efficiency, emission, operational cost, and required infrastructure of each concept. The concept that emerged as the most promising option was that of a fully electric tilt-wing vehicle. The detailed design of the chosen vehicle concept is the focus of the final phase. The process and results obtained during the detailed design are the focus of the present work.

Overview of Final Design

A render of the final design configuration is shown below, in addition to a table which summarised some of the key parameters of the Healios UAV.

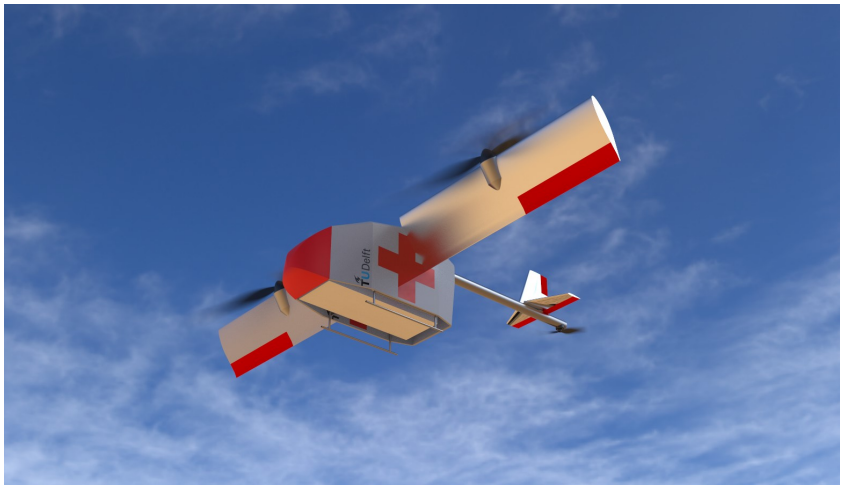

Figure 1: Render of the Healios UAV

Parameter	Value
MTOW	355 [kg]
Wingspan	6.1 [m]
Height	1.52 [m]
Length	3.96 [m]
Rotor Diameter	2.6 [m]
Max. Speed	586 [km/h]
Max. Range	333 [km]
Max. Endurance	2.16 [h]

Table 1: Parameter Overview

Subsystem Design

In order to have a clear overview of the detailed design process, its essential to provide a global overview of the individual subsystems that make up the entire engineering department. The design of the vehicle was divided into 4 subsystems, namely: Aerodynamics, Structures, Power & Propulsion, and Control & Stability.

Aerodynamics

During the aerodynamic design the elements that affect the aerodynamics properties of the vehicle the most were designed in detail. The four components designed included the wing, the horizontal and vertical tail, and the fuselage.

The design process started with the wing design, as this component has the largest effect on the overall design. The design approach included an iterative process, where based on several inputs, the NACA 643-41 aerofoil was selected, followed by the optimisation of the three-dimensional wing, and the output of the information required to evaluate its performance.

For the first iteration, the inputs were based on the preliminary design, and for later solutions, the inputs from other sub-systems were used. For the optimisation of the three-dimensional wing, a numerical method was developed based on the lifting-line theory. A final design was selected after five iterations. The final design was highly influenced by the structural design requirements, as it required a single spar to pass through from one wingtip to the wingtip on the other side. The final design consists of a uniform chord of 0.66 metres, and a wingspan of 2.65 metres, with a twist of 3 degrees. The results of the design were validated using the vortex lattice method.

The horizontal and vertical tail design methodology is very similar to the wing, as many of the design parameters are the same. The main difference is given by the fact that the task of each of these components is different. The tail section aims not to provide lift, but to provide the required lateral and longitudinal stability. As the control group gave stability requirements, a large part of the iteration process was taken up. Once the final stability requirements were chosen, the NACA 0010 airfoil was selected. As the process

was less iterative, an analytical approach was chosen. The horizontal tail's final dimensions include a root chord of 0.5 metres, a tip chord of 0.25 metres, and a span of 1 metre. For the vertical tail, the height is 0.5 metres, and the root chord is 0.5 metres, while the tip chord is 0.25 metres long. The horizontal tail results were validated using lifting-line theory, and the vertical tail was validated using the stability derivatives.

The purpose of the fuselage is to provide a secure attachment for the carried payload and the UAV components, which results in a large volume. This chapter aimed to optimise this volume as such, that it produces as little drag as possible. Based on the control team's work, the minimum cross-sectional area of 0.72 m^2 was given. The drag could be further reduced by giving the design a more aerodynamic shape, by adding a nosecone and other aerodynamic elements. For this report's purpose, the design method was limited in selecting an achievable drag coefficient by comparing the design to simile objects. Based on this data, the selected drag coefficient is 0.2.

Lastly, the effects of the propellers in front of the wings were discussed. A conclusion was drawn that based on past literature, the propellers would positively affect the vehicles aerodynamic performance, but at this stage, it was not possible to give an exact value to these advantages.

Structures & Materials

The scope of the structures & materials subsystem was to design a wing, fuselage, and tail structure that would be able to withstand the internal and external loads applied at all critical flight phases. As the structural design of the three components are independent from each other, each one is explained separately.

The wing structural design was the most extensive analysis out of the three. The inputs for design was dictated from the Aerodynamics subsystem based upon the wing planform and geometry that was obtained, as well as specific design parameters such as the fact that the wing had to be rotate-able. Once the fixed design parameters were identified, the wing's loading condition was analysed. From the analysis, it was concluded that the wing would be experiencing 4 external loads, namely : lift (distributed load), drag (distributed load), weight of the wing (distributed load) and the engine (point load), and the thrust (point load). Once all the external loads were identified and analysed, the internal reaction forces and moments could be computed. Through the internal reaction forces and moments, the internal stress which the wing would be experiencing due to the 4 external loads could also be identified. The stresses that were analysed were : Bending, Shear, Torsion, and Buckling. Through the bending analysis, the dimensions of the main spar was obtained. Through the shear & torsion analysis, the dimensions of the ribs and skin were obtained. Through the buckling analysis, the dimensions of the stiffener and also the skin were obtained.

The fuselage structural design had to main objectives: firstly, to design a fuselage structure that was able to withstand all the internal loads exerted by the electronics, equipment, batteries and payload, and able to direct/transfer these loads to the main wing and tail spar. Two concepts were analysed, namely a monocoque structure and a truss structure. The design opted for the latter choice due to lower manufacturing and part costs, complexity, and easier maintainability. Thus the truss structure was analysed in the critical condition of banking 30 °, and it's dimensions were sized accordingly. The second objective in the fuselage design was the payload design, which investigated how and where the payload would be stored inside the fuselage, and how the vehicle was going to accommodate for the fact that it had to be able to handle two separate payloads with different dimensions : 140x50x50 [cm^3] and 70x70x70 [cm^3]. The chosen method for the payload attachment was through the use of actuated lead screws which would lock onto the payload, according to the attachment points, and it would be lowered by allowing the screws to have 2 degrees of freedom.

The tail structural design mainly focused on the design of the main tail spar which connected the tail, and the auxiliary engine from the fuselage and the wing spar. A similar method as the wing spar analysis was conducted as they both could be modelled as a cantilever beam experiencing point/distributed loads.

Once each analysis was complete, the results were first verified through the use of different unit and system tests, then validated by comparing the analytical model of the wing, truss, and tail spar with a FEM model using SOLIDWORKS and ANSYS. Lastly, the final wingbox, truss, and tail-spar dimensions were presented, as well as future recommendations that could be considered.

Control and Stability

The function of the control and stability subsystem is to ensure stability and controllability in all flight stages in order to to ensure safe mission completion. The subsystem must be robust, in the sense that inaccuracies of measurements and failures of power should not stop the subsystem from maintaining the vehicle's control. Furthermore, the vehicle must be able to follow a set of desired coordinates that are provided by the mission computer in the form of path-planning.

The UAV has three flight modes; hover, transition, and cruise. Firstly, the general equations of motion for the vehicle are derived. Based on these equations a static stability analysis is performed for both hovering and cruising flight. It was found that the vehicle is statically stable in these flight regimes. Thereafter, the dynamic stability was analysed for both hover and cruise. The dynamic stability analysis consisted of an exploration of the characteristic modes of the vehicle during hover and cruise by constructing the relevant state-space models and analysis the resulting eigenmotions. It was found that the vehicle is not dynamically stable in all flight conditions. In particular, the phugoid motion was found to be unstable for both cruise and hover. In addition, the spiral motion (cruise) an dutch roll (hover) were also found to be unstable modes. This leads to the need for an active flight control system.

The control system design is a continuously running loop updated by the error of the current state and the desired state. The current state is estimated with a state space model and on-board sensors, while the desired state stems from the flight planning. Actuators are driven by the control system's output to obtain the desired state.

In order to address the dynamic stability during hover, the preliminary design of a controller was performed. A controller architecture is presented, explaining how the different control inputs are structured and how they related to the control output. The system is designed with proportional, integral, derivative (PID) controllers. The tuning of these controllers could not be performed in the present work due to time constraints. Finalising the design of the hover controller therefore remains as one of the the main outstanding items related to the design of the control and stability subsystem, to be performed in future design iterations. A successful tuning of this controller is vital for the vehicle to operate safely while hovering.

For cruise, two controllers are developed; one for symmetric flight and one for asymmetric flight. The decoupling of the longitudinal and lateral eigenmotions, which is a consequence of the performed linearisation and the assumed mass symmetry of the vehicle, allows for the analysis to be split in this manner. Splitting the controllers in the longitudinal and lateral simplifies the development while maintaining accuracy, as long as the deviations from the linearised state remain small. A simplified altitude hold, speed hold and heading hold are designed. These control loops were all tuned proportionally. As a result, it was found that the system becomes dynamically stable if controlled. A comparison of the the open-loop (unstable) response and the closed-loop (stabilised) response of the vehicle is presented and discussed. For future design iterations, these controllers should be replaced by PID controllers to improve the response characteristics of the UAV.

Transition is qualitatively analysed. The general transition principles and common pitfalls are discussed, while an approach to transition for the Healios vehicle is presented. The control system allows for a smooth transition between the flight envelopes related to hover and cruise. Performing transition in the vehicle's transition corridor implies that, in principle, the flow around the wing can not detach, opting out any unpleasant flight behaviour. Nevertheless, further analysis must be performed to ensure this is the case. Transition is characterised by complex, non-linear flow over the propellers and the wing. Thus, a thorough quantitative analysis of this flight phase is deemed to be beyond the scope of the present work.

The flight controller is implemented as presented above. Consequently, the vehicle is able to operate safely in all flight regimes.

Hardware and Software

Highly accurate electronic computing and sensing devices are now available thanks to technology, and a human operator is no longer needed. Together with the use of software, the model's physics and controls can be modelled.

There are a multitude of hardware components necessary to make an autonomous vehicle operate. Primary computers systems are in charge of all the critical functions of the vehicle: machine vision is processed by a graphical processor; its logic is performed by the mission computer, and its controls are performed by the flight controller and its peripherals. An inertial navigation system is present for global positioning and attitude sensing. Air traffic separation is provided by means of cameras, transponder and a FLARM unit. In any event where a human operator has to take control of the vehicle, the radio link between the operator and the ground control station accommodates for a smooth control transfer.

Software is custom made to execute all necessary operations more efficiently. The main development tool is Linux and all its available subprograms. Before the Healios goes to market, LynxOS is used instead of Linux to offer customers maximum security. All control and logic software are designed according to the DO-178B standard to ensure certifiability.

Propulsion and Performance

The design of the power and propulsion systems consisted of several steps. To provide guidelines for design trade-offs, it was analysed whether the power required in horizontal flight or vertical flight would be more determining for the maximum take-off mass. It was concluded that the horizontal flight was critical and is mainly be optimised for.

From this point the propeller diameter was established to be 1.3m, the maximum diameter possible, preserving the required clearances. This was done to lower the disc loading in vertical flight and only having small compromise in the propeller efficiency in forward flight. This could only be achieved with one engine per wing and therefore it was decided to fix the number of engines. The risk of a single-engine failure, was mitigated by using a twin-engine system for the propeller.

Once the diameter was established an iterative loop was entered for the calculation of the required powers and as a result the battery and engine size. Since the mass of the battery and propulsion was around half of the total take-off mass, small changes in the power required for the flight, would lead to large changes in the calculated maximum take-off mass. Therefore, the calculations for the required power were performed in tandem with the calculation of the required aerodynamic and structural characteristics. The iterations converged to a maximum take-off mass of 355 kg and battery mass of 117 kg. This battery mass was determined a result of the power required for vertical and horizontal flight of 8.4 and 97.7 kW respectively and a battery density of 400 kW/kg.

With these masses the required powers during the different phases of the mission were estimated. From here the propellers were optimised for horizontal flight and the thrust provided in hover was calculated with the blade element method. This was done to ensure that the propellers were able to deliver sufficient thrust to hover out of ground for the required time. Next to that, the Saluqi P20S4 engine was selected for the design.

Lastly, the performance of the vehicle was analysed. A broader vision on the power required could be established with the propeller parameters. This was visualised by constructing power curves. From which the maximum speed was calculated to be 163 m/s, the maximum range 333.3 km and the maximum endurance 2.16 hrs. The noise level was estimated to be 123 dB at 150 m distance.

System Characteristics

This part of the report presents the characteristics of the system that is not directly related to the subsystems. This mainly consists of: the certification plan, future project planning, sustainable development strategy, cost breakdown structure, and the resource allocation.

Certification

In order for the vehicle to get certified and operable by 2025, there are two main steps. The first is the compliance to the previously found and determined requirements. All of the relevant driving and key requirements have been met with the exception of a vibrational analysis, and most of the additional requirements have been met as well. These include requirements that came from the Vertical Flight Society's Re-

quest for Proposal, the requirements set by the Joint Authorities for Rulemaking on Unmanned Systems (JARUS) (presented in previous work, see the Baseline Report), and further requirements out of practicality and possibility. Additional to the requirement compliance matrix, a risk assessment was performed. This risk assessment was split in two parts, namely the general risk assessment and the Strategic Operations Risk Assessment (SORA) specifically required for certification. The general risk assessment consists of financial, process, operations, design, and project risks that were devised based on experience, similar projects and general prediction. All of these risks were given a likelihood and consequence level, which when combined leads to a risk level. Then, the risks were mitigated by either a preventive action, corrective action or both. This way the likelihood and consequence levels changed and new risk levels were assigned. For the overview these risks were then displayed in risk maps to show the effectively of mitigation. Regarding the SORA, a plan has been written and specific levels for the ground and air risk class have been found. Using these, one can assemble a safety portfolio that is required for certification.

Project Planning

To ensure that the development of the UAV could be continued after this phase, a planning was constructed. The plan consisted of four phases describing the flow and distribution of upcoming tasks. Firstly, the design would be further developed in the research phase, followed by a production phase. The production of the UAV will be outsourced and therefore the tasks associated with this mainly concern the preparation and overseeing of the production. After this, the tasks that occur during the operational life time of the UAS were described and lastly, the process for the disposal of the UAV was constructed.

Sustainable Development Strategy

During the design of the UAV the main goals set by the driving requirement have been followed strictly and greatly influenced design choices. However the impact which the UAV will have on sustainability has always been taken into account as well and had its share on the influence of the design. First, during the concepts trade off, a configuration has been decided upon based on the low environmental impact an EV could have, showing that sustainability was already being taken into account. Other aspects of sustainability have been taken into account during the detailed design by each subsystem, allowing for specific design choices to be made in order to improve the impact on sustainability. The social impact is taken into account through safety by providing redundancy in the control system, through noise emission by having an electrical engine and an optimal propeller design, and by providing services to everyone. A life cycle assessment using EDUPACK 2020 is performed by looking at the impact of production of the UAV and its operations. Sustainable design choices were made regarding material selection, on board electronics and drone efficiency during operations. A goal was set as to keeping the carbon footprint and energy consumption of the materials and components needed as low as possible, and this goal has been achieved when a comparison is made between the UAV and its main competitors. In fact, the UAV has a lower carbon footprint than conventional fuel powered cars (23,000 [kg] less) and than current on the market electric cars (12,000 [kg] less). The UAV has been designed in such way that its end of life impact on environment is minimal. Most of the components are made in such way that they can be reused on other drones. Furthermore the use of aluminium in most structural components allows for the material to be recycled easily and lowers the carbon footprint. Most of the parts can thus be recycled, the only waste generated comes from the ones that can not be fully recycled, which are mainly the rotor blades, fuselage fairing, and the battery pack. It is recommended to, in the future, mainly focus on the CO2 and energy expenditure footprint of the batteries as they have the greatest impact (60% of the total footprint). Then cost of the electrical components should be reduced by looking at economies of scale and in house production for the propulsion system. Lastly, to improve social sustainability, it is recommended to keep the software updated to ensure safety even more and employ people that live in the region so as to stimulate local economies.

Cost Breakdown Structure

At this stage of the design an estimate of the costs related to the design and production of a prototype have to be studied and discussed. The costs can be categorised into 4 main sections being : Research and development, Manufacturing and construction, Operation and support, Decommissioning and disposal. The first cost can be estimated by combining the working hours needed for the design phase, the software needed for

this as well as the costs related to testing the components before starting big scale production. The salaries used for the calculation are based averages depending on the work sector. All combined, these costs sum up to 257 400€. Secondly are the production costs, which combine the working hours needed by the available manpower (23 520€), the cost of the off shelf components (60 517€), the UAV produced components costs (2974.8€) and the assembly costs related to the manpower needed and (126 00€). Furthermore, the estimated costs related to operations are purely related to the working hours needed to maintain the operations going and lead to 416 000€. Finally the disposal costs, which is the lowest of all costs, is related to the disposal cost of components that cannot be reused and is mainly influenced by the recycling cost of different components which are difficult to recycle. With these costs in mind the UAV unit cost can be found by setting a cost required to break even with the expenses. In order to break even the first year, 4 drones have to be sold at a realistic cost of 270 000€. It is expected that after the break even point has been reached, more drones will be sold during a span of 4 years.

Resource Allocation and Budget Breakdown

Having an initial estimate of the mass, power and costs related to the different subsystems of the UAV is crucial and referred to in order to maintain coherence amongst these subsystems. The first cost estimation made has been overestimated by more than 100% compared to the current estimation, leading to a more feasible and attractive product costing 270 000€. Furthermore the mass estimations have overall been overestimated as well. The propulsion system is most off nearly 600 [kg] lighter than the first estimate. The upper bound set to the MTOW has well been defined and was overestimated by 145 [kg], leading to a more lightweight estimation of 355 [kg]. The power budget follows the same pattern as the two previous ones. It had initially been overestimated by 32 [kW] leading to a more efficient UAV design. All in all the upper bounds set at an earlier stage have not been overshot and the new estimates are beneficial for the design leading to a more lightweight, more efficient and cheaper design than expected.

Contents

Nomenclature

Acronyms & Symbols

Acronym	Description	Acronym	Description
(N)LH	(new) likelihood	ID	identifier
(N)RL	(new) risk level	INS	inertial navigation system
2D / 3D	two or three dimensional	JARUS	joint authorities for rulemaking on unmanned systems
ABS	acrylonitrile butadiene styrene	LC	labour cost
AGL	above ground level	LCA	life cycle assessment
AIDS	acquired immunodeficiency syndrome	NACA	national advisory commission for aeonautics
AR	aspect ratio	NGO	non-government organisation
ARC	air risk class	OLT	operating life time
ATC	air traffic control	OS	operating system
C	consequence	OSO	operational safety objectives
CBS	cost breakdown structure	PAV	personal air vehicle
CCD	charged coupled device	PCIe	peripheral component interface express
CFD	computational fluid dynamics	PID	proportional, integral, derivative
CFRP	composite fibre reinforced polymer	POS	project objective statement
COTS	commercial off-the-shelf	P&P	power and propulsion
CPH	cost per hour	RAMS	reliability, availability, maintainability and safety
DOF	degree of freedom	RF	reference frame or radio-frequency
DSE	design synthesis exercise	RFP	request for proposal
EOL	end-of-life	ROS	robot operating system
EOM	equations of motion	RPM	rotations per minute
ESC	electronic speed controller	Resp	responsibility
EV	Electric Vehicle	SAIL	specific assurance and integrity levels
FBS	functional breakdown structure	SORA	strategic operations risk assessment
FEM	finite element method	TBD	to be determined
FFD	functional flow diagram	TMPR	tactical mitigation performance requirement
FH	flight height	UA	unmanned aircraft
FLOPS	floating point operations per second	UART	universal asynchronous receiver-transmitter
GCS	ground control station	UAS	unmanned aerial system
GFRP	glass fibre reinforced polymer	UAV	unmanned aerial vehicle
GPS	global positioning system	VFS	vertical flight society
GRC	ground risk class	VLM	vortex lattice method
HIGE	hover in ground effect	VTOL	vertical take-off and landing
HIV	human immunodeficiency viruses	V&V	verification and validation
HOGE	hover out of ground effect	WBS	work breakdown structure
ICEV	internal combustion engine vehicle	WFD	work flow diagram

Symbol	Description	Symbol	Description	Symbol	Description
"	inches	K_h	induced velocity factor	ν	Poisson's ratio
η	efficiency	L_{tot}	total lift force [N]	ϕ	roll angle [°]
A	cross-sectional area [m^2]	M	moment [Nm]	ψ	yaw angle [°]
AR	wing's aspect ratio	P	load [N]	ρ	air density [kg/m^3]
C_L	lift coefficient	PL	power loading [W/N]	τ	torque [Nm]
C_N	normal force coefficient	P_{cr}	critical load [N]	θ	pitch angle [°]
C_d	airfoil drag coefficient	R	reaction force [N]	b	wing span [m]
C_l	airfoil lift coefficient	S	wing surface area [m^2]	c	chord [m]
C_m	airfoil pitching moment	S_F	fuselage surface area [m^2]	c_n	airfoil normal force coefficient
$C_{D,i}$	induced drag coefficient	S_h	horizontal tail surface area [m^2]	c_{l_n}	lift curve, effective angle of attack
C_{DF}	fuselage drag coefficient	T	thrust force [N]	e	oswald efficiency factor
C_{L_C}	ideal cruise lift coefficient	U	power density [kW/kg]	g	gravitational acceleration constant [m^3/kg/s^2]
$C_{L_{\max}}$	maximum lift coefficient	V_c	cruise velocity [m/s]	i_p	wing tilt angle [°]
C_{l_i}	ideal airfoil lift coefficient	V_h	horizontal tail velocity [m/s]	l_h	horizontal tail arm [m]
C_{thrust}	thrust coefficient	V_i	induced velocity	m	mass of the aircraft [kg]
C_{torque}	torque coefficient	V_∞	freestream velocity [m/s]	p	roll rate [°/s]
$C_{L_{C\,w}}$	wing cruise lift coefficient	W_{TO}	maximum take-off weight [N]	q	pitch rate [°/s]
$C_{L_{\max\,w}}$	maximum airfoil lift coefficient	W_{eng}	engine weight [N]	q_∞	dynaimc pressure [Pa]
D	damping factor	$W_{\text{preliminary}}$	preliminary weight of aircraft [N]	r	yaw rate [°/s]
DL	disc loading [W/m^2]	W_{wing}	wing weight [N]	σ_{cc}	critical buckling stress [Pa]
D_F	fuselage drag force [N]	Γ	vortex strength [rad/s]	σ_{cr}	critical internal stress [Pa]
D_{tot}	total drag force [N]	α	angle of attack [°]	t	time [s]
E	Young's modulus [Pa]	α_i	induced angle of attack [°]	u	flight velocity in x direction [m/s]
F	force [N]	α_{eff}	effective angle of attack [°]	v	flight velocity in y direction [m/s]
FoM	figure of merit	β	side-slip angle [°]	w	flight velocity in z direction [m/s]
I	moment of inertia [m^4]	δ	deflection of a control surface [°]	w_e	effective width [m]
K	controller gain	ϵ	downwash angle [°]	y_n	y-coordinate along wing span [m]

1 Introduction

"Immediate access to crucial medical supplies during emergencies is often extremely hard or impossible. Even developed countries have difficulties in providing fast medical supply access after natural disasters or epidemics, especially in remote locations where infrastructure is poor or non-existent. The COVID-19 pandemic has been a harsh reminder of how fast medical supply availability can make the difference between life and death. The current emergency response vehicles rely on infrastructure which is highly vulnerable to natural disasters such as roads, rail, airports, and seaports. As a result, response time can be delayed by hours, days, or even weeks under emergency situations. In addition, 1 billion people live in developing countries without access to all-season roads, making conventional delivery methods to such regions extremely difficult or impossible. Moreover, emergency vehicles such as helicopters are very costly and rely on human operators, which can create a bottleneck in the supply chain. This work explores the opportunity to alleviate the current emergency relief limitations by designing a vertical lift aircraft capable of autonomously delivering urgent medical supplies." [1].

This is the fourth and final report of the DSE Group 3 UAV series that documents the progress of this Design Synthesis Exercise (DSE). The goal of the project is to design an autonomous vertical take-off vehicle capable of carrying 50 kg of emergency payload to an end user 50 km away or to a logistics centre 200 km away. This document continues the work from the Midterm Report [2], where three vehicle configurations were compared in a trade-off and a winning design was chosen. The focus is now on the detailed design of this winning vehicle configuration and its subsystems, as extensively as possible. In addition, it includes a market analysis, a sustainable development strategy, a financial plan, and a description of the operations and logistics involved in the mission, including two case studies.

The report content begins with Chapter 2, where the reasoning behind the need for this vehicle is explained and defended by taking a look a the current emergency relief sector and performing a market analysis. Then, an overview of the project and its main goals and requirements are laid out in Chapter 3, right before a brief summary of the concept generation and trade-off done in the past, shown in Chapter 4. Then, an overview of the vehicle's configuration is given and visualised in Chapter 5, to give the reader an impression of the design before going into the details. Next up, Chapter 6 gives an overview of the main subsystems of the vehicle and the approach to their design and verification and validation procedures. After this, the technical side of the report comes to life, beginning with the vehicle aerodynamics in Chapter 7, where different wing and tail designs and configurations are studied, compared and ultimately selected for the best performance. Next, Chapter 8 explains the physical structure of the vehicle and goes into detail on how the loads are supported, both analytically and with the use of simulations. Then, the control and stability of the vehicle is extensively described in Chapter 9, where the flight behaviour of the vehicle is described and discussed alongside the derivation of the equations of motion and the stability analysis during various stages of flight. Furthermore, Chapter 10 presents the means of generating power and propulsion for the vehicle by first providing a design approach, and then making the necessary calculations to support the mission's needs. Last but not least, the final subsystem is presented in Chapter 11, where the required hardware and software for the autonomous operation of the vehicle are described, together with the flight planning and obstacle avoidance strategies. Next, moving on to the non-technical side of the report, Chapter 12 contains the operations and logistics approach for the mission, including two use cases and a detailed description of the typical mission procedures. Then, Chapter 13 is dedicated to the certification of the vehicle, by showing the compliance of the project and the vehicle design to the requirements received by stakeholders, and providing a risk analysis. The sustainability of the project is presented in Chapter 14, where a sustainable development strategy is presented, including the efforts by the team to contribute to the cause, a life cycle assessment and an end-of-life procedure description. The resources are described in Chapter 15 Then, Chapter 16 gives a brief cost breakdown estimation for the project, vehicle, and operations. Lastly, the overall project planning is presented in Chapter 17, and the report is closed with a conclusion in Chapter 18.

2
Market Analysis

The market analysis is an essential step in understanding customer needs and market conditions. Market indicators such as volume, supply, and demand are key in establishing a competitive product price which influences the final design. These indicators decide whether the final design will be taken into production.

First, general issues in the emergency relief sector are investigated in Section 2.1. Then, Section 2.2 explores the current solutions supplied in the emergency relief market. The stakeholders are presented in Section 2.3. Section 2.4 investigates the customer needs to determine if there is a mismatch between the customer demand and the market supply. Accordingly, Section 2.5, clearly identifies the gap between the customer demand and the market supply to have a clear understanding of what gap the system aims to fill.

Now that a clear market gap has been identified; a potential solution of using drones to bridge this gap is investigated. A general overview of the current UAV market is given in Section 2.6. This is done to investigate if a pre-existing design can be used to fulfil the goal. From which it is clear that although the general market for UAV is vast; a UAV specifically designed for emergency relief is still a gap in the market.

Thereafter, Section 2.7 investigates the competition that attempts to (partially) satisfy this market gap, and analyses how the system can offer a different/better solution. Lastly, Section 2.8 provides a price point estimation for the solution, which is based on current competitors.

2.1. Problem Statement

Currently, the disaster relief sector faces multiple issues in order to increase the efficacy of its operations. One of the main issues is the lack of solutions to access natural disaster zones, where damaged infrastructure prevents the use of traditional vehicles such as trucks or cars. Helicopters provide a solution to this. However, due to their high operational costs, the issue still persists [3].

2.2. Emergency Relief Sector

To better understand the topic at hand, the current emergency relief solutions provided in the market are discussed, analysing the supply side.

The emergency relief sector consists of industry establishments that provide basic human needs (food, shelter, medical relief) to victims of domestic or international disasters. Disasters entail natural disasters (earthquakes, fires, tornadoes, hurricanes), human disasters (e.g. hazardous material spills), and acts of terrorism[1].

The emergency relief market is segmented by the vehicle platform, these are land, marine, and airborne platforms [3]. The land platform is the cheapest and most simple solution. However, in the case of damaged infrastructure, it might not be able to reach the affected zone or have a very slow response time. Since failing infrastructure must be considered in the case of natural disasters, this issue is very limiting for the land platform [3]. The marine platform is used in scenarios such as floods, and in those cases, small boats can navigate the disaster area. This procedure is typically risky due to unknown objects and floating debris in the water which can damage the boat, putting the rescuer's and the victims in the boat at risk[3]. The airborne platform is the most resilient platform to locally damaged infrastructure. Two airborne solutions exist, namely aircraft and helicopters. Aircraft are used to deliver large quantities of supplies to a nearby airfield which is still intact, and in some cases, they are also used to drop packages over the zone during flight. Thus, in cases where 'delicate' payloads are to be delivered, aircraft cannot fulfil the need for transporting these payloads without a runway. Helicopters have two main uses in disaster relief; delivering cargo to locations inside the affected area, or rescuing people from the area. Thus helicopters are a good contender

[1] https://www.ibisworld.com/united-states/market-research-reports/ [visited on 1/12/2020]

for a solution of emergency relief. However, the problem of the scarcity of helicopters is a current problem which typically bottlenecks the capacity at which aid can be supplied [3].

With these general solutions that are currently supplied by the market laid out, it is clear that the current emergency relief sector is having difficulty providing satisfying solutions. The demand for an efficient and reliable solution for emergency relief still exists. The following section (Section 2.3) will identify the stakeholders, after which, Section 2.4 will analyse the mismatch between the customer demand and the market supply.

2.3. Stakeholder Identification

All stakeholders need to be identified to fully understand the needs and expectations of major interests outside the project environment. Following this, requirements were derived based on these stakeholders in [4]. The following list presents the identified stakeholders:

1. Project partners
2. Customers (see 2.4.1)
3. End Users
4. Employees
5. Competitors
6. Suppliers
7. Regulatory bodies
8. Legislative bodies
9. (Local) community
10. (Local) government
11. Investors
12. NGO's
13. Environmental groups
14. Labour unions

Strategic project partnerships could be established to give the project an edge on aspects regarding which the team lacks knowledge and experience (eg. NGO for humanitarian mission expertise). A distinction should be made between the customers & end-users. Customers buy and operate the drone, while end-users are the victims who receive supplies from the drone. Employees are highly relevant to the project since their role is crucial to make the project a success. Competitors are important because the market conditions depend on them, thus it is important to continuously investigate what their next step is in order to make strategic decisions. A good relationship with suppliers is paramount since they are a crucial cog in the manufacturing process and can be the driver behind the drones unit cost. Regulatory and legislative bodies set the rules that the drone needs to fulfil to be allowed to operate. Local communities and government are important to keep good relationships with as they could press legal charges or hinder operations if they do not feel fairly treated. Investors are crucial to the project as they provide the funding, they will have opinions on what should be prioritised such that the project is profitable, therefore it is important that their needs are satisfied. NGO's and environmental groups are important to keep close since if they disagree with certain operations of the company they could hinder progress. Lastly labour unions effect the employees of the company.

2.4. Customer Analysis

The general problem in the industry was previously discussed in Section 2.1, however, for a deeper and detailed understanding of the problem, the customers need to be evaluated. The previous sections provided a supply-side analysis of what is currently provided by the market. This section can be seen as a demand-side analysis.

2.4.1. Identifying Customers

During disaster relief, the organisations managing the disaster are making decisions under high stress, in a time-constrained environment, and with limited information [5]. The customers can be segmented into 3 groups:

1. Governmental organisations
2. Humanitarian non-governmental organisations
3. Private entities

Private companies are relevant because they can cause disasters by, for example, being responsible for a large hazardous material spill, and in that case, they could have the responsibility of fixing it.

2.4.2. Customer Needs

1. Speed - For all customers, the time-constraint is the most important criteria as human lives are at risk. Therefore the speed at which the solution can be implemented on the location is crucial.
2. Capacity & Scarcity - The capacity & scarcity of available vehicles can be used as important criteria, as they go hand in hand with the the required for solutions to be implemented.
3. Cost - Another important criterion is the cost of the solution. In the case of government organisations, the cost is not the highest priority, however, they are often budget constraint meaning the cost of the solution is highly relevant. In the case of humanitarian NGO's, these organisations typically depend on donations and have limited funding. Lastly, if a private entity is responsible for managing a disaster they caused, they are probably in a tough financial situation due to the disaster itself, and therefore it is expected that the cost of the solution is highly important to them.

2.5. Market Gap

Based on Section 2.4 it is clear that there is a gap between the customers' needs and what is supplied by the market. The customers' main priorities are solutions that can be implemented fast at a relatively low cost. Now, to summarise the gap between customer needs and the current solutions in the emergency relief sector:

1. Land Platform - Although the land platform fulfils the cost aspect of the customer needs, it lacks when it comes to the speed at which solutions can be implemented. In addition, when dealing with damaged infrastructure, it performs even slower thus it is not suitable for most scenarios.
2. Marine Platform - The marine platform can perform well in the cases of floods, and other natural disasters where a body of water is present, however as it cannot provide solutions in numerous other scenarios, it always creates a demand for a new or additional solution.
3. Airborne Platform (Aircrafts) - The aircraft platform is great when it comes to delivering large quantities of supplies at great speed; however due to the fact that a runway is needed, in the case of damaged infrastructure; it still creates a demand for another solution.
4. Airborne Platform (Helicopters) - The helicopter platform is the best current solution to emergency relief as it is the most resilient platform to locally damaged infrastructure, allowing it to operate in most situations. However, there have been many issues with the implementation of helicopters in emergency management due to their lack of availability due to the limited amount of helicopters spread over large geographic areas. Therefore a peak demand for a disaster management situation is difficult to satisfy. Secondly, helicopter solutions are expensive. The cost is not the main criterion in these situations because there are often no other alternatives. However, it would play a large role in the case of competition or substitute solutions.

The specific gap Project Healios is aiming to fill with our solution is point 4. In short, the market needs a quick to implement, low cost, airborne delivery of packages/cargo solution. Section 2.6 analyses how this gap can be filled using UAV's.

2.6. UAV Sector

A possible solution to the problems the emergency relief sector is facing is the use of UAVs to bridge the gap. Since drones are an emerging industry and not yet established in the emergency relief industry, a separate supply-side analysis for the drone market is provided in this section.

2.6.1. Segmentation and Size

UAV technology is currently used for a wide variety of purposes. A top-level characterisation of the uses of UAV is comprised of the use by consumers for recreational purposes; the use for military purposes (e.g. warfare, intelligence, reconnaissance); and the use by commercial and civil entities (i.e. commercial and government use). The market size of these sub markets is represented in Figure 2.1. In the case of the current project, the market to adhere to belongs to the civil category with a market size of $13 billion (€11 billion) in the year 2020 [2]. The civil market is expected to increase to $1.5 trillion (€1.26 trillion) or higher

[2] https://www.goldmansachs.com/insights/technology-driving-innovation/drones/ [visited on 17/11/2020]

in 2040 [3], this shows that there will be high growth in the coming decades with an average growth of 13% annually.

Within this market segment, civil and commercial entities use drones in a wide range of industries and sectors. These include but are not limited to agriculture, conservation of biomass and habitat protection (i.e. environmental conservation), architecture and construction, logistics and delivery of cargo, wireless internet access, and media and imaging [6].

The target sub-market that this team aims for is that of cargo logistics and delivery. Specifically, the target market is that of urgent medical supply delivery during natural disasters and global epidemics such as the current COVID-19 pandemic, which has highlighted the need for quick and reliable means of transportation of critical medical supplies to remote areas.

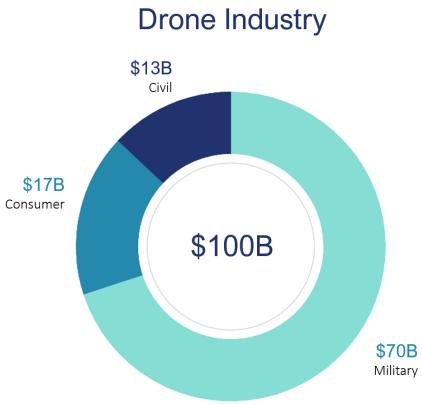

Figure 2.1: Drone Market Size in 2020 [2], Expected 13% Annual Growth from 2020 - 2040 [3]

As shown by Figure 2.1, the civil market is only 13% of the entire market, and the market for urgent medical supply delivery is a tiny fraction of that. This means that the current drones on the market aren't designed for similar missions, where a payload of 50kg is required, with a high-speed requirement, as well as delicate payload handling. Thus there is still a need for a new design of a drone that is suited for urgent medical supply delivery.

2.6.2. Market Dynamics and Trends

Currently, strict government regulations have been an obstacle to the deployment of drones across the healthcare sector [7]. However, several countries are progressively allowing the entry of drones in the healthcare industry by altering and creating new regulations to enable the entry of drones. These government initiatives are expected to drive the deployment of these drones and fuel the increasing market growth[4]. Public opinion on autonomous UAV's has also become more accepting over the past years. This is extremely beneficial for the drone industry as the creation of new progressive regulation depends to some extent on the public opinion. Lastly, climate change has been correlated to the increase of natural disasters and has been increasing over the past century [5]. This is another market driver for disaster relief services.

2.7. Competition

The competition is analysed to understand how the drone can be positioned with respect to current solutions. As stated before, the main competition is the use of helicopters. However similar logistical drones must also be considered as a competitor. Helicopters are the largest competitors in today's market. However, with the advancement of technology, drones may become the main competitor in the near future. Drones are not seen as a large competitor presently because their use is not widespread, and because companies manufacturing them do not have the resources to mass-produce them.

2.7.1. Helicopters

Helicopters are not direct competitors since there are considerable differences between a helicopter and a UAV. A logistic drone is not able to fully substitute a helicopter since it cannot evacuate people from a zone. However, it can substitute the delivery of cargo/packages that helicopters do. In disaster management, these two solutions could go hand in hand. The drone frees up capacity for the helicopters to specifically focus on evacuating people. While the drone can focus on bringing supplies in specific locations within the disaster

[3] https://www.morganstanley.com/ideas/autonomous-aircraft [visited on 25/11/2020]
[4] https://www.polarismarketresearch.com/industry-analysis/medical-drones-market [visited on 17/11/2020]
[5] https://www.ibisworld.com/united-states/market-research-reports/ [visited on 04/01/2021]

zone. In this situation the drone offers the advantage that the supplies are distributed in a decentralised manner. In disaster situations this can be beneficial as victims are typically dispersed over areas, and it is hard for victims to move even short distances. Therefore a decentralised distribution ensures that supplies are brought closer to the victims. For the drones to be viable, their cost still needs to be lower than that of a helicopter. Further analysis can be found in the price point estimation in Section 2.8.

2.7.2. UAV's

From preliminary market research, various companies that provide similar services in the UAV logistics and delivery market were identified. These are summarised in Table 2.1. These UAVs have payloads ranging from 1.75 kg up to 200 kg and range from 15 km to 500 km. Furthermore, note that not all of these companies are dedicated solely to the delivery of medical supplies. Some of them focus on the delivery of cargo packages, while others are more versatile and provide services in multiple market segments. Other specifications of the products such as cost are unknown for these concepts [4].

Table 2.1: Overview of main competitors in the logistics UAV market

Company	Description/Market	Vehicle Configuration	Max. payload [kg]	Range [km]
EHang[6]	Focused on the development of air mobility solutions in general. Products include PAVs, short-to-medium haul aerial logistics, and others.	Quadcopter (Falcon B) Octocopter (Ehang 216)	5 200	19 35
Zipline[7]	Focused on the delivery of medical supplies, blood delivery, and other healthcare logistics.	Fixed-wing	1.75	80
Matternet[8]	Fast, predictable and reliable transportation of diagnostic samples and medical items between healthcare facilities.	Quadcopter	2	20
Amazon Prime Air[9]	Delivery of packages from warehouses to end-users.	Hexacopter	25	16
Elroy Air[10]	End-to-end aerial cargo delivery for cargo, humanitarian, and military applications.	Hybrid (fixed-wing w/ quadcopter)	135	480
Wings For Aid[11]	Focused on the delivery of humanitarian supplies (food, water, any other life saving commodities).	Fixed-wing	160	500
UPS Drone[12]	Delivery of packages from warehouses to end-users	Quadcopter	25	N/A

2.7.3. SWOT of the UAV in the market context

With the competitors in mind, a SWOT analysis of the UAV solution can be performed. Strengths, weaknesses, opportunities and threats are identified in the market context.

[6] (https://www.ehang.com/Logistics/ [visited on 18/11/2020]
[7] https://flyzipline.com/how-it-works/) [visited on 18/11/2020]
[8] https://mttr.net/product [visited on 18/11/2020]
[9] https://www.amazon.com/Amazon-Prime-Air/b?ie=UTF8&node=8037720011) [visited on 18/11/2020]
[10] https://www.elroyair.com/ [visited on18/11/2020]
[11] https://www.wingsforaid.org/ [visited on22/01/2021]
[12] UPS Drone (https://www.ups.com/us/en/services/shipping-services/flight-forward-drones.page [visited on 17/11/2020]

Table 2.2: SWOT of the UAV in the market context

Strengths	**Weaknesses**
Product: S1: Faster response time to the emergency area compared to current solutions S2: Fast recovery in disaster/pandemic zones S3: Deployable from any open area S4: Better distribution of medical supplies compared to helicopters S5: Potentially more cost-effective compared to current solutions S6: Lower risk of human lives (no pilot) S7: Can be operated in difficult terrain S8: Purpose-built	**Product:** W1: Few similar products on the market W2: Certification can be a hurdle W3: Trained staff needed for continuous monitoring W4: Heavy medical equipment cannot be delivered by UAV W5: The 'smarter' the drone the higher the weight and cost W6: If batteries are used as the power source, battery life and power density is of high concern W7: Low tolerance to adverse environmental conditions
Opportunities	**Threats**
Product: O1: The UAV can transport medical supplies to rural areas (in non-emergency situations) O2: UAV can transport organs quickly without risk of traffic jam O3: The UAV can provide solutions to other industries (e.g. commercial) **Market:** O4: Money is available for emergency relief solutions O5: Global high investment in UAV technology O6: Public opinion becoming more open to UAV technology	**Product:** T1: Other products that solve the same problem are in development T2: Helicopters are a close competitor T3: Costly product certification T4: Safety of the drone: medical UAV can be mistaken for the military and be attacked by armed forces T5: UAV may interfere with air traffic and cause confusion to commercial planes **Market:** T6: Strong safety regulations need to be passed T7: Helicopters are current best option

2.8. Price Point Estimation

As discussed in Section 2.4, the price of the solution has a strong influence on the purchasing decision of the customer. The price of the solution can be estimated by investigating prices of comparable solutions. Ideally, the price point would be established based on the price of comparable UAVs in the market. However, since these competitors are not yet well established in the market, limited information is available on the price of these solutions. Due to this, the price point is estimated by analysing the price point of helicopters. For the drone to be an attractive competitor as a new entrant of the market it must be priced lower than helicopters.

The cost per hour (CPH) for each kg of payload transported is calculated for helicopters. The total cost is calculated based on the fixed costs and variable costs of the helicopter. Where fixed are annual costs, irrespective of the number of hours flown, consist of depreciation, insurance, taxes, crew costs, overheads, interest, and capital equipment. On the other hand variable costs directly vary with the number of hours flown, and consist of: fuel and oil, (un)scheduled maintenance labour, engine overhaul, airframe overhaul, and airframe lifted items. Under the assumption that the helicopter flies 450 [13] hours each year, the CPH/kg of the payload is between 1.34€ and 2.44€, for typical helicopters used in emergency relief scenarios. The ranges in price mainly depend on the size of the helicopter, larger helicopters having a lower CPH/kg, while smaller helicopters have a higher CPH/kg. Based on these calculations the drone must have a CPH/kg of payload lower than 1.34€ to be a competitive solution in the market and to be economically sustainable. The exact value of the CPH/kg and it's corresponding unit costs is further discussed in Chapter 16.

[13] https://www.ainonline.com/aviation-news/aerospace/2013-03-05/honeywell-sees-helicopter-sales-growth-ahead [visited on 04/01/2021]

3
Project Overview

In the previous chapter (Chapter 2), a market analysis was performed to recognise the gap in the market for the distribution of medical supplies in emergency relief scenarios.

The objective of this chapter is to present a general overview of our solution to the problem found in the market analysis, after which the mission is presented in a more technical description, with its functional requirements.

3.1. Project Healios

The market analysis (Chapter 2) shows that the current emergency relief sector is not able to fully meet the market needs. Based on the customer needs and the competitive landscape, the use of a logistics delivery UAV for the transport and delivery of medical supplies in disaster management situations presents itself as an attractive, suitable, and competitive solution. It is clear from the market analysis that the autonomous aerial distribution of products can be far more beneficial than existing solutions such as helicopters. The benefits arise due to the easy implementation of the solution and its lower cost.

Therefore, the goal of Project Healios is to develop a technology in which the distribution of medical supplies and other commodities for disaster relief can be expedited through the use of autonomy. The project was proposed and initiated by Dr. M.D. Pavel and derives most of its requirements from the Vertical Flight Society's Request for Proposal (RFP) for their *38th Annual Student Design Competition* [8] sponsored by Boeing. A detailed description of the requirement identification process for Project Healios is given in Section 3.5; here, it is sufficient to state that the project is broadly described in the RFP as:

Project Description

"Developing an unmanned vertical lift concept that can deliver, at high speed, up to 50 kg payloads to end-user customer sites up to 50 km radius, and to logistics centres up to 200 km away. The sizing is such that the vehicle can make a difference within a future pandemic or natural disaster. Responses shall include only current year (2020) technologies in order to support an initial entry into service in 2025" — *from the Vertical Flight Society Request for Proposal* [8]

The mission need statement (MNS) of Project Healios can therefore be defined as:

Mission Need Statement

To provide autonomous vertical lift delivery of emergency medical payloads to remote end-users or logistic centres, ready for service by 2025.

Similarly, the project objective statement (POS) is:

Project Objective Statement

To design an autonomous aerial vehicle capable of delivering emergency payloads in 10 weeks by 10 students, while complying with the regulations stipulated by in the VFS's 38th Annual RFP.

3.2. System Description

The goal of our mission is to provide a service in which medical supplies and other urgent commodities can be delivered at high speeds to remote areas, and other locations not accessible by the traditional methods

of transportation. Although the focus of the project is the development of the UAV itself, it is important to recognise that significant operational, logistic, and ground operations infrastructure would be required to ensure the successful completion of the mission.

For the remainder of this document, the word *system* is used to refer to the combination of the vehicle itself and all of the external infrastructure needed to support the vehicle's operations. This includes a base where the payload and the vehicle(s) are stored which serves as the centre of operations and the necessary personnel to maintain and operate the base. A detailed description of the operations and logistics needed to support Project Healios is given in Chapter 12.

3.3. Mission Profile

With the goals that the system must accomplish clearly defined, let us now shift our attention to *how* those goals are to be realised by the system. Firstly, the specific mission profiles that the vehicle must be able to perform are described in this section. Then, the functions that must be performed by the vehicle in order to complete the mission profiles are presented in Section 3.4.

The mission profiles that the vehicle must perform are taken from the VFS' Request for Proposal [8]. Again, note that a detailed description of the requirement identification process is given in Section 3.5. Here, the focus is placed on the guidelines provided by the VFS regarding the mission profiles alone.

Specifically, there are two separate missions that the system must be able to complete:

- **Local Delivery Mission:** Delivery of up to 50 kg payload to end-users in a range of 50 km. The vehicle must perform a two-way delivery mission within 33 minutes (excl. return trip) at high speed.
- **Logistics Mission:** Delivery of up to 50 kg payload to logistic centres within a 200 km range. The vehicle must perform a one-way trip operation within 80 minutes at high speed to safely deliver the package.

Both missions are divided into various segments, which together make up the mission profile. The VFS also provides specific requirements on certain segments for the missions, such as the duration of a specific segment or the altitude of the vehicle at that point in the mission.

The mission profile corresponding to the local delivery mission is given in Figure 3.1, and the explanation of the various segments of the mission is given in Table 3.1. Similarly, the logistics mission is represented visually in Figure 3.2, and its segments are summarised in Table 3.2.

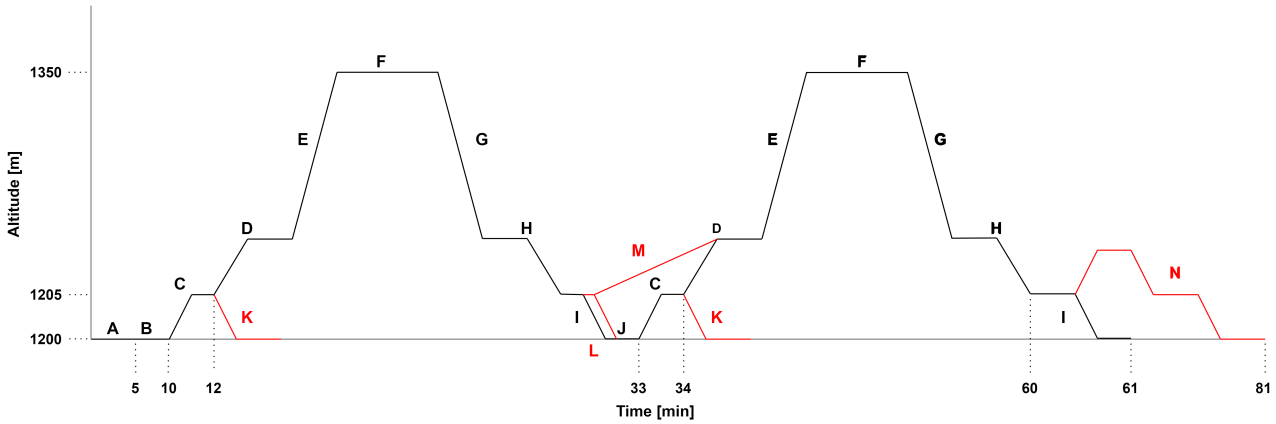

Figure 3.1: Mission profile of local delivery mission

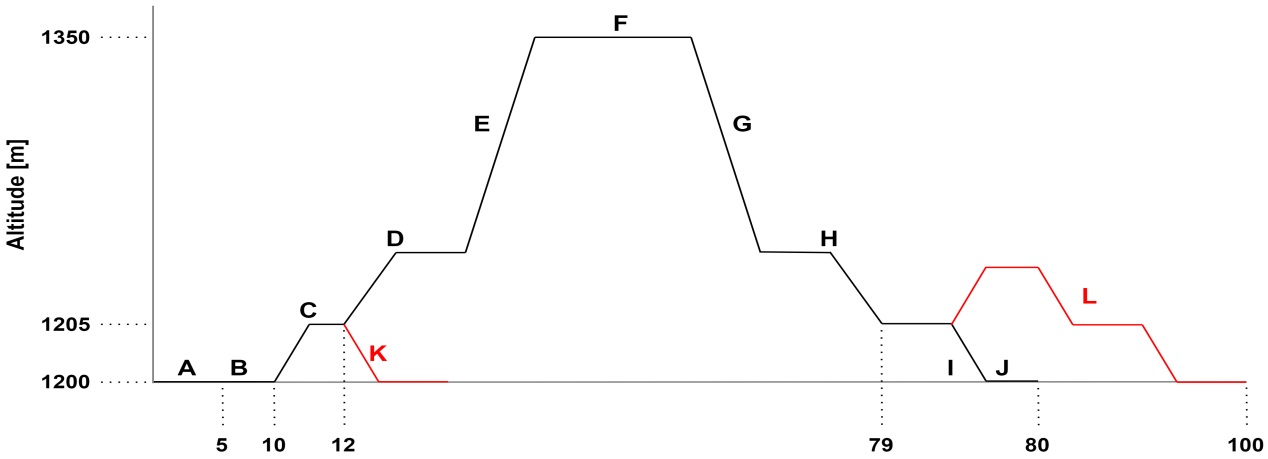

Figure 3.2: Mission profile of logistics mission

Table 3.1: Mission segment description of local delivery mission

#	Segment Name	Duration [min]	Segment Description
A	Preparations	5	Pre-flight vehicle inspections and payload handling.
B	Warm-up	5	Warming up the engines, and request for take-off.
C	Take-off HOGE	2	Take-off and climbing out of ground effect height to ensure hovering is possible without the aid of ground effect.
D	Transition: Horizontal		Vertical climb to transition altitude, and transition to horizontal flight.
E	Climb		Horizontal climb to cruise altitude.
F	Cruise		Cruising for 50km.
G	Descent	21	Horizontal descent to transition altitude.
H	Transition: Vertical		Horizontal descent to transition altitude, and transition to vertical flight.
I	Land HOGE		Hovering out of ground effect height, and landing.
J	Unload Payload		Autonomous payload ejection, and confirmation of delivery.
K	Abort Take-off		Emergency segment of abort take-off in the case a subsystem malfunction.
L	Contingency Landing	20	Emergency segment of relocating to a contingency landing spot.
M	Abort Return to base		Emergency segment of abort payload delivery, and returning to base.
N	Loiter Land at base		Emergency segment of abort nominal landing procedures, and loiter until landing is possible.

Table 3.2: Mission segment description of logistics mission

#	Segment Name	Duration [min]	Segment Description
A	Preparations	5	Pre-flight~vehicle inspections and payload handling.
B	Warm-up	5	Warming up the engines, and request for take-off.
C	Take-off HIGE	2	Take-off and hover in ground effect.
D	Transition: Horizontal		Vertical climb to transition altitude, and transition to horizontal flight.
E	Climb		Horizontal climb to cruise altitude.
F	Cruise		Cruising for 200km.
G	Descent	68	Horizontal descent to transition altitude.
H	Transition: Vertical		Horizontal descent to transition altitude, and transition to vertical flight.
I	Land HOGE		Hovering out of ground effect to ensure landing is possible without ground effect.
J	Unload Payload		Human-aided unloading of payload at logistics centre.
K	Abort Take-off	20	Emergency segment of abort take-off in the case a subsystem malfunction.
L	Loiter Land at base		Emergency segment of abort nominal landing procedures, and loiter until landing is possible.

As can be seen from the mission profiles the two missions share similar mission characteristics. However, there are a few key differences between the two:

- **HOGE & HIGE** - The first main difference between the two missions are related to its take-off procedures. For the local delivery mission; it is a mission requirement for the vehicle to first go through

a hover out of ground effect (HOGE) phase; in order to ensure that the engines are fully capable of delivering the lift required to hover, and to climb.[9]

- **Abort Procedures** - As can be seen in the table above, the segments corresponding with a red identifier relate to the abort segment procedures. For the local delivery mission; there are 4 instances where a planned abort is possible. Whereas for the logistics there are only 2 instances. This difference is due to the fact that the local delivery mission encounters an extra take-off and landing sequence.

3.4. Functional Analysis

Now that the mission profile has been analysed, a functional analysis of the system can be conducted. The functional analysis identifies the main functions that must be performed by the system, breaking them down into various levels of detail and organising them in a structured way. This allows the team to (a) gain a deeper understanding of the system, and (b) identify any potential additional requirements that could be added to the ones provided by the VFS to improve the performance of the system.

The functional analysis covers the functions that the *system* must perform, which includes everything from setting up the bases to the end-of-life (EOL) of the mission. In order to derive a complete and cohesive set of system functions from the mission requirements as presented in Section 3.3, two tools will be used. These are the functional breakdown structure (FBS)(Section 3.4) and functional flow diagram (FFD)(Section 3.4).

Functional Breakdown Structure

The FBS presents all the functions that the system must accomplish. It lists all the low-level functions pertaining to each of the high-level tasks. Whereas the FFD presents how the functions are to be performed in sequential order; the FBS relates the functions based on which high-level function it corresponds to.

Functional Flow Diagram

The FFD presents the functions to be performed by the system in sequential order, emphasising the relationships between them. The focus of the functional flow diagram is the functions that the product itself (i.e. the vehicle) must perform. Nevertheless, it is important to place these functions within the framework of the collection of function that the entire system must perform since the mission profile represents the main functions that the entire system needs to accomplish, and the vehicle is just a sub-part of that system.

Therefore, the FFD has been subdivided at the top level into the phases shown below. Please note that the first, second, and last phase are added mainly for the purpose of completeness, but the focus of the FFD (and therefore the phase that is constructed in most detail in the diagram) is the third phase, the actual operation of the system. The complete FFD is presented on a separate page at the end of this Chapter for clarity.

- **Design System** → As the name suggests, this phase deals with the design of the system. This phase is essentially encapsulated by Chapters 4 to Chapter 5.
- **Manufacture System** → This phase includes the functions that must be performed between the end of the design and the beginning of the operations of the system. This includes the manufacturing stage of the vehicle, the construction of the necessary bases and/or control centres, and the distribution of those vehicles to the respective bases.
- **Operate System** → This is the main branch of the FFD. It deals with the operation of the system, which can be subdivided into establishing contact with customers, carrying out pre-flight operations, delivering the payload to the customer/end-user, and finally, carrying out post-flight operations.
- **Retire System** → Finally, when the system reaches its EOL, it must be retired. This phase describes the process through which both the vehicles and the bases and/or logistic centres will be disposed of. It is vital to consider this phase of the life-cycle of the system to ensure that the EOL also complies with the organisational approach of the team, such as sustainability and risk assessment.

3.5. Requirement Identification

The basis of our design process depends on the requirements set for the final design, derived from various stakeholders. Thus, the first step in requirement identification was to perform stakeholder identification to

ensure that each of their wishes are taken into account, and reflected by the project.

Once all the stakeholders have been identified, through the use of multiple different analyses such as : market analysis (Chapter 2), technical risk assessment (Chapter 13), sustainable development strategy (Chapter 14), and functional analysis (Section 3.4). A set of requirements can be established. Combined with these constraints, the majority of the top-level requirements are derived directly from the *'Request for Proposal'* from the Vertical Flight Society (VFS) [8], and from the official JARUS guidelines for certification of the *Specific* category [10]. A more detailed description of the overall requirement identification process can be found in the Baseline Report [4].

The requirements that were identified were categorised in 2 main groups: Technical & Non-technical. Technical requirements were those that were directly related to a specific subsystem. Thus, these were used to drive the design scope in the respective subsystem departments, and presented at the beginning of each subsystem chapter. Non-technical requirements were those that were not directly related to a subsystem. Although these requirements were not driving in the scope of designing the vehicle, specific considerations were given for these and will be presented in Chapter 13.

Healios

- Design System 1.0
- Manufacture System 2.0
  - Manufacture Vehicle 2.1
    - Construct Manufacturing Plan 2.1.1
      - Explore manufacturing methods 2.1.1.1
      - Design manufacturing methods 2.1.1.2
    - Buy Material stock and components 2.1.2
    - Manufacture part 2.1.3
    - Assemble parts into sub-assemblies 2.1.4
    - Assemble final assembly 2.1.5
    - Test and validate final product 2.1.6
  - Build Base(s) 2.2
    - Study Optimal locations from market analysis 2.2.1
    - Select locations based on terrain, costs, and distribution 2.2.2
    - Construct Bases 2.2.3
    - Buy and install operational equipment for base 2.2.4
    - Hire & train personnel 2.2.5
    - Distribute Vehicles to bases 2.2.6
- Operate System 3.0
  - Establish contact with user 3.1
    - Receive order request 3.1.1
    - Check if destination is within operational range 3.1.2
    - Request Necessary parameters 3.1.3
      - Check Payload Mass 3.1.3.1
      - Check Payload Volume 3.1.3.2
      - Check Payload Content 3.1.3.3
      - Check Delivery Deadline 3.1.3.4
    - Confirm/Reject Order 3.1.4
  - Pre-Flight Operations 3.2
    - On-site payload handling & preperation 3.2.1
      - Receive Payload 3.2.1.1
      - Inspect Payload & make inventory 3.2.1.2
        - Check Mass 3.2.1.2.1
        - Check Volume 3.2.1.2.2
        - Check Content 3.2.1.2.3
      - Handle & Distribute payload to drone 3.2.1.3
      - Load Payload 3.2.1.4
    - Flight Planning 3.2.2
      - Input delivery coordinates into flight system 3.2.2.1
      - Construct Flight Plan 3.2.2.2
        - Check weather conditions 3.2.2.2.1
        - Select Contingency landing sites 3.2.2.2.2
        - Establish Flight Path 3.2.2.2.3
        - Verify U-Space 3.2.2.2.4
        - Initialize drone software & synchronize flight plan 3.2.2.2.5
    - Taxi drone to take-off area 3.2.3
    - Perform pre-flight vehicle check 3.2.3
      - Check control surfaces 3.2.3.1
      - Perform software checks 3.2.3.2
      - Establish contact with ATC and request for take-off 3.2.3.3
      - Standby for mission confirmation 3.2.3.4
  - Deliver payload to end-user 3.3
    - Take-Off 3.3.1
      - Check for obstacles and debris 3.3.1.1
      - Set engines and control system in take-off mode 3.3.1.2
      - Lift Off 3.3.1.3
      - Climb to cruise altitude 3.3.1.4
    - Perform Cruise Phase 3.3.2
      - Transition engines and control system into cruise mode 3.3.2.1
      - Lock in and align with flight path 3.3.2.2
      - Follow Flight Path 3.3.2.3
    - Perform Approach Procedure 3.3.3
      - Transition to hover mode 3.3.3.1
      - Initialize obstacle avoidance software 3.3.3.2
      - Detect Landing site characteristics 3.3.3.3
      - Identify obstacle/debris 3.3.3.4
      - Establish Landing/Drop Zone 3.3.3.5
    - Perform Descent Procedure 3.3.4
      - Set engines and control system in deployment/ landing mode 3.3.4.1
      - Activate animal/human deterrence system (if necessary) 3.3.4.2
      - Descend to landing site 3.3.4.3
      - Deliver Payload 3.3.4.4
      - Confirm Deliver Payload 3.3.4.5
    - Perform Abort Procedure 3.3.5
      - Abort to contingency landing site 3.3.5.1
  - Return to base 3.4
    - Set engines and control system in take-off mode 3.4.1
    - Repeat Take-Off Procedure 3.4.2
    - Repeat Cruise Procedure 3.4.3
    - Repeat Landing Procedure at base 3.4.4
    - Land at base 3.4.5
    - Turn off engines 3.4.6
    - Enter standby mode 3.4.7
  - Perform post-flight operations 3.5
    - Inspect the vehicle 3.5.1
      - Inspect Landing Gear 3.5.1.1
      - Inspect Payload attachment mechanism 3.5.1.2
      - Inspect Sensors 3.5.1.3
    - Cleaning and Maintenance 3.5.2
      - Perform maintenance and cleaning of vehicle 3.5.2.1
      - Perform maintenance and cleaning of base 3.5.2.2
    - Refueling/Recharging 3.5.3
- Retire System 4.0
  - Recycle Vehicles 4.1
    - Disassemble Vehicle 4.1.1
    - Erase/Destroy parts with sensitive information 4.1.2
    - Disposal of non-sensitive parts 4.1.3
      - Reuse common parts as spare stock 4.1.3.1
      - Retire unusable parts 4.1.3.2
        - Disposal of recyclable materials (e-waste) 4.1.3.2.1
        - Disposal of non-recyclable materials 4.1.3.2.2
  - Refurbish Base 4.2
    - Make inventory of remaining equipment 4.2.1
    - Erase/Destroy parts with sensitive information 4.2.2
    - Disposal of non-sensitive equipment 4.2.3
      - Dispose of recyclable materials 4.2.3.1
      - Sell remaining equipment 4.2.3.2
    - Sell Building and/or property 4.2.4

Functional Flow Overview

Design System 1.0 → Manufacture System 2.0 → Operate System 3.0 → Retire System 4.0

Legend

Lighter tones represent depth of detail

Operate System 3.0 — Function Description — Function Identifier

Normal Procedures

Abort Procedures

Manufacture System

Manufacture Vehicle 2.1 → Build Base(s) 2.2

2.0

Construct Manufacturing Plan 2.1.1 → Buy Material stock and components 2.1.2 → Manufacture part 2.1.3 → Assemble parts into sub-assemblies 2.1.4 → Assemble final assembly 2.1.5 → Test and validate final product 2.1.6

2.1

Study Optimal locations from market analysis 2.2.1 → Select locations based on terrain, costs, and distribution 2.2.2 → Construct Bases 2.2.3 → Buy and install operational equipment for base 2.2.4 → Hire & train personnel 2.2.5

2.2

Operate System

Establish contact with user 3.1 → Pre-Flight Operations 3.2 → Deliver payload to end-user 3.3 → Return to base 3.4 → Perform post-flight operations 3.5

3.0

Receive order request 3.1.1 → Check if destination is within operational range 3.1.2 → Request Necessary parameters 3.1.3 → Confirm/Reject Order 3.1.4

3.1

Check Payload Mass 3.1.3.1 → Check Payload Volume 3.1.3.2 → Check Payload Content 3.1.3.3 → Check Delivery Deadline 3.1.3.4

3.1.3

On-site payload handling & preperation 3.2.1 → Flight Planning 3.2.2 → Taxi drone to take-off area 3.2.3

3.2

Receive Payload 3.2.1.1 → Inspect Payload & make inventory 3.2.1.2 → Handle & Distribute payload to drone 3.2.1.3 → Load Payload 3.2.1.4

3.2.1

Check Mass 3.2.1.2.1 → Check Volume 3.2.1.2.2 → Check Content 3.2.1.2.3

3.2.1.2

Input delivery coordinates into flight system 3.2.2.1 → Construct Flight Plan 3.2.2.2

3.2.2

Check weather conditions 3.2.2.2.1 → Select Contingency landing sites 3.2.2.2.2 → Establish Flight Path 3.2.2.2.3 → Verify U-Space 3.2.2.2.4 → Initialize drone software & synchronize flight plan 3.2.2.2.5

3.2.2.2

Perform pre-flight vehicle check 3.3.1 → Take-Off 3.3.2 → Perform Cruise Phase 3.3.3 → Perform Approach Procedure 3.3.4 → Perform Descent Procedure 3.3.5 → Perform Abort Procedure 3.3.5

3.3

Check control surfaces 3.3.1.1 → Perform software checks 3.3.1.2 → Establish contact with ATC and request for take-off 3.3.1.3 → Standby for mission confirmation 3.3.1.4

3.3.1

Check for obstacles and debris 3.3.2.1 → Set engines and control system in take-off mode 3.3.2.2 → Lift Off 3.3.2.3 → Climb to cruise altitude 3.3.2.4

Abort to contingency landing site 3.3.5.1

3.3.2

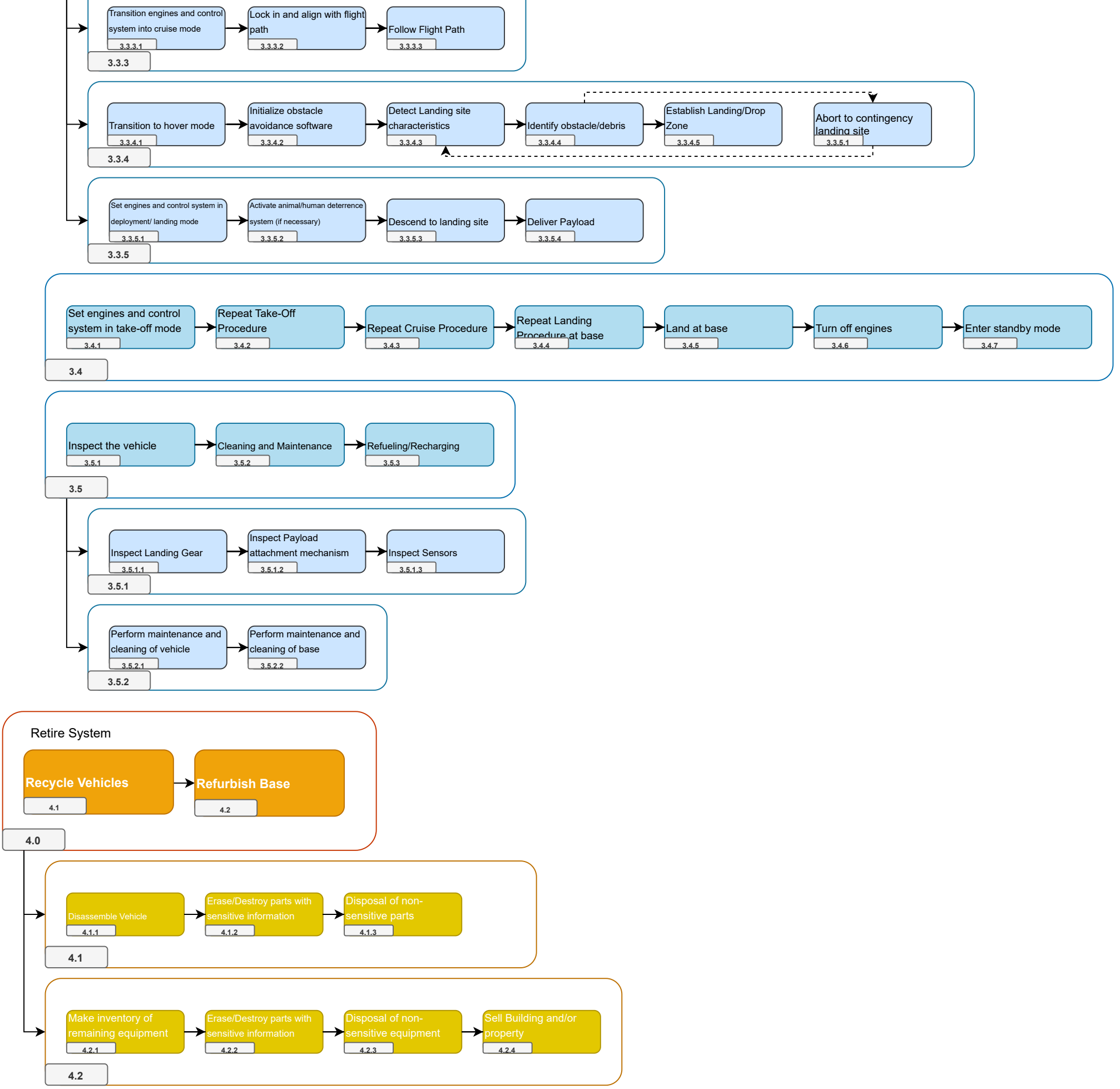
Transition engines and control system into cruise mode
3.3.3.1
Lock in and align with flight path
3.3.3.2
Follow Flight Path
3.3.3.3
3.3.3
Transition to hover mode
3.3.4.1
Initialize obstacle avoidance software
3.3.4.2
Detect Landing site characteristics
3.3.4.3
Identify obstacle/debris
3.3.4.4
Establish Landing/Drop Zone
3.3.4.5
Abort to contingency landing site
3.3.5.1
3.3.4
Set engines and control system in deployment/ landing mode
3.3.5.1
Activate animal/human deterrence system (if necessary)
3.3.5.2
Descend to landing site
3.3.5.3
Deliver Payload
3.3.5.4
3.3.5
Set engines and control system in take-off mode
3.4.1
Repeat Take-Off Procedure
3.4.2
Repeat Cruise Procedure
3.4.3
Repeat Landing Procedure at base
3.4.4
Land at base
3.4.5
Turn off engines
3.4.6
Enter standby mode
3.4.7
3.4
Inspect the vehicle
3.5.1
Cleaning and Maintenance
3.5.2
Refueling/Recharging
3.5.3
3.5
Inspect Landing Gear
3.5.1.1
Inspect Payload attachment mechanism
3.5.1.2
Inspect Sensors
3.5.1.3
3.5.1
Perform maintenance and cleaning of vehicle
3.5.2.1
Perform maintenance and cleaning of base
3.5.2.2
3.5.2
Retire System
Recycle Vehicles
4.1
Refurbish Base
4.2
4.0
Disassemble Vehicle
4.1.1
Erase/Destroy parts with sensitive information
4.1.2
Disposal of non-sensitive parts
4.1.3
4.1
Make inventory of remaining equipment
4.2.1
Erase/Destroy parts with sensitive information
4.2.2
Disposal of non-sensitive equipment
4.2.3
Sell Building and/or property
4.2.4
4.2

4

Summary of Concept Generation & Trade-off

Now that the top level depiction of the project has been given, this chapter will include a summary of the trade-off process performed to arrive at the final concept to be taken into the detailed design.

4.1. Concept Generation

The initial step to developing a suitable design that can satisfy the requirements was to generate ideas. After this, the different design options could be evaluated. In this step, overlooking no options. The preliminary concepts were grouped in the following families: conventional rotorcraft/helicopter, compound (fixed-wing) with VTOL, and blended-wing with VTOL. The concepts in each family were analysed and based on the outcome of this analysis the 'best' concept is brought to the trade-off [2]. This was done to ensure a limited number of feasible designs were analysed.

4.2. Trade-off

The trade-off method is used to select one of the concepts from the concept generation phase. The trade-off is based on independent and measurable criteria that can show differences between the concepts. The goal was to cover as many requirements as possible with these criteria. The concepts were scored with the following criteria: Operational cost, Risk, Emissions, Infrastructure, Resilience and complexity. Each criterion had a scoring function and a weight. Weights are given to each criterion based on their relative importance. The importance was decided on based on the stakeholders' requirements and the groups' judgement. In Figure 4.1 a summary is provided of the performed trade-off.

Criteria	Oper. Cost	Risk	Emission	Infra.	Resilience	Complexity	Final Scores
Helicopter	0.13	0.14	0.09	0.07	0.11	0.15	**0.67**
Tilt-Wing C	0.19	0.14	0.13	0.07	0.10	0.10	**0.73**
Tilt-Wing H	0.19	0.12	0.13	0.06	0.10	0.09	**0.69**
Tilt-Wing E	0.20	0.15	0.14	0.06	0.09	0.10	**0.74**
Tailsitter C	0.20	0.14	0.14	0.07	0.09	0.07	**0.71**
Tailsitter H	0.19	0.13	0.13	0.06	0.07	0.06	**0.65**
Tailsitter E	0.20	0.15	0.14	0.06	0.09	0.07	**0.71**

Figure 4.1: Trade summary table

Once the result of the trade-off was obtained, a sensitivity study was carried out to test the robustness of the trade-off and to verify the results. The analysis was done by fluctuating the criteria weights and observe how this influenced the trade-off winner. Additionally, there were uncertainties regarding the final design parameters of each concept. Therefore, these design parameters were changed within the uncertainty range to understand how that would affect the trade-off's winner. It was concluded that the trade-off was robust enough, with the winning concept winning 70% of the time in various sensitivity scenarios.

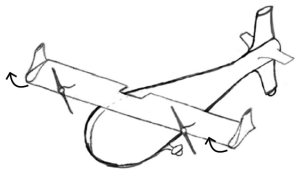

Figure 4.2: Electric Tilt-Wing

4.3. Final Concept

The winning concept from the trade-off was the electric tilt-wing vehicle (Figure 4.2). This is an artistic representations of the concept and the exact shape, size or form of the concept has not been determined at this stage. Throughout the rest of this report the exact design of the concept will be discussed.

5
Final Layout

The final configuration is displayed below in Figure 5.1, Figure 5.2, and Figure 5.3. Note that both payloads are shown overlapping each other (in blue and in yellow). The vehicle is displayed during transition, with its wings tilted 45°. Furthermore, the internal layout of the vehicle is a volumetric approximation to house all of the components in such a manner that the centre of gravity is within acceptable bounds and everything can be structurally fastened. The lights, cabling, small sensors, fasteners, and other smaller components are not modelled.

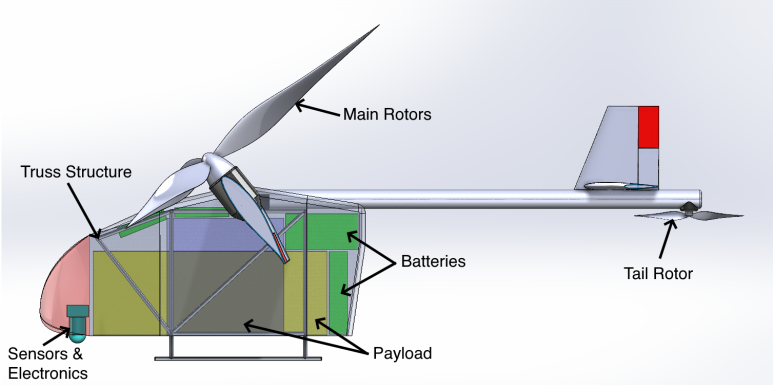

Figure 5.1: Side view of the vehicle

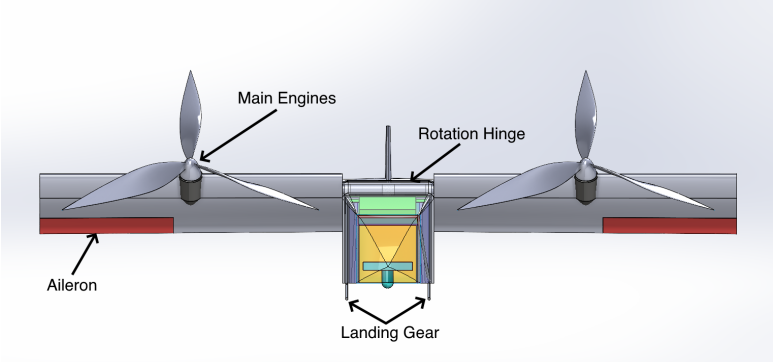

Figure 5.2: Front view of the vehicle

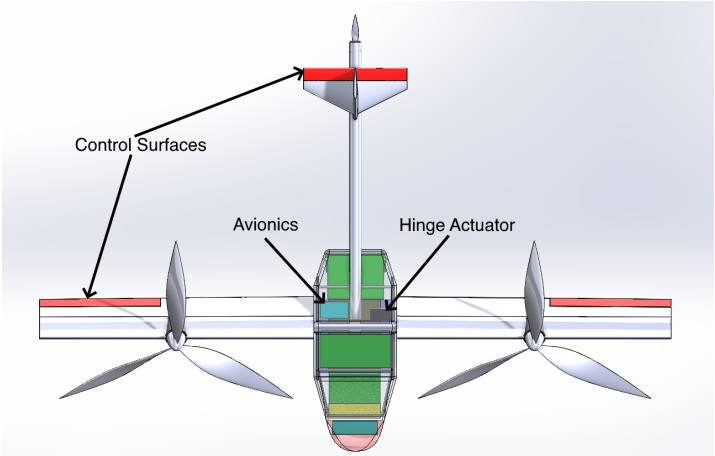

Figure 5.3: Top view of the vehicle

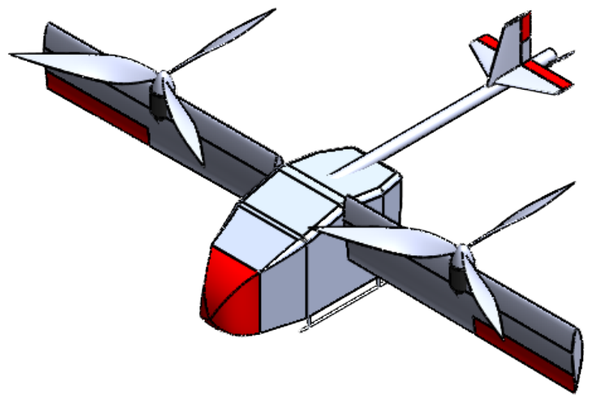

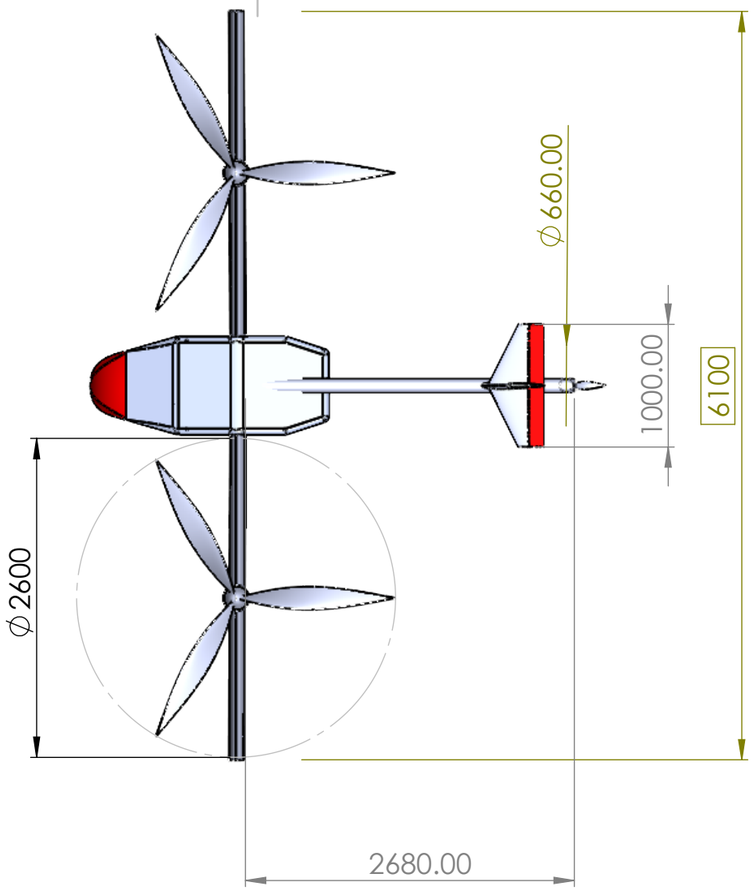

Name	Dimension
Wing Span	6100
Wing Chord	630
Wing Aerofoil	NACA 643-418
Twist	3°
Horizontal Tail Span	1000
Horizontal Tail Root Chord	500
Horizontal Tail Tip Chord	250
Vertical Tail Height	500
Vertical Tail Root Chord	500
Vertical Tail Tip Chord	250
Horizonta/Vertical Tail Aerofoil	NACA 0010
Tail distance to C.G.	2500
Propeller Diameter	1300
Propeller Aerofoil	Clark Y
Engine Distance To Centre Line	1730
Engine Distance To Centre Line	1730
Aux Engine Arm	2600
C.G. from Wing LE	280

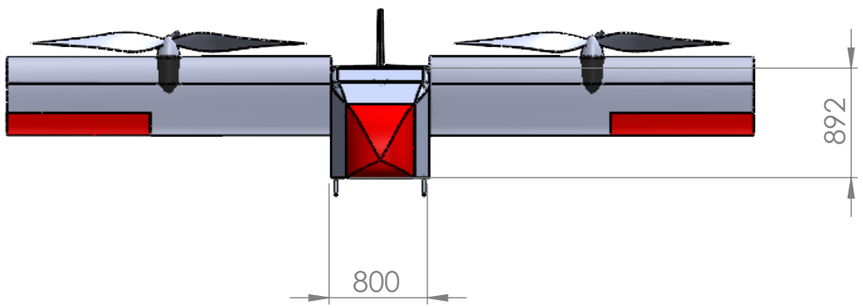

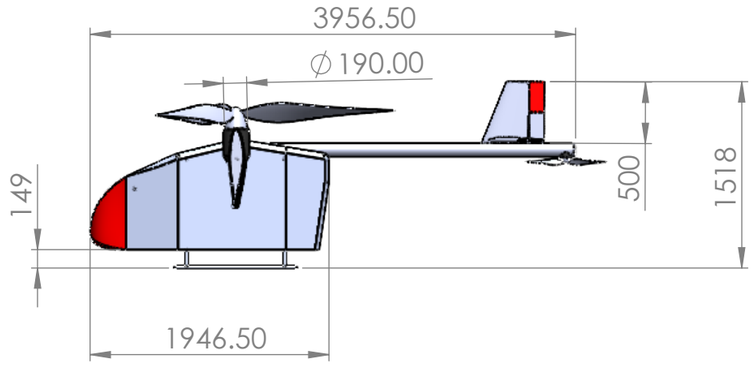

Units: Millimetres, unless stated otherwise | REVISION A

TITLE:

HEALIOS

DWG NO. 1 | A3

SCALE:1:50 | SHEET 1 OF 1

6
Design Methodology

Now that the final layout of the vehicle has been presented in Chapter 5, the overall design methodology can be presented. In order to have a clear overview of the detailed design process, this chapter aims to provide a global overview of the individual subsystems that will make up the entire engineering department, and how they will interact with each other in order to have a coherent design from each technical department's perspective. The foundation of the entire process is based upon the results obtained from the midterm trade-off as described in Chapter 4. Section 6.1 provides an overview of the scope and objectives of each subsystem. Then in Section 6.2, a general approach to the subsystem design and the subsystem structure of the report are presented. Section 6.3 describes how the different subsystems will be integrated together, and shows the general process for the iterative design. Finally, Section 6.4 includes the general guidelines for the verification & validation methods to be used throughout the design process.

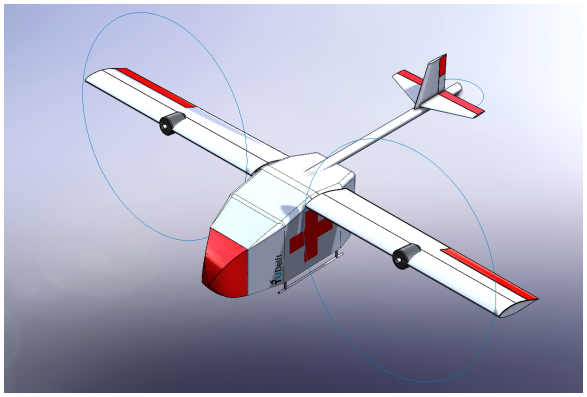

Figure 6.1: Healios in cruise mode - front view

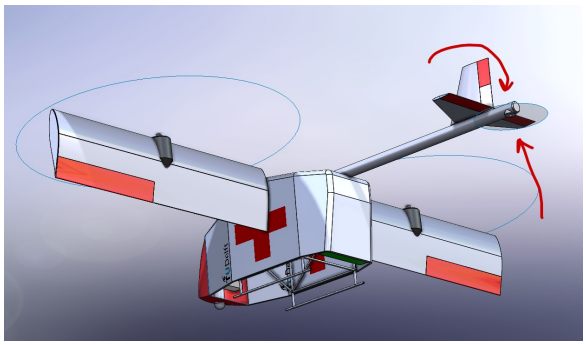

Figure 6.2: Healios in hover mode - back view

6.1. Subsystem Overview

This section aims to present an overview of the scope and objectives of each subsystem.

Aerodynamics - The outline of the Aerodynamics department has begins with the airfoil design, where the analysis will be performed to choose an aerofoil for a given set of constraints. Estimations are done to achieve the aerodynamic characteristics of said airfoil. Then once an airfoil has been decided on, the 3D wing design will be based on iteratively optimising the wing planform for the given geometrical constraints and aerodynamic constraints.

Structures & Materials - The Structures & Materials department began with a wing box design, by first identifying the different loading conditions the wing would experience. This analysis has been performed analytically and iteratively as the wing planform changed. It is verified using FEM software. The fuselage design consists of developing a lightweight truss structure to form a load path from the payload and batteries towards the main wing spar. Finally, the connection between the tail to the wing and fuselage will also be designed based upon the loading it experiences.

Control & Stability - The scope of the Control & Stability department has been to design a subsystem which can ensure that the vehicle is stable and controllable in all flight conditions. The attention is then placed on performing a thorough analysis of the static (trim) and dynamic (eigenmotion) stability of the vehicle for both cruising and hovering flight. This is on its turn used to perform the preliminary design of controllers to ensure the vehicle is stable and controllable in cruise (longitudinally and laterally) and in hover.

Transition flight is examined and risk analysis is performed. It is worth noting that although the Control &

Stability subsystem was not directly affected by iterations regarding the MTOW, a significant effort was made to ensure coordination with the other subsystems. For example, the use of aerodynamic analysis software to determine the stability derivatives of the vehicle, and the coordination with the Propulsion department to size the auxiliary engine.

Power & Propulsion - The power and propulsion subsystem are described by developing detailed and specific mass and power calculations. These tools are used in an iterative approach, to find the converged parameters. In addition to the power and mass calculations, the battery is sized and the engine chosen. The propeller is designed to adhere to the requirements and noise calculations are performed.

6.2. Subsystem Design & Structure

It is crucial that each subsystem has the same general approach to present the steps and method used in the design. This way, it can be ensured that the design process is coherent and concise between each subsystem. This section presents the basic structure of each subsystem and what it will be consisting of.

1. **Design Overview** - The design overview aims to provide the reader with a brief recap of everything that has been done for the said subsystem.
2. **Requirements and Functional analysis** - The functional analysis identifies the priorities and the driving requirements for the specific subsystem.
3. **Risk & Sustainability analysis** - The risk & sustainability analysis aims to present the various risk and sustainability aspects that can be taken into account during the design of a specific subsystem.
4. **Design approach** - The design approach lays out the specific scope of each of the subsystem and the process each subsystem will take in a qualitative manner.
5. **Design process and results** - The design process will contain the majority of the actual detailed design, where the quantitative analysis of each subsystem design will take place.
6. **Sensitivity Study** - The sensitivity study aims to investigate how robust our design choices are, looking into if there is a radical change in the design for a slightly different design inputs/choices.
7. **Verification and Validation** - The V&V section aims to discuss the procedure that has been taken to ensure all calculations are done correctly and works as it is intended to.

6.3. Subsystem Integration & Design Iterations

Before beginning the individual subsystem design, it is crucial to have an overview of how each subsystem will affect the other. Since poor overview of the inter-relations between the subsystem will lead to poor communication between them, not keeping them into account might result in an unfeasible design.

There are 3 main subsystem groups that are mainly affected by the change in MTOW, namely the aerodynamics, structures, and power & propulsion. Control and stability was not taken into account during this iterative design due to the fact that it is only implicitly related to the MTOW. The changes due to a change in MTOW will only affect the control system if the weight grows above a certain threshold. This would mean that heavier COTS control actuators should be chosen.

1. **Aerodynamics** - The aerodynamics department will begin the design process based on the lift that is required to have a steady flight, as well as performing manoeuvres. Thus the design process begins with an MTOW for which the wing is designed.The wing plaform can be determined afterwards.
2. **Structures** - The structures department can be split into 2 groups: the wing structure, and the fuselage structure. The fuselage structure will be designed with the instrumentation, avionic equipment and payload in mind. However once it has been designed, the overall structure to support these will not deviate dramatically. On the other hand, the wing structure will heavily depend on the aerodynamics department, and thus whenever a new wing plan-form is outputted, a new wing structure should be designed. In addition, depending on the MTOW, the landing gear design will vary as well.
3. **Power & Propulsion** - The P&P department will begin the design process based upon the thrust that is required to have a steady flight, as well as performing manoeuvres. Thus the design process begins with the output from the aerodynamics department, the wing's aerodynamic performance, to see how much thrust is required to overcome the drag. Also, MTOW will inherently affect the thrust that is required.

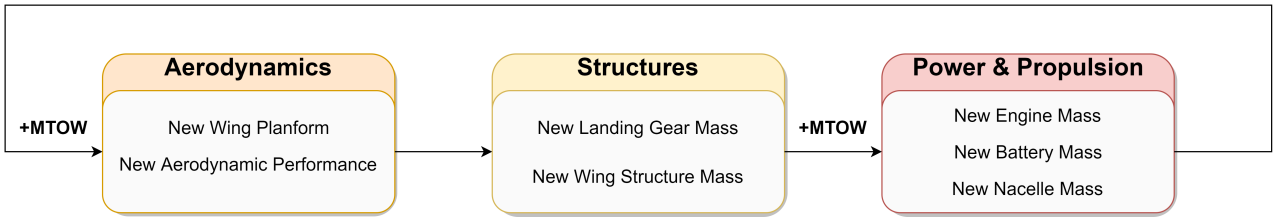

Figure 6.3: Visualization of the Iterative Process

Figure 6.3 displays a visual representation of the overall design iteration process. For a given MTOW, the process begins with the aerodynamics department creating a wing planform, which outputs new aerodynamic coefficients and wing dimensions. Next, given the new wing dimensions, the structures department creates the inner structure of the wing. Which on its turn affects the overall MTOW, which affects the landing gear mass. Now with this new MTOW, and new drag coefficients, the Power & Propulsion department can size their batteries and engines given the drag force it must overcome, and generate enough thrust to support the new MTOW. Then this new MTOW with the new battery, engine, and nacelle mass gets fed back into the aerodynamics. This process will continue until an MTOW has been converged upon.

6.4. Verification & Validation Procedures

Verification & validation (V&V) are essential procedures that ensure that the final design meets its requirements and fulfils its intended purpose. This was previously presented in the Midterm Report[2], thus the aim of this section is to recap the general approach and guidelines for the V&V which will be performed within each subsystem and adapted for the detailed design.

6.4.1. Verification

This section outlines the verification procedures that will be implemented in the design process. In addition, as different tools are used to support the design process, specific methods for the verification procedure of design tools are also presented.

Verification Methods

Common verification methods used in aerospace design are listed below.

- **Test** is to analyse the product to prove it passes a specific requirement. Generally, tests are the most reliable confirmation that a product adheres to a set of requirements. However, as it can only be performed when the system or subsystem has been produced, it will be omitted from the main verification methods to be used for each subsystem.
- **Analysis & Simulation** uses a mathematical model of the product to show that it meets a set of requirements. Logic, mathematics, or computations could be classified as analysis. Examples of typical analyses are thermal, electrical, mechanical, functional & operational analyses. In all engineering designs, analysis is used extensively as a verification tool. A simulation is a specific form of analysis using computers to show that the products behave in the predicted manner, and meet the requirements. Test inputs can be used to compare a model to a validated simulation. However as the design size increases, the complexity of creating test input increases, making it less practical.
- **Review of Design** or also called inspection, aims to review the design and compare it to standards outlined by the relevant authority. This is done to investigate if the product answers the requirements. It is treated as an informal verification technique because it is based on interpretation and subjectivity. For certifiability, inspection is a required verification technique, to ensure the systems comply with the requirements [11], [12].
- **Verification Through Similarity** is based on the fact that another component with similar performance and operating requirements will meet its own performance requirements. This method is largely based on experience with another component in similar operating conditions. The operating conditions of a similar component must be equivalent to the operating conditions of the part being designed. To verify by using similarity, a 'Letter of Similarity' is used in the aircraft industry. This letter justifies the past use of the component as verification for the requirements [11].

Verification Procedures for Design Tools
It is important to investigate the level of accuracy of the tool before use, and to analyse whether the assumptions made for the tool can be applied. Thus this subsection lists numerous verification procedures to be used for the design tools.

- **Unit Tests** - a small part of the software is tested. For example, one formula can be tested. This is done by implementing variables into the equation of which the output is known. When performing an unit test using literature, it is crucial to specify the source, the type of test, and the expected output given a certain input. By properly performing unit tests, the time consumed by debugging can be minimised as there will be fewer defects during the later stages [13]. Additionally, Python's built-in 'unit test' function will be used to perform unit tests and verify any python scripts that were used in the design process [1].
- **Integration Tests** - Integration tests are performed when different units have been put together. This verifies that the individual codes work together. These tests can be split into two: importing data and comparing the final solution with an analytical solution. If the design tool imports data from a file, verification is needed to check that the right data is imported. [13]

6.4.2. Validation
System validation is the "Confirmation, through objective evidence, that the developed system effectively achieves its intended purpose and meets the user needs it was developed to address." In other words, validation attempts to determine whether the right system has been built.[2] A system is usually validated by comparing simulation or analytical data with physical test results.

The scope of this project does not reach as far as manufacturing and testing, therefore the system can not be validated. However, the used methods can be validated since method validation is the process of "determining if the simulation results accurately represent the physical problem" [14]. This method of validation can be done in multiple ways:

- Comparing result to current technologies
- Running different programs with similar constraints and comparing results
- Using papers and studies to compare the method to

This way, by validating the methods, the chance of the system performing as expected and required is maximised without the need of system validation. Naturally, this system validation is a requirement for further research and design. That is if the project was to be continued.

[1] https://www.datacamp.com/community/tutorials/unit-testing-python [visited on 02-12-2020]
[2] https://connected-corridors.berkeley.edu/developing-system/system-validation-and-verification-plans [visited on 02-12-2020]

7
Aerodynamics

The vehicle's aerodynamic design is the key to keeping it in the air. An efficient aerodynamic design helps keep the vehicle in the air longer. Studying the motion of air around the UAV allows the calculation of forces acting on it. This chapter aims to design the UAV elements as such, that sufficient lift is achieved to keep it in the air, while minimising the resistance acting on it.

Section 7.1 gives an overview of the past of this design. Whereas Section 7.2 displays their relevant requirements, and the functions to be investigated. This is followed by three sections discussing the design elements: Section 7.3 provides the design of the wing, Section 7.4 discusses the design of the horizontal and vertical tail, and Section 7.5 shows the design of the fuselage. Section 7.6 shortly discusses the effects of the propellers on the design. Finally, Section 7.7 provides the verification and validation of the design methods, Section 7.8 gives a view on the sustainability of the design, and Section 7.9 suggests some recommendations for future research.

7.1. Design Overview

During the preliminary design phase a number of elements related to the aerodynamic design have been calculated. These include:

- **Maximum take-off weight estimation:** This is one of the most crucial inputs for the aerodynamics' detailed design. As the system designed in this project uses electric propulsion, the MTOW is equal to the cruise weight, meaning it directly reflects the lift required to keep the UAV in the air.
- **Wing area estimation:** As the wingspan of the aircraft is limited by requirements, the required wing area highly reflects the wing's shape.
- **Stall speed estimation:** The stall speed shows at what speed the vehicle is still required to produce enough lift to keep the UAV in the air.

The detailed design uses these inputs to perform iterations on the design.

7.2. Requirements and Functional Analysis

The relevant requirements for the aerodynamic design are listed in Table 7.1

Table 7.1: Requirements for Aerodynamic Design

ID	Requirement
OP-CER-UAS-07	The UA minimum safe speed or the minimum steady flight speed for each flight configuration and phase of flight shall be determined.
OP-CER-UAS-17	The UA shall be controllable and manoeuvrable, within the demonstrated flight envelope at all loading conditions for which certification is requested.
OP-MI-PER-03	The UA planform shall be less than or equal to 6.1m x 6.1m.
FU-STR-18	The loads acting upon all relevant structural components shall be determined in response to the flight load conditions.

The three elements that are considered in this section are:

- **Wing:** The wing's primary function is to generate sufficient lift to keep the UAV in the air.
- **Horizontal and vertical tail:** These components are present to provide trim, stability and control.
- **Fuselage:** It provides a secure attachment for the carried payload, aerodynamic surfaces and other UAV components.

The design of each of these components are discussed in the upcoming sections. As the UAV is in cruise configuration for the large majority of the mission, the aerodynamics are optimised for this phase, with additional considerations for the fact that wings incidence angle is adjustable.

7.3. Wing Design

The focus of this chapter is the detailed design of the wing. The wing may be considered as the most important component of an aircraft since its geometry, and its features influence every other aircraft component.

Its primary function is to generate the required lift force, which results in two addition elements, namely the drag force and pitching moment. The design aims to provide the required lift while minimising the drag and pitching moment. Design constraints are derived from performance requirements, stability and control requirements, producibility requirements, operational requirements, cost, and flight safety.

7.3.1. Wing Design Approach

First, the constraints set for the wing design are introduced:

1. A single wing design is used to limit the additional weight needed by the rotatable wing.
2. The design has a high wing configuration: This provides the required ground clearance for payload loading and prevents dust or gravel injection in the engines.
3. No high lift devices are used: This is since the wing incidence angle is variable; therefore, extra lift can be generated using the engines at any time. This constraint further helps to decrease the weight of the wing structure.

Given these constraints, the design process is planned in accordance with [15]. As the wing design is an iterative process and the calculations are usually repeated several times, the design process block diagram is drawn accordingly in Figure 7.1.

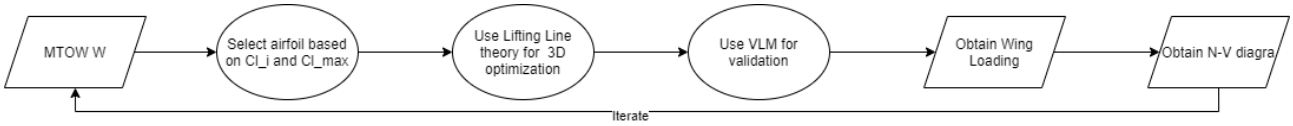

Figure 7.1: Wing Design Process

Each activity, represented by the blocks in the diagram, is further explained in the next subsections.

7.3.2. Wing Airfoil Selection

The airfoil section is responsible for generating the optimum pressure distribution on the top and bottom surfaces. There are two ways of determining an airfoil, which are related to the first block in Figure 7.1: designing the airfoil or selecting one from previously existing designs.

As the design of an airfoil is a very time consuming and complex activity, as the subsection's title suggests, the airfoil is selected from an existing list of airfoils. Two proven airfoil sources are NACA and Eppler [15]. The airfoil selection follows the process proposed by [15] which suggests tailoring it to the design needs. The following criteria for the airfoil selection are considered:

- Choose the airfoil with the highest maximum lift coefficient.
- Choose the airfoil with the proper ideal or design lift coefficient.
- Choose the airfoil with the lowest minimum drag coefficient.
- Choose the airfoil with the highest lift-to-drag ratio.
- Choose the airfoil with the highest lift curve slope.
- Choose the airfoil with the lowest pitching moment coefficient.
- Choose the proper stall quality in the stall region.
- The airfoil must be structurally reinforceable.
- The airfoil must be such that its cross-section is manufacturable.

Generally, it is impossible to obtain an airfoil that has an optimum value for all these criteria. Therefore a compromise has to be made. The practical steps to select an airfoil are the following:

1. The ideal cruise lift coefficient is calculated using the weight obtained from the preliminary weight estimation, see Equation 7.1.
2. The wing cruise lift coefficient is calculated. This is given as a ratio showing what percentage of the lift the wing generates [15]. Equation 7.2 is based on statistics.

$$C_{L_C} = \frac{2W_{\text{preliminary}}}{\rho V_c^2 S} \tag{7.1}$$

$$C_{L_{Cw}} = \frac{C_{L_C}}{0.95} \tag{7.2}$$

3. The wing airfoil ideal lift coefficient is calculated. This assumes a constant wing chord, no sweep angle, no dihedral angle, and an infinite wingspan. This relation is also based on statistics[15], see Equation 7.3.
4. The maximum lift coefficient is calculated according to:

$$C_{l_i} = \frac{C_{L_{C_w}}}{0.9} \tag{7.3}$$

$$C_{L_{\max}} = \frac{2W_{TO}}{\rho_O V_s^2 S} \tag{7.4}$$

5. With the relation described in step 2, the wing's maximum lift coefficient C_{Lmax_w} is calculated.
6. All airfoils that deliver the required C_{Lmax_w} and C_{l_i} are listed. The one that performs the best, according to the listed criteria, is selected.

As step 6 indicates, the NACA 643-418 is selected from a list of applicable airfoils [15], based on the previously given criteria. The non-dimensionalised lift, drag, and pitching moment, relative to the angle of attack, are presented below for a Reynolds number of 1 million[1].

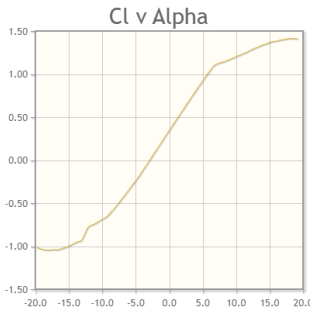

Figure 7.2: Lift against angle of attack

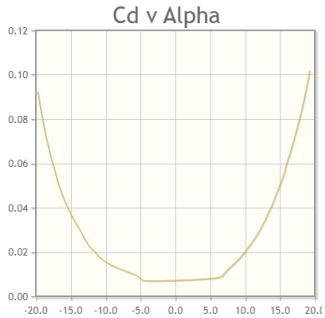

Figure 7.3: Drag against angle of attack

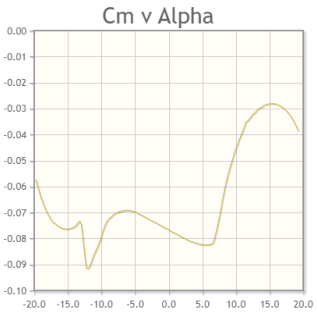

Figure 7.4: Moment against angle of attack

From Figure 7.2 five significant features can be deducted:

- **Stall Angle:** Approximately 15 degrees.
- **Maximum Lift Coefficient:** Approximately 1.25 degrees.
- **Zero Lift Angle of Attack:** Approximately -3 degrees.
- **Lift Curve Slope:** (α * 0.116) + 0.339 for the linearised region between -5 and +5 degrees.
- **Stall behaviour:** Not abrupt.

From Figure 7.3 the following can be deducted:

- The drag coefficient does not change considerably between -5 and +5 degrees angle of attack. Therefore, the ideal lift coefficient is between these values.
- Drag Curve Slope: (α*0.000136) + 0.00832 for the linearised region between -5 and +5 degrees.

From Figure 7.4 the following can be deducted:

[1] http://airfoiltools.com/airfoil/details?airfoil=naca643418-il [visited on 15/12/2020]

- The negative slope of the curve between the linearised region of -5 and +5 degrees is desirable, as it stabilises the flight if the angle of attack is disturbed by a gust.
- Moment Curve Slope: (α*0.005) - 0.076 for the linearised region between -5 and +5 degrees.

7.3.3. Wing Planform Design Method

As the airfoil is selected, the next step based on figure Figure 7.1 is to design the 3D wing. The input of this process are the airfoil properties and the output consists of the following variables: wing area, aspect ratio, taper ratio, tip chord, root chord, mean aerodynamic chord, span, twist angle, sweep angle, dihedral angle and incidence angle.

The effect of these variables has been documented intensively in past literature. A very extensive overview is given in "Aircraft Design. A Systems Engineering Approach" by M. H. Sadraey [15]. The book provides a method for choosing these values analytically as well as choosing them based on the experience of past designs. As the layout of the UAV in question does not completely overlap with previous categories, a different approach is selected.

Lifting-line Theory

To calculate the optimum value for the variables discussed in subsection 7.3.3, an aerodynamic technique is required that calculates the resulting lift and drag forces as well as the pitching moment. In the recent past, a variety of tools and software-based numerical methods have been developed. These tools include: Computational Fluid Dynamics based solutions using Navier–Stokes equations; the Vortex Lattice Method, and other methods. The application of such tools would be unnecessary and time extensive at this phase of designing. Therefore, a simpler method, the lifting-line theory, is introduced.

This technique was initially introduced by Ludwig Prandtl in 1918. As this method is linear theory, it is only applied in the linear regions of the non-dimensionalised properties, namely between -5 and +5 degrees. Furthermore, limitations include swept wing, and low aspect ratio wings. As displayed in Figure 7.1, results are validated using the Vortex Lattice Method in XFLR5. This process is then further explained in Section 7.7. The method used for these tasks was derived from "Fundamentals of Aerodynamics" [16] by Anderson. The steps to use this method are the following:

1. The semi wingspan is cut into N+1 number of segments. The spacing of these segments is non-uniform, where the segments closer to the wingtip are shorter. Literature [16] suggests using a N+1 of at least 100. Note, each segment has its own geometry.
2. For a selected alpha, the elliptical lift distribution is assumed, corrected later, and gives: $\Gamma_1, ..., \Gamma_{N+1}$.
3. Using the assumed distribution, the induced angle of attack is calculated for each section:

$$\alpha_i(y_n) = \frac{1}{4\pi V_\infty} \int_{-b/2}^{b/2} \frac{(d\Gamma/dy)dy}{y_n - y} \tag{7.5}$$

   With which Simpson's rule becomes:

$$\alpha_i(y_n) = \frac{1}{4\pi V_\infty} \frac{\Delta y}{3} \sum_{j=2,4,6}^{k} \frac{(d\Gamma/dy)_{j-1}}{(y_n - y_{j-1})} + 4\frac{(d\Gamma/dy)_j}{y_n - y_j} + \frac{(d\Gamma/dy)_{j+1}}{y_n - y_{j+1}} \tag{7.6}$$

   The integral is evaluated numerically.
4. The effective angle of attack at each section is calculated using:

$$\alpha_{\text{eff}}(y_n) = \alpha - \alpha_i(y_n) \tag{7.7}$$

5. Where the distribution of effective angle of attack is calculated and the sectional lift coefficients are obtained using the lift curve slope:

$$c_{l-n} = (0.000136\alpha_{eff}) + 0.00832 \tag{7.8}$$

6. Using the newly calculated sectional lift coefficients, a new circulation distribution can be calculated using the Kutta-Joukowski theorem and the definition of the lift coefficient:

$$L'(y_n) = \rho_\infty V_\infty \Gamma(y_n) = \frac{1}{2}\rho_\infty V_\infty^2 c_n (c_l)_n \quad (7.9) \qquad \Gamma(y_n) = \frac{1}{2} V_\infty c_n (c_l)_n \quad (7.10)$$

7. The new Γ distribution is compared to the one calculated in step 3. If they do not match, a new input is generated using:

$$\Gamma_{\text{input}} = \Gamma_{\text{old}} + D(\Gamma_{\text{new}} - \Gamma_{\text{old}}) \quad (7.11)$$

   Here, D is the damping factor, which has been experimentally found to equal 0.05. Iterations are repeated until convergence.
8. From the converged Γ distribution the lift and drag coefficients are obtained using:

$$C_L = \frac{L}{q_\infty S} = \frac{2}{V_\infty S}\int_{-b/2}^{b/2} \Gamma(y)dy \quad (7.12) \qquad C_{D,i} = \frac{D_i}{q_\infty S} = \frac{2}{V_\infty S}\int_{-b/2}^{b/2} \Gamma(y)\alpha_i(y)dy \quad (7.13)$$

   The integration is again carried out using Simpson's rule. Information regarding the moment coefficient can be obtained using the local angle of attacks and the airfoil's non-dimensional relations.

7.3.4. Wing Planform Design Optimization

Peter Sharpade from MIT created an open-source Python library called AeroSandbox, where he combined the previously derived lifting-line theory in subsection 7.3.3 with CasADi, an open-source symbolic framework for numeric optimisation.

Setup

Using this Python library, it is possible to split the wing into geometrical sections and set the dimensions as variables. In this case, the wing's geometry is defined at two points: the root and the tip. Furthermore, the same airfoil shape is used throughout the wing section. The variables used are: root chord, tip chord, twist angle, tip x-location, tip y-location and angle of attack.

The upper bound of the root chord is limited by the fuselage length, while the minimum aspect ratio limits the lower bound. The lower bound of the tip chord is limited by manufacturability, while the minimum aspect ratio limits the upper bound. The tip's location in the X-direction is limited by geometrical constraints. While in the Y direction, it is limited by the system requirements. The airfoil data limited the upper bound of the angle of attack. The goal of the optimisation was to minimise the drag coefficient. Further constraints that were introduced for the optimisation include:

1. The lift generated has to equal the cruise weight.
2. The velocity for the lift calculation is set to the cruise speed.
3. The density is set to the cruise altitude density.
4. The number of panels is set to 100[16].

Wing Optimisation

As mentioned above, the aim of the optimisation is always to minimise drag. For restricting the variable's bounds multiple options were used, based on the current iteration. The Power and Propulsion group gave the MTOW for each iteration, which is 168 kilograms in the beginning. The results of each iteration are presented here.

1st Iteration For the first iteration, a low bound on the maximum angle of attack was used. By applying a lower angle of attack during cruise, the V-N diagram can be expended for a lower stall speed. The inputs and outputs are summarised in Table 7.2 and Table 7.3:

Furthermore, the results can be plotted with Python's Plotly library, which is able to plot data in 3D shown in Figure 7.5. The V-N diagram is presented in Figure 7.6. This diagram is constructed using the lifting-line theory, previously described in subsection 7.3.3 for several velocity values, and using the angle of attack range of -5 to +5 degrees. It was used as an output to determine the approximate stall speed, which is the speed at N=1, and for the structures group to see the maximum achievable N factor based on the intersection of the curves and the maximum speed. If needed, this N-value is limited artificially. The expected loads and maximum N are further explained in Chapter 8.

The result is a trapezoidal wing with a low aspect ratio, stemming from the low angle of attack, which requires a larger wing area. This shape's main advantage lays with its achievable high speed. Therefore, it is clearly not well suited for this use-case. The V-N diagram is plotted between -5 and +5 degrees of angle of attack in the airfoil's linear region. Which results in a stall speed that is even lower than shown on the graph.

Table 7.2: Wing geometry variables

Variable Name	Lower Bound	Upper Bound	Initial value
Root Chord	0.5	2	0.6
Tip Chord	0.1	2	0.6
Twist angle	0	3	1
Tip X-location	0	1.5	0.5
Tip Y-location	2.3	2.05	2.05
Angle of Attack	0	1	0.5

Table 7.3: Outputs of the first iteration

Name	Value	Unit
CL	0.3779	-
CD	0.1411	-
Cm	-0.2395	-
Lift	1657.3	N
Drag	61.9	N
Root Chord	1.193	m
Tip Chord	0.201	m
Twist	3	degree
Tip X-location	0.737	m
Tip Y-location	2.3	m
Alpha cruise	1	degree

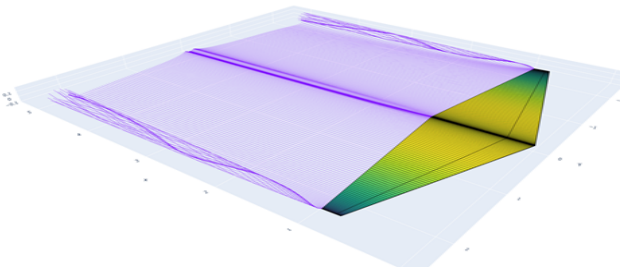

Figure 7.5: Visualisation first iteration

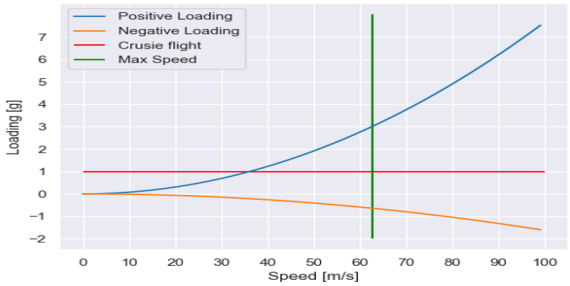

Figure 7.6: V-N diagram first iteration

2nd Iteration For the second iteration, the upper bound of the angle of attack has been increased to 4 in the hopes of providing lower drag and a more fitting shape to achieve a lower required wing area. The inputs are summarised in Table 7.4, and the outputs in Table 7.5. The outputs are then visualised in Figure 7.7, and the V-N diagram is shown in Figure 7.8. In this case, the results are much better fitted for the use-case. The drag is decreased by close to 35 percent. Negative consequences can be found for the Cm value which has decreased by a large margin. The other obvious downside is the decrease in the flight envelope.

Figure 7.8 again shows the bounds between -5 and +5 degrees angle of attack. For this wing planform, the stall velocity is calculated for an angle of attack of 15 degrees. This is done by using the output of the optimisation as the input for the numerical lifting-line theory calculation described previously as a linearisation of the non-dimensional curves near 15 degrees. This shows that the stall speed is around 35 metres per second, which is within the accepted range for the transition.

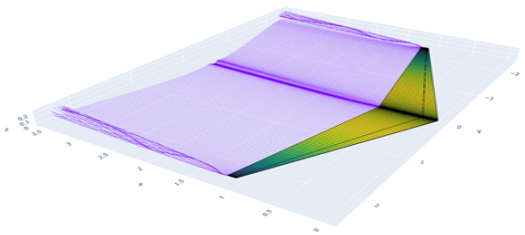

Figure 7.7: Visualisation of the second iteration

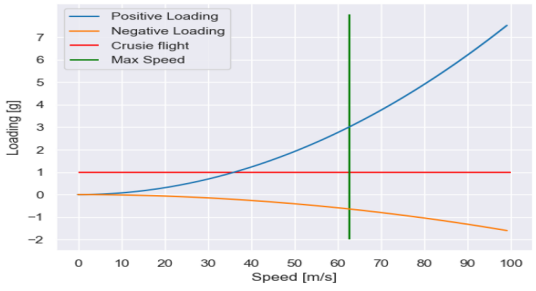

Figure 7.8: V-N diagram of the second iteration

Table 7.4: Wing geometry variables

Variable Name	Lower Bound	Upper Bound	Initial value
Root Chord	0.5	2	0.6
Tip Chord	0.1	2	0.6
Twist angle	0	3	1
Tip X-location	0	1.5	0.5
Tip Y-location	2.3	2.05	2.05
Angle of Attack	0	4	0.5

Table 7.5: Outputs of the second iteration

Name	Value	Unit
CL	0.643	-
CD	0.017	-
Cm	-0.77	-
Lift	1657.3	N
Drag	44.07	N
Root Chord	0.720	m
Tip Chord	0.1	m
Twist	2.5	degree
Tip X-location	1.086	m
Tip Y-location	2.3	m
Alpha cruise	4	degree

3rd Iteration The following iteration was completed to investigate the effects of increasing the span to the secondary boundary of 6.1 metres defined by OP-MI-PER-03. This is done with the hopes that using a larger span results in a lower required angle of attack during cruise. This increases the flight envelope. The second desire is to have Cm values closer to zero. The input table is presented in Table 7.6.

As shown in Figure 7.9, the obtained wing has a much lower sweep angle and taper ratio while having a similar drag, and a lower cruise angle of attack than the previous iteration. The lower sweep and taper are highly favourable for the wing group as the wing is rotatable. The lower Cm value is favourable for the Control group. The V-N diagram looks as shown in Figure 7.10.

The diagram is very similar to that of Figure 7.6 due to the same angle of attack conditions imposed during the cruise. Given the properties described above, this is the chosen design for the given constraints. The optimisation problem's output is shown in Table 7.7, again followed by its visualisation in Figure 7.9.

Table 7.6: Input variables for the third iteration

Variable Name	Lower Bound	Upper Bound	Initial value
Root Chord	0.5	2	0.6
Tip Chord	0.1	2	0.6
Twist angle	0	3	1
Tip X-location	0	1.5	0.5
Tip Y-location	2.3	2.65	2.05
Angle of Attack	0	1	0.5

Table 7.7: Outputs of the third iteration

Name	Value	Unit
CL	0.447	-
CD	0.012	-
Cm	-0.38	-
Lift	1657.3	N
Drag	46	N
Root Chord	0.702	m
Tip Chord	0.172	m
Twist	3	degree
Tip X-location	0.675	m
Tip Y-location	2.65	m
Alpha cruise	1	degree

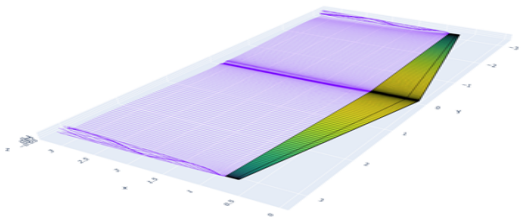

Figure 7.9: Visualisation of the third iteration

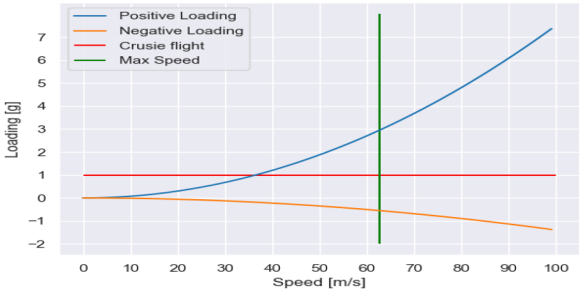

Figure 7.10: V-N diagram of the third iteration

4th Iteration Following iterations are required as the MTOW of the system changed after iterations performed by other departments. The new MTOW given by the Propulsion group is 345 kilograms. This, more than doubled weight is a challenge for the aerodynamic design. The surface area is to be increased substantially. For these iterations, only the larger dimensional limit of 6.1 metres is considered. The input table is shown in Table 7.8.

The solution, similar to the first iteration, has a trapezoidal wing shape. Before, this indicated a small surface area, compared to the generated lift. It could be solved by increasing the wingspan or increasing the angle of attack during the cruise, of which neither is possible. The reduction in lift-to-drag ratio is also noticeable compared to previous iterations. The V-N diagram is similar to the previous iteration where the angle of attack was 4 degrees. This is shown in Figure 7.12.

Table 7.8: Input variables for the forth iteration

Variable Name	Lower Bound	Upper Bound	Initial value
Root Chord	0.5	2	0.6
Tip Chord	0.1	2	0.6
Twist angle	0	3	1
Tip X-location	0	1.5	0.5
Tip Y-location	2.3	2.65	2.05
Angle of Attack	0	4	0.5

Table 7.9: Outputs of the third iteration

Name	Value	Unit
CL	0.580	-
CD	0.021	-
Cm	-0.42	-
Lift	3372.3	N
Drag	124.35	N
Root Chord	1.504	m
Tip Chord	0.1	m
Twist	3	degree
Tip X-location	1.185	m
Tip Y-location	2.65	m
Alpha cruise	4	degree

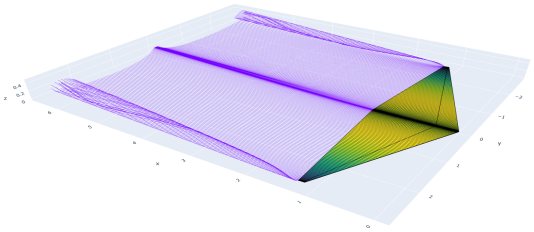

Figure 7.11: Visualisation of the fourth iteration

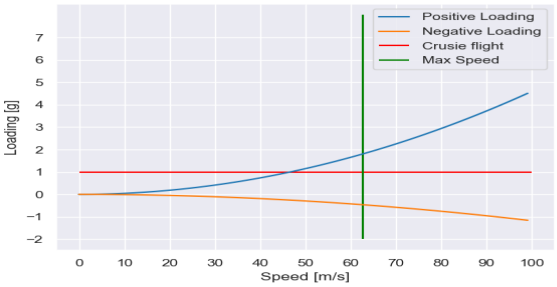

Figure 7.12: V-N diagram of the fourth iteration

5th Iteration The new iteration is completed by the request of the Structures group. Their requirement is that a single spar perpendicular to the fuselage should be able to pass from one wingtip to the wingtip on the other side. The spar is placed at 25 percent of the MAC. This is only possible if the wing design has no sweep. To tackle this issue, the inputs of the optimisation problem are changed such that the tip X-location is fixed at zero, and the taper ratio is set to 1. With these changes, the input table is presented in Table 7.10. The results obtained and their visualisation are presented in Table 7.11 and Figure 7.13 respectively.

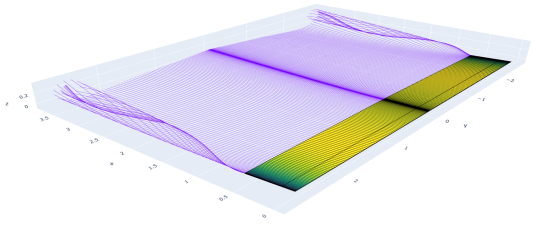

Figure 7.13: Visualisation of the fifth iteration

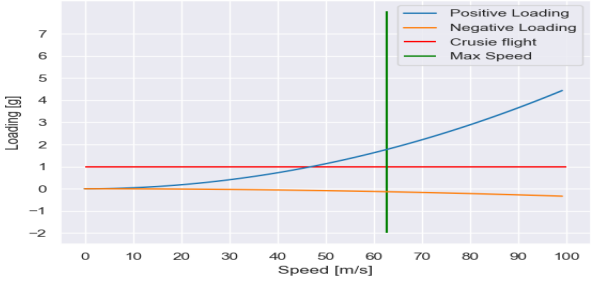

Figure 7.14: V-N diagram of the fifth iteration

Table 7.10: Input variables for the fifth iteration

Variable Name	Lower Bound	Upper Bound	Initial value
Root Chord	0.5	2	0.6
Tip Chord	-	-	Root Chord
Twist angle	0	3	1
Tip X-location	-	-	0
Tip Y-location	2.3	2.65	2.05
Angle of Attack	0	4	0.5

Table 7.11: Outputs of the fifth iteration

Name	Value	Unit
CL	0.739	-
CD	0.0324	-
Cm	-0.185	-
Lift	3372.3	N
Drag	148.68	N
Root Chord	0.631	m
Tip Chord	0.631	m
Twist	3	degree
Tip X-location	0	m
Tip Y-location	2.65	m
Alpha cruise	4	degree

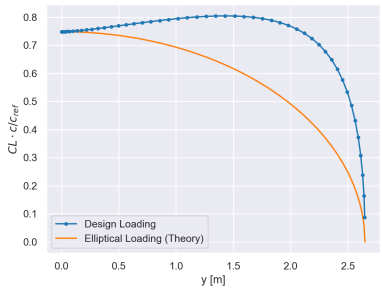

Figure 7.15: Loading diagram of the fifth iteration

The Cessna style wing's main disadvantage is that the loading distribution is not close to elliptical, as shown in figure Figure 7.15. This results in a higher induced drag. Compared to the previous iteration, the drag increase is 17 per cent, which is high compared to the previous iteration. However, it is only 6 per cent compared to the vehicle's total drag, as explained in the following section. The V-N diagram shown in Figure 7.14 is similar to the previous case since the alpha in cruise has not changed. As explained for the second iteration, the stall speed can be estimated using an angle of attack of 15 degrees. The non-dimensional curves are linearised near 15 degrees, which show a stall speed of 33.6 metres per second.

7.3.5. Wing Optimisation Results

After the iteration process is completed, the final design is presented in this subsection. The wing design has the properties summarised in Table 7.12.

Table 7.12: Designed wing planform variables

Name	Value	Unit
Wing Area	3.34	m^2
Aspect Ratio	8.4	
Taper Ratio	1	-
Tip Chord	0.631	m
Root Chord	0.631	m
MAC	0.631	m
Span	5.3	m
Twist Angle	3	degrees
Sweep Angle	0	degrees
Dihedral Angle	0	degrees
Incidence Angle	Variable	degrees

7.4. Horizontal and Vertical Tail Design

The next logical [15] step after the design of the wing is the tail design. Many aspects regarding the tail design are similar to that of the wing design. The difference between the wing and the tail lifting surfaces is their function. While the wing's function is to generate the maximum amount of lift, the tail is present to provide trim, stability and control. The horizontal tail's primary function is longitudinal moment balance and control. The vertical tail's primary function is to provide lateral stability and yaw control.

The variables for which values are to be obtained are the following, for both the horizontal and the vertical tail: planform area, tail arm, airfoil section, aspect ratio, taper ratio, tip chord, root chord, mean aerodynamic chord, span, sweep angle, dihedral angle, and incidence.

7.4.1. Horizontal Tail Design Approach

To design the horizontal tail, the approach presented by the book of "Aircraft Design" [15] is chosen. The steps to take are the following:

1. Select the horizontal tail location
2. Select the horizontal tail volume coefficient
3. Determine the optimum tail arm
4. Determine planform area
5. Select the right airfoil
6. Determine the sweep and dihedral angles
7. Determine the aspect and taper ratio
8. Calculate the setting angle

Steps in between 1-3 are determined by the Control group, which is expanded upon in subsection 9.5.1. The inputs are the following:

Table 7.13: Horizontal tail calculation input

Name	Value	Unit
Tail arm	2.5	m
Tail lift coefficient	-0.154	-
Volume ratio	0.438	-
Horizontal Tail Area	0.375	m^2

To determine other variables, compared to the wing design, a more analytical approach is taken for the design. Each variable is analysed, and a decision is made on its value. The previously described lifting-line theory is used to verify the results.

7.4.2. Horizontal Tail Design

Airfoil Selection A horizontal tail is a lifting surface, similar to the wing, and requires a similar airfoil section. The airfoil cross-section should be able to generate the required lift with minimum drag and minimum pitching moment. Since the aircraft's centre of gravity could move with different missions, the airfoil section must be able to create both positive and negative lift, therefore a symmetric airfoil is recommended.

For the tail to be beyond the compressibility effect, the tail lift coefficient is determined to be less than the wing lift coefficient. The flow Mach number at the tail must be less than the flow Mach number at the wing to ensure this requirement. Therefore, selecting a horizontal tail airfoil section to be thinner than the wing section is required. The selected airfoil for the wing is the NACA 643-418, therefore a section below 18 per cent thickness-to-chord has to be selected.

The selected aerofoil is the NACA 0010, selected from the recommended airfoils for general aviation aircraft in [15]. This airfoil has a lift coefficient curve of 0.1046 α + 0.00644 and a drag coefficient curve of 0.0001116 α^2 + 0.006253.

Parameter Design The tail incidence/setting angle's primary requirement is to nullify the vehicle's pitching moment about the centre of gravity during cruise. Using the lift coefficient curve, the incidence angle is set at 3.2 degrees.

Most of the tail aspect ratio effects are very similar to those related to the wing, but on a smaller scale due to the decreased amount of lift force generated. Generally, as the tail's aspect ratio is increased, the tail's lift curve slope steepness is increased as well. Furthermore, an elliptical lift distribution is not required for the tail, and a smaller aspect ratio is suggested, which decreases the structural weight when the bending moments are generated by the elevator. As a general rule of thumb the aspect ratio of the horizontal tail can be determined using:

$$AR_h = \frac{2}{3} AR_w \tag{7.14}$$

As the wing's aspect ratio is 8.4, the aspect ratio of the horizontal tail should be around 5.6. This is decreased to a lower value of 2.7 to mitigate the effects of the propellers, further explained in Section 7.6.

Since the elliptical lift distribution is not a requirement for the tail, the main motivation behind the value for the tail taper ratio is to lower the tail weight. The tail taper ratio is typically between 0.7 and 1 for GA aircraft, and between 0.4 and 0.7 for transport aircraft. Due to the layout of the aircraft, a taper ratio of 0.5 is selected.

The value of the horizontal tail sweep and its dihedral angle is often the same as the wing's sweep and dihedral angle. Therefore, no sweep nor dihedral is selected for the design. The summary of the horizontal tail properties are the following:

Table 7.14: Horizontal tail properties

Name	Value	Unit	Name	Value	Unit
Planform area	0.375	m^2	Mean aerodynamic chord	0.389	m
Tail arm	2.5	m	Span	1	m
Airfoil section	NACA 001	-	Sweep angle	0	°
Aspect ratio	2.7	-	Dihedral angle	0	°
Taper ratio	0.5	-	Tail installation	Conventional	-
Tip chord	0.25	m	Incidence	3.2	°
Root chord	0.5	m			

7.4.3. Vertical Tail Design Approach

Similarly to the horizontal design approach, the vertical design approach follows an analytical approach. This approach is validated using lifting-line theory. Very similarly the design steps that are taken are:

1. Select the vertical tail location
2. Select the vertical tail volume coefficient
3. Determine the optimum tail arm
4. Determine planform area
5. Select the right airfoil
6. Determine the sweep angle
7. Determine the aspect and taper ratio

The location of the vertical tail is selected to coincide with the location of the horizontal tail. Furthermore, the tail coefficient is selected to be 0.06 based on statistics. From the volume coefficient, the area can be calculated as 0.212 m^2.

7.4.4. Vertical Tail Design

Airfoil Selection The vertical tail airfoil section is responsible for the generation of the vertical tail's lift. The airfoil must result in the required lift coefficient with a minimum drag coefficient. To ensure symmetry of the aircraft, the vertical airfoil section must be symmetric. In general aviation, similar airfoils are used, as

for the horizontal tail, as the requirements are similar. In this project, the same NACA 0010 is chosen as for the horizontal tail.

Parameter Design If the engines, wing, horizontal tail, and fuselage are symmetric, the vertical tail is not required to produce any lift for maintaining directional trim in normal flight conditions. For this reason, the vertical tail incidence must initially be zero.

The vertical tail's aspect ratio affects multiple parameters: the height of the system, structural requirements, and stability properties. The literature suggests an initial value between 1 and 2. In this case, 1.3 is selected because it provides similar dimensions as the horizontal tail.

A large taper ratio negatively affects the stability of the aircraft. At the same time, a small taper ratio increases the complexity of the tail. To balance the up- and downsides, a taper ratio of 0.5 is selected.

A sweep angle for the vertical tail is highly beneficial for T-tail configurations. For a traditional inverted T shape, benefits are limited. Therefore, no sweep is assigned. Due to the required symmetry, a dihedral angle is not possible. All variables can be calculated using Equation 7.15 and Equation 7.16:

$$\mathrm{AR_v} = \frac{b_\mathrm{v}}{\bar{C}_\mathrm{v}} = \frac{b_\mathrm{v}^2}{S_\mathrm{v}} \qquad \lambda_\mathrm{v} = \frac{C_{\mathrm{v_{tip}}}}{C_{\mathrm{v_{root}}}} \tag{7.15}$$

$$\bar{C}_\mathrm{v} = \frac{2}{3} C_{\mathrm{v_{root}}} \left(\frac{1 + \lambda_\mathrm{v} + \lambda_\mathrm{v}^2}{1 + \lambda_\mathrm{v}} \right) \qquad S_\mathrm{v} = b_\mathrm{v} \cdot \bar{C}_\mathrm{v} \tag{7.16}$$

A summary of the selected variables is presented in the table below:

Table 7.15: Selected variables for the vertical tail

Name	Value	Unit	Name	Value	Unit
Planform area	0.212	m2	Root chord	0.5	m
Tail arm	2.5	m	Mean aerodynamic chord	0.4	m
Airfoil section	NACA 001	-	Span	0.5	m
Aspect ratio	1.3	-	Sweep angle	0	°
Taper ratio	0.5	-	Dihedral angle	0	°
Tip chord	0.25	m	Incidence	0	°

7.5. Fuselage Design

The fuselage function is to provide a secure attachment for the payload to be carried and the components of the UAV. The aerodynamic fuselage design aims to minimise the drag created by this component.

The drag force created by the fuselage can be calculated with the general drag equation:

$$D_F = C_{DF} \cdot \frac{1}{2} \rho V^2 S_F \tag{7.17}$$

Where D_F is the drag force created by the fuselage, the C_{DF} is the non-dimensional drag coefficient, and S_F is the cross-sectional area of the fuselage. There are two options to minimise the drag force created: Minimising the drag coefficient or minimising the cross-sectional area.

Since the cross-sectional area can only be changed by rearranging the location of the internal components, it affects the centre of gravity of the UAV. This on its turn affects the general stability derivatives. Therefore, a constraint was given to the Control team: Arrange the internal components such that it minimises the cross-sectional area. The output from the control team is the following:

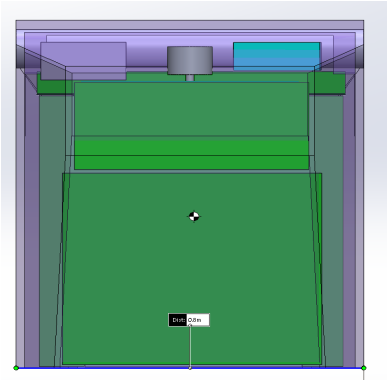

Figure 7.16: Fuselage front view

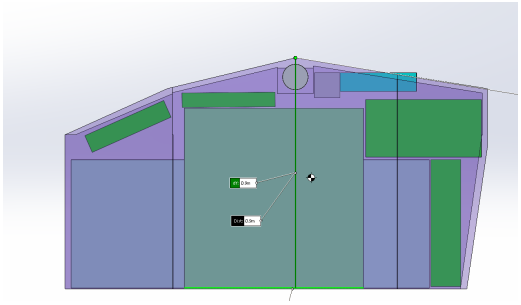

Figure 7.17: Fuselage side view

This shows that the fuselage's width is 0.8 m, and the height is 0.9 m, resulting in an area of 0.72 m^2. Obtainable drag coefficients are bases on statistics of different shapes summarised in Table 7.16.

Table 7.16: Drag coefficient of different shapes

Type of Object	**Drag Coefficient**	**Type of Object**	**Drag Coefficient**
Streamlined body	0.04	Saloon Car, stepped rear	0.4-0.5
Long stream-lined body	0.1	Cube	0.8
Airplane wing, stalled	0.15	Thin Disk	1.1
Modern car like a Tesla model 3 or model Y	0.23	Solid Hemisphere flow normal to flat side	1.17
Sports car, sloping rear	0.2 - 0.3	Squared flat plate at 90 deg	1.17
Motorcycle and rider	1.8	Rectangular box	2.1

Based on this table, the assumption was made that a drag coefficient of 0.2 is achievable for the UAV's fuselage. This is based on Equation 7.17 results in the drag force of 196 Newtons for only the fuselage. This value is about 1.5 times the value of the drag of the wing, which shows that the optimisation of the fuselage shape is of extreme importance.

Optimisation could be carried out using computational fluid dynamics software for the nosecone and to streamline the outside of the body. These methods are out of scope for this report, as team members do not have the required expertise to carry out validated calculations with these solutions. Resulting in an approximate nosecone that has been created for visualisation purposes, shown in Figure 7.18.

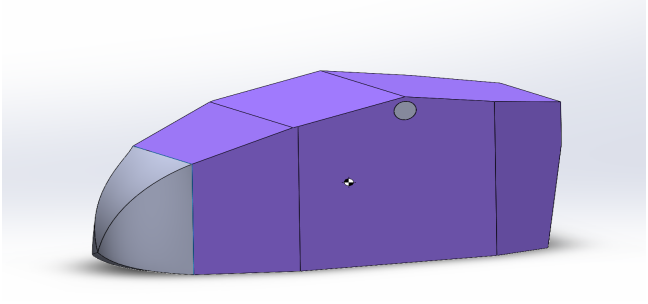

Figure 7.18: Visualisation of the nosecone

7.6. Effects of the Propellers on Aerodynamics

An element that was simplified in the aerodynamic model is the propellers' effect on the wing design. Since the UAV's propellers were optimised for vertical take-off, the propellers' size is much larger than a conventional propeller-powered aircraft. The size of the propellers in this design is close to the size of the wing.

The effect of propellers in front of the wing has been studied by papers such as [17], [18], [19], [20]. These papers show two things: the propellers have a positive effect on the wing's aerodynamic properties and

harm the tail's control capabilities during cruise flight. Positive effects on the wing include a delayed stall, which is highly useful during the transition, and an increase in wing lift. This shows that if the calculations do not take these effects into account, they are more conservative. The negative effect on the tail design's control capability was considered, where a lower volume ratio was selected for the tail. This provided a higher level of control, on the expense of stability.

The decision was made to ignore these effects during the aerodynamic design, since the analysed literature has not shown a simple analytical implementation of these effects at the propeller scale of this design. Furthermore, the conservative approach, while likely to increases the drag over the wings, has shown that the fuselage has a larger effect on the total drag than to the wing.

7.7. Verification and Validation

This section includes the verification and validation procedures used for the design of different components. Some of the methods include the use of alternative methods for calculations, while others use available data from literature. As the fuselage estimation is based on statistics, there is no clear way to validate the results without the use of experiments or CFD simulations. That is why it was ommited from this section.

7.7.1. Wing Design Verification

The main tools used for the calculations related to the wing design are Python and Matlab scripts which adopt the lifting-line theory described in subsection 7.3.3. For the first calculations, a self-developed program in MATLAB was used. It was validated using hand calculations based on the same method. The method was later extended using Peter Sharpade's Python package, which implemented an optimisation with CasADi. The results of this package were verified using the self-developed Matlab package, providing the same outputs from the same inputs.

The optimisation results for the parameters were compared to the verification method, showing that the direction of the optimisation indeed provides the expected results.

7.7.2. Horizontal and Vertical Tail Design Verification

As the calculations were based on analytical methods, integration tests were carried out which confirmed that given inputs based on existing data, the provided output is in line with the provided output data. Furthermore, unit tests were carried out confirming that individual components provide the expected outputs given the inputs.

7.7.3. Wing Design Validation

To validate the results given by the lifting-line theory, an alternative method is used. This method is the Vortex Lattice Method, used by XFLR5. The wing geometry specified in Table 7.12 is used to generate the same wing planform. After applying the same simulation conditions, the results of the two methods are compared:

Table 7.17: Comparison of methods

Name	LLT	VLM
Lift Coefficient	0.739	0.702
Drag Coefficient	0.0324	0.03

Results show a 5 percent difference in the lift coefficient and an 8 percent difference in the drag coefficient. Other than the application of different methods, these differences are also related to the fact that XFLR5 has access to more accurate airfoil data. The presented accuracy of the data is deemed sufficient for a validated result.

7.7.4. Horizontal and Vertical Tail Design Verification

To validate the results given by the analytical methods and related calculations, the lifting-line theory described in subsection 7.3.3 is used with the designed horizontal tail geometry. The visualisation of the horizontal tail is shown:

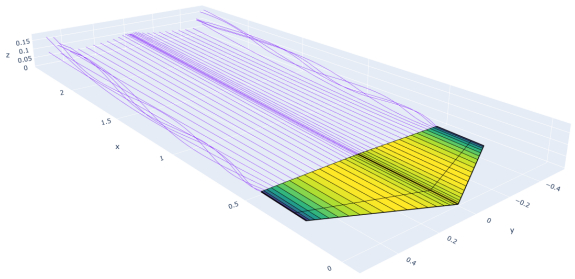

Figure 7.19: Visualisation of the horizontal tail

The required lift force of the wing was defined by the control group to be 112.88 Newtons based on the stability derivation. The lift force given by the numerical method is 102.03 Newtons, which is deemed acceptable for the validation of the results.

To validate the design of the vertical tail, the control derivatives from XFLR5 are used, which are further described in Chapter 9.

7.8. Sustainability Approach

A sustainable aerodynamic design can be achieved in two ways: by minimising drag, and by minimising the complexity of the design. A low drag design has multiple advantages from a sustainability point of view. The main advantage is that with the lower drag force, the power required decreases as well. This directly decreases the UAV's footprint, and indirectly it creates a snowball effect. Multiple components can be down-sized, which further reduces the footprint of the system. Another advantage of a lower drag is that it reduces the noise generated by the vehicle. As the UAV's flight altitude is not very high, the lower noise emission, the better. Decreasing the complexity of the aerodynamic elements decreases the costs related to production considerably. Aerodynamic elements that can be produced with simple methods on a large scale have a large effect on these costs. Furthermore, less complex elements require less research, which further decreases the development process's costs and the resources required.

7.9. Future Recommendations

Future recommendations for the aerodynamic design include: adding components that are too complex to model and components that would require more resources than available. These are out of the scope of the undergraduate competition. As discussed in Section 7.6, the effect of the large propellers on the aerodynamic performance of the UAV should be investigated further. Possible solutions are: developing a numerical model, which can be solved with the CFD method, or performing wind-tunnel tests.

For the wing design, further iterations could be completed with the collaboration of the Structures team, improving the design's efficiency. Further considerations could include the addition of wing-tips in order to reduce the induced drag. Further iterations can be carried out with the addition of CFD packages and experimental wind-tunnel tests. The main concern regarding the current design is the use of a positive twist angle. This parameter allows the wing to have a much higher aspect ratio, but could cause issues regarding manoeuvrability during stall. Some preliminary calculations on the problem show that with the current configuration, an elliptical lift distribution is achievable with a negative twist of 3 degrees. That would require half the aspect ratio to provide sufficient lift, which would further increase the weight making the MTOW diverge. The effects of this parameter should be considered together with the effects of the propeller. In the case where the MTOW of the UAV can be reduced, the twist can be also lowered.

The parametrisation of the nosecone design, with the help of a CFD package, can be optimised to achieve the suggested drag coefficient.

Finally, a sensitivity analysis should be carried out with the main focus of the wing design. Preliminary results show that a small change of input parameters for the optimisation could have a small effect on the output of the method. These changes should be quantified and verified in the future.

8
Structures and Materials

The structural design of the vehicle is a fundamental feature in the aerospace industry as the failure of a single path structural component can result in a crash of the vehicle. An overly designed structure will cause performance losses, resulting in higher overall costs. In addition, manufacturing processes, and sustainability considerations are dependant on the material selection and other design choices. Thus, the scope of the structural design is to find the optimal structural mass, whilst being able to withstand the loads and stresses the vehicle will be experiencing in its operation. The structure of the chapter is as follows: Section 8.1 summarises the work that has been done during the Midterm and Section 8.2 presents the functional analysis of the structures subsystem, and the requirements which drive the scope of the design. Then Section 8.3 presents the overall design approach for the design of the structure regarding namely: wing, fuselage, and tail. Section 8.4 presents the formulas and results that were used in the design, and Section 8.5 presents the verification & validation procedures for the structural design. Finally, Section 8.6 presents the sustainability analysis of this section, and Section 8.7 presents future work and recommendations if the project were to continue.

8.1. Design Overview

As previously mentioned, the structural design of the vehicle is critical as the output heavily affects numerous subsystems. In addition, the inputs of the structural design are heavily dependant on other subsystems' outputs. With this in mind, the focus during the Midterm design was conducting the trade-off between the different vehicle configurations at a much broader scope. Meaning that the structural design of the vehicle were not analysed in-depth, and mainly analysed in terms of its overall configurations i.e: comparing the structural design and performance of a blended wing-body and a fixed-wing compound.

8.2. Requirements and Functional Analysis

The functional analysis is conducted in order to have a general overview of the scope of the subsystem design. For the structures & materials subsystem, this can be split into three main groups: wing, fuselage, and tail.

Functional Analysis: Wing - The wing structure will be designed such that the wing box can withstand any of the loads it will experience during operation, as well as accounting for the ultimate load factor.

Functional Analysis: Fuselage - The fuselage structure will be designed such that all the loads inside the fuselage (i.e: payload, batteries) can be transferred to the main wing spar. In addition to this, the payload bay will also be designed, with the autonomous payload handling system attached.

Functional Analysis: Tail - The tail structure will be designed mainly in regards to the tail spar, which connects the tail to the rest of the fuselage. The tail spar will be designed such that it can withstand the bending due to the horizontal and vertical tail, and the auxiliary motor. The inner structure of the horizontal and vertical can be examined in future iterations, as the majority of resources were spent on the wing design.

As previously mentioned in Section 3.5, the basis of the design process depends on the requirements set for the final design, derived from various stakeholders. The following requirements are the key/driving requirements set for the structures subsystem.

Table 8.1: Overview of requirements

ID	Requirement	Type
OP-CER-UAS-01	The limits for mass and centre of gravity that provide for the safe operation of the UA shall be determined.	CS-UAS.2100 JARUS

Table 8.1: Overview of requirements

ID	Requirement	Type
OP-CER-UAS-25	The MTOM of the UA shall not exceed 3715 kg.	CS-UAS.2000 JARUS
OP-MI-PER-01	The system shall be able to carry at most 50 kg payload for the LDM and LM	RFP
OP-MI-PER-03	The UA planform shall be less than or equal to 6.1 m x 6.1 m.	RFP
OP-MI-PER-05	The UA shall be able to carry a payload with dimensions of 70cmx70cmx70cm	RFP
OP-MI-PER-06	The UA shall be able to carry a payload with dimensions of 140cmx50cmx50cm	RFP
FU-SYS-18	Equipment containing high-energy rotating parts shall be designed or installed such that, in the event they fail: they are safely contained, or they cannot damage other systems or subsystems	CS-UAS.2550 JARUS
FU-STR-01	The structural design envelope shall be determined, which describes the range and limits of UA design and operating parameters	CS-UAS.2200 JARUS
FU-STR-10	The structural internal and external design loads at all critical combinations of parameters, at and within the boundaries of the structural design envelope shall be determined	CS-UAS.2210 JARUS
FU-STR-12	The flight load conditions shall be determined, to ensure vibration, including air resonance, and buffeting does not result in structural damage up to the maximum design speed.	CS-UAS.2215 JARUS
FU-STR-24	The limit loads, which are equal to the structural design loads shall be determined.	CS-UAS.2230 JARUS
FU-STR-25	The ultimate loads, which are equal to the limit loads multiplied by a 1.5 factor of safety shall be determined.	CS-UAS.2230 JARUS
FU-STR-48	Each part of the UA, shall have adequate provisions for ventilation and drainage.	CS-UAS.2255 JARUS
FU-STR-49	For each part that requires maintenance, preventive maintenance, or servicing, a means into the UA design to allow such actions to be accomplished shall be incorporated.	CS-UAS.2255 JARUS
FU-STR-50	There shall be enough clearance between movable or rotating parts (such as propellers or rotor blades) and other parts of the structure to prevent the movable or rotating parts from striking any part of the structure during any operating condition including emergency recovery.	CS-UAS.2255 JARUS
SUS-SOC-DaC-6	There shall be a positive means to keep the landing devices in the landing position.	CS-UAS.2305 JARUS
SUS-SOC-DaC-7	There shall be an alternative means available to bring the landing devices in the landing position when a nondeployed system position would be a hazard	CS-UAS.2305 JARUS

8.3. Design Approach

In order to design for the structural elements of the UAV, a clear and concise approach to the design has to be set. Constructing a concice methodology when designing a part can be very beneficial and could mean the difference between system that works, and one that does not. The general design approaches for the three different structural elements will be presented, before diving into the detailed design methodology in Section 8.4.

An important aspect to take into account is the loading condition which the following analysis are based upon. From Chapter 7, and more specifically , Figure 7.14, it was found that the critical load factor would be $n = 2$. Now one must identify which flight condition this load factor needs to be applied to. When looking

at hover, a thrust force with a $n = 2$ loading would never be achieved as the engines cannot provide this force. The question remains whether transition or cruise flight is the most critical, which depends on the combination of the vertical component of the thrust force with the related lift force compared to pure lift in cruise. When comparing these two conditions it is clear that cruise is the most critical, which is further explained in subsection 8.4.1. The flight envelope is plotted based on the different limiting speeds and the maximum load factors described in Chapter 7 and shown in Figure 8.1, where n_{max} and n_{min} are the maximum and minimum load factors, V_{stall} the load factor at $C_{L_{max}}$, V_D the dive speed and V_C the cruise speed. The gust load factors have not been plotted as they do not put a higher limit to the maximum load factor.

Aluminium alloys are widely used in the aerospace industry as they have great properties regarding weight and strength. The material used for the spar, ribs, truss and stiffeners will be AL7075 T6, as for the skin, AL2024 T3 will be used [1]. Using aluminium is beneficial for the harsh environment in which Healios will operate. Aluminium alloys are easy to work with, reusable and are by far the most produced base metals worldwide [2]. This allows for cheap and fast production which are more necessary in these uncertain environments. Finally, from a sustainability point of view aluminium alloys have a high recycle fraction, and lower embodied footprint when compared with other material options such as CFRP as further explained in Section 14.2. For the payload attachment mechanism, titanium is used due to its strong and lightweight properties (see subsection 8.4.4).

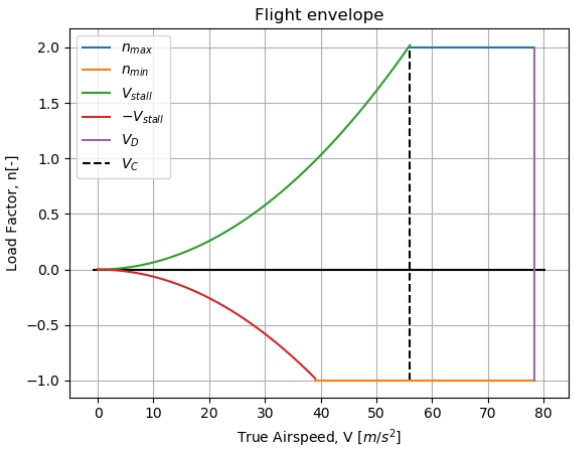

Figure 8.1: Manoeuvre flight envelope

8.3.1. Wing Design

The initial inputs to the wing design were derived from Chapter 7, where the wing planform, and the aerodynamic parameters were outputted. The main critical feature that had to be taken into account for the structural design configuration was the fact that the wing should be able to rotate in order to allow for VTOL capabilities. In order to allow for this, it was decided that the main spar going through the wing would rotate from the torque exerted by an on-board actuator motor. From this, a design parameter was fixed; namely, the that the wing planform would be uniform, have no taper ratio, and no sweep. As the only way of rotating the wing with a cylindrical spar going through would mean the main spar would also need to be completely uniform, which would also reduce the complexity relative to if it were to be swept and tapered.

The main spar was chosen to be going through the aerodynamic centre of the wing at each cross-section due to multiple reasons. Firstly; the a.c is the region with the highest thickness-to-chord ratio, allowing for a larger diameter. However, as the spar is located on the a.c of the wing; the resultant aerodynamic forces could create a torque on the main spar, which is also analysed in Figure 8.4.1.

Once the design parameter regarding the main spar was fixed, the loads other than the lift had to be computed. These were related to the thrust provided by the engine, the engine weight and the wing weight itself. These loads were taken based on the most critical load case, which has been derived in 7.3.4. From these external loads, internal loads and moments could be calculated at each cross-section. Based on these internal forces, moments, and the initial wing cross-section, a stress analysis could be performed comprising of the bending, shear and buckling stresses which the wing would encounter. Note that the current analysis only focuses on the cruise configuration, as it was found to be the limiting case.

By analysing the different stresses the wing would experience, the cross-sectional elements inside the wingbox could also be designed. Firstly, through the bending analysis, the minimum spar thickness can be obtained, then through the buckling analysis, the skin thickness, and if necessary any stiffener dimensions

[1] https://www.experimentalaircraft.info/articles/aircraft-aluminum.php [visited on 25/01/2020]

[2] https://www.visualcapitalist.com/all-the-worlds-metals-and-minerals-in-one-visualization/ [visited on 25/01/2020]

could be obtained. Finally once the cross section of the wing box was defined, through the shear/torsion analysis, skin thickness and the rib spacing could be obtained. Note that both the shear and buckling analysis defines the minimum skin thickness, and the larger value is chosen, as it will be the limiting case.

When final values were set for the aforementioned variables, the wing design was implemented into SolidWorks. In order to validate the results, the design was subjected to a FEM analysis using Ansys Workbench. This FEM analysis allowed for a comparison with the values retrieved from the analytical model. Once the validation had been performed, the wing model was imported to the complete UAV design made in SolidWorks.

8.3.2. Fuselage Design

The fuselage is an integral component of the vehicle, as it must protect the payload, transfer loads, and house the necessary components while adding minimal drag and weight. The aim of this section is to provide the general approach and the scope of the fuselage design.

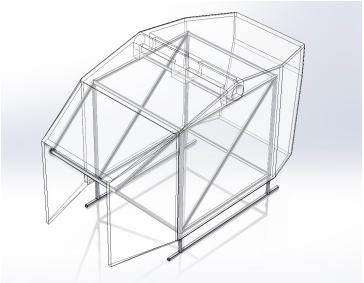

Figure 8.2: Fuselage Truss structure

The fuselage design can be split into two main principles, the design of the fuselage structure and the design of the payload attachment & handling system.

The structure of the fuselage shall be able to handle and transfer multiple loads from the payload, batteries, and avionics component weights to the wing and the tail. Two structural concepts have been devised to withstand and transfer the loads: a monocoque composite shell, and a truss structure with an outer aerodynamic shell. It has been decided to opt for the latter for multiple reasons, including lower part and manufacturing costs, simpler design, and easier maintainability. Despite it being heavier and less stiff than a monocoque shell, it is considered adequate for the purposes and scope of this project. This truss is manufactured simply by riveting or bolting the pipe sections together. The analysis of the truss design assumes the scenario of banking 30 degrees as it would be the most critical case. This is due to the fact that as can be seen from Figure 8.2, there is a horizontal truss member missing in order to accommodate for both payload sizes. Meaning, when banking, the vertical truss members will have no constraints in deflction, thus resulting in the most critical condition.

The analysis was conducted to find the minimum thickness of the rods, given a diameter of 4cm, and to have deflection no greater than 1[mm]. By analysing each truss member separately, one can also optimise the thickness required for each member, as they all experience different types of loads. This analysis is developed further in subsection 8.4.3.

Next, regarding the payload attachment structure, as previously analysed, the automation of the payload handling mechanism was a key requirement for the design of the vehicle. The main difficulty for designing such a system was the fact that the vehicle had to accommodate two different payload sizes as shown in Figure 8.4. The attachment of the payload to the vehicle was achieved through the use of four lead screws that would be attached to an actuator on each the sides of the payload bay to allow movement in and out of the payload and to accommodate for the difference in the width of the two payloads. An additional actuator would be required to allow the 4 screws to have vertical movement in order to allow the payload to be lowered once the vehicle has landed, this is visualised in Figure 8.3. The sizing of the 4 lead screws are developed further in Figure 8.4.4

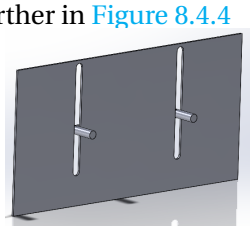

Figure 8.3: Payload attachment & lowering mechanism

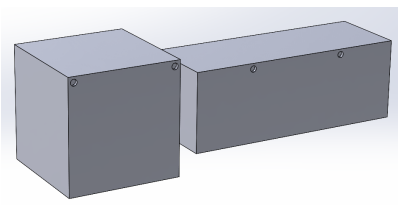

Figure 8.4: Payload attachment points for both sizes

8.3.3. Tail Design

The UAV needs to have a tail for both the VTOL and cruise configurations. For the VTOL, the tail needs to provide a reaction moment to counteract the moment generated by the thrust with respect to the centre of gravity, and to provide pitch authority. This is accomplished by the use of a third "auxiliary engine" located under the tail (see Figure 8.5). During cruise configuration, the tail needs to counteract the moments produced by the aerodynamic forces of the wing and fuselage in addition to providing pitch and yaw authority. Thus, the loads which the tail spar needs to accommodate for are the bending moment due to the auxiliary engine during hover/transition, and the bending moment generated by the maximum lift the horizontal tail can produce. The design of the tail spar will assume the most critical condition, which will be during cruise, as the maximum force which the horizontal tail can produce during cruise, obtained from Chapter 7 was calculated to be **453 [N]**, whilst the maximum thrust the auxiliary engine was calculated to be **150 [N]** obtained from Chapter 9.

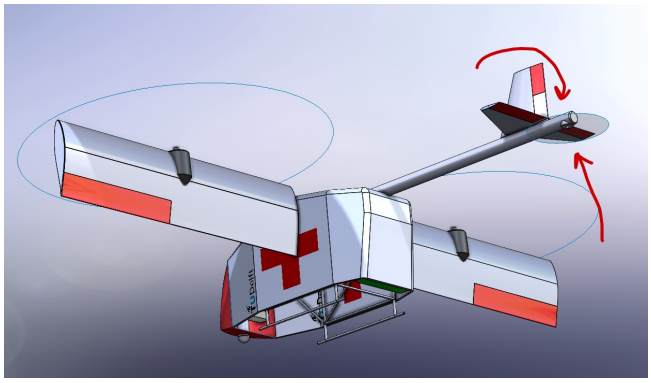

Figure 8.5: View of the auxiliary motor.

8.4. Design Methodology & Results

8.4.1. Wing Design

Rotation Mechanism The rotation of the wings is an essential feature of the design, which of course requires an adequate structure and mechanism to work. The idea is that both wing sides are connected by a spar which goes across the fuselage and is supported by three radial bearings (two on the fuselage edge and one in the centre line) and is rotated by means of a motor attached to a gear system. This allows for rotation but constrains forces in all directions. The attachment point of this rod to the wings is strategically positioned at the aerodynamic centre at the quarter-chord point to minimise the torque required for the wing's rotation. It was decided that a closed-loop high-torque electric stepper motor powerful enough to rotate the wing, engines, and propellers connected via a gear system to the wing rod was ideal for this application because it can provide precise rotation and send position feedback to the control system. Some data was found from other vehicles which also had wing-tilting mechanisms [3], and a list of a wide range of commercially-available motors was found to estimate the required mass. It was estimated that allocating a maximum of 21 kg for this motor and a gear transmission system was reasonable based on the available data.

Wingbox Design As mentioned previously the wing design has started using necessary outer wing dimensions and a specific airfoil selected by the aerodynamics department. The aerodynamic loads which the wing will encounter were also given and a load analysis was first performed with the previously stated $n = 2$ load factor on each force. To perform the analysis, some assumptions had to be made are stated along the design process. The loads analysed for the wing design are the most critical, following:

- **Lift:** The lift distribution along the wing will be considered as a uniformly distributed load. This is a valid assumption as the wing taper ratio is 1. This assumption is conservative as the maximum loads will not be underestimated and the internal moment will be slightly higher than in reality.
  Total Lift (per half span): 3372.3 N
- **Drag:** As with lift, the drag will be considered as being a uniformly distributed load along the span of the wing.
  Total Drag (per half span): 148.68 N
- **Weight:** The weight of the wing is mainly influenced by the weight of the spar and is also considered uniform along the span as the spar will span the entire wing and maintain its cross-sectional properties. Also, the weight of the engine is taken into account and will be identified as a point load at 1.4 m

[3] https://journals.sagepub.com/doi/pdf/10.1243/09544100JAERO666

from the root.
Wing Weight: 539.55 N, Engine Weight: 392.26 N

- **Thrust:** The forward force acting on the wing will be delivered by the main engines. These will also be analysed as point loads acting on the wing.
  Thrust (per engine): 392 N

The following free body diagrams show the load distributions on the wing in two planes:

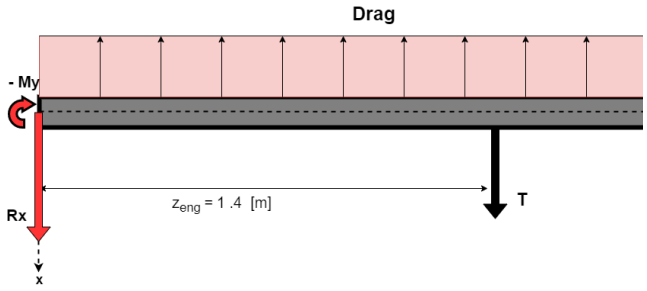

Figure 8.6: Wing free body diagram (x-z)

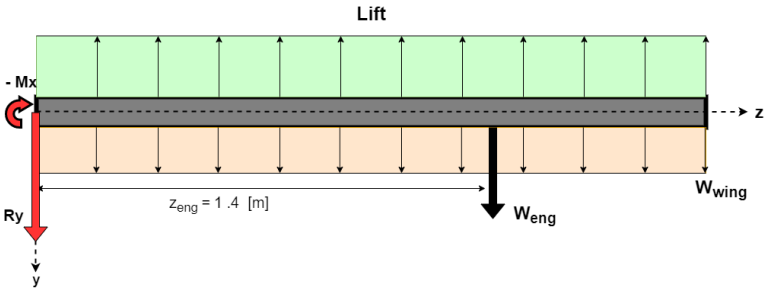

Figure 8.7: Wing free body diagram (x-z)

From the external load distribution, an analysis on the internal loads can be performed. The resulting forces and moments at the root of the wing have been computed with the following relations:

$$\begin{aligned} \sum F_x = 0 &\implies T - D_{tot} = -R_x \\ \sum F_y = 0 &\implies -L_{tot} + W_{wing} + W_{eng} = -R_y \end{aligned} \qquad \begin{aligned} \sum M_x = 0 &\implies (-L_{tot} + W_{wing}) \cdot \frac{b}{2} + W_{eng} \cdot \frac{b}{2} = M_{x,0} \\ \sum M_y = 0 &\implies -D_{tot} \cdot (\frac{b}{2}) + T \cdot \frac{b}{2} = M_{y,0} \end{aligned} \tag{8.1}$$

$R_{x,y}$ being the resultant forces at the root in both x and y direction respectively, $M_{x,y}$ the resultant moments at the root in both x and y direction respectively, T the engine thrust and $W_{wing,eng}$ the wing weight and engine weight respectively. From these, the internal shear and moment variation can be computed. The shear force in both x- and y-direction as well as the internal moments have been found and follow the relation shown in the following relations:

$$\begin{aligned} V_y(z) &= Lift(z) - W_{Wing}(z) - R_y - W_{eng}[z - \frac{b}{2}] \\ V_x(z) &= Drag(z) - R_x - T[z - \frac{b}{2}] \end{aligned} \qquad \begin{aligned} M_y(z) &= -M_{y,0} + R_x \cdot z - Drag(z) \cdot \frac{z}{2} + T[z - \frac{b}{2}] \\ M_x(z) &= Lift(z) \cdot \frac{z}{2} - M_{x,0} - W_{wing}(z) \cdot \frac{z}{2} - W_{eng}[z - \frac{b}{2}] \end{aligned} \tag{8.2}$$

When plotting these force and moment functions along the span of the wing (see Figure 8.9 and Figure 8.10), the points of maximum shear and moment can be found. Because of the assumptions made earlier, the maximum moments and forces will be found at the root of the wing. Several structural components have been analysed in order to achieve the most lightweight design possible while ensuring a safe UAV. Thus the design has been split into three main sections.

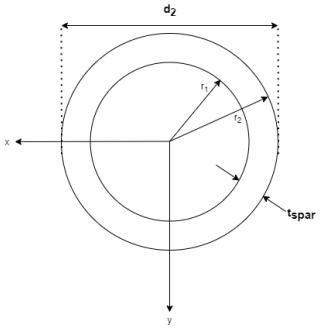

Figure 8.8: Spar cross section

Spar Design - Bending A design choice was made by setting a main circular spar at the aerodynamic centre of the wing. This would minimise the torque needed from the main actuator in order to rotate the wing and avoid high-stress concentrations near the root as a constant moment will be applied [16]. Conventional aircraft usually have a wing box spanning most of the wing which would take up most of the bending loads and axial loads [21]. Furthermore, it is assumed that at the location of the ribs, the shear force is transferred entirely

to the spar, which also has to withstand the torsional loads. In this case, the circular spar takes the role of the wing box.

The spar dimensions are first set by the available space within the wing. In Chapter 7 the airfoil needed is selected and a wing chord is set. From this and other wing shape parameters, the outer dimension of the spar cannot exceed 0.09$[m]$. The outer diameter remains fixed at the maximum possible diameter, which is also beneficial with regards to bending. The parameter to be found is t_{spar}, the thickness of the spar.

This parameter is dependent on the maximum normal stress that is found in the spar and is optimised for minimum weight without failing. Several failure modes are analysed such that a final thickness can be chosen, including the minimum spar thickness. An upper limit to the maximum allowed stress is set to $\frac{Y}{1.5}$ where Y is the yield strength of the material used, which for AL7075 is 503 MPa. All calculations have been performed using Python scripts.

- Bending stress is the first case to be analysed. For this analysis, the spar will be subject to all previously mentioned external loads and the maximum shear stress is found as a function of the beam thickness. The formula [22] used is:

$$\sigma_z = \frac{\left(M_x I_{yy} - M_y I_{xy}\right) y + \left(M_y I_{xx} - M_x I_{xy}\right) x}{I_{xx} I_{yy} - I_{xy}^2} \tag{8.3}$$

  Where σ_z is the normal stress at the given x, y location from the centroid. In this case, $I_{xy} = 0$ as the beam is assumed to be symmetric.
  The maximum bending moment is found at the root of the wing, and the maximum stress at the furthest distance from the neutral axis of the beam. With this value fixed, a minimum thickness for the beam can be computed. Several points along the cross-section have been plotted and the maximum stress value has been kept. When the UAV is subjected to a $2g$ loading, the minimum allowed thickness is $t_{min} = 1.3[mm]$.
- An assumption made during the design of the wing is that at each rib location, the shear loads will be transferred from the skin to the spar through the rib. This design choice follows from the fact the circular spar has great resistance to torsion as well as from the goal of minimising the skin thickness by having the loads taken up by the spar. So the maximum shear stress that the beam would encounter is analysed with the following formula:

$$\tau_{\max} = \frac{V_{max} \cdot Q}{I_{xx,yy} \cdot b} + \frac{T}{2 \cdot t_{spar} \cdot A_m} \tag{8.4}$$

  Where V_{max} is the maximum shear force, Q is the first moment of the cross-sectional area, I is the second moment of inertia about either axis (because of symmetry) and b is given by $b = 2 \cdot (r2 - r1)$ where r1 is the inner radius and r2 the outer radius. The second term on the right hand side is due to the contribution of the aerodynamic moment generated by the airfoil at the critical loading condition with T the torque, t_{spar} the spar thickness and A_m the enclosed area. This formula[4] analyses a pure shear scenario. A minimum thickness of 0.1$[mm]$ is required in order to have a stress value not exceeding the upper limit set before.
- The next constraint which sets a lower bound to the spar thickness is the deflection of the wing. The wing deflection can have an impact on its aerodynamic efficiency. Furthermore, as the wing deflects the axis in which the thrust force acts will change and induce an additional bending moment which will have to be accounted for. Furthermore a higher deflection would lead to greater normal forces acting on the skin of the wing, leading to early buckling which will in turn be compensated by adding stiffeners and thus adding weight. This value is set to a maximum of 2% of the wing span, which is 13.5 [cm]. The deflection of a beam is computed using (from [22]):

$$M(z) = -EI\frac{\mathrm{d}^2 v}{\mathrm{d}z^2} \tag{8.5}$$

  The maximum deflection is found at the wing tip and does not exceed 5.3 [cm] if $t_{spar} \geq 6.5[mm]$.

[4] http://www.faculty.fairfield.edu/wdornfeld/ME311/BasicStressEqns-DBWallace.pdf [visited on 15/12/2020]

- When beams are put under bending, there is ovalisation of the cross-section occurring which may decrease the maximum bending load which it can withstand before failing. This effect is expressed as the Brazier effect [23]. As a beam bends and deforms its cross-sectional properties vary in a non-linear fashion which can lead to an anticipated failure. For beams having a uniform cross-section, the critical moment load before failure is approximated by:

$$M_{cr} \approx 0.98 \cdot E \cdot r \cdot t^2 \tag{8.6}$$

  where r is the inner spar radius, E the elastic modulus of the material, t is the spar thickness [23]. It is assumed that the material used is Al7075. The modulus of elasticity for this material is $E = 7.2 \cdot 10^{10}$. Following this equation, the beam must have a minimum thickness of $t_{min} = 1.5[mm]$ in order not to fail in this mode.

From this analysis, a minimum thickness has been computed for the wing main spar which is influenced by the maximum deflection allowed and leads to a spar thickness $t_{spar} \geq 6.5[mm]$.

Shear & Torsion - Cross Sectional Design In order to design for the skin thickness of the wing, a shear analysis has to be made as it is assumed that the skin will only take up shear loads and transfer them to the spar through the ribs. The skin will have to resist the maximum shear stress which will be accumulated between two subsequent rib locations. Once the maximum shear force which the skin will have to account for is computed, the cross-sectional properties of the wing will be computed leading to the calculation of the maximum shear stress found in the skin.

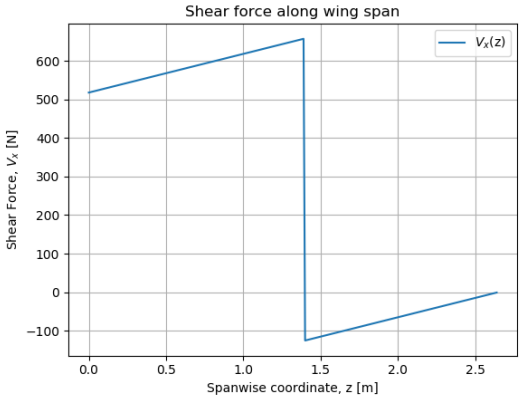

Figure 8.9: V_x shear force along the span

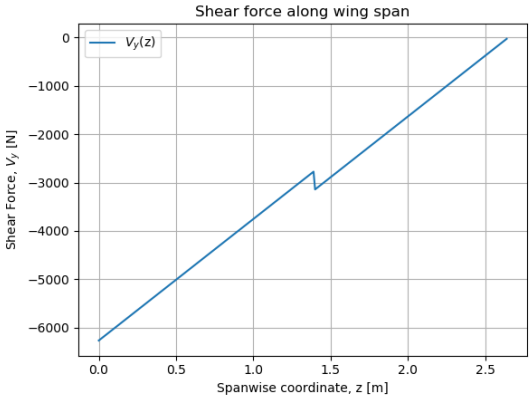

Figure 8.10: V_y shear force along the span

With an initially assumed rib spacing of 20 [cm] a shear force difference can be computed. From the plots shown above, it is clear that V_x is going to have the greatest influence of the shear stress within the skin. The maximum load that the skin will have to carry is 214 N. With the maximum shear force found, the cross-sectional properties of the wing have to be computed. The methodology used following the methodology from [22] and is as follows:

- Idealisation of the cross-section
- Computing the moments of inertia
- Finding the open section boom contribution to the shear flow, and from that the closed section shear flow
- Computing the shear centre of the cross-section and the resulting torque
- Finding the maximum shear stress in the skin and from that, the allowed thickness

The cross-sectional shape of the wing is dictated by the airfoil used, thus it is important to represent this shape when idealising. The booms are placed along the skin of the wing and will be point areas accounting for the thickness of the skin and the possible stiffener.

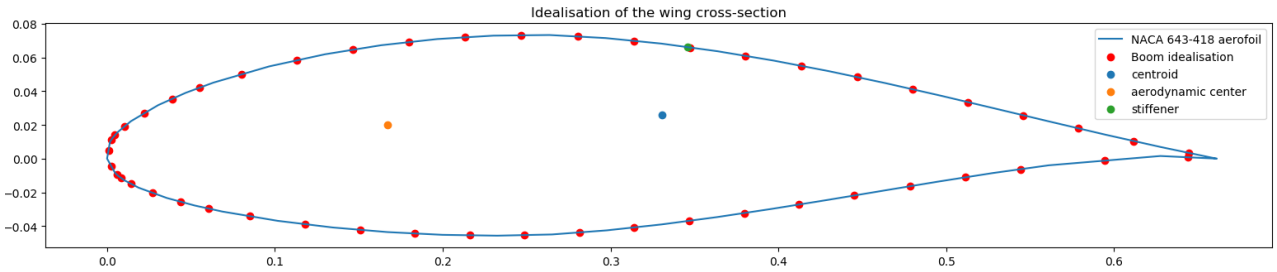

Figure 8.11: View of the idealised cross section (NACA 643-418)

Here, the booms are depicted in red and the centroid of the cross-section in orange. An additional stiffener has been placed on the upper skin and is shown as a blue dot in Figure 8.11. Having the boom areas and their location from the centroid, the moments of inertia can found using the following formula [22]:

$$I_{xx} = \sum_{i=1}^{n} y_i^2 B_i \quad I_{yy} = \sum_{i=1}^{n} x_i^2 B_i \quad I_{xy} = \sum_{i=1}^{n} y_i x_i B_i \tag{8.7}$$

With the forces known, and the cross section properties computed the shear flows can be computed. As a closed section is being analysed, a cut has to be made in order to perform the calculations on an open section. The shear flow between each boom can be found with :

$$q_s = q_b + q_{s0} = -\frac{V_y I_{yy} - V_x I_{xy}}{I_{xx} I_{yy} - I_{xy}^2} \left[\sum_{r=1}^{n} B_r y \right] - \frac{V_x I_{xx} - V_y I_{xy}}{I_{xx} I_{yy} - I_{xy}^2} \left[\sum_{r=1}^{n} B_r x \right] + q_{s0} \tag{8.8}$$

(from [22]) with q_b represents the contribution of each boom to the shear flow within the idealised cross-section. It is a function of the boom location with respect to the centroid and its area. The second term on the right-hand side, q_{s0}, is the shear flow that accounts for the cut made in the cross-section, and can be computed as follows:

$$q_{s0} = -\frac{\oint (q_b / Gt)\, ds}{\oint ds / Gt} \tag{8.9}$$

The total shear flow can thus be computed and plotted. From Figure 8.12 it can be seen that the shear flow does represent the flow that would be present in a closed section and the q_b initial and end values match.

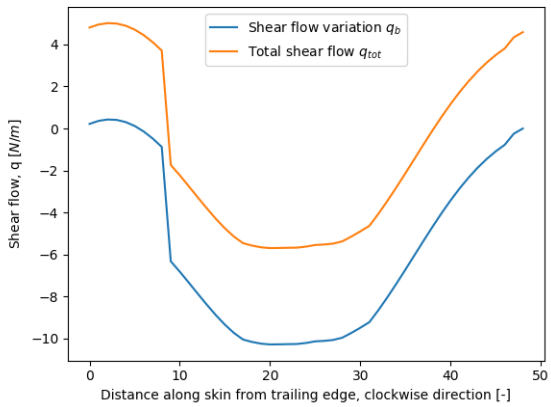

Figure 8.12: Shear flow within the cross-section due to a unit force Vy

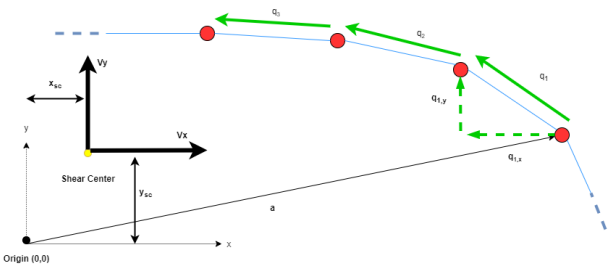

Figure 8.13: Analysis of the shear centre

The shear flows which have now been computed are found for the scenario in which there is pure shear applied on the cross-section, meaning a shear force going exactly through the shear centre. As the airfoil has no axis of symmetry and an arbitrary shape, the shear centre has to be computed analytically. This is done by applying, at the location of the shear centre, unit loads in the x and y direction respectively and performing a moment equilibrium about a chosen point, such that:

$$V_x x_{sc} - V_y y_{sc} = \oint p q_{b_i} ds + 2A_i q_{s_0} \tag{8.10}$$

Where x_{sc} and y_{sc} are respectively the y and x location of the shear centre of the cross-section, and A_i the enclosed area. Figure 8.13 shows the methodology behind the shear centre calculation.

Now that the total shear flow is computed for each interval between the booms, the total shear stress can be computed and compared to the maximum allowed shear stress. As for the case of bending, an upper limit to this allowed shear stress is set to $\frac{Y}{1.5}$ with Y being the yield strength of the material used. The shear stress is computed using:

$$\tau_{max} = \frac{q_{max}}{t_{skin}} \tag{8.11}$$

The maximum value for the shear flow is found to be -1174.93 [N/m] for a rib spacing of 20 [cm]. This value is very low and does not put a constraint on the skin thickness, for this reason buckling has to be analysed. A skin thickness of 0.7 will be assumed for the first iteration, this value should reduce as the iteration process goes on (refer to Section 8.7). This will allow for calculations to be performed. It is recommended to further iterate on the shear flow calculations and skin thickness as they have not been optimised.

Skin Buckling - Skin, Stiffener & Ribs Design For the buckling analysis, the entire wing was sectioned into 9 smaller panels, which encompassed two ribs on either side, and stiffening elements added on the upper part of the skin. However as the chosen wing planform from subsection 7.3.4 was designed to have no sweep or taper ratios, only one panel was to be analysed. The following analysis uses the equations derived from the Structural Analysis & Design lecture notes [24].

$$\sigma_{cr} = \frac{k\pi^2 E}{12(1-\nu^2)}\left(\frac{t}{b}\right)^2 \tag{8.12}$$

$$P_{cr} = \sigma_{cr} A \tag{8.13}$$

First, a panel without any stiffening elements was analysed, using Equation 8.12, where σ_{cc} is the critical buckling stress, k is the buckling coefficient function of the boundary conditions and the aspect ratio of the plate, E is Young's modulus, ν is Poisson's ratio, t is the thickness of the plate, and b is the width of the plate. The buckling coefficient is a function of the boundary condition and the aspect ratio of the plate, where the values were obtained from Figure 8.14. For the analysis, the boundary condition was assumed to be simply supported on all sides. Once the critical buckling stress was obtained, the critical buckling load was calculated using Equation 8.13, where P_{cr} is the critical buckling load, and A is the cross-sectional area of the skin.

From the bending analysis performed in Figure 8.4.1, the maximum normal force the wing would experience was calculated to be 15 [kN] Figure 8.4.1. From this, it was clear that the panel required some stiffening elements as the critical buckling load was calculated to be 141.71 [N] for a panel with $t = 0.7$ [mm].

Next, the same analysis was performed, but now with a stiffener. For the analysis, an Omega stiffener was chosen with the geometry and dimension as shown in Figure 8.15. To calculate the crippling stress of the stiffener, a similar method is used as calculating the plate buckling stress, but each segment of the stiffener is viewed as a plate, and then the weighted average of the crippling stress is taken. Thus Equation 8.14 is a combination of Equation 8.12 corrected for a stiffener with a semi-empirical correction factor α and n based upon experimental data [24]. Which for aluminium alloys equals to $\alpha = 0.8$, n = 0.6, and $\sigma_y = 450$ [MPa], which is the yield strength. Once each segment's crippling stress was calculated, the weighted average was obtained using Equation 8.15, where A_i is the cross-sectional area of each stiffener section.

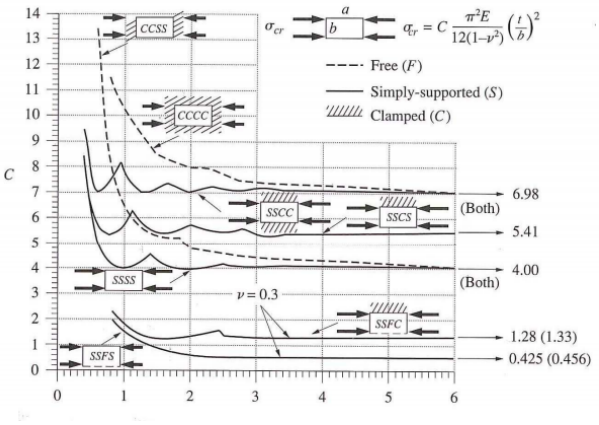

Figure 8.14: Buckling Coefficient as a function of aspect ratio for several different boundary conditions.

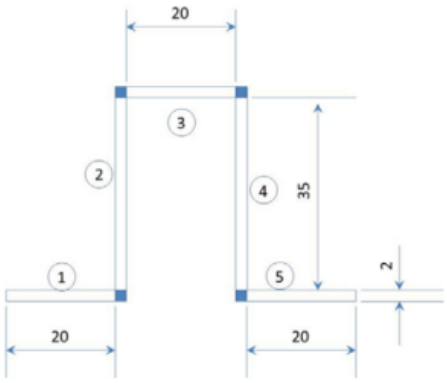

Figure 8.15: Stiffener geometry

Once the crippling stress of the stiffener was obtained, the critical buckling stress of the reinforced panel could be obtained by using the following formulas:

$$\sigma_{cr}^{i} = \alpha \left(\frac{k}{\sigma_y} \frac{\pi^2 E}{12(1-\nu^2)} \left(\frac{t}{b} \right)^2 \right)^{1-n} \tag{8.14}$$

$$\sigma_{cc} = \frac{\sum \sigma_{cc} A_i}{\sum A_i} \tag{8.15}$$

$$2w_e = t\sqrt{\frac{k\pi^2}{12(1-\nu^2)}}\sqrt{\frac{E}{(\sigma_{cc})_{stiff}}} \tag{8.16}$$

$$\sigma_{cc_{panel}} = \frac{(A_{stiff} + 2w_e t_{skin})(\sigma_{cc})_{stiff} + (b - 2w_e)t_{skin}\sigma_{cr}}{A_{stiff} + b t_{skin}} \tag{8.17}$$

To do so, first, the effective sheet width, which is essentially the new width of the panel in which the skin experiences the critical crippling stress of the stiffener, instead of the critical skin buckling stress is calculated using Equation 8.16, where all variables have previously been explained above. Once the effective sheet width has been calculated, the critical skin buckling stress is re-calculated using the new width, as now some part of the skin experiences the reinforcement, the width has become smaller, or to be exact $b - 2w_e$. Then the weighted average of the new critical skin buckling stress and the reinforced crippling stress of the panel is taken. Finally, the critical load can be found using Equation 8.13, only now A should include the entire cross-section including the stiffeners, and σ_{cr} should be of the entire panel with reinforcements.

8.4.2. Final Wingbox Design

Following the analyses performed to determine the skin thickness, ribs placement, stiffener pitch, and wing spars; the final configuration of the wing is presented in the following subsection. Table 8.3 presents a summary of the key parameters obtained, and Figure 8.16 presents the bird's eye view of the wingbox section. From the figure, the spar location at quarter-chord, and the rib spacing of 20 [cm] can be observed. Note that the red section in the figure represents the ailerons, which the structural component has not been designed yet, due to time constraints.

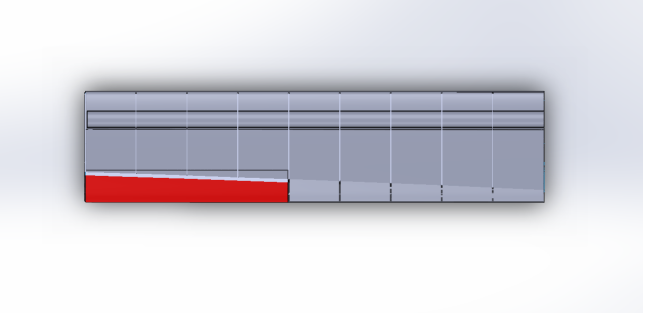

Figure 8.16: Bird's eye view of the wingbox section

8.4.3. Truss Design

Table 8.2: Summary of the wingbox elements

Element	Material	Thickness [mm]	Mass [kg]
Skin	Al2024-T3	0.7	13.6
Spar	Al7075-T6	6.5	28.86
Ribs	Al7075-T6	[-]	4.8
Stiffener	Al7075-T6	[-]	7.74

Table 8.3: Summary of the spar design

Property	Value
Material	AI7075 T6
E-Modulus	72 [GPa]
Yield Strength	503 [MPa]
Outer Diameter	0.09 [m]
Thickness	6.5 [mm]
Length	2.65 [m]

The truss structure is designed to be a simple structure constructed of hollow cylindrical beams welded together. The layout has been designed in such a way that allows direct load paths from the main structural elements (Battery, Payload, and Wings) and makes efficient use of the available space. See Figure 8.2 for the final layout.

The analysis of the truss design assumes the scenario of banking 30 degrees as it would be the most critical case. And the analysis was conducted to find the minimum thickness of the rods, given a diameter of 4cm, and to have deflection no greater than 1[mm].

[h]

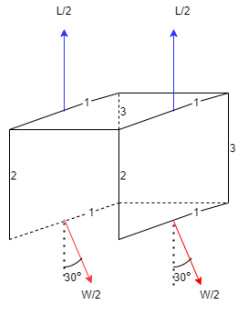

Figure 8.17: Free Body Diagram of the fuselage Truss in the limiting case of banking 30°

Thus, the analysis begins with simplifying the truss on Figure 8.2 to a idealised model as shown on Figure 8.17, and it was split into 3 separate studies, based upon the different types of loading each truss member would experience. **Member 1** will be modelled as an S.S beam with a point load in the middle. **Member 2** will be decoupled into 2: a rod in pure tension, and as a cantilever beam with a tip load. **Member 3** will be modelled as a rod in pure tension.

Simply supported beam members (I) See Equation 8.18 for an expression derived from the Flexure formula which yields the maximum displacement of the beam. Equation 8.19 is the moment of inertia for a thin-walled circular beam.

$$\delta = \frac{P \cdot L^3}{48 \cdot E \cdot I} \quad (8.18) \qquad \text{with} \qquad I = \frac{\pi \cdot t \cdot d^3}{8} \quad (8.19)$$

Where P is the point load, L is the length of the beam, E is Young's modulus and I is the moment of inertia of the section. The load applied is the maximum lift times the maximum load factor, plus the weight of the components attached to the truss (Batteries + Payload) divided by two (two sides of the truss). Resulting in Equation 8.20

$$P = \frac{3750N \cdot 2 + (105kg + 50kg) \cdot 2}{2} = 4510.2N \quad (8.20)$$

By using Equation 8.18, Equation 8.19, and plugging in the variables, it is possible to solve for the required thickness, yielding 2cm, meaning that the section must be solid.

Axially loaded beam members (II) The formula derived from the Flexure formula for axial displacement in a beam is shown in Equation 8.21.

$$\delta = \frac{P \cdot L}{A \cdot E} \quad (8.21) \qquad P = \frac{(155kg \cdot 9.81m/s^2 + 3750N \cdot 2}{4} = 4130N \quad (8.22)$$

Where P is the point load, L is the length, A is the cross-sectional area and E is Young's Modulus. The force applied is the sum of the weight carried (Payload + Batteries) by the member and the lift times the maximum load factor, all divided by four since there are four members loaded axially. Solving for the thickness (implicit in the area) by using Equation 8.21 yields a thickness of 5mm.

Cantilever beam members (III) Since these members are also loaded axially, a new thickness is computed and whichever is greater is taken. The displacement formula derived from the Flexure formula is shown in Equation 8.23.

$$\delta = \frac{P \cdot L^3}{3 \cdot E \cdot I} \tag{8.23}$$

In this case, the load applied laterally at the tip is $P = W/4 \cdot \sin(30deg)$, with the weight divided over four beams at the maximum bank angle of 30°. Again, solving for thickness in Equation 8.23 yields a thickness of 2mm, and thus is neglected since the thickness for axial loading is greater (5mm).

8.4.4. Payload Design

The payload and its recipient are the reason why this vehicle is needed, so an effective system to load and unload the payload from the vehicle is necessary.

Payload Bay The payload bay refers to the internal volume of the vehicle where the payload is accommodated. The payload is fixed to the body by an attachment mechanism, described below. To unload the payload, first, the payloads are lowered by a pair of linear actuators, until they are resting on ground height. Then, the pins are mechanically released to detach the payload from the vehicle and the deployment status is verified. The actuators now return to their stowed position and the vehicle is ready to lift-off and returns to base.

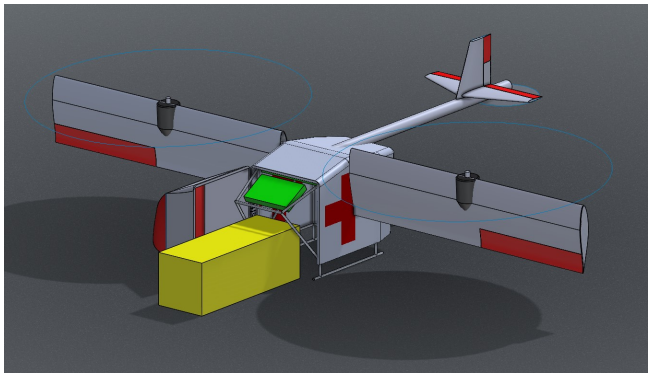

Figure 8.18: Payload loading procedure

In order to load the vehicle, the nose of the fuselage swings open like a door to expose the internals. This is also the main access hatch for inspections and maintenance. The operator at the ground base can then carry the payload from storage to the vehicle, slide it into the payload bay and secure the attachments on the side. The nose door is closed, and the vehicle is ready for start-up and delivery. See Figure 8.18 for a representation of the loading procedure.

Payload Attachment Mechanism To design the four lead screws, the following analysis will be conducted for the case of the payload 1 (70x70x70) , as it is the most critical case, with a longer rod, whereas for payload 2, the rod would be retracted, thus creating a much smaller bending moment. To design the rod to support the 50kg payload the following assumptions were made:

1. The rods shall not deflect more than 1mm even with a limiting manoeuvre of 2g.
2. The mass of the payload is homogeneous and the load will be evenly distributed amongst the 4 rods, thus resulting in a point force of 245.25 [N]
3. The lead screws can be assumed to be supported as a cantilever beam, and the weight of the payload can be assumed to be a point force at the tip of the beam.

Then using the Flexure formula simplified for a cantilever beam with a point force applied at the tip, the following relation is obtained as shown in Equation 8.24:

$$v = -n\frac{PL^3}{EI} \tag{8.24}$$

$$I = \frac{\pi r^4}{4} \tag{8.25}$$

Where v is the vertical displacement of the rod at the tip, n is the load factor applied, P is the tip load, L is the length of the rod, E is the Young's modulus, and I is the moment of inertia of the cross-section

of the cantilever beam. As the beam in the analysis is supposed to depict a circular lead screw, the cross-section of the beam is assumed to be a solid circular section and its moment of inertia can be obtained using Equation 8.25, where r is the radius of the rod.

The analysis considers two different materials, namely Titanium 6AL-4V and Stainless Steel 17-4PH. Both have pros and cons, and the results of the analysis can be seen below in Table 8.4

Table 8.4: Summary of the lead screw material selection

	Stainless Steel 17-4PH	Ti 6AL-4V Grade 5
Radius [cm]	2	2
Length [cm]	12	12
Density [kg/m^3]	7750.373[5]	4428.785[6]
E-Modulus [GPa]	200	110
Cost per rod [€]	4.66[7]	8.36[8]
Tip Deflection [mm]	0.025	0.046

As can be seen above, both materials allow negligible deflection. The stainless steel allows for smaller deflection, due to it's higher E-Modulus, however, comes at a higher density. Whereas the Titanium allows for a larger deflection, which comes at a higher overall cost. However as weight is a driving constraint in the aerospace industry, and in addition, the higher cost of the titanium rods would be negligible relative to the overall cost of the vehicle, the Titanium rods were chosen to be used. Note that in this analysis, the radius of both materials was fixed, as the analysis was conducted based upon 'off the shelf materials', and the cost of a smaller diameter rod could not be obtained. In addition, the current analysis only considers the rod to be in pure shear, whereas in reality; due to the nature of lead-screws, some of the load would also be carried through tensile loading, meaning the tip deflection would be even smaller.

8.4.5. Tail Spar Design

The analysis of the tail spar was to obtain the minimum thickness of the tail spar, given the critical loading conditions of pulling $n = 2$, and given that the minimum spar diameter was 11 [cm] in order to fit the auxiliary engine. For the analysis, a very similar method as for the main wing spar was used to size the tail spar. By using Equation 8.5, and by setting the maximum allowable deflection to be 1[cm], a minimum spar thickness of 2.5[mm] is obtained based on the maximum yield stress of the material and the maximum moment generated by the tail relative to the CG (1019.25 Nm). Using the material properties of Al 7075-T5, this results in a tail boom mass of 5kg.

8.5. Verification & Validation

Once the structural design has been done, it is important to perform verification and validation of these results. For verification, 2 methods were used, in order to verify the python scripts. For Validation, a numerical model of the main spar was created through Ansys in which the bending results are validated.

8.5.1. Verification

Given that most of the analytical calculations were performed using Python, it is imperative that meticulous verification procedures are performed. Due to the fact that all codes were developed individually, meaning there was no integration of two separate codes, by performing a unit test on the individual pieces of codes were enough for verification, also due to the fact that the overall complexity of the developed software was relatively low. Thus unit tests were performed for 3 separate python scripts namely: bending script, buckling script, and the axial script for the truss design. For each script, input variables were given a random

[5] www.azom.com/article.aspx?ArticleID=6778 [visited on 06/01/2021]
[6] www.azom.com/properties.aspx?ArticleID=1547 [visited on 06/01/2021]
[7] www.onlinemetals.com/en/buy/stainless-steel/0-125-stainless-round-bar-17-4-ph-cond-a-cold-finish/pid/20783 [visited on 06/01/2021]
[8] www.onlinemetals.com/en/buy/titanium/0-125-titanium-round-bar-6al-4v/pid/4618) [visited on 06/01/2021]

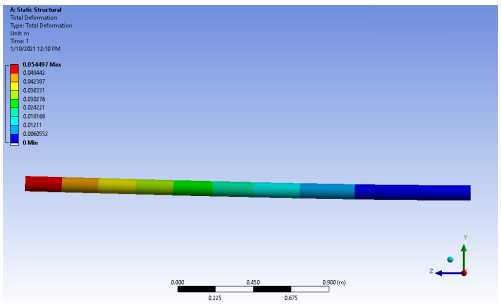

Figure 8.21: Total Deformation

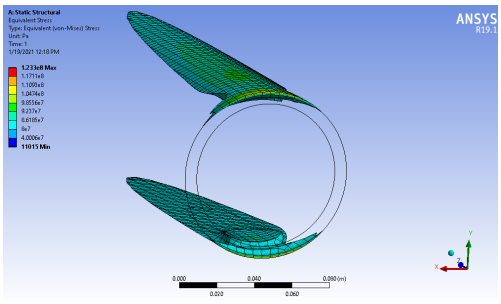

Figure 8.22: Maximum Von-Mises

numerical value, in which they were compared to hand calculations. By ensuring that the output from the script matched the hand calculations, one can be sure that there were no typos of any kind in the script. The numerical tool used for the shear analysis does has been verified in several ways. The computation of the shear centre is not accurate and has thus failed verification at that part.

8.5.2. Validation

Spar Design Validation The calculations of the spar design were based on analytical methods, therefore a different method is selected for the validation of the original method. This method is a static steady-state finite element analysis, using Ansys Workbench. Ansys Workbench is selected instead of Ansys APDL or HyperWorks Optistruct, as workbench provides an interface which automates many of the required inputs. The trade-off is, that following an analysis, the input and output file is to be investigated thoroughly, that no possible mistakes were made.

For meshing two different elements were used: SOLID186 a quadratic 3-D element, and SURF154 which is used for the loads and are overlaid onto the area face of the solid elements.

A very small element size of 0.005 metre is used, as it allows the use of multiple elements in the cross-section of the spar, shown in Figure 8.19.

For the loading conditions, the Lift force is distributed over the lower surface, the Drag over the front surface, the Thrust and the Weight of the engine where the attachment point is located, and the Weight of the wing is distributed over the entire surface. The attachment point of the spar is fully constrained. Loading and boundary conditions are presented in Figure 8.20.

Figure 8.21 show the total deformation of the spar. The maximum deformation is 0.054 metres, while the analytical solution gave 0.0538, of which the deformation in the X-direction is minimal 0.005 metre.

For the stress analysis the Von Mises value is used to determine if a given material will yield. Alternatively, the Tresca method could be used, but it is a more conservative method, therefore Von Mises is selected. The maximum stress is located at the root as shown on Figure 8.22. Even at the location of stress-concentrations the value is below yield, and matches the analytical solution closely. Based on the results the design method is deemed valid.

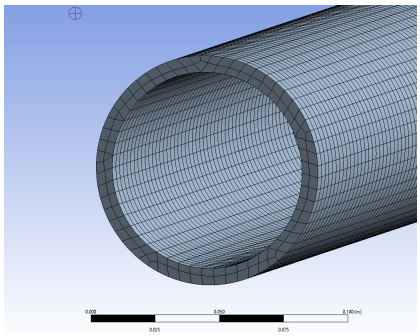

Figure 8.19: Element size

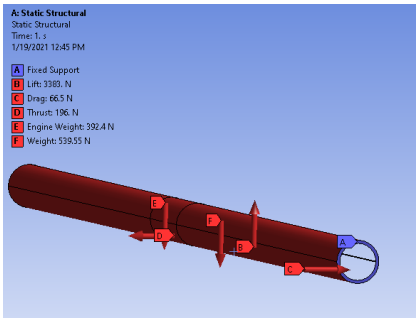

Figure 8.20: Fuselage side view

Skin and Stiffener Validation For the validation of the buckling analysis, eigenvalue/linear buckling analyses could be used, which predicts the theoretical buckling strength of an ideal elastic structure. The issue with this approach is that material and production imperfections prevent most structures from reaching their eigenvalue predicted buckling strength. Also, this type of analysis is not capable of predicting post-buckling behaviour.

Therefore, the suggested approach, is to perform an eigenvalue buckling analysis on a given mesh, and using ANSYS APDL's "UPGEOM" command, updating the location of the nodes of the undeformed mesh using the shape of the critical eigenvalue multiplied with a very small factor. This way, imperfections are introduced to the mesh. After this step, a nonlinear-buckling analysis can be setup on the new mesh, which should provide more accurate buckling behaviour. As the evaluation of these results are very timely and outside of the scope of the project, the method is omitted from this report.

8.6. Sustainability Analysis

The structural design of the entire system was influenced by the sustainable development strategy especially when it came to the materials that were chosen to be used. As previously mentioned, the majority of the structural components in the aircraft are made up of AL-7075 T6. This choice was made not only based upon the good mechanical properties that the material had, it also has a high recycle fraction as explained in Section 14.2. During the iterative process, the team initially considered using a range of CFRP composites to build the main spar and the upper skin of the wing. However, in the end, the material chosen for these components was AL-7075, thus improving the sustainability of the vehicle.Furthermore, it is decided to not make extensive use of composites, which despite their great performance, are more expensive and difficult to manufacture than metals. In addition, composites are very difficult for repairs in the unlikely event of an accident, and they have a highly negative environmental footprint and reduced recycling capabilities.

8.7. Future Recommendations

Given the limited nature of this project, the level of detail is constrained by the available resources: time, knowledge, and manpower. The team is aware of some shortcomings and limitations of the design in its current stage and would like to provide recommendations for a hypothetical future design phase. These areas of improvement were given a lesser priority than that of the contents of this report and were discussed internally to work on what made the most sense.

To begin, the wing structure can be further optimised to achieve a lighter structure overall. The placement of the spars and webs has been partially estimated analytically and then via the use of a FEM analysis, however, time constraints have limited the number of iterations possible during this design stage. The next recommendation is to perform a sensitivity analysis on the materials of various structural elements such as the wing skin or ribs. The use of lighter metals or custom composites can further help reduce weight overall and possibly increase stiffness and strength. However, sustainability shall not be forgotten and must be taken into account for this analysis, striving for a minimal carbon footprint.

The tail can also receive structural improvements, more specifically regarding the attachment points to the tail and the inner structure of the airfoils, which must sustain flight forces. The truss structure can be further optimised to be lighter as well. By making use of composite materials and/or structural optimisation techniques such as natural design, the weight and load-carrying capabilities can be improved. Furthermore, instead of a truss structure, a monocoque design can also be investigated, which could also allow for performance gains.

Furthermore, on all the design choices that were made, a sensitivity analysis should be conducted in order to determine how robust the design choices were. For example, a sensitivity analysis on how the manufacturability/cost would change depending on the materials used should be investigated.

Lastly, a manufacturing plan must be created where all components of the vehicle must be checked for ease of manufacturability and assembly, and technical drawings must be drafted together with a complete bill of materials.

9
Control and Stability

In order for the UAV to perform its mission, it shall be able to fly according to inputs provided by the path planning computer, following this path while remaining stable and maintaining controllability throughout the entire flight envelope. The control system is responsible for this. This chapter describes the design process and results for the control and stability subsystem of the Healios UAV.

Firstly, the functions of the control system are described and the requirements to which the subsystem must adhere to are listed (Section 9.1 and Section 9.2). The approach to the technical design of the subsystem is then presented in Section 9.3. A general framework to assess the stability and controllability characteristics of the vehicle is developed in Section 9.4. Based on this framework, the static and dynamic stability of the vehicle is investigated for both the hover and cruise flight modes in Section 9.5, 9.6.1, and 9.6.2. From the dynamic stability it is found that the UAV needs active control, therefore controllers are presented for cruise and the new stable responses are analysed (subsection 9.7.1). A control architecture is presented for hover (subsection 9.7.2), and a general transition control strategy is discussed (Section 9.8). Verification and validation is provided for the cruise and hover analysis (Section 9.9). The risk and sustainability considerations are then discussed in Section 9.10 and 9.11. Finally, the chapter ends with recommendations to be implemented in future design iterations (Section 9.12).

9.1. Design Overview

The control and stability subsystem was not considered before the Midterm phase of the project. Preliminary control and stability considerations were made for the various concepts presented in the trade-off during the conceptual design stage, but these were not explicitly included in the trade-off itself since the team was unable to determine an accurate method to score the concepts based on their controllability. The control and stability are therefore considered at this stage, during the detailed design stage of the vehicle.

9.2. Requirements and Functional Analysis

In order to design the subsystem in charge of providing control and stability to the vehicle, it is crucial to understand the functions that the subsystem must perform and the requirements that are related to its design.

9.2.1. Functional Analysis

The scope of the control and stability subsystem is to ensure stability and controllability in all flight stages. The subsystem must be robust, in the sense that inaccuracies of measurements and failures of power should not stop the subsystem from maintaining the vehicle stable and to stay controllable. Furthermore, it is to able to follow a set of desired coordinates provided by the flight planning computer.

9.2.2. Requirements

In the previous design phases, the following requirements were generated for the control and stability subsystem [4]:

Table 9.1: The key and driving requirements for the power and propulsion subsystem

ID	REQUIREMENT
SUS-SOC-REL-1	The UA shall be controllable and manoeuvrable, within the demonstrated flight envelope with a reversible flight control system failure.
SUS-SOC-REL-2	The UA shall be controllable and manoeuvrable, within the demonstrated flight envelope with a propulsion system failure.

Table 9.1: The key and driving requirements for the power and propulsion subsystem

ID	REQUIREMENT
FU-PPI-11	The system shall provide a means for the Flight Control System or the remote crew to override the automatic function
FU-PPI-10	Any single failure or likely combination of failures of a power or thrust control system shall not prevent continued safe flight and landing of the UA.

9.3. Design Approach

Now, that the main requirements and functions relevant to the subsystem design can be identified, it is possible to begin the technical design. This section presents the approach taken to perform the technical design of the control subsystem. By presenting this information, a clear overview is provided to the reader. A very general overview of this design process can be seen in Figure 9.1.

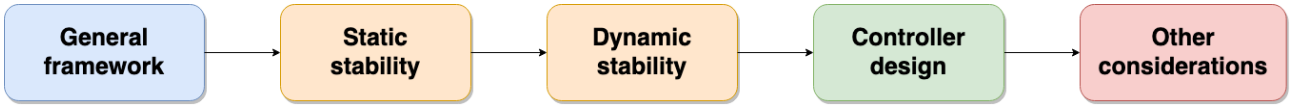

Figure 9.1: Top level view of the design approach for the control and stability subsystem

The design begins by constructing a general framework that can be used to describe the stability, dynamics, and control of the vehicle. This framework is composed of a general set of equations of motions derived from certain assumptions. Furthermore, the framework contains the control allocation of the vehicle, which describes the general approach to control the vehicle in all of its flight conditions. The construction of this general framework is the focus of Section 9.4.

The next step in the design process focuses on ensuring that the vehicle is statically stable. Evidently, static stability is a necessary prerequisite before the dynamic stability of the vehicle can be considered. Ensuring that the vehicle is statically stable both in cruise and hover is the focus of Section 9.5. The focus is then shifted to analysing the dynamic stability of the vehicle. This is done both for cruise (subsection 9.6.1) and hover (subsection 9.6.2). The general equations of motion previously derived are further simplified to represent these flight conditions, after which a state-space model of the vehicle is constructed to analyse its characteristic modes.

After analysing the dynamic stability of the vehicle, the team focuses on performing a preliminary design of the necessary controllers to ensure that the vehicle is stable in all flight conditions. This is the focus of subsection 9.7.1 and subsection 9.7.2. Last but not least, some final considerations are made. These include discussing the approach to ensure controllability and stability while transitioning from hover to cruising flight (Section 9.8) and performing risk analysis in the context of the controllability of the vehicle (Section 9.10), amongst others.

9.4. General Framework

The first step in the design of the control and stability subsystem is the construction of a general framework to analyse the stability, controllability, and dynamic behaviour of the vehicle. That is the focus of this section. Firstly, some important assumptions are presented in addition to the reference frames used throughout the remaining of this chapter. Then, a general set of equations of motion that is applicable to all flight conditions (cruise, hover, and transition) is derived. Lastly, the control allocation for the vehicle is discussed.

9.4.1. Assumptions and Reference Frames

It is vital to begin the analysis of the controllability and stability of the vehicle by providing a clear overview of the used reference frames. The main references frames used in subsequent sections are:

- Vehicle-carried normal Earth reference frame (F_E) — The origin of this frame is placed at the vehicle's

centre of gravity. The Z_E axis points straight down towards the centre of the Earth. The X_E axis is directed to the north, and the Y_E to the east (90°to the right of X_E). This frame is particularly useful to describe the heading of the vehicle with respect to the Earth.

- Body-fixed reference frame (F_b) — The origin is placed at the centre of gravity of the vehicle. The X_b axis then points towards the noise of the aircraft, the Z_b axis points straight down towards the centre of the Earth, and the Y_b axis completes this right-handed reference frame (points towards the right side of the aircraft).
- Aerodynamic reference frame (F_a) — This reference frame is coupled to the aerodynamic velocity vector V_a, that is, the velocity vector of the centre of gravity of the vehicle. The origin of the frame is the same as that of F_b, but the X_a axis points in the direction of V_a. The Z_a lies in the symmetry plane of the aircraft, and the Y_a axis completes this right-handed reference frame.

The relation between the latter two frames is shown graphically in Figure 9.2.

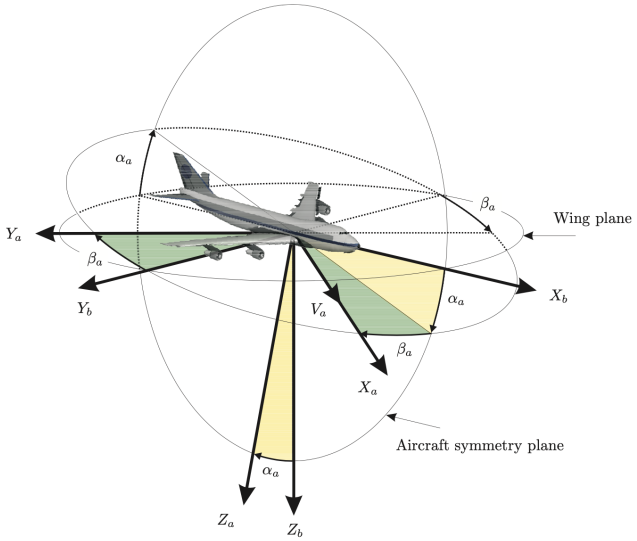

Figure 9.2: Body-fixed and aerodynamic reference frames [25, p.27]

Furthermore, various assumptions are made in order to derive the relevant equations of motion. These are summarised below:

- **Earth is flat and non-rotating** — This implies that the curvature of the Earth is neglected, as well as centrifugal and Coriolis accelerations due to the Earth's rotation with respect to an inertial reference frame. Therefore, in the following, an Earth-centered reference frame is assumed to be inertial.
- **Vehicle is a rigid body with constant mass** — This implies neglecting aeroelastic effects in the derivation of the equations of motion, in addition to variations in the mass distribution and changes in mass (due to e.g. fuel losses, which are not applicable to the Healios vehicle).
- **Vehicle has a plane of mass symmetry** — The body-fixed reference frame is chosen such that I_{xy} and I_{yz} are zero. This implies that the vehicle is assumed to have mass symmetry about the $X_b - Z_b$ plane.
- **Effects of rotating masses are neglected**, such as gyroscopic forces from propellers, which are counter-rotating.
- **Gravity is constant** — The changes to the gravitational acceleration due to altitude changes are neglected.

9.4.2. Control Allocation

Since the Healios UAV must be capable of flying in three different flight modes (see Figure 9.3) it is important to have a control architecture that can offer active control for all the degrees of freedom of the vehicle motion during all flight modes. During cruise the vehicle behaves similarly to traditional aircraft: the ailerons are used for roll control, the rudder for yaw control, and the elevators for pitch control. The throttle setting of the engines is used to control the longitudinal component of the velocity along the body axis. When

in hover mode, the UAV uses the main engines as well as the auxiliary engine (located in the tail) for roll, pitch and yaw control, while the ailerons offer additional yawing authority (both the rudder and elevator have no control authority during hover due to the lack of forward speed and hence are not used in this flight mode). Furthermore, transition is performed by using all control devices (main and auxiliary engines, rudder, elevator and ailerons), while also modifying the wing tilt angle. It is worth noting that the differential thrust of the engines is not actively used during cruise, but it provides redundancy in yawing during that flight phase.

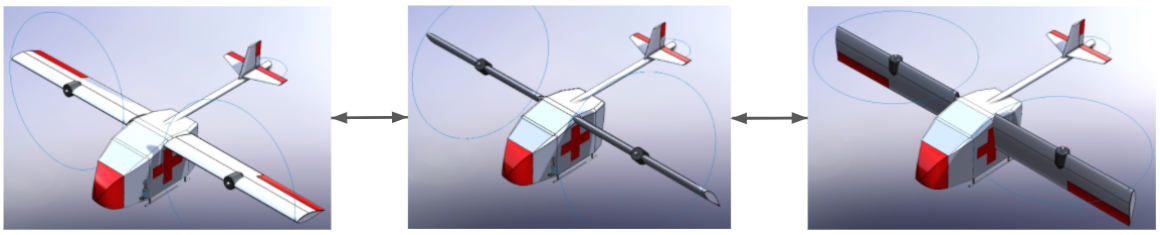

Figure 9.3: UAV flight modes: cruise (left), transition (middle), VTOL (right)

Moreover, when deriving the equations of motion and state space models in the following chapters, a state (**x**) and control vector (**u**) are needed:

$$\mathbf{x} = \left[u, v, w, p, q, r, \theta, \phi, \psi\right]^{\mathrm{T}} \qquad \mathbf{u} = \left[\omega_{\mathrm{left}}, \omega_{\mathrm{right}}, \omega_{\mathrm{aux}}, i_p, \delta_a, \delta_e, \delta r\right]^{\mathrm{T}} \tag{9.1}$$

Here u, v, and w are the components of the velocity along the X_b, Y_b, and Z_b axes; p, q, and r are the pitch, roll, and yawing rates; θ, ϕ, ψ are the so-called Euler angles that describe the attitude of the vehicle, the ω's represent the angular velocities of the left, right, and auxiliary engines: ; i_p is the tilt angle of the wing, and finally δ_a, δ_e, and δ_r are the deflection angles of the aileron, elevator, and rudder, respectively.

9.4.3. Equations of Motion

In order to analyse the dynamics of the UAV, a general set of equations of motion is derived. These equations of motion include the forces caused by the control devices, aerodynamics, engines, and the UAV weight. Figure 9.4 shows a free body diagram of the vehicle in an arbitrary configuration.

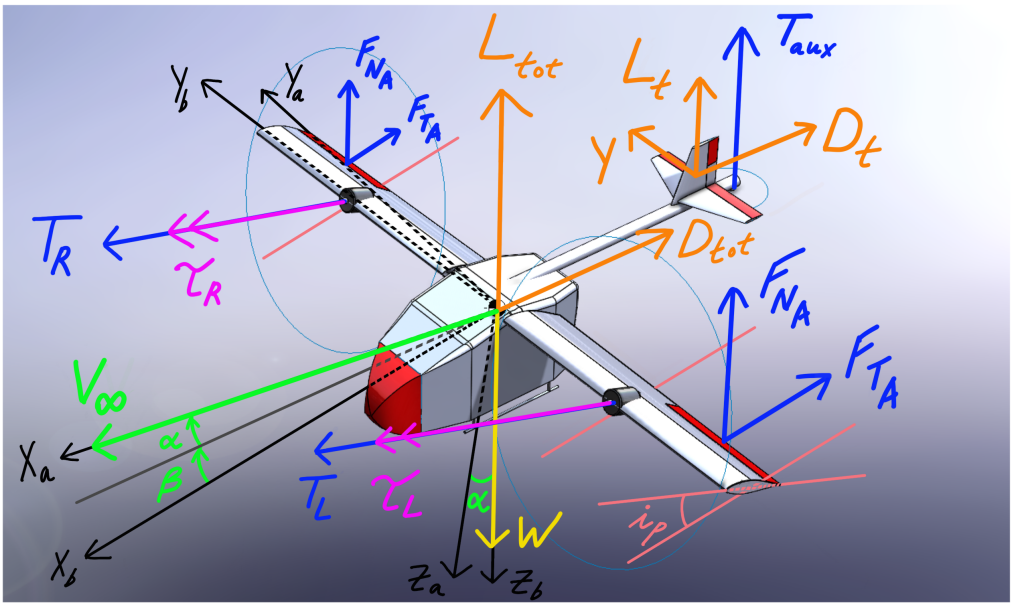

Figure 9.4: Free body diagram of the flying UAV (the aerodynamic control surfaces are highlighted in red)

In order to derive a set of equations of motion from Figure 9.4 that accurately describes the forces and

moments experienced by the vehicle, all of the forces should be expressed in the same reference frame. The chosen reference frame is the body-reference frame, F_b. Nevertheless, instead of writing all of the forces and moments directly in F_b, it is easier to derive each force in whichever reference frame is most convenient for that force and then converting all forces to F_b using a transformation matrix. Therefore, some forces are described in F_E, some in F_a, and some directly in F_b.

To transform the forces expressed in F_E and F_a to F_b, two transformation matrices are needed to convert between the Earth-fixed and aerodynamic reference frames to the body-fixed reference frame. This is done by using the corresponding Euler angles (θ, φ and ψ for the Earth-fixed frame, and α and β for the aerodynamic frame). These matrices are shown in Equations 9.2 and 9.3 [25]:

$$\mathbb{T}_{bE} = \begin{bmatrix} \cos\theta\cos\psi & \cos\theta\sin\psi & -\sin\theta \\ \begin{pmatrix}\sin\varphi\sin\theta\cos\psi \\ -\cos\varphi\sin\psi\end{pmatrix} & \begin{pmatrix}\sin\varphi\sin\theta\sin\psi \\ +\cos\varphi\cos\psi\end{pmatrix} & \sin\varphi\cos\theta \\ \begin{pmatrix}\cos\varphi\sin\theta\cos\psi \\ +\sin\varphi\sin\psi\end{pmatrix} & \begin{pmatrix}\cos\varphi\sin\theta\sin\psi \\ -\sin\varphi\cos\psi\end{pmatrix} & \cos\varphi\cos\theta \end{bmatrix} \tag{9.2}$$

$$\mathbb{T}_{ab} = \begin{bmatrix} \cos\beta_a\cos\alpha_a & \sin\beta_a & \cos\beta_a\sin\alpha_a \\ -\sin\beta_a\cos\alpha_a & \cos\beta_a & -\sin\beta_a\sin\alpha_a \\ -\sin\alpha_a & 0 & \cos\alpha_a \end{bmatrix} \tag{9.3}$$

Then, using these transformation matrices, the equations of motion can be expressed in the body frame as:

$$\begin{pmatrix}\sum F_X^b \\ \sum F_Y^b \\ \sum F_Z^b\end{pmatrix} = \begin{pmatrix}F_X^b \\ F_Y^b \\ F_Z^b\end{pmatrix} + \mathbb{T}_{bE}\begin{pmatrix}F_X^E \\ F_Y^E \\ F_Z^E\end{pmatrix} + \mathbb{T}_{ab}^T\begin{pmatrix}F_X^a \\ F_Y^a \\ F_Z^a\end{pmatrix} \tag{9.4}$$

$$\begin{pmatrix}\sum M_X^b \\ \sum M_Y^b \\ \sum M_Z^b\end{pmatrix} = \begin{pmatrix}M_X^b \\ M_Y^b \\ M_Z^b\end{pmatrix} + \mathbb{T}_{bE}\begin{pmatrix}M_X^E \\ M_Y^E \\ M_Z^E\end{pmatrix} + \mathbb{T}_{ab}^T\begin{pmatrix}M_X^a \\ M_Y^a \\ M_Z^a\end{pmatrix} \tag{9.5}$$

where (for example) F_X^E represents the sum of forces in the X_E direction of *only* the forces that are initially expressed in F_E. The forces that can be directly described in the body reference frame F_b are the thrust forces of the engines, the forces from the ailerons, and the force from the auxiliary engine (those shown in blue in Figure 9.4. Therefore the sum of the forces and moments that are described directly in F_b are described below in Equations 9.6 to 9.11. The forces that are first described in the aerodynamic frame (such as the lift and drag. generated by the vehicle) are shown in Equations 9.17 to 9.22). Lastly, the forces described in the Earth frame are shown in Equation 9.24.

$$F_X^b = (T_L + T_R + \tau_L + \tau_R)\cos(i_p) + 2X_A - 2D_a\cos i_p \tag{9.6}$$

$$F_Y^b = Y_A \tag{9.7}$$

$$F_Z^b = -(T_L + T_R + \tau_L + \tau_R)\sin(i_p) - T_{\text{aux}} + 2Z_A \tag{9.8}$$

$$M_X^b = (T_L - T_R + \tau_L - \tau_R)\sin(i_p)y_{\text{eng}} + \sin(i_p)y_{\text{eng}} - 2Z_A y_A \tag{9.9}$$

$$M_Y^b = (T_L + T_R)\sin(i_p)x_{\text{eng}} - T_{\text{aux}}x_{\text{aux}} - 2Z_A x_A - 2X_A z_A \tag{9.10}$$

$$M_Z^b = (T_L - T_R + \tau_L - \tau_R)\cos(i_p)y_{\text{eng}} + 2X_A y_A \tag{9.11}$$

(which are taken with respect to the centre of gravity, the corresponding moment arms been x_{eng}, y_{eng}, and z_{eng} for the distance between the main engines thrust and the cg, and x_{aux}, y_{aux}, and z_{aux} for the distance between the auxiliary engine thrust and the cg)

where X_A, Y_A, and Z_A are the components of force generated by a single aileron along the axis of F_b; T_L and T_R are the thrust forces of the left and right engines; τ_L and τ_R are the corresponding torques, i_p is the tilt angle of the wing from the local horizontal plane; x_{eng}, y_{eng}, and z_{eng} are the distances from the point of action of the thrust forces to the centre of gravity along the X_b, Y_b, and Z_b axes; and finally x_{aux}, y_{aux}, and z_{aux} are those distances but to the auxiliary engine instead of the main rotors.

The thrust forces are calculated using blade element theory. Chapter 10 presents a detailed description of the derivation of various formulas used to compute the thrust of the rotors. In particular Equations 10.18 and 10.19 are combined to derive the following equation for the thrust of the rotors:

$$T = 2\int_0^1 \frac{\sigma C_l R^2}{2} dR \cdot A_{\text{disc}} \cdot (\omega R)^2 \tag{9.12}$$

where C_l is the lift coefficient of the blades (dependent on the angle of attack and twist of the blades, and i_p), σ is the blade solidity, R is the radius of the rotor, A_{disc} the rotor area, and ω the rotational velocity. The forces generated by the ailerons can be modelled as follows. Firstly, note that the forces generated by the ailerons can be decomposed in the body frame by:

$$\begin{aligned} X_A &= -F_{T_A}\cos(i_p) - F_{N_A}\sin(i_p) \\ Z_A &= +F_{T_A}\sin(i_p) - F_{T_A}\cos(i_p) \\ Y_A &= 0 \end{aligned} \tag{9.13}$$

Where F_{N_A} and F_{T_A} are the normal and tangential forces generated by the aileron in its local reference frame (that is, along the chord direction of the wing). These are two components of the resultant aerodynamic force of the aileron, F_A. This force is made up of two components, namely $F_A = (F_A)_{\text{wetted}} + (F_A)_{\text{unwetted}}$. Since in the case of the Healios vehicle the aileron is fully submerged in the slipstream of the rotor this equation reduces to $F_A = (F_A)_{\text{wetted}}$, which is dependent on the aileron deflection δ_a and the local velocity seen by the aileron V_A. The local velocity seen by aileron is given by [26]:

$$V_A = \sqrt{u^2 + v^2 + (w - v_i)^2} \tag{9.14}$$

where u, v, and w are the X, Y, and Z components of the freestream velocity in the body axis, and v_i is the velocity induced by the rotor. This is calculated according to [27]:

$$v_i = \sqrt{\frac{T}{S_A}\frac{2}{\rho} + u^2} \tag{9.15}$$

where T is the thrust generated by the rotor (computed using Equation 9.12) and S_A is the total surface area of the aileron. The equations for the tangential and normal forces generated by the aileron can then be written as:

$$F_{N_A} = C_{N_{\delta a}}\left(\delta_a - \delta_{a_0}\right)\cdot\frac{1}{2}\rho V_A^2 \cdot S_A \qquad F_{T_A} = C_{T_{\delta a}}\left(\delta_a - \delta_{a_0}\right)\cdot\frac{1}{2}\rho V_A^2 \cdot S_A \tag{9.16}$$

where $C_{N_{\delta a}}$ and $C_{T_{\delta a}}$ are the derivatives of the normal and tangential force coefficient of the aileron with respect to aileron deflection, δ_{a_0} is the aileron deflection at which the aileron does not generate a tangential force, and V_A is computed according to Equation 9.14.

The forces and moments that are described in the aerodynamic frame are:

$$F_X^a = D_{\text{fuselage}} + D_{\text{wing}} + D_{\text{tail}} \tag{9.17}$$
$$F_Y^a = Y_{\text{tail}} \tag{9.18}$$
$$F_Z^a = -L_{\text{wing}} - L_{\text{fuselage}} - L_{\text{tail}} \tag{9.19}$$
$$M_X^a = 0 \tag{9.20}$$
$$M_Y^a = +M_{\text{wing}} + L_{\text{wing}}x_{\text{wing}} - L_{\text{tail}}x_{\text{tail}} \tag{9.21}$$
$$M_Z^a = -L_{\text{rudder}}x_{\text{tail}} \tag{9.22}$$

Here, L stands for lift force and D for drag force. The aerodynamic forces generated by the wing, fuselage and tail are modelled as follows:

$$L = C_L\frac{1}{2}\rho V^2 S \qquad M = C_m\frac{1}{2}\rho V^2 S\bar{c} \tag{9.23}$$

Where L and M are the lift and moment generated by the aerodynamic device, C_L and C_M are the corresponding lift and moment coefficients, S is the wing or fuselage reference area, and $\bar{c}$ is the reference

length, namely the mean aerodynamic chord in the case of the wing and the fuselage length in the case of the fuselage.

Finally, the only force left to be described is the weight. This is written in the Earth-fixed reference, which yields:

$$F_Z^E = W = mg \qquad F_X^E = F_Y^E = 0 \tag{9.24}$$

Furthermore, the right-hand side of the equations of motion (if written in $\sum F = ma$ format) is given by:

$$\sum F_X^b = m(\dot{u} + qw - rv) \tag{9.25}$$
$$\sum F_Y^b = m(\dot{v} + ru - pw) \tag{9.26}$$
$$\sum F_Z^b = m(\dot{w} + pv - qu) \tag{9.27}$$
$$\sum M_X^b = I_{xx}\dot{p} + \left(I_{zz} - I_{yy}\right)qr - I_{xz}(\dot{r} + pq) \tag{9.28}$$
$$\sum M_Y^b = I_{yy}\dot{q} + (I_{xx} - I_{zz})\,rp + I_{xz}\left(p^2 - r^2\right) \tag{9.29}$$
$$\sum M_Z^b = I_{zz}\dot{r} + \left(I_{yy} - I_{xx}\right)pq - I_{xz}(\dot{p} - rq) \tag{9.30}$$

In addition, the kinematic equations of the Euler angles are described by:

$$\begin{aligned} \dot{\varphi} &= p + q\sin\varphi\tan\theta + r\cos\varphi\tan\theta \\ \dot{\theta} &= q\cos\varphi - r\sin\varphi \\ \dot{\psi} &= q\frac{\sin\varphi}{\cos\theta} + r\frac{\cos\varphi}{\cos\theta} \end{aligned} \tag{9.31}$$

9.4.4. Linearisation

The equations presented in the previous section are incredibly versatile since they can be applied to essentially any vehicle that follows the assumptions presented in subsection 9.4.1. Nevertheless, the general equations of motions presented in the previous section are also coupled and non-linear. These non-linear equations could in principle be studied (and solved analytically) using integration techniques provided by software. Another alternative is the linearisation of these equations. In the context of performing the analysis of the dynamics of a system, linearisation is an attractive solution for two main reasons [25]:

- **It allows one to study the characteristics modes of the system** — Linearising the system allows one to study the eigenmotions of the vehicle, which describe its dynamic stability.
- **It allows one to construct linear flight controllers** — By linearising the system one can use the well-established theory of linear controllers, avoiding having to resort to much more complex non-linear controller architectures. The latter evidently have their appropriate use cases, advantages, and disadvantages, but they are deemed to be beyond the scope of the current work.

Based on the reasons above, linearisation presents itself as a really valuable tool in the analysis of the dynamics of the vehicle. The equations of motions presented in Section 9.4 must therefore be linearised about the flight conditions of interest. Linearisation is the process of approximate a function by taking the first-order Taylor series expansion of the function about the point of interest. For that reason, results obtained from linearisation are only valid in a so-called "validity region" around the point about which the equation was linearised.

In general, the linearisation of a function g which is dependent on many variables ($g = f(x_1, x_2, ...x_n)$) can be written as $g_0 + \Delta g$, where g_0 is the evaluation of the function about the center of linearisation and $\Delta g = \frac{\partial g}{\partial x_1}\Delta x_1 + \frac{\partial g}{\partial x_2}\Delta x_2 + ... + \frac{\partial g}{\partial x_n}\Delta x_n$. The following sections of this Chapter discuss how to apply this general methodology to linearise the equations of motion for the specific flight conditions of interest.

9.5. Static Stability Analysis

When designing for the control and stability of the vehicle, the first step is to design a control architecture that can be trimmed to provide force and moment equilibrium both for the cruise and hover conditions. subsection 9.5.1 discusses the approach to tail sizing in order to provide static stability during cruise, while subsection 9.5.2 explores different options to provide moment and force equilibrium during hover.

9.5.1. Cruise

To ensure the static stability of the UAV during flight, a tail is needed both to counteract the moments generated by the wing and to trim the yawing motion of the aircraft. In order to design the tail, an iterative approach is conducted. Firstly, a conventional tail design is chosen due to its simplicity and deep stall characteristics compared to other tails such as the T-tail. Then, given that a high manoeuvrability is needed for transition control, the horizontal and vertical tail volume coefficients are initially chosen to be 0.738 and 0.06 respectively [15] (similar to some fighter jets). Then, with a first estimation of the most fwd and aft cg, the tail arm is calculated to minimise the fuselage drag [15]:

$$l_{\text{opt}} = K_{\text{c}} \sqrt{\frac{4\bar{C}S\bar{V}_{\text{H}}}{\pi D_{\text{f}}}} \tag{9.32}$$

Where $\bar{C}$ is the wing mac, S the wing surface area, $\bar{V}_{\text{H}}$ is the horizontal tail volume coefficient and D_{f} the fuselage drag (the fuselage is assumed to have a circular cross section for simplicity). Additionally a correction factor K_{c} of 1.4 is used to account for the fact that the tail arm design is not conical [15]. A preliminary centre of gravity calculation is used together with the initial wing characteristics (see Chapter 7) to establish longitudinal moment equilibrium and estimate the required tail lift. This is done with the following relation [15]:

$$\sum M_{\text{cg}} = 0 \Rightarrow M_{\text{o}_{\text{wf}}} + L_{\text{h}} \cdot l_{\text{opt}} + L_{\text{wf}} (h - h_{\text{o}}) \bar{C} = 0 \tag{9.33}$$

Where $M_{\text{o}_{\text{wf}}}$ is the moment of the main wing, L_{wf} is the wing's lift, L_h the tail's lift, and $(h - h_0)$ the wing's moment arm. Then the lift's requirements are fed to aerodynamics who selects the airfoil characteristics and area of the tail (see Section 7.4). After this, the geometry of the tail outputted from the aerodynamic calculations is implemented onto XFLR and the stability of the whole UAV during cruise is analysed. If the static stability needs are not met, iterations are done until the tails arm, cg range, and tail characteristics provide static stability. Furthermore, Table 9.2 summarises the main results from the static stability analysis:

Table 9.2: Main results from the static stability sizing:

Tail arm [m]	Horizontal Tail Volume Ratio	Vertical Tail Volume Ratio	FWD cg [m]	AFT cg [m]
2.5	0.438	0.006	0.274	0.280

As it can be seen in Table 9.2, the cg locations (with respect to the wing's leading edge) barely change. This is because the payload cg has been aligned as much as possible with the empty cg of the UAV in order to reduce the cg excursion.

9.5.2. Hover

As explained in subsection 9.4.2, when in vertical flight mode, the tail has little control authority due to the lack of incoming aerodynamic flow onto the tail surfaces. In order to control the pitch of the UAV, a control strategy other than deflecting the tail's elevator is needed. To do so, two control strategies were considered. The first one entails actively controlling the wing tilt angle i_p by changing the torque of the wing's actuator in order to adjust the moment generated by the thrust with respect to the cg, thus balancing the UAV's pitch. This has two main drawbacks, the first one being that since the wing is a heavy part (close to 90kg with the engines) the wing actuator needed would be heavy and subjected to overheating if a hydraulic mechanism is used. The second drawback is that to compensate the moment created by the engines, the thrust needs to be vertically aligned with the cg, causing the vehicle to have a non zero pitching angle while in hover, which might result in some hazards when landing. Thus the second design option is chosen, which consists on placing a small auxiliary engine in the tail that can help control the pitching behaviour of the aircraft by modifying the thrust it produces. In order to size this engine, a moment equilibrium is done to ensure that when in hover mode, the pitching moment generated by the main engines is balanced by the auxiliary engine, meaning that the UAV can hover with a pitch angle of 0 degrees. This calculations are described

in subsection 10.4.6, where the auxiliary engine is sized together with the main engines. Furthermore, the main engines rotate in opposite directions, which means that they balance each others torques, meaning that no yawing moment is generated when in hover. However the auxiliary engine at the back induces an extra yawing moment. To compensate for this, the ailerons are deflected at a trim angle to compensate this yawing moment.

9.6. Dynamic Stability Analysis

Now that the static stability of the vehicle has been discussed, an analysis of its dynamic stability can be performed for the cruise and hover conditions.

9.6.1. Cruise

This section presents the analysis of the dynamic stability of the vehicle during cruise, while subsection 9.6.2 discusses the analysis during hover.

The first step in the analysis of dynamic stability during cruise is to linearise the general equations of motion presented in Section 9.4 about the flight condition of interest which allows one to create a linear system that approximates the behaviour of the vehicle in that condition. Here the flight condition of interest is that of cruise. The most common flight condition in cruise is that of steady flight. In particular, are considered two steady cruise conditions: one corresponding to steady, straight, *symmetric* flight, and the other to steady, straight, *asymmetric* flight. The reason why these motions can be decoupled is the following.

As a consequence of the assumed mass symmetry about the X_bZ_b plane and the linearisation procedure, it is known that the *symmetric* variables can only affect the *asymmetric* motions with terms that are multiplied by higher-order derivatives (that is, derivatives of order two or higher) [25]. The same is true for the changes caused by *asymmetric* variables on the *symmetric* motion. Therefore, assuming that the deviations from the initial conditions remain small, it can be stated that the symmetric and asymmetric eigenmodes of the vehicle are uncoupled [25]. For this reason, the symmetric and asymmetric cruise eigenmotions is analysed separately in the following.

Linearisation about symmetric flight condition The condition of steady, straight, *symmetric* flight has the following properties [25]:

$$\begin{array}{llll} u \neq 0 & \dot{u} = 0 & p = 0 & \dot{p} = 0 \\ v = 0 & \dot{v} = 0 & q = 0 & \dot{q} = 0 \\ w \neq 0 & \dot{w} = 0 & r = 0 & \dot{r} = 0 \\ \varphi = 0 & \dot{\varphi} = 0 & X \neq 0 & \dot{X} = 0 \\ \theta \neq 0 & \dot{\theta} = 0 & Y = 0 & \dot{Y} = 0 \\ \psi = 0 & \dot{\psi} = 0 & Z \neq 0 & \dot{Z} = 0 \end{array} \tag{9.34}$$

The variables that are relevant for this condition are those that are non-zero, namely the horizontal and vertical components of the velocity (u and z), the pitch angle θ, and the pitch rate q. These are non-dimensionalised so that the UAV's performance can be compared with that of other aircraft. Furthermore, this variables are also combined to construct the state vector for the symmetric case as shown:

$$\hat{u} = \frac{u}{V} \qquad \alpha = \frac{w}{V} \qquad \theta = \theta \qquad \hat{q} = \frac{q\bar{c}}{V} \qquad \longrightarrow \qquad \mathbf{x}_s = \left[\hat{u}, \alpha, \theta, \frac{q\bar{c}}{V}\right]^T \tag{9.35}$$

Linearisation about asymmetric flight condition Similarly, the condition of steady, straight, *asymmetric* flight has the following properties [25]:

$$\begin{array}{llll} u = 0 & \dot{u} = 0 & p \neq 0 & \dot{p} = 0 \\ v \neq 0 & \dot{v} = 0 & q = 0 & \dot{q} = 0 \\ w = 0 & \dot{w} = 0 & r \neq 0 & \dot{r} = 0 \\ \varphi \neq 0 & \dot{\varphi} = 0 & X = 0 & \dot{X} = 0 \\ \theta = 0 & \dot{\theta} = 0 & Y \neq 0 & \dot{Y} = 0 \\ \psi = 0 & \dot{\psi} = 0 & Z = 0 & \dot{Z} = 0 \end{array} \tag{9.36}$$

The relevant variables are the lateral velocity v, the roll angle φ, the roll rate p, and the yaw rate r. These are non-dimensionalised in the same way as the symmetric variables. The resulting non-dimensional state variables and state vector are:

$$\beta = \frac{v}{V} \qquad \varphi = \varphi \qquad \hat{p} = \frac{pb}{2V} \qquad \hat{r} = \frac{rb}{2V} \qquad \longrightarrow \qquad \mathbf{x}_\mathrm{a} = \left[\beta, \varphi, \frac{pb}{2V}, \frac{rb}{2V}\right]^\mathrm{T} \tag{9.37}$$

State-space model The equations of motion are then non-dimensionalised following the procedure in [25]. Each component of the linearised forces and moments is turned into its corresponding non-dimensional coefficient. For instance, the change in force in the X direction due to a change in the horizontal velocity (X_u) is non-dimensionalised as follows:

$$C_{X_u} = \frac{1}{\frac{1}{2}\rho V S} \cdot \frac{\partial X}{\partial u} \neq \frac{\partial C_X}{\partial \hat{u}} \tag{9.38}$$

The same procedure was used to non-dimensionalise all of the coefficients present in the linearised equations. These coefficients are the so-called stability derivatives, which describe how changes in the state variables affect the forces and moments experienced by the vehicle.

State space for symmetric motion The non-dimensionalised simplified equations of motion for the symmetric case are given by [25]:

$$\begin{bmatrix} C_{X_u} - 2\mu_c D_c & C_{X_\alpha} & C_{Z_0} & C_{X_q} \\ C_{Z_u} & C_{Z_\alpha} + \left(C_{Z_{\dot{\alpha}}} - 2\mu_c\right) D_c & -C_{X_0} & C_{Z_q} + 2\mu_c \\ 0 & 0 & -D_c & 1 \\ C_{m_u} & C_{m_\alpha} + C_{m_{\dot{\alpha}}} D_c & 0 & C_{m_q} - 2\mu_c K_Y^2 D_c \end{bmatrix} \begin{bmatrix} \hat{u} \\ \alpha \\ \theta \\ \frac{q\bar{c}}{V} \end{bmatrix} = \begin{bmatrix} -C_{X_{\delta_e}} & -C_{X_{\delta_t}} \\ -C_{Z_{\delta_e}} & -C_{Z_{\delta_t}} \\ 0 & 0 \\ -C_{m_{\delta_e}} & -C_{m_{\delta_t}} \end{bmatrix} \begin{bmatrix} \delta_e \\ \delta_t \end{bmatrix} \tag{9.39}$$

where $D_c = \frac{\bar{c}}{V}\frac{d}{dt}$ is the non-dimensional time derivative operator, $\mu_c = \frac{m}{\rho S \bar{c}}$ is the non-dimensional mass parameter, and $K_Y^2 = \frac{I_{yy}}{m\bar{c}^2}$ is the non-dimensional moment of inertia about the Y_b axis. These equations must now be written in state space form. This is done by first noting that the state space representation is

$$\dot{\mathbf{x}} = \mathbf{A}\mathbf{x} + \mathbf{B}\mathbf{u} \tag{9.40}$$

where $\mathbf{x}$ is the state vector and $\mathbf{u}$ the control vector. The resulting state space models are presented below. In the case of symmetric flight the state vector is $\mathbf{x} = \mathbf{x_s}$, and the control vector is simply composed of the elevator deflection and thrust setting, $\mathbf{u} = [\delta_e, \delta_t]^\mathrm{T}$. In order to transform Equation 9.39 into state space form is noted that an intermediate form of the state space system is given by the equation:

$$\mathbf{P}\dot{\mathbf{x}} = \mathbf{P}\frac{d\mathbf{x}}{dt} = \mathbf{Q}\mathbf{x} + \mathbf{R}\mathbf{u} \tag{9.41}$$

where $\mathbf{Q}$ is the matrix on the left hand side of Equation 9.39, while $\mathbf{R}$ is the right hand side matrix. Then, the state space model can be constructed by the following matrix multiplication:

$$\dot{\mathbf{x}} = \mathbf{P}^{-1}\mathbf{Q}\mathbf{x} + \mathbf{P}^{-1}\mathbf{R}\mathbf{u} = \mathbf{A}\mathbf{x} + \mathbf{B}\mathbf{u} \tag{9.42}$$

This results in the following equations for the $\mathbf{A}$ and $\mathbf{B}$ matrices:

$$\begin{bmatrix} \dot{\hat{u}} \\ \dot{\alpha} \\ \dot{\theta} \\ \frac{\dot{q}\bar{c}}{V} \end{bmatrix} = \begin{bmatrix} x_u & x_\alpha & x_\theta & 0 \\ z_u & z_\alpha & z_\theta & z_q \\ 0 & 0 & 0 & \frac{V}{\bar{c}} \\ m_u & m_\alpha & m_\theta & m_q \end{bmatrix} \begin{bmatrix} \hat{u} \\ \alpha \\ \theta \\ \frac{q\bar{c}}{V} \end{bmatrix} + \begin{bmatrix} x_{\delta_e} & x_{\delta_t} \\ z_{\delta_e} & z_{\delta_t} \\ 0 & 0 \\ m_{\delta_e} & m_{\delta_t} \end{bmatrix} \begin{bmatrix} \delta_e \\ \delta_t \end{bmatrix} \tag{9.43}$$

The coefficients of the matrices are assigned variables such as x_u, x_α, etc... for the sake of clarity. Each of those coefficients follows from the matrix multiplication of Equation 9.42. The formulas for all of these coefficients are omitted for the sake of brevity. Nevertheless, as an example, the formula for the coefficient m_u is:

$$m_u = \frac{V}{\bar{c}} \frac{C_{m_u} + C_{Z_u} \frac{C_{m_{\dot{\alpha}}}}{2\mu_c - C_{Z_{\dot{\alpha}}}}}{2\mu_c K_Y^2} \tag{9.44}$$

The state-space system in Equation 9.43 can be analysed using numerical software such as MATLAB. By computing the eigenvalues of the **A** matrix, the symmetric eigenmotions of the vehicle can be analysed.

State space for asymmetric motion In the asymmetric case, the state vector is $\mathbf{x} = \mathbf{x_a}$, and the control vector is simply composed of the aileron and rudder deflections $\mathbf{u} = [\delta_a, \delta_r]^T$. The non-dimensional simplified equations of motion for the asymmetric case are given by [25]:

$$\begin{bmatrix} C_{Y_\beta} + \left(C_{Y_{\dot{\beta}}} - 2\mu_b\right) D_b & C_L & C_{Y_p} & C_{Y_r} - 4\mu_b \\ 0 & -\frac{1}{2} D_b & 1 & 0 \\ C_{\ell_\beta} & 0 & C_{\ell_p} - 4\mu_b K_X^2 D_b & C_{\ell_r} + 4\mu_b K_{XZ} D_b \\ C_{n_\beta} + C_{n_{\dot{\beta}}} D_b & 0 & C_{n_p} + 4\mu_b K_{XZ} D_b & C_{n_r} - 4\mu_b K_Z^2 D_b \end{bmatrix} \begin{bmatrix} \beta \\ \varphi \\ \frac{pb}{2V} \\ \frac{rb}{2V} \end{bmatrix} = \\ = \begin{bmatrix} -C_{Y_{\delta a}} & -C_{Y_{\delta r}} \\ 0 & 0 \\ -C_{\ell_{\delta a}} & -C_{\ell_{\delta r}} \\ -C_{n_{\delta a}} & -C_{n_{\delta r}} \end{bmatrix} \begin{bmatrix} \delta_a \\ \delta_r \end{bmatrix} \tag{9.45}$$

where $D_b = \frac{b}{V}\frac{d}{dt}$ is the non-dimensional time derivative operator for the asymmetric case, $\mu_b = \frac{m}{\rho S b}$ is the non-dimensional asymmetric mass parameter, and $K_X^2 = \frac{I_{xx}}{mb^2}$, $K_Z^2 = \frac{I_{zz}}{mb^2}$ and $K_{XZ}^2 = \frac{I_{xz}}{mb^2}$ are the corresponding non-dimensional moments of inertia.

Following the same steps described in Equation 9.41 and 9.42, the state form for the asymmetric case has the form:

$$\begin{bmatrix} \dot{\beta} \\ \dot{\varphi} \\ \frac{\dot{p}b}{2V} \\ \frac{\dot{r}b}{2V} \end{bmatrix} = \begin{bmatrix} y_\beta & y_\varphi & y_p & y_r \\ 0 & 0 & 2\frac{V}{b} & 0 \\ l_\beta & 0 & l_p & l_r \\ n_\beta & 0 & n_p & n_r \end{bmatrix} \begin{bmatrix} \beta \\ \varphi \\ \frac{pb}{2V} \\ \frac{rb}{2V} \end{bmatrix} + \begin{bmatrix} 0 & y_{\delta_r} \\ 0 & 0 \\ l_{\delta_a} & l_{\delta_r} \\ n_{\delta_a} & n_{\delta_r} \end{bmatrix} \begin{bmatrix} \delta_a \\ \delta_r \end{bmatrix} \tag{9.46}$$

where again the coefficients follow from the matrix multiplication of Equation 9.42. Note that all of the coefficients in Equation 9.43 and Equation 9.46 depend on the stability and control derivatives. Therefore, before one can analyse the state-space models derived in this section, the value of a wide range of stability derivatives must be determined, both for the symmetric and asymmetric cases.

Stability and control derivatives As stated previously it is necessary to compute the stability derivatives of the vehicle during cruise in order to compute the coefficients of the state space model given in Equation 9.43 and Equation 9.46. The calculation of values for the stability derivatives is the purpose of this section. Ideally the value of these derivatives would be derived experimentally using a wind-tunnel. Evidently, this is not possible at this stage of the design. For that reason, the aerodynamic software XFLR5 was used to model the vehicle in its cruise condition and find an approximation for the value of the stability derivatives.

In order to construct the aerodynamic model of the vehicle in XFLR5, various steps were taken. First, the 2D airfoil shape of the wing and tail obtained based on aerodynamic considerations (see Chapter 7) was plotted inside the program, and 2D aerodynamic analyses were performed on these airfoils. This is a necessary step since XFLR5 uses this 2D data to perform the 3D analysis. The 2D analyses yielded the aerodynamic polars of the airfoils as a function of angle of attack at a wide range of Reynolds numbers (chosen so that the Reynolds number corresponding to the cruise condition was included in the analysis) [28].

Once the 2D airfoil analysis was conducted a 3D model of the vehicle was constructed. The model can be seen in Figure 9.5. The model is comprised of the 3D planform of the wing and tail (see Chapter 7) and a number of point masses which represent all of the components inside the fuselage of the vehicle (e.g. batteries, sensors, main wing actuator, etc...).

Once the vehicle was modelled inside XFLR5, the 3D analysis could be performed. The software performs the 3D analysis based on the Vortex Lattice Method (VLM). VLM models the lifting surfaces of the vehicle as an infinitely thin sheet of discrete vortices to calculate the lift and induced drag. Like any other method, VLM has its limitations. The theory assumes the flow to be incompressible, inviscid, flow. However, these assumptions are deemed to be acceptable for the Healios vehicle, since the cruise condition is significantly below the Mach number were compressibililty effects become relevant ($M_{\text{cruise}} \approx 0.16$). Another drawback of XFLR5's VLM method is the fact that the viscous drag of the wing is merely an interpolation of 2D viscous drag from local wing lift, meaning it underestimates the total drag of the vehicle.

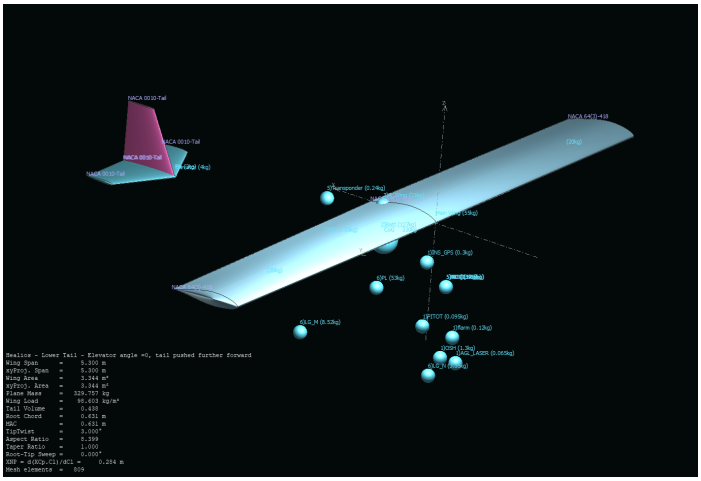

Figure 9.5: Three dimensional model of the wing, tail, and component point masses of the vehicle in XFLR5.

With the XFLR5 software setup as described above, a stability analysis was conducted to find approximate values of the necessary derivatives for both symmetric and asymmetric flight. Two types of derivatives must be found: stability derivatives and control derivatives.

The stability derivatives describe how the forces and moments experienced by the vehicle are affected by changes in the *state* variables. Their non-dimensional form is used to compute the coefficients of the A matrix in the state-space system. The control derivatives describe the changes caused by changes to the *input* variables. Their non-dimensional form are used to compute the coefficients of the B matrix. Although the control derivatives are not strictly necessary to examine the eigenmotions of the vehicle (since these are described by the eigenvalues of the A matrix), their calculation is provided here since they form an integral part of the state-space system. Furthermore, the control derivatives are needed in order to design the corresponding controllers for the systems, see subsection 9.7.1.

The stability derivatives were computed by performing a stability analysis on the 3D model of the vehicle using XFLR5. A necessary prerequisite for studying the dynamic stability of the model is to have a statically stable vehicle, that is, to ensure that $C_{m_\alpha} < 0$. As explained in subsection 9.5.1 the process of sizing the tail surface to ensure appropriate static stability was an iterative one since it heavily depends on the MTOW of the vehicle and the location of the centre of gravity. For that reason those iterations were performed first and only then was the stability analysis conducted in XFLR5. This ensured that the stability analysis was performed on the finalised (and statically stable) vehicle geometry.

The stability analysis conducted in XFLR5 yielded values for a wide range of stability derivatives, all of which are necessary to continue with the analysis of the eigenmotions of the vehicle in cruise. The non-dimensional values of these derivatives are shown below in Table 9.3. These are obtained by taking the dimensional derivatives obtained from XFLR5 and dividing them by the corresponding dvisor following the methodology from [25]. The divisors for the symmetric case are either $\frac{1}{2}\rho VS$ (e.g. for C_{X_u}), $\frac{1}{2}\rho V^2 S$ (e.g. for C_{X_0}), $\frac{1}{2}\rho VSc$ (e.g. for C_{m_u}), $\frac{1}{2}\rho VSc^2$ (e.g. for C_{m_q}). The divisors for the asymmetric case are the same but using the span b instead of the chord c.

Table 9.3: Stability derivatives for the symmetric (left) and asymmetric (right) flight conditions

Non-dimensional derivative	Value [-]	Non-dimensional derivative	Value [-]
C_{X_u}	-0.0293	C_{Y_β}	-0.1705
C_{X_α}	0.2751	C_{Y_p}	0.0928
C_{X_q}	0	C_{Y_r}	0.1522
C_{Z_u}	-0.8993	C_{l_β}	0.0063
C_{Z_α}	-4.2841	C_{l_p}	-0.5364
C_{Z_q}	-2.0731	C_{l_r}	0.1452
C_{M_u}	-0.0036	C_{n_β}	0.0781
C_{M_α}	-0.2571	C_{n_p}	-0.1152
C_{M_q}	-4.7382	C_{n_r}	-0.0700

It is worth noting that two additional stability derivatives had to be computed. These are the derivatives related to the rate of change of the angle of attack $\dot{\alpha}$, namely $C_{Z_{\dot{\alpha}}}$ and $C_{m_{\dot{\alpha}}}$. These stability derivatives are not given by XFLR5 and therefore they had to be computed according to [25]. The reason why these terms appear in the equations of motion has to do with the fact that after a sudden change in the angle of attack, it takes a certain amount of time for the flow around the horizontal stabiliser to "feel" this change in the flow. These terms account for this time-delayed effect after the angle of attack changes. They were computed according to the equations below [25]:

$$
\begin{aligned}
C_{Z_{\dot{\alpha}}} &= -C_{N_{h_\alpha}} \left(\frac{V_h}{V}\right)^2 \frac{d\varepsilon}{d\alpha} \frac{S_h l_h}{S\bar{c}} \\
C_{m_{\dot{\alpha}}} &= -C_{N_{h_\alpha}} \left(\frac{V_h}{V}\right)^2 \frac{d\varepsilon}{d\alpha} \frac{S_h l_h^2}{S\bar{c}^2}
\end{aligned}
\tag{9.47}
$$

Here $C_{N_{h_\alpha}}$ is the derivative of the normal force coefficient of the horizontal stabiliser with respect to the local angle of attack at the tail. $\frac{V_h}{V}$ is the ratio of velocities between the tail and the freestream, $\frac{d\varepsilon}{d\alpha}$ is the change in downwash angle per unit change of angle of attack. All of these terms were obtained from XFLR5. The remaining terms are obtained from the tail geometry: S_h is the surface area of the horizontal stabilised, l_h the distance between the aerodynamic centre of the tail and that of the wing. S is the surface area of the wing and $\bar{c}$ the mean aerodynamic chord.

The computation of the control derivatives was slightly more involved than that of the stability derivatives, since these values are not provided directly by XFLR5. In the case of symmetric flight the control derivatives are those related to the elevator ($C_{X_{\delta_e}}$, $C_{Z_{\delta_e}}$ and $C_{m_{\delta_e}}$) and those related to the throttle setting ($C_{X_{\delta_t}}$, $C_{Z_{\delta_t}}$ and $C_{m_{\delta_t}}$). In the case of asymmetric flight the control derivatives are those related to the aileron ($C_{Y_{\delta_a}}$, $C_{l_{\delta_a}}$ and $C_{n_{\delta_a}}$) and those related to the rudder ($C_{Y_{\delta_r}}$, $C_{l_{\delta_r}}$, $C_{n_{\delta_r}}$).

Elevator control derivatives The control derivatives related to the elevator were calculated by performing aerodynamic analysis of the vehicle at elevator deflections ranging between -10°and 10°in steps of 2.5°. The value of the total lift coefficient C_L, drag coefficient C_D and pitching moment coefficient C_m were recorded at each elevator deflection. The results are shown below in Figures 9.6, 9.7, and 9.8, in addition to the regressions used to fit the data and obtain relations between the elevator deflection and the relevant quantities.

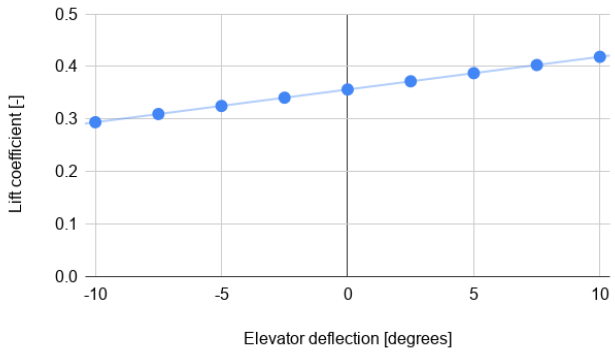

Figure 9.6: C_L against δ_e

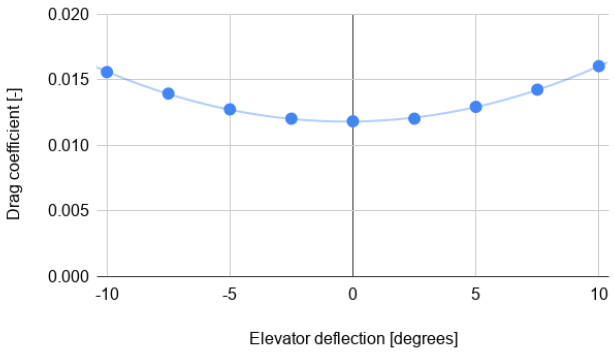

Figure 9.7: C_D against δ_e

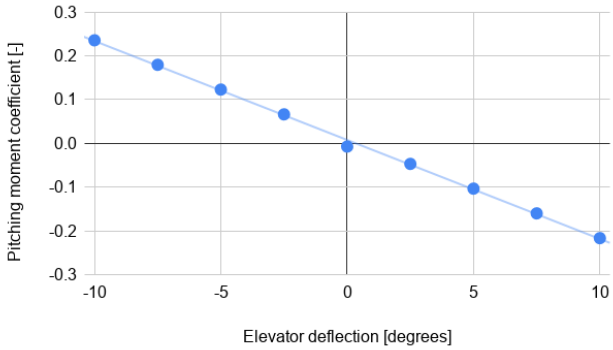

Figure 9.8: C_m against δ_e

The regressions were then used to calculate an approximation of the elevator stability derivatives. This was done by simply relating the change in lift coefficient to the forces in the Z direction, the drag to forces in the X direction, and leaving the moment unchanged. This is justified due to the fact that the angle of sideslip β was set to zero, and because the angle of attack remained constant throughout [25]. The computed values for the elevator derivatives are given in Table 9.4 (next page).

Aileron control derivatives A similar approach was taken to compute the control derivatives related to the aileron. In this case, the rolling moment L and yawing moment N of the vehicle were recorded at aileron deflections ranging from 0°to 20°. For each of these deflections, the right and left ailerons were deflected in opposite directions (with right elevator having a positive deflection and the left one having a negative deflection). The results are shown below in Figures 9.9 and 9.10. The computed values for the aileron derivatives are given in Table 9.4 (next page).

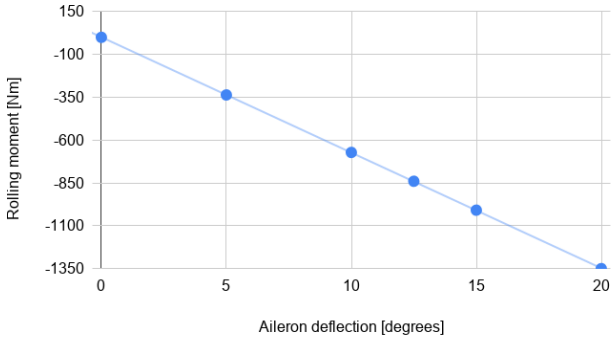

Figure 9.9: Rolling moment against δ_a

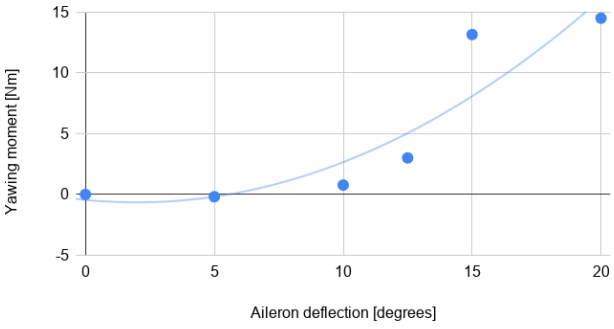

Figure 9.10: Yawing moment against δ_a

Rudder control derivatives The main function of the rudder is the generation of a side force Y due to a rudder deflection. The rudder derivatives were all calculated as a function of the change in side force due

to a change in rudder deflection, Y_r. If that value is known, the change in rolling and/or yawing moment can easily be calculated by multiplying Y_r with the corresponding vertical or horizontal distance from the centre of gravity to the point of action of the side force, namely the aerodynamic centre of the rudder.

The value of Y_r was calculated by performing various aerodynamic analyses of the rudder at rudder deflections between -10°and 10°. The value of Y_r was found to be 899.5437 Newtons per degree of rudder deflection. The rudder derivatives which depend on this value are summarised in Table 9.4.

Thrust setting control derivatives The derivatives related to the thrust setting were computed by simply reasoning the effect of a change to the forces and moments on the vehicle due to a change in the thrust setting. The change in force in the X direction is simply $C_{X_{\delta_t}} = 1$, since the thrust itself is a force in the X direction. For the same reason, the change in force in the Z direction is $C_{Z_{\delta_t}} = 0$. Lastly, the change in pitching moment is $C_{X_{\delta_t}}$ multiplied by the corresponding moment arm, which yields $C_{m_{\delta_t}} = -0.284$.

Summary of control derivatives The control derivatives related to the elevator, ailerons, and rudder are summarised below in Table 9.4.

Table 9.4: Summary of control derivatives related to elevator (left), aileron (middle), and rudder (right) deflections

Non-dimensional derivative	Value [-]	Non-dimensional derivative	Value [-]	Non-dimensional derivative	Value [-]
$C_{X_{\delta_e}}$	-0.000021	$C_{Y_{\delta_a}}$	0	$C_{Y_{\delta_r}}$	0.1268
$C_{Z_{\delta_e}}$	-0.3570	$C_{l_{\delta_a}}$	-0.1027	$C_{l_{\delta_r}}$	-0.000444
$C_{m_{\delta_e}}$	-1.2949	$C_{n_{\delta_a}}$	-0.000314	$C_{n_{\delta_r}}$	0.2973

Analysis of eigenmotions The eigenmotions of the vehicle during cruise can now be examined by computing the eigenvalues of the A matrix using the stability and control derivatives derived in the previous section.

The eigenvalues of the symmetric and asymmetric eigenmodes are plotted in Figure 9.11 and Figure 9.12. These correspond to the characteristic modes of the vehicle in the longitudinal and lateral directions, respectively. Furthermore, the values of the eigenvalues are summarised in Table 9.5.

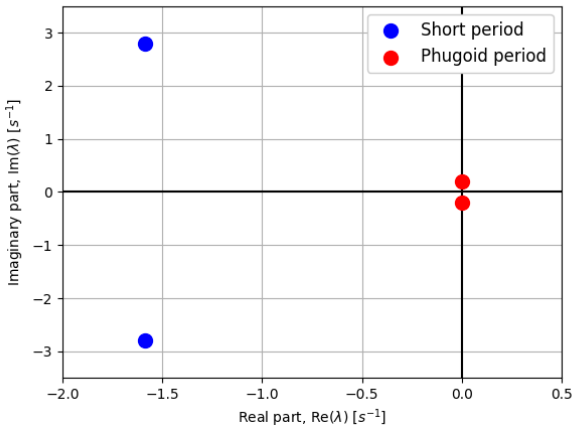

Figure 9.11: Eigenvalues of the symmetric eigenmotions during cruise

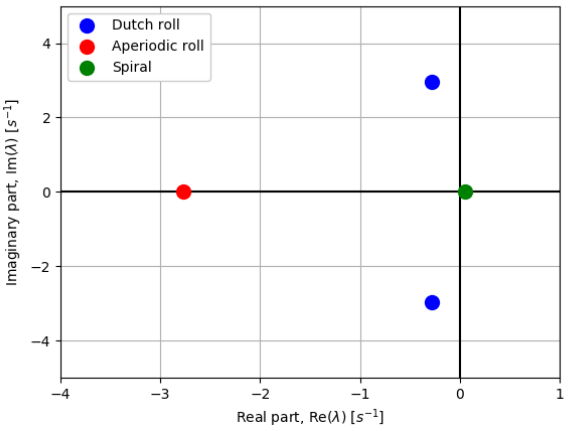

Figure 9.12: Eigenvalues of the asymmetric eigenmotions during cruise

In the longitudinal case two clear eigenmotions can be observed in Figure 9.11. Each of them correspond to a conjugate pair of eigenvalues, which indicates the oscillatory nature of the motions. The eigenmotion

represented by the blue dots is stable, since the real components of the eigenvalues are negative, indicating damping of the eigenmotion over time. This corresponds to the short period of the aircraft, a highly damped oscillatory motion with a period in the order of a couple of seconds. On the other hand, the second eigenmotion is slightly unstable. Although Figure 9.11 appears to show the eigenvalues on the y axis, their real component is slightly positive. This eigenmotion corresponds to the phugoid, an oscillatory motion which a much longer period (in the order of tens of seconds or even minutes [25] depending on the aircraft). Even though the real component of these eigenvalues is really close to zero the motion is still unstable. This means that, if left uncontrolled, the aircraft would slowly start experiencing oscillations in its pitch angle, pitch rate, angle of attack and horizontal velocity that would diverge over time. For this reason, a controller needs to be designed and implemented to ensure this motion is stabilised (see subsection 9.7.1).

Table 9.5: Eigenvalues of the symmetric (S) and asymmetric (A) characteristic modes

Motion	**Eigenmode**	**Real component**	**Imaginary component**
Symmetric	Phugoid	+0.0006	$\pm 0.2000\,i$
Symmetric	Short period	−1.5886	$\pm 2.7942\,i$
Asymmetric	Dutch roll	−0.2779	$\pm 2.9576\,i$
Asymmetric	Aperiodic roll	−2.7716	$0.0000\,i$
Asymmetric	Spiral	+0.0477	$0.0000\,i$

In terms of lateral motion, three clear eigenmotions can be observed in Figure 9.12. Two eigenmotions lie in the x-axis (i.e. their imaginary components are equal to zero), which indicate that these motions are aperiodic (they do not oscillate). The most stable of those motions is the so-called aperiodic roll (or roll subsidence), a highly damped rolling motion represented by the red dot in Figure 9.12. The second aperiodic motion is the spiral, which in this case is unstable (note the positive real component in Table 9.5). The spiral motion is a combination of increased velocity and roll angle which causes the aircraft to enter a spiral dive with a continuously decreasing turn radius. This eigenmode tends to be unstable for many conventional aircraft [25] and could result in fatal consequences if left uncontrolled (e.g. complete structural failure of the airframe due to increasing loads). For this reason a lateral controller must also be designed, to not only stabilise the unstable motion but also to improve the response of the system to the stable motions.

Lastly an oscillatory motion can also be observed in Figure 9.12, indicated by the conjugate pair of complex eigenvalues shown in the figure as blue dots. This motion is the so-called Dutch roll, a coupling of yawing and rolling motion which results in the nose of the aircraft "drawing" an elliptical shape in the horizon. This motion is oscillatory but stable, with the oscillations being damped out over time.

9.6.2. Dynamic Stability Analysis

In order to assess the flying performance of Healios during take-off and landing, it is important to understand the hovering characteristics of the UAV. Hovering entails having the vehicle in a fixed position in the air without moving forwards, backwards or laterally. This section analyses the longitudinal (Equation 9.6.2) and lateral (Equation 9.6.2) hovering dynamics of the UAV in order to asses its performance under different eigenmotions.

When analysing hover, several simplifications and assumptions are made in regards to the used control devices. This further simplifies the general equations of motion (see subsection 9.4.3) :

- The hover control devices are the main and auxiliary engines, and the ailerons. The tail is not used for hover control due lack of aerodynamic authority.
- Ailerons are deflected equal in magnitude but opposite in direction, meaning their net effect on the X and Z axis forces is zero.
- Ailerons only affect yaw (no pitch authority due to wing chord alignment with center of gravity)
- Aileron drag is the same for the right and left ailerons, hence no rolling moment is induced due to the deflection of the ailerons.
- The wing is in vertical position ($i_p = 90°$).

- i_p is not a control variable since tilting the wing actively would overload the actuator.

Furthermore, similarly to the cruise dynamic analysis, the symmetric and asymmetric hovering motions are analysed by first linearising the general equations of motion from subsection 9.4.3 around the hover condition (which is specified for the symmetric and asymmetric conditions in Subsections 9.6.2 and 9.6.2). These equations are then written in state-space format ($\dot{\mathbf{x}} = \mathbf{A}\Delta\mathbf{x} + \mathbf{B}\Delta\mathbf{u}$), and the eigenvalues of the A matrix are examined to calculate the eigenmotions of the UAV. In order to do this, the general state and control vectors for hover are defined as:

$$\mathbf{x} = [u, v, w, p, q, r, \theta, \phi, \psi]^{\mathrm{T}} \qquad \mathbf{u} = \left[\omega_{left}, \omega_{right}, \omega_{aux}, \delta_a\right]^{\mathrm{T}} \tag{9.48}$$

Similarly to the analysis of the dynamic stability during cruise presented in subsection 9.6.1, the resulting state-space system that describes the vehicle's dynamics during hovering is heavily dependent on stability derivatives. These stability derivatives need to be computed to analyse the characteristic modes of the vehicle during hover. Unlike for cruising flight, aerodynamic analysis tools such as XFLR5 are not well suited for the hovering case; thus, an alternative approach to find these derivatives was taken.

A brief literature review on the controllability and stability of tilt-wing and tilt-rotor aircraft was conducted to understand which parameters are the determining factor related to stability during hover. In particular, references [29, 30] proved to be extremely valuable. They are a series of technical notes published presented by NASA which explore the longitudinal and lateral stability characteristics of a tilt-wing aircraft with VTOL capabilities, including a series of model flight tests used to validate their methodology. The authors present an analytical methodology used to identify the main factors that influence the stability of tilt-wing aircraft like the Healios vehicle during hover.

The validated method presented in references [29, 30] was therefore chosen to proceed with the analysis of the stability of the vehicle during hover. The references were used to chose which of the many stability derivatives are important during hovering. Values for those derivatives were then computed by dimensionalising the non-dimensional values provided in the references to adapt them to the configuration of the Healios vehicle.

Symmetric Hover When linearising, the symmetric hovering condition around which the general equations of motion are linearised (see subsection 9.4.3) and the symmetric state and control vectors are defined as:

$$\begin{array}{cccc} u=0 & \dot{u}=0 & p=0 & \dot{p}=0 \\ v=0 & \dot{v}=0 & q\neq 0 & \dot{q}=0 \\ w=0 & \dot{w}=0 & r=0 & \dot{r}=0 \\ \varphi=0 & \dot{\varphi}=0 & X=0 & \dot{X}=0 \\ \theta\neq 0 & \dot{\theta}=0 & Y=0 & \dot{Y}=0 \\ \psi=0 & \dot{\psi}=0 & Z=0 & \dot{Z}=0 \end{array} \qquad \mathbf{x} = [u, w, q, \theta]^{\mathrm{T}} \qquad \mathbf{u} = \left[\omega_{left}, \omega_{right}, \omega_{aux}\right]^{\mathrm{T}} \tag{9.49}$$

In the case of symmetric hovering flight, references [29, 30] show that the main stability derivatives that need to be taken into consideration are X_u, M_u, and X_θ. These are:

$$X_u = \frac{\partial \dot{u}}{\partial u} \qquad M_u = \frac{\partial \dot{q}}{\partial u} \qquad X_\theta = \frac{\partial \dot{u}}{\partial \theta} = -g \tag{9.50}$$

Then, the eigenvalues of the original **A** matrix (left hand side of Equation 9.51) can be approximated by the eigenvalues of the modified **A'** matrix (right hand side of Equation 9.51), which only includes the derivatives from Equation 9.50. Thus the **A'** matrix is used to calculate the eigenvalues and corresponding eigenmotions of the system, which are analysed in Equation 9.6.2.

$$\mathbf{A} = \begin{bmatrix} \frac{\partial \dot{u}}{\partial u} & \frac{\partial \dot{u}}{\partial w} & \frac{\partial \dot{u}}{\partial q} & \frac{\partial \dot{u}}{\partial \theta} \\ \frac{\partial \dot{w}}{\partial u} & \frac{\partial \dot{w}}{\partial w} & \frac{\partial \dot{w}}{\partial q} & \frac{\partial \dot{w}}{\partial \theta} \\ \frac{\partial \dot{q}}{\partial u} & \frac{\partial \dot{q}}{\partial w} & \frac{\partial \dot{q}}{\partial \dot{q}} & \frac{\partial \dot{q}}{\partial \theta} \\ 0 & 0 & 1 & 0 \end{bmatrix} \qquad \mathbf{A'} = \begin{bmatrix} \frac{\partial \dot{u}}{\partial u} & 0 & 0 & -g \\ 0 & 0 & 0 & 0 \\ \frac{\partial \dot{q}}{\partial u} & 0 & 0 & 0 \\ 0 & 0 & 1 & 0 \end{bmatrix} \tag{9.51}$$

Asymmetric Hover When linearising, the asymmetric hovering condition around which the general equations of motion are linearised (see subsection 9.4.3) and the asymmetric state and control vectors are defined as:

$$\begin{array}{cccc} u = 0 & \dot{u} = 0 & p \neq 0 & \dot{p} = 0 \\ v = 0 & \dot{v} = 0 & q = 0 & \dot{q} = 0 \\ w = 0 & \dot{w} = 0 & r \neq 0 & \dot{r} = 0 \\ \varphi = 0 & \dot{\varphi} = 0 & X = 0 & \dot{X} = 0 \\ \theta = 0 & \dot{\theta} = 0 & Y = 0 & \dot{Y} = 0 \\ \psi \neq 0 & \dot{\psi} = 0 & Z = 0 & \dot{Z} = 0 \end{array} \qquad \mathbf{x} = [v, p, \phi, r]^{\mathrm{T}} \qquad \mathbf{u} = \left[\omega_{left}, \omega_{right}, \delta a\right]^{\mathrm{T}} \tag{9.52}$$

In the case of asymmetric hovering flight, references [29, 30] show that the main stability derivatives that need to be taken into consideration are Y_v, Y_p, L_v, N_r. These are:

$$Y_v = \frac{\partial \dot{v}}{\partial v} \qquad Y_p = \frac{\partial \dot{v}}{\partial p} \qquad L_v = \frac{\partial \dot{p}}{\partial v} \qquad N_r = \frac{\partial \dot{r}}{\partial r} \qquad \frac{\partial \dot{v}}{\partial \phi} = g \tag{9.53}$$

Then, the eigenvalues of the original **A** matrix (left hand side of Equation 9.54) can be approximated by the eigenvalues of the modified **A'** matrix (right hand side of Equation 9.54), which only includes the derivatives from Equation 9.53. Thus the **A'** matrix is used to calculate the eigenvalues and corresponding eigenmotions of the system, which are analysed in Equation 9.6.2.

$$\mathbf{A} = \begin{bmatrix} \frac{\partial \dot{v}}{\partial v} & \frac{\partial \dot{v}}{\partial p} & \frac{\partial \dot{v}}{\partial \phi} & \frac{\partial \dot{v}}{\partial r} \\ \frac{\partial \dot{p}}{\partial v} & \frac{\partial \dot{p}}{\partial p} & \frac{\partial \dot{p}}{\partial \phi} & \frac{\partial \dot{p}}{\partial r} \\ 0 & 1 & 0 & 0 \\ \frac{\partial \dot{r}}{\partial v} & \frac{\partial \dot{r}}{\partial p} & \frac{\partial \dot{r}}{\partial \phi} & \frac{\partial \dot{r}}{\partial r} \end{bmatrix} \qquad \mathbf{A'} = \begin{bmatrix} \frac{\partial \dot{v}}{\partial v} & \frac{\partial \dot{v}}{\partial p} & \frac{\partial \dot{v}}{\partial \phi} & 0 \\ \frac{\partial \dot{p}}{\partial v} & 0 & 0 & 0 \\ 0 & 1 & 0 & 0 \\ 0 & 0 & 0 & \frac{\partial \dot{r}}{\partial r} \end{bmatrix} \tag{9.54}$$

Analysis of Eigenmotions The eigenmotions of the UAV during hover can be examined by computing the eigenvalues of the **A'** matrices and using the stability derivatives stated in Subsections 9.6.2 and 9.6.2.

The eigenvalues of the symmetric and asymmetric eigenmodes are plotted in Figure 9.13 and Figure 9.14. These correspond to the characteristic modes of the hovering UAV in the longitudinal and lateral directions. Furthermore, the values of the eigenvalues are summarised in Table 9.6:

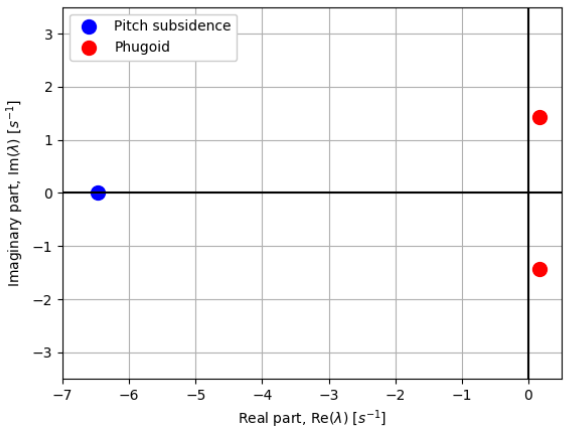

Figure 9.13: Eigenvalues of the symmetric eigenmotions during hover

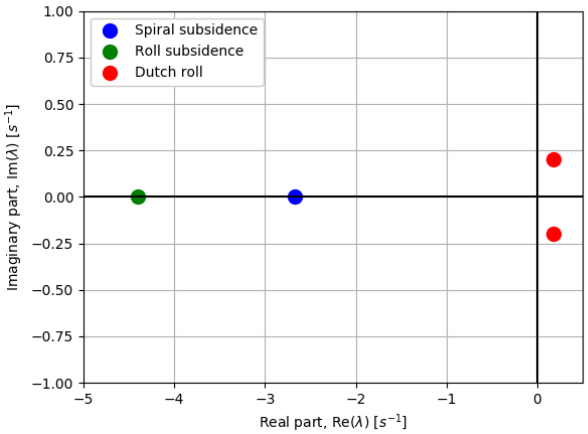

Figure 9.14: Eigenvalues of the asymmetric eigenmotions during hover

Regarding the symmetric motions, two sets of eigenvalues are observed in Figure 9.13. One of them is real and negative (the pitch subsidence) indicating a non-oscillatory damping of the motion over time, while the other is complex and and its real part is positive (the phugoid), indicating an unstable oscillatory behaviour over time. Furthermore, Figure 9.14 shows three asymmetric eigenmotions, two of them are real and on the negative axis (namely the spiral and roll subsidences) indicating a non-oscillatory damped behaviour over time, and the third eigenmotion, corresponding to the Dutch roll, is complex and its real part is positive, indicating an unstable oscillatory behaviour over time.

Table 9.6: Eigenvalues of the symmetric and asymmetric characteristic modes

Motion	**Eigenmode**	**Real component**	**Imaginary component**
Symmetric	Pitch Subsidence	-6.4642	$0.0000\,i$
Symmetric	Phugoid	$+0.1611$	$\pm 1.4342\,i$
Asymmetric	Roll Subsidence	-4.4021	$0.0000\,i$
Asymmetric	Spiral Subsidence	-2.6698	$0.0000\,i$
Asymmetric	Dutch Roll	$+0.1732$	$\pm 0.2004\,i$

Thus in summary, five eigenmotions are observed for the hover condition. Three of them are on the negative real axis (the pitch, roll, and spiral subsidences), indicating damped motion, and a stable open-loop response of the system. Additionally, the other two eigenmotions (the Dutch roll and phugoid) show an unstable oscillatory behavior, hence the open-loop response of the system is unstable for these motions. Thus, a hover controller architecture is needed both to make the Dutch roll and phugoid motions closed-loop stable and to improve (if needed) the response for the pitch, roll and spiral subsidences (see Section 9.7).

9.7. Controllers

This section presents the controllers necessary to ensure that the vehicle remains stable during all flight conditions. For cruising flight two controllers are designed and implement, one for longitudinal and one for lateral motion. In the case of hover and transition, a single controller is presented and its architecture described in detail.

9.7.1. Cruise Controllers

This section presents the controllers used in cruise. The design philosophy is the development of two separate controllers; a longitudinal and lateral motion controller. Separating the cruise controllers into the longitudinal and lateral motions simplifies the development of the controllers without losing significant accuracy [31], given that the vehicle experiences small deviations from both cruise conditions, as the state-

space models used are linearised around this longitudinal and lateral cruse conditions. Furthermore, the system is solely controlled with proportional controllers, as these can be analytically tuned, however it is acknowledged that they have some limitations regarding the control response and steady state error reduction, ans that in the future more complex controllers can be used to improve the performance of the flight control system. subsection 9.7.1 presents the controller for longitudinal (symmetric) flight and Figure 9.7.1 presents the controller for lateral (asymmetric) flight.

Longitudinal Controller The longitudinal controller architecture is shown in Figure 9.15. The top loop is the velocity control and the bottom outer loop is the altitude control, with the pitch controller nested inside the altitude controller.

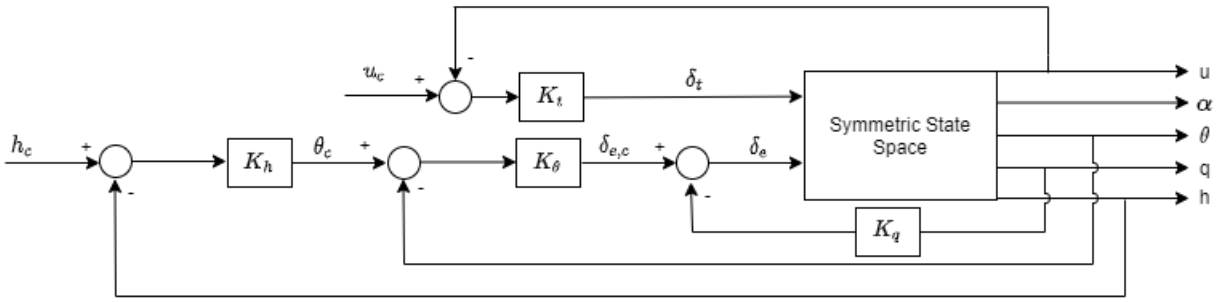

Figure 9.15: Controller for Symmetric Flight

The horizontal speed (u) is controlled by a gain (K_u) with a unitary feedback. The bottom loop is the altitude control where (K_h) is the altitude gain. The pitch control is nested within the altitude control, where (K_θ) is the pitch gain. The pitch rate feedback (K_q) was implemented, which improves the short period damping.

In order to have the altitude feedback into the controller, an altitude state needs to be added in the state space matrix for symmetric flight, which was obtained from Equation 9.6.1. The assumptions made to accommodate for altitude in the state vector (ie: that the flight path angle is small enough to make a small angle approximation) to construct a relation between the V and γ and the vertical velocity $\dot{h}$ is then calculated with relation 9.55 [32]:

$$\dot{h} \approx V\gamma = v(\theta - \alpha) \tag{9.55}$$

Figure 9.16 shows the horizontal velocity step response. To ensure that the vehicle has a good efficiency, the velocity controller should have a slow response (low acceleration) and no overshoot. Increasing the gain K_t reduces the overshoot and reduces the rise time (which increases the acceleration). Thus, there is a compromise to be made between acceleration and overshoot. In addition, the controller has a steady-state error, the response levelling out at 0.98 instead of 1. As stated before, the response should be slower, however the slower the response the larger the steady-state error. The steady-state error could be reduced with the use of an additional integral term in the controller, and the response can be made slower, more energy-efficient, with a derivative term.

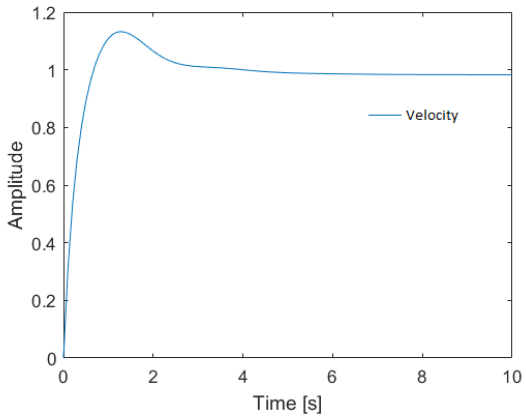

Figure 9.16: Velocity Step Response

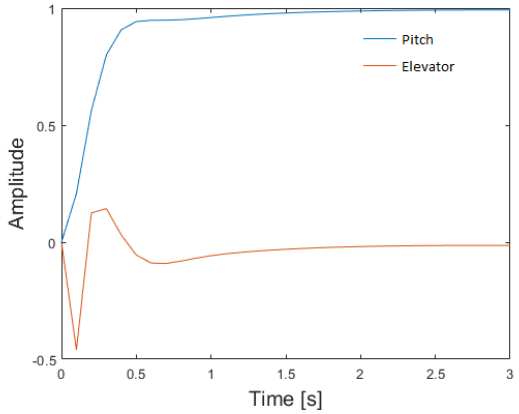

Figure 9.17: Pitch Step Response (pitch = blue, orange = elevator)

Figure 9.17 shows the step response of the pitch controller to a step input, the elevator response is also included (in orange). The use of a proportional controller to control the pitch introduces a steady-state error, to reduce this error the pitch gain (K_θ) needs to be as large as possible. However, as the pitch gain increases the short period damping deteriorates. Therefore a pitch rate feedback (K_q) was implemented which improves the short period damping while allowing (K_θ) to be larger. The steady-state error of the pitch is 0.1, and the closed-loop has a short period damping of 0.762 at a speed of 9.66[rad/s]. The phugoid is critically damped and has speeds of 8.71[rad/s] and 1.34[rad/s]. The pitch settles at around 0.9.

Figure 9.18 shows the step response of the altitude controller. For energy efficiency, the response of the altitude controller must be relatively slow and have no overshoot. A slow response has been achieved with a rise time of around 5 seconds. The altitude controller has a steady-state error of 0.1 and it levels off to its final value after 20 seconds. This steady-state error could be eliminated by adding an integrator term to the controller. Figure 9.19 shows the pitch and elevator response to a unit step input to the altitude controller. The pitch increases and then returns to zero after 5 seconds, which is the time it takes for the altitude to arrive at its final value.

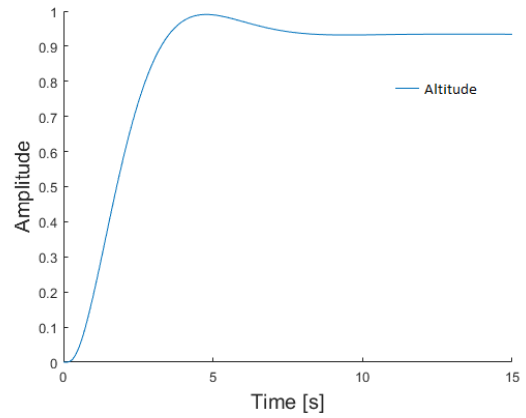

Figure 9.18: Altitude Step Response

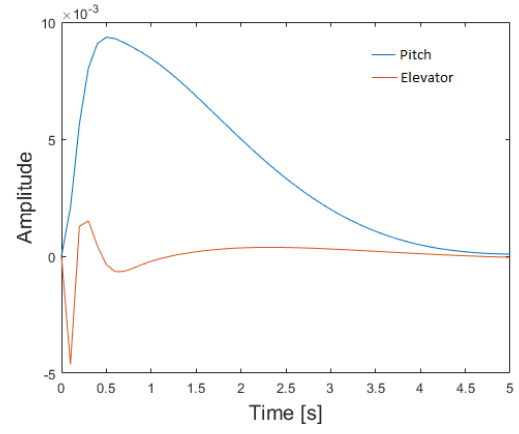

Figure 9.19: Pitch and Elevator Response to Altitude Step Input

Lateral Controller Figure 9.20 shows the control architecture for lateral (asymmetric) flight. The outer top loop is the heading hold which is controlled with the proportional controller K_ψ. The roll control is nested inside the heading control, and is controlled by K_ϕ. The outer bottom loop is the sideslip angle control which is controlled by K_β. The yaw damper is nested within the side slip control, and improves the dutch roll damping, it has a gain of K_r.

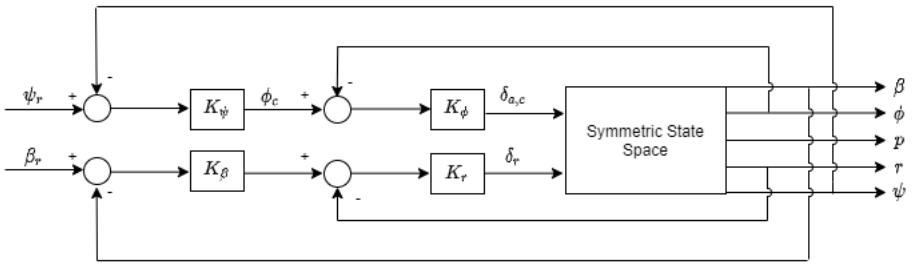

Figure 9.20: Heading Controller Architecture

To be able to feed back the yaw angle, the state space system found in Equation 9.6.1 needs to be extended to accommodate for (ψ). ψ was calculated using Equation 9.56[32]:

$$\psi = \frac{r}{s\cos\theta} \tag{9.56}$$

Figure 9.21 shows the roll step response, a small steady-state error of 0.04 is present. The steady-state error can be decreased by decreasing the roll gain (K_ϕ). However, a lower roll gain leads to a faster response, therefore the gain was chosen such that the roll acceleration wasn't too high and that the steady-state error was acceptable. The steady-state error can be tailored as explained before.

Figure 9.22 shows the yaw step response. The yaw response in this graph is too slow with a rise time of 100 seconds. The response could be made faster with a larger yaw gain (K_ψ). However, the larger yaw gain leads to unfeasible roll angles. This is probably due to the assumption that the heading is only changed by the ailerons. In reality this would be done with a combination of aileron and rudder deflections. For this step response, a gain was chosen such that maximum roll angle was below 30 degrees.

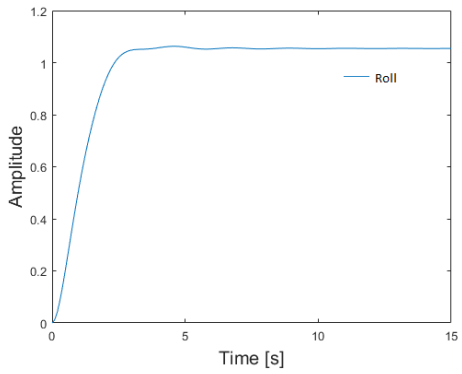

Figure 9.21: Roll Step Response

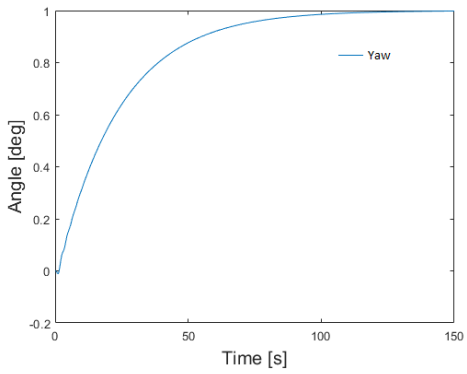

Figure 9.22: Yaw Step Response

The side slip controller could not be tuned with proportional controllers. Figure 9.23 shows the root locus of the $\frac{\beta}{\delta_r}$ transfer function. There is a pole and a zero on the right, unstable side of the plane. Negative gain can not be used to tune the closed-loop. The control can still be tuned with a PID controller where the integral and derivative terms shift the unstable pole and zero to stabilise the motion.

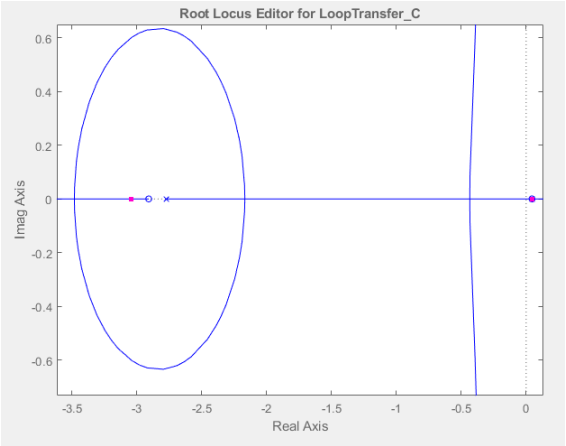

Figure 9.23: Side Slip Root Locus

9.7.2. Hover Controller

This section desribes the control system the UAV used during hover. The control system is developed based on a quadcopter Simulink model [1]. The general approach is outlined for the control design during hover and the control architecture presented.

General Control Strategy A control system needs inputs and outputs to complete its assigned operations. Outputs are returned and fed back into the control loop. The goal of the controller program itself is to manipulate the input by applying operations such that it results in the outputs. Some assumptions for the hover control strategy have been given below:

- Under-actuated system (5 control inputs, 6DOF)
- Wing stays stationary in the upward position
- The hover condition is stabilised around an arbitrary x, y, z position in the global reference frame and a desired heading (ψ)
- Position is the only vehicle variable that can be accurately observed

The presented control architecture (Figure 9.24) can be applied to the whole flight regime. From hover to cruise, take-off and landing provided that the necessary adjustments are made e.g. adjust for wing tilt angle. The inputs to the control system relate to the three dimensional position of the vehicle as well as its desired heading. The path planning software generates the coordinates for the positional input. The outputs of the control system consist of: the rotational speeds of the main proprotors, auxiliary proprotor and aileron deflection. For simplicity it is assumed that the ailerons deflect the same amount in opposite directions, such that they create a yaw moment. The vehicle output equals the estimated state of the state space model. This estimated state is combined with the sensor data to accurately depict the new state. This is then fed back into the control system.

PID Controllers The operations are done by a PID (proportional-integrate-derivative) control function. The controller calculates the error value relating to the difference between the desired set point and the process variable in a loop. The PID controller then applies a correction based on scaling the proportional, derivative and integral terms. Correct tuning of these scales, called gains, achieves a vehicle that moves as desired in every flight situation. As tuning is typically a time consuming process it is considered out of scope for this report. A typical discrete PID control function calculates its output on a computer as given in Equation 9.57 [2] [3].

$$u_k = K_p(e_k + \frac{T_d}{T_s}e_k + \frac{T_s}{T_i}\sum_{n=1}^{n_t} e_n) \tag{9.57}$$

[1] https://github.com/wilselby/MatlabQuadSimAP [visited on 10/01/2021]
[2] https://www.pid-tuner.com/pid-control/ [visited on 10/01/2021]
[3] https://www.elprocus.com/the-working-of-a-pid-controller/ [visited on 10/01/2021]

Where e_k indicates the error between the desired set point and the process variable, u_k is the output of the PID controller, K_p is the proportional gain, T_i the integral gain and T_d the derivative gain. Knowing the controller's update time, dependent on the hardware the control program runs on, the sampling time (T_s) can be determined. The value of n_t depends on how much history is dedicated to integral control.

Control System Architecture The control system is depicted in Figure 9.24 and described below. The architecture is split up in different controller blocks which contain one or more PID controllers.

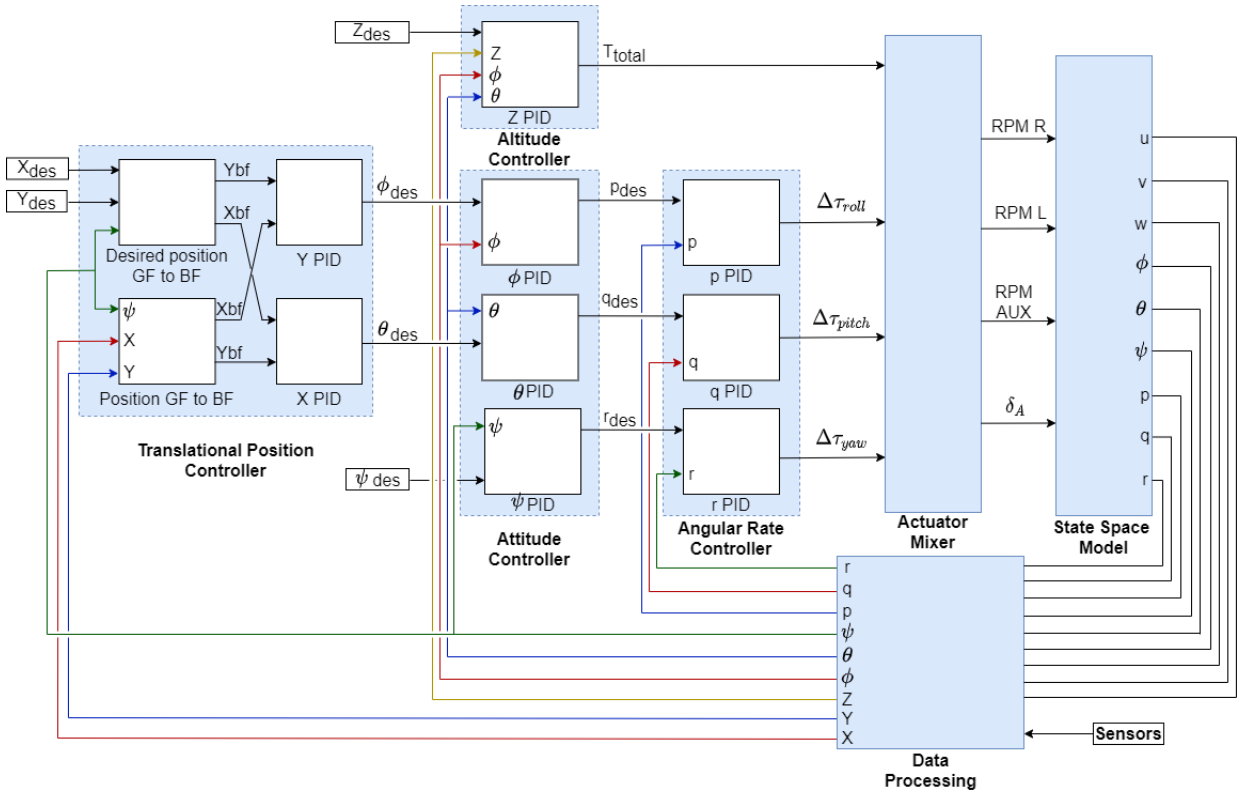

Figure 9.24: Hover control architecture

The translational position controller relates the coordinates to an attitude that makes the vehicle fly along the flight trajectory. The inputs into the control program get loaded in the translational controller block along with their feedback counterparts. After transformation, the body coordinates are plugged into a PID controller to calculate the desired roll and pitch angles. This output is saturated such that the actuator can not exceed its physical limits.

Controlling the altitude during hover is directly related to the total thrust produced by the UAV. However, the total thrust also influences the translational motion. Due to the control strategy assumptions, the vertical acceleration is decoupled from attitude angles. The altitude PID controller takes the z coordinate from the control program input, some feedback angles and the vehicle's weight to compute the total thrust required for all engines.

The attitude controller's task is to compute the necessary angular speeds to move the aircraft in the desired attitude. In this new state, the vehicle's cumulative thrust vector is pointed in the desired direction. The angular speeds are determined by means of a PID controller, the desired Euler angles and the feedback ones.

Using the error between the desired angular rates and the current angular rates, the angular rate controller calculates the moment input needed to achieve this rate difference.

These moment inputs must be communicated to the vehicle. The actuator mixer calculates the necessary RPMs for the 3 motors and the aileron deflection. This block contains no PIDs, it is a calculator that converts the output of the control system to the physical UAV control inputs. These signals are then translated to the

appropriate actuator protocol. The calculator's general relation is shown in Equation 9.58.

$$\begin{bmatrix} F_T^b \\ \tau_\phi \\ \tau_\theta \\ \tau_\psi \end{bmatrix} = \begin{bmatrix} 1 & 1 & 1 & 0 \\ 1 & -1 & 0 & 0 \\ 1 & 1 & -1 & 0 \\ 0 & 0 & 1 & 1 \end{bmatrix} \begin{bmatrix} \omega_{\text{left}}^2 \\ \omega_{\text{right}}^2 \\ \omega_{\text{aux}}^2 \\ \delta_a \end{bmatrix} \tag{9.58}$$

With F_T^b the thrust force in the body reference frame, τ torque related to its respective Euler angle, ω the rotational speed of a rotor and δ_a the cumulative aileron deflection.

9.8. Transition Flight

Transition is a complex flight regime to discuss. Due to time limitation, this report does not provide a concrete control architecture for this regime, but attempts to understand its limitations by analysing the transition model and control architecture of existing analytical and experimental research. Starting with a general description of the transition principle (subsection 9.8.1) and its common pitfalls (subsection 9.8.2) before moving on to how a transition looks like for the Healios UA (subsection 9.8.3). This qualitative presentation attempts to lay a foundation for future controller design work.

9.8.1. Transition Principle

Most of the research done on tilt-wing aircraft has been focusing on the hover and transition regime, not so much on cruise. As the flight envelopes relating to the tilt-wings cruise and hover flight condition are disjoint, transition provides a principle to connect these disjoint flight envelopes by means of a generated transition trajectory. Representing the physical states of the vehicle, which are inherently continuous, by a discrete system is possible as long as the mission computer's logic to switch from one flight regime to another is well defined [33].

Control can be simplified by assuming that the transition is purely symmetric. The state matrix elements according to the lateral speed in Y direction (global reference frame), roll and yaw angles can be assumed to be zero. That way, the generated transition trajectory only contains values related to the pitch angle and speeds along the X and Z axes (global reference frame).

When the limitation of the dynamics have been taken into account properly when modelling and controlling the transition, the tilt-wing is perfectly flyable in all three flight regimes.

9.8.2. Common Pitfalls and Solutions

The wing stall during transition is unfavourable [34]. Not only does it cause erratic dynamic behaviour that is hard to predict, its consequences are more broad. Wing stall during transition causes an increase in power required as well as extensive vibration and buffeting. If the engines are not capable of delivering this extra acceleration to decrease the local angle of attack of the wing, the vehicle pitches down until the flow is reattached. When this happens close to the ground, it can cause emergency situations. Thus, the goal is to minimise the risk of entering a stall. Several methods to mitigate this risk include: the application of high lift devices, increase of chord or choosing another airfoil. Basically, increasing the lift for the same angle of attack so the flow stays attached longer.

There are limitations on how fast the vehicle can accelerate during the transition. To prevent a stall, the transition must be flown in a very specific way at a very specific velocity range. When this velocity range is computed for every tilt angle and plotted, the resulting plot is called a transition corridor. Such a transition corridor, example shown in Figure 9.26, can be constructed using 5 distinct operating velocities [35]:

- **Point 1**: the forward velocity at hover, usually this is equal to zero (starting point in graph)
- **Point 2**: the maximum forward speed in hover (higher limit)
- **Point 3**: the maximum forward speed during transition at a wing tilt angle of 45° (higher limit)
- **Point 4**: the maximum forward speed during horizontal flight (higher limit, end point in graph)
- **Point 5**: the minimum forward speed during horizontal flight (lower limit, end point in graph)

It was decided to do the transition using a pre-generated reference trajectory. The autonomous vehicle can change its state during the transition manoeuvre as long as the position error is such that it does not result in a flight condition outside of the transition corridor.

9.8.3. Transition for the Healios UA

Remarking that the main goal during transition is to mitigate the stall condition such that loss of altitude is prevented, a main strategy for the transition modelling and control is described.

After take-off, a maximum hover limit is set as 10m AGL. This limit is chosen such that in the case of a partial engine failure during hover and if the engines are shut off at such a low altitude, the propeller keeps its partial rotational velocity which slows down freefall and decrease possible damage to the vehicle [36]. This maximum hover altitude limit is similar to what a helicopter would do in a comparable situation.

To check whether the Healios would not enter a stall at a specific tilt angle, a python script was written to compute the necessary velocity to keep the local angle of attack below 15°, which is the stall angle of attack. For this wing stall analysis, it is assumed that the local airspeed over the wing is the vector sum of the induced velocity from the rotors and the freestream velocity. Then, the angle of attack can be calculated using the wing tilt angle (i_p). A simple model such as the one shown in Figure 9.25 can be used for the computation.

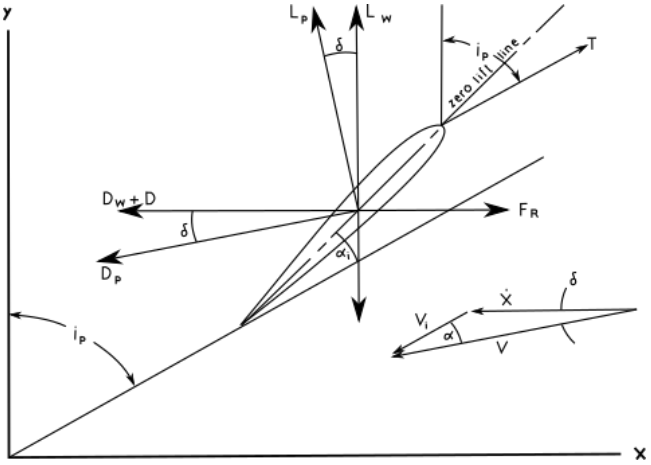

Figure 9.25: Forces on a tiltwing aircraft [36]

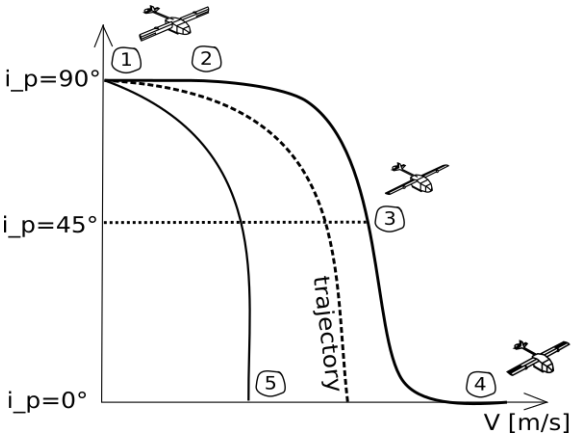

Figure 9.26: Conversion corridor [37]

In Figure 9.25, V represents the velocity, V_i the induced velocity, V_{inf} the freestream velocity, i_p for the wing tilt angle and a for α (local angle of attack). Where V can be decomposed in its freestream and induced components. Now, a relation between the x and y component of V can be found using the figure:

$$\frac{V_x}{V_y} = \tan(\alpha + 90° - i_p) \tag{9.59}$$

As V_y only consists of the vertical component of the induced velocity if the freestream is assumed to be horizontal only, V can be computed for every tilt angle as well as its associated acceleration. This would mean that to keep the wing from stalling, an accelerated climb should be performed during the transition flight regime. Equation 9.59 can be used to determine a possible path in the conversion corridor, taking into account the singularity at i_p equal to 15°. For a more accurate corridor representation, all forces should be modelled such that a more accurate representation can be given of the transition corridor. As the thrust is tilted forward with the wing, the y component of the thrust does not provide adequate lift for the vehicle anymore, thus the y component of the lift should be such that the aircraft is in equilibrium again.

9.9. Verification and Validation

In the design of any aerospace system is it crucial to perform verification and validation to ensure the system behaves as expected and produces reliable and meaningful results. Validation cannot be performed at

this stage of the design due to a lack of real-life testing data (from a test flight or wind tunnel experiment) to compare the results. However, verification should and was performed for the tools used to analyse the control and stability of the vehicle. In particular, this section focuses on comparing the obtained eigenvalues for cruise and hover to those corresponding to similar vehicles. It is assumed that if the computed eigenvalues have the correct shape and location, and represent the typical eigenmotions of similar vehicles, then the used methodology has been verified.

9.9.1. Verification of Cruise Analysis

To verify the eigenvalues related to cruise, the Cessna Citation II (Model 550) aircraft is used as a reference. This aircraft is used for two reasons: firstly, the Healios vehicle is essentially a conventional aircraft in cruise configuration; secondly, and most importantly, a complete set of stability derivatives and eigenvalues were readily available from literature for this vehicle. Stability derivatives for the reference vehicle were taken from [25]. The eigenvalues corresponding to the various eigenmotions of the vehicle are also provided in [25]. This allows for two different verification steps to be performed. Firstly, the stability derivatives were used to compute the eigenvalues of the reference aircraft. These matched those presented in [25], which verifies the scripts used to compute the eigenvalues based on a set of given stability derivatives.

Secondly, the stability derivatives of the Healios vehicle are verified by comparing the found eigenvalues with those of the reference vehicle. The comparison of the eigenvalues corresponding to the longitudinal eigenmotions are shown in Figure 9.27; those for the lateral eigenmotions are shown in Figure 9.28.

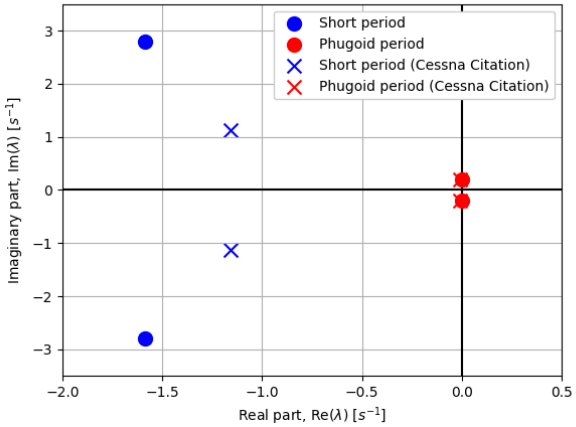

Figure 9.27: Verification of symmetric cruise eigenvalues

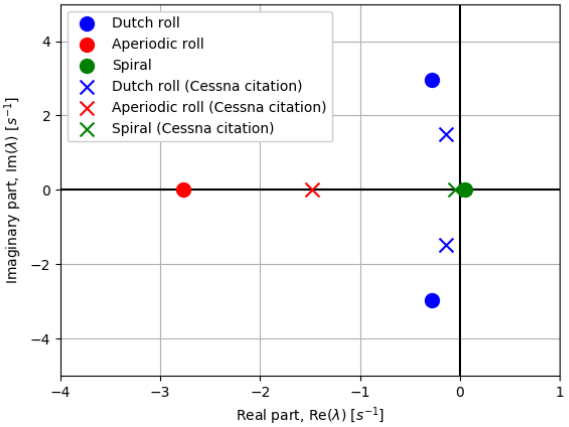

Figure 9.28: Verification of asymmetric cruise eigenvalues

It can be seen from Figure 9.27 and Figure 9.28 that the computed eigenvalues have the correct size and location, which verifies that they represent the correct characteristics motions of the vehicle. In the symmetric case, both the short period and the phugoid motion appear to be represented accurately. The only difference with the reference vehicle is the fact that it has a stable phugoid motion (this is slightly difficult to see in Figure 9.27, but the eigenvalues corresponding to the phugoid lie within the left half of the plane). In the case of the Healios vehi,cle this motion is unstable. This difference is attributed to the differences in configuration and geometry between the two aircraft, which evidently results in different values for the stability derivatives. This is deemed acceptable since a more accurate analysis of the stability needs to be performed at later stages of the design (see Section 9.12). The focus here is placed on checking the structure and location of the computed eigenvalues, which in this case verify the computed stability derivatives and methodology employed to analyse the symmetric eigenmodes of the vehicle during cruise.

In the case of asymmetric motions, the eigenvalues are verified by Figure 9.28. The reference aircraft also possess an two non-oscillatory eigenmodes (the aperiodic role and the spiral). The spiral appears to be stable for the reference vehicle, although flight tests have demonstrated it to be slightly unstable in practice [25]. The oscillatory Dutch roll also matches exceptionally well with that of the reference vehicle. This

verifies the asymmetric motions as well, demonstrating that the analysis performed to analyse the cruise performance of the vehicle produces reasonable results.

9.9.2. Verification of Hover Analysis

Verification of the analysis of the vehicle during hover is analogous to that of cruise. In this case the reference vehicle is a tilt-rotor aircraft, namely the Bell XV-15. The reference eigenvalues are taken from [38]. A comparison of the eigenmotions corresponding to the longitudinal motion is shown in Figure 9.29, while those corresponding to the lateral eigenmotions are shown in Figure 9.30.

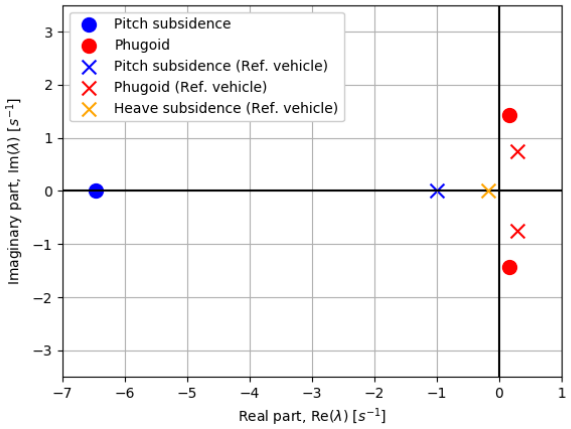

Figure 9.29: Verification of symmetric hover eigenvalues

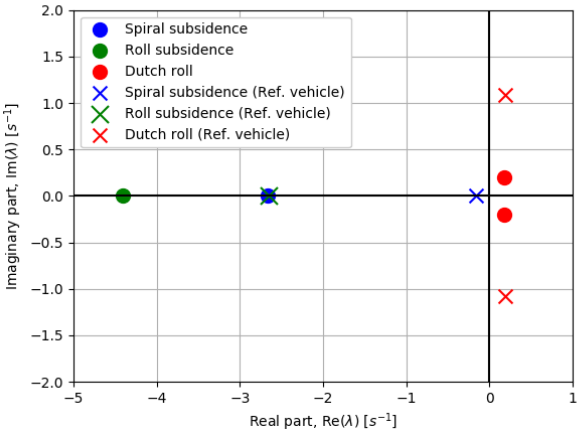

Figure 9.30: Verification of asymmetric hover eigenvalues

In the case of the symmetric motions (Figure 9.29), the pitch subsidence and phugoid appear to match very well with the reference vehicle. Nevertheless, the reference vehicle clearly also has an eigenvalue corresponding to the heave subsidence, which the methodology presented in this Chapter failed to reproduce. This is due to the simplifications made to the A matrix of the state space model corresponding to the hovering conditions. It is possible that by neglecting some of the stability derivatives this eigenmotion was lost. Upon further investigation it was found that the derivatives Z_α and M_α have significant effect for the heave subsidence [39]. The lack of an eigenvalue corresponding to the heave subsidence is attributed to the fact that both of these derivatives were neglected in the analysis. This verifies the method but demonstrates that a more accurate determination of the stability derivatives during hover (from measurements from a wind tunnel experiment or a flight test) would greatly improve the accuracy of the results.

The longitudinal eigenvalues match extremely well with those of the reference vehicle (Figure 9.30). Two aperiodic modes are present (spiral and roll subsidence), in addition to one oscillatory mode (Dutch roll). In this case, the simplifications made to the A matrix appear to yield perfectly reasonable results, including the correct number, location, and structure of the eigenvalues. This further verifies the method itself. The issue of accuracy in the estimation of the stability derivatives remains open and should be the focus of future work.

9.10. Risk Analysis — Failures and Emergency Protocols

An emergency situation would be defined as any state of the vehicle that is not part of the nominal set of operations. Components can fail, and it is important to analyse these failures before they happen. When every risk is identified, appropriate risk mitigation can be applied to the design of the UAV. If the autonomous vehicle encounters one of these failures, the program computer knows what to do since the mitigation strategy is present in memory. This section aims to give an explanation of how the vehicle complies with the failure related regulations set out by the aviation safety authority.

In the case of hover for a conventional helicopter, a region called the dead man's curve is defined in the plot relating to the relation of altitude and flight velocity. The main idea is that, in case of a catastrophic failure,

the helicopter should have enough energy to perform autorotation. This can be done by converting enough kinetic or potential energy to kinetic energy of the rotor blades. Hovering at low altitudes and speeds just after take-off or before landing can be risky as well. If the engine fails in such a situation, the blades still contains a residual rotational speed. If the altitude is kept low enough, this residual rotational speed can allow the helicopter to land safely with the diminishing thrust it still has. This principle is also applied to the tilt-wing UAV.

To ensure flight loads are kept within bounds, actuator control signals are saturated to an acceptable minimum and maximum deflection. This section defines an actuator failure as a condition where the actuator is not functioning as expected. This can be due to any internal failure of the component itself. Except in a case where fire is detected. In this situation, the UAV must land as quickly as possible to prevent damage to personal property.

9.10.1. Hover Emergency Protocol

After take-off, to mitigate the risk of engine failure and reduce the amount of engines required for multi-engine reliability, the maximum hover altitude is set to 10m. This way, all engines are shut off in case of an engine failure during hover and the aircraft touches down by means of the residual rotational velocity as described above for the helicopter case. During the transition, a climb is initiated to keep the wing from stalling. When an engine failure occurs during this flight phase, the engines are shut off and the wing must be rotated at a faster rate than would be the case in nominal operations. If the wing is rotated to the horizontal position, the UAV can perform either a horizontal landing directly at a contingency site or at a resupply centre depending on the severity of the failure. These contingency landing sites and their appropriate approach trajectory are constantly considered by the path planning algorithm. The higher the flight altitude, the more time the vehicle has to consider more contingency sites than already calculated by the flight path planner. The UAV then loiters with both engines off until the abundant speed and altitude is bled off and the approach trajectory can be initiated.

Performing horizontal landing manoeuvres would result in catastrophic damage to the rotors, and potentially damage the landing skids as well, since these are designed for VTOL operations. Tests should be performed to test its effectiveness and propeller damage during horizontal landing. If the skids do not perform as desired, they should be replaced by land sleds or even wheels. In any case, these horizontal landing manoeuvres would only take place if absolute necessary, and they will need to be studied in more detail in future design iterations.

9.10.2. Control Surface Failure

Apart from an engine failure, the other control actuator failures have to be taken into account as well. The classic control surfaces which have been taken from a fixed-wing aircraft have inherent redundancy built into the design. Ailerons work as redundancy for the rudder and vice versa for directional control. If both are compromised, the engines can be used for differential thrust application to create a yawing moment. If the control architecture and internal system model is such that it gives an accurate depiction of the forces and moments of the vehicle, it also accommodates all the redundancies described above.

For longitudinal control, the control moments about the centre of mass are controlled by the main engines, auxiliary engine and elevator. Auxiliary engine and elevator are considered each other's backup to compensate the moment in the event of a failure. In a situation where both these actuators are out of function, no longitudinal control is guaranteed. As a redundancy, an extra flight mode can be built and loaded in the flight controller to give the ailerons authority to perform elevon functionalities. To conclude, all these functionalities depend on how well the control architecture is designed. If these failures are taken into account during the design and implementation of the control program the Healios UAV is able to successfully perform the logistic mission as well as the user supply mission with triplex redundant directional and longitudinal control. If a failure occurs during flight, it is able to land safely. Cases where the vehicle would be unable to hover or perform transition, are labelled critical failures since they compromise mission completion.

9.10.3. Auxiliary Engine Failure

A special case of failure would be related to auxiliary engine failure. This kind of failure would compromise the controllability in hover. Redundancy can be provided by the use of the elevon flight mode described above. When the wing is tilted upward, the elevons allow pitching control to balance the longitudinal moment created by the main engines. In cruise, the auxiliary engine is turned off. A heartbeat signal is sent to the mission computer by every actuator. Its logic detects the faulty actuator through its missing heartbeat signal. Then, it determines which flight mode must be communicated to the flight controller.

9.10.4. Wing Actuator Failure

The actuator which controls wing tilting is related to one of the most critical failures the Healios UAV can encounter. If it fails on its own, a horizontal landing can be performed where control can be guaranteed by triplex redundancy. Hover would not be possible and the mission is compromised. Thus, the tilting mechanism failing is defined as a critical failure. Any cascading failures on top of a wing actuator failure results in an uncontrollable vehicle. Future design iteration should aim to understand the failure modes described in this section more thoroughly. Experimentation should be able to determine if failures which are cascaded on top of critical failures can be mitigated by the use of control or if a ballistic rescue parachute should be added as a last resource.

9.10.5. Data Handling During Emergencies

In an emergency situation, the flight controller is instructed to land horizontally if necessary. The transition altitude is chosen at 10m such that when an emergency is declared in hover, the engines are disarmed and the aircraft has minimum damage due to the partial lift of the de-spinning propellers. No damage should be present to the payload container in this case. In case of a hardware failure, a preset flight trajectory generated by the flight panning software is flown. In the case this is not possible, a grave emergency is called and the human operator is notified to engage a manual override. To incorporate the manual override, the RF control receiver has auxiliary data connections to the control surface actuators so a glide to horizontal landing can be performed. The human operator should be trained to react within two seconds to take control of the aircraft when it is not possible to autonomously control itself. In case of a partial battery failure, assuming the battery does not fail completely since it is split in separate modules, the mission computer needs to evaluate how much energy is left and act accordingly. A small reserve battery could be included to provide auxiliary power to a low-voltage bus to ensure communication can be maintained during an emergency.

Machine vision is used for obstacle avoidance, which is defined as an emergency situation. During the flight, the optical sensors perform 360-degree scans constantly analysing the images through the graphical processor. When an obstacle is detected, an interrupt is send to the flight controller overriding the desired Euler angles and motor inputs to prevent collision. Since a machine vision system based on a neural network is defined as a non-deterministic system, it may present problems with regards to the key requirement of ensuring certifiability by 2025. Although not ideal, this is not impossible to certify. The plan is to certify the machine vision system based on certification by similarity. This principle allows the certification of non-deterministic systems by proving that they their performance is, at minimum, equal to that of a trained human pilot. In this case, the chosen benchmark is the fact that humans need to see and react to an obstacle in under 12.5 seconds to prevent a collision. Thus, the system is certifiable if is proven that the systems can react faster than a safe human pilot [40].

9.11. Sustainability

The control system design was influenced by the sustainable development strategy on three different fronts; social, economic, and environmental sustainability. Social sustainability mainly influences features that relate to the safety of the UAV, such as safety protocols and redundancies within the control system that minimises the risk of people getting injured. Further, the flight planning software, which avoids areas with higher population densities, ensures that the 'livability' of areas is not reduced. The economic sustainability is addressed on the hardware front by using cheaper and more durable hardware, in order to minimise the life cycle cost of the UAV. Lastly, economic sustainability is addressed by the controller design and the hardware choice. The controllers must be designed such that vehicle flies efficiently, by not accelerating fast

or not overshooting the target velocity or target altitude. As for the hardware, hardware can be chosen that has a lower carbon footprint.

9.12. Future Recommendations

The work presented in this Chapter provides an overview of the stability and controllability of the Healios vehicle. Nevertheless, future design iterations are required to further investigate certain aspects of the design of the Control and Stability subsystem of the vehicle. This section briefly describes some of those items. These should be the focus of further work related to the stability and control of the Healios UAV.

Firstly, a significant amount of resources should be allocated to the detail study of the transition phase. The eigenmotions of the vehicle should be studied in transition. Furthermore, a conversion corridor for the Healios vehicle should be constructed. In addition, the non-linear flow around the propellers, wing, and aerodynamic surfaces during transition should be studied. The occurrence of flow separation should be understood and reported, and the aerodynamic design (of the wing and the control surfaces) should be iterated accordingly.

This detailed analysis of transition could be aided by performing wing-tunnel testing on a scale model of the vehicle. This could provide valuable information such as the stability derivatives at various points in transition, similarly to the work performed by Chambers and Grafton [29, 30]. Furthermore, the data obtained from wind tunnel testing could be used to construct more accurate models of the vehicle during cruise and hover. Additional resources could be spent on performing CFD analysis of the model. This type of analysis, in conjunction with real life data obtained from wind-tunnel tests, should be used to perform the next design iterations of the vehicle, until a suitable design is found, verified, and validated.

Another key point for future design iterations is the improvement of the current control architectures. Although the presented cruise controllers are functional and can provide control of the vehicle, they can be improved. Implementing PID controllers instead of the used proportional controllers could improve the closed-loop response of the system, by for example reducing response time and overshoot. The architecture for the hover and transition controller should be implemented and tuned. Ideally, all controllers would be modelled using software such as Simulink, thus constructing a fully connected model for the closed-loop vehicle dynamics. This model could be used to test how the UAV responds to a variety of complex disturbance patterns. The model could then be adapted to analyse, test, and improve the trajectory followed by the vehicle given a set of coordinates from the flight planning software. Lastly, the controllers should be extended to include all of the emergency protocols described in Section 9.10.

Moreover, the possibility of using the tilt angle of the wing as an active control variable should be explored. This has not been explored so far since it was assumed that the sudden changes to the wing tilt angle would overwork the wing actuator and potentially cause failure of the hydraulic system. Nonetheless, this is not known with certainty and it is heavily dependent on the specific type of actuator used. For this reason, the wing tilt angle i_p has been included in the general equations of motion derived in Section 9.4. By doing so, the same equations of motions derived in the present work can be used to easily adapt the state space models and develop controller architectures that use the tilt angle as a control variable.

Lastly, additional design iterations could be done in the design of the auxiliary engine. The use of counter rotating coaxial propellers could be explored. This would result in an increase in weight and complexity. Nevertheless, it would provide redundancy and would counteract the torque generated by the auxiliary engine.

10
Power, Propulsion Performance

10.1. Design overview
The power and propulsion subsystem design incorporates the propulsion system, propeller sizing, engine selection, distribution of power and the mass estimations. All other subsystem designs influence the propulsion design and it has therefore been iterated upon numerous times. This chapter explains the different design steps taken during this subsystem design and the results and conclusions that follow.

10.2. Requirements and Functional Analysis
Before the start of a design phase, it is crucial to analyse the function and requirements of a subsystem. This ensures a fitting design solution for the problem.

10.2.1. Subsystem Functions
The subsystem consists of two main components; the power storage and the powerplant. The function of these components can be defined by its interaction with other components. It has been decided that the vehicle is fully electrical. Therefore the battery delivers not only power to the mission computer, flight controller and landing gear, but also to the powerplant during all phases of the mission. The powerplant converts this energy to forces and moments to fly and control the UAV. Both the weight of the battery and the powerplant contribute to a large part of the maximum take-off weight. By using off-the-shelf technology these weights can be minimised.

10.2.2. Requirements
The requirements established for the power and propulsion system of the UAV are represented in Table 10.1.

Table 10.1: The key and driving requirements for the power and propulsion subsystem

ID	REQUIREMENT
OP-MI-UAS-08	For the Local Delivery Mission, the UA shall not be refuelled or recharged at the delivery site.
OP-MI-PER-02	The maximum range shall be 200km carrying maximum payload.
OP-MI-PER-10	The maximum operational altitude shall not exceed 1350m above sea level.
FU-SYS-10	The on-board generation, storage, distribution and supply of power to each system shall be designed and installed to ensure no single failure or malfunction will prevent the system from supplying the essential loads required for continued safe flight and landing or emergency recovery.
FU-SYS-11	The on-board generation, storage, distribution and supply of power to each system shall be designed and installed to have enough capacity, if the primary source fails, to supply essential loads, including non-continuous essential loads for the time needed to complete the function, required for safe flight and landing or emergency recovery.
FU-PPI-10	Any single failure or likely combination of failures of a power or thrust control system shall not prevent continued safe flight and landing of the UA.
FU-PPI-18	The design shall allow in flight shutdown of any powerplant or groups of powerplants if required by continued safe flight.
FU-PPI-19	The design shall allow in flight restart of any powerplant if required by continued safe flight.
FU-PPI-22	Each system shall be designed to provide independence between multiple energy storage and supply systems so that a failure of any one component in one system will not result in the loss of energy storage or supply of another system.

Table 10.1: The key and driving requirements for the power and propulsion subsystem

ID	REQUIREMENT
SUS-SOC-REL-3	In a non-catastrophic failure scenario, the UA shall be capable of a continued safe flight for 15 minutes.

10.3. Design Approach

The full design of the power and propulsion subsystem consists of multiple steps. First of all, a sensitivity analysis was performed on the required power during horizontal and vertical flight with respect to the maximum take-off mass. This is done to have a guideline as to which configuration is optimised when design trade-offs had to be made.

To proceed to more detailed calculations, it was important to establish the propeller diameter of the vehicle. To have the optimal performance of a tilt-wing design, the propeller diameter should be maximised. This lowers the disc loading, with only small comprises in the propeller efficiency in forward flight and still being able to obtain a 0.85 propeller efficiency in forward flight [41].To ensure the largest diameter, the number of propellers was set at one propeller per wing. The maximum dimensions of the vehicle were indicated in the Request for Proposal [8]. Recognising the required clearance of the propeller, the diameter was established. [8] As a result of having only one propeller per wing, a single-engine failure would lead to a catastrophic failure. This problem was mitigated by deciding that the propeller is driven by a twin-engine system with a belt drive. This ensures that if one engine fails, only half the power is lost and a safe landing can still be performed. Moreover, the mass of the power and propulsion subsystem is a big part of the total mass of the vehicle. As a result, these small changes in the power required for the flight, would lead to large changes in the calculated maximum take-off mass. This parameter again greatly influences other subsystem designs. Therefore, the powers required were established with an iterative process. With the power required found; the battery was sized, and the structural and control subsystems designed. Since the vehicle is electric and batteries can be connected in both series and parallel, a combination of these allows for partial failure while still being able to land in a safe and controlled manner. Additionally, the 20 minutes reserve was taken into account with the sizing of the batteries.

Using the estimation on the required power, the propellers could be optimised for horizontal flight. From the sensitivity study, it was clear that a propeller design that would lead to high propeller efficiency was optimal. The power required and thrust provided for the vertical flight with this propeller were calculated using the blade element method.

Once, the propeller design was known, the propeller dimensions could be used again to give more insight into the power required during the different phases of the mission. A distinction was made between the power required for the horizontal and vertical flight. The power was plotted for both modes as a function of velocity. Lastly, the engine could be selected for the full range of powers of the mission.

10.4. Design Process and Results

Firstly, the sensitivity analysis is presented, followed by the mass power iteration loop and the propeller design. This was followed by the power curves, the power and thrust of the propellers and the engine selection.

10.4.1. Influence of Flight Configurations

The objective of the power and propulsion subsystem is to deliver enough power to fulfil every part of the mission. Optimally, this is done with the highest thrust to weight ratio. However, this mission consists of two different configurations that have to be optimised for: horizontal flight and vertical flight. For simplicity in this stage, it was assumed that the transition is part of the hovering phase. Therefore, it was decided to investigate which power required (either in hover, or horizontal flight) had the biggest influence on the mass of the subsystem. The configuration that most strongly determines the mass is the configuration that is optimised for first, as the mass can create a snowball effect in the power required again. The required power is always be highest in hover and therefore this power determines the engine size. [42] Lastly, it is assumed that the continuous power required for other subsystems are negligible compared to the power

required for the propulsion. The mass of the subsystem is therefore calculated with Equation 10.1.

$$m_{pp} = \frac{P_{hover}}{U_{engine}} + \frac{P_{hover} \cdot t_{hover} + P_{cruise} \cdot t_{cruise} + P_{transition} \cdot t_{transition}}{U_{battery}} \tag{10.1}$$

In this equation, U_{engine} is the power density of the engine in kW/kg. This value has been estimated at 2.5 kW/kg. [1] Moreover, $U_{battery}$ is the energy density of the battery in Wh/kg and this value has been estimated at 400 Wh/kg.[2] The hover time and cruise time are restricted to 5 minutes for hover and 23 minutes for cruise for the local delivery mission and 3 minutes for hover and 72 minutes for the logistics mission[8]. To get a first estimate of the range of powers that can be expected for the mission, the powers required were calculated for the initial mass from the concept selection (168 kg) [2] and a mass 250 kg above this (418kg), to allow for the mass increase as a result of the design.

In hover, the thrust must equal weight and therefore by the momentum equation the power required can be described with Equation 10.2. [42]

$$P_{hover} = T\sqrt{\frac{T}{2\rho A_{disc}}} = W\sqrt{\frac{W}{2\rho A_{disc}}} \tag{10.2}$$

In this equation, the P_{hover} is the hover power in W, the weight (W) is given in N, ρ is the density in kg/m^3 that has been estimated at 1.08997 for the height given. [8] Lastly, for the disc area (A_{disc}) it was decided that the disc radius is maximised to increase efficiency. [43] The maximum radius is constraint by the dimensions of the design and clearances and therefore estimated to be 1.3 m. [8] These calculations resulted in a range of 19.7 kW for the lowest weight of the vehicle and 77.1 kW for the highest weight of the vehicle.

And the power required for cruise is given by Equation 10.3. [21]

$$P_{cruise} = \frac{1}{2}\rho_\infty V_\infty^3 A_{wing} C_{D_0} + \frac{W^2}{\frac{1}{2}\rho_\infty V_\infty A_{wing} \pi e AR} \tag{10.3}$$

In this equation, the P_{hover} is the cruise power in W, the weight (W) is given in N, ρ is the density in kg/m^3 that has been estimated at 1.0739 for the height given for cruise. [8] Next to that, the parameters for the wing design were estimated in Chapter 7: A_{wing} is 3.5 m^2 , the aspect ratio (AR) is 6. The C_{D_0} and Oswald factor for this type of aircraft can be estimated to be 0.028 and 0.78 respectively. [15] Lastly, the velocity (V) was calculated by dividing the distance that has to be covered by the available time. This resulted in a velocity for the local mission and the logistics mission in m/s. The calculated powers are given in Table 10.2.

Table 10.2: Cruise powers required for different missions at different vehicle masses

Powers (kW)	m = 168 kg	m = 418
Local Mission	27.2	39.9
Logistics Mission	54.3	65.4

From this table, it is clear, that the logistics mission is critical for the sizing and this range is used in the further comparison. The mass described in Equation 10.1 is plotted against the power required in cruise or hover in Figure 10.1. When the cruise power is the input, the hover power is kept constant at its maximum value and vice versa.

From the graph, it can be seen that a change in cruise power has a bigger influence on the mass of the subsystem. Therefore, the proprotor is optimised for cruise performance. After which the system is checked to see if it meets the hover performance requirements.

[1] https://cleantechnica.com/2020/02/19/bloombergnef-lithium-ion-battery-cell-densities%2D-have-almost-tripled-since-2010/ [visited on 25/01/2021]

[2] https://insideevs.com/news/440727/elon-musk-400-whkg-cells-not-far/ [visited on 25/01/2021]

10.4.2. Mass calculations

In order to move on from the original concept to a more detailed and specific design, parameters and requirements had to be set and further defined. During this process, the original power calculations that were used in the midterm report were used as a starting point to ensure a consistent approach. An overview of the method to compute the power loading required for the mass calculations can be found below. Because the hover and transition power could be calculated using the old system, and the cruise power could be estimated based on general aircraft performance calculations, the total mass of the vehicle and accompanying features could be found. The method for calculating initial hover and transition power is explained below and comes from Kamal and Ramirez-Serrano.[44]

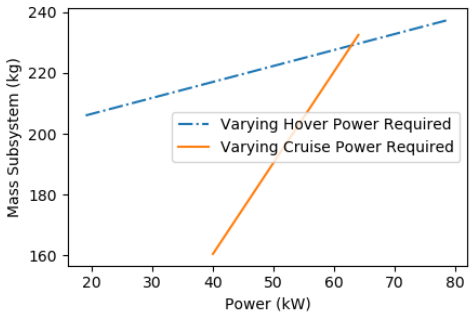

Figure 10.1: The influence of the power required on the mass of the subsystem

The hover power loading is given by:

$$(PL) = FoM\sqrt{\frac{2\rho}{(DL)}} \tag{10.4}$$

where FoM is the figure of merit, ρ is the density at 1200 m, and DL is the disk loading. This figure of merit was kept below 0.73 by tweaking the number of blades and angular velocity while still complying with all other ranges.

The transition power loading is given by:

$$(PL) = \frac{1}{\frac{k_i}{\sin(\theta_{\text{tilt}})}\sqrt{\frac{-V_\infty^2}{2} + \sqrt{\left(\frac{V_\infty^2}{2}\right)^2 + \left(\frac{(DL)}{2\rho\sin(\theta_{\text{tilt}})}\right)^2} + \frac{\rho V_{Tip}^3}{(DL)}\left(\frac{\sigma C_d}{8}\left(1+4.6\mu^2\right)\right) + \left(0.5\rho_o V_\infty^3 C_{Do}\frac{1}{(WL)} + \frac{2K}{\rho_o V_\infty}(WL)\right.}} \tag{10.5}$$

where V_∞ is the freestream velocity during the transition, θ_{tilt} and α_{rotor} are two relevant angles explained below, C_{D_0} is the zero-lift drag coefficient of the vehicle, μ is the advance ratio given by Equation 10.6, and K is given by Equation 10.7 where e is the vehicle's Oswald efficiency factor, and AR is the aspect ratio.

$$\mu = \frac{V_\infty \cos(\alpha_{rotor})}{V_{\text{tip}}} \tag{10.6}$$

$$K = \frac{1}{\pi e AR} \tag{10.7}$$

Here θ_{tilt} is the angle between the rotor axis and the vehicle's longitudinal axis (measured counterclockwise), while α_{rotor} is the angle between the rotor disk and the freestream velocity.

The required power in aeroplane configuration for the cruise period of the mission is given by:

$$Pr = (0.5\cdot\rho_{cruise}\cdot V_\infty^3\cdot S_w\cdot CD_{0cruise} + ((W^2/(0.5\cdot\rho_{cruise}\cdot V_\infty\cdot S_w))/(\pi\cdot e\cdot AR_{wing})))/\eta_{propulsive} \tag{10.8}$$

Where $\eta_{propulsive}$ is the efficiency between the engine and propeller which is assumed to be 0.85. [41]

Using these preliminary power estimations a method was developed to calculate the mass. This was done in the following manner:

Using the requirements from the VFS Request for Proposal [8], the mission duration and required velocity in all stages of the mission were defined. This was done by applying time duration's and power requirements to each part of the mission. Then, knowing the cruise altitude and estimating general aeroplane performance in climb and descent the time and distance to climb and the descent was calculated. This was done using the procedure explained below.

Using simplified power curves based on aeroplane performance, the maximum power discrepancy between the power available and required was found. The value of this discrepancy is the climb power. Additionally, a climb angle of 11 deg was chosen as climb angle based on climb angles of other aircraft. [45] From this climb angle and available power, the required time to climb and horizontal distance to climb was found. Using these parameters, the cruise time and distance were redefined.

This was done using the following relation:

$$t_{cruise} = t_{block} - t_{hover} - t_{transition} - t_{unload} - 2 \cdot t_{climb} \tag{10.9}$$

Then, using all these power and time inputs the required battery mass could be calculated based on the initial maximum take-off mass. Assuming a mass fraction of 0.4, the new maximum take-off mass was calculated by subtracting $0.4 \cdot MTOM$ and adding the new battery weight. This iteration was then performed until convergence, after which the maximum take-off mass was communicated with the other subsystems and continuously updated and iterated when new masses were found and set as constants. Ultimately this iteration loop was combined with all subsystem design groups and led to the final conclusion of a maximum take-off mass of 355 kg.

10.4.3. Propeller Design

For the propeller design, multiple options were available. One could choose and pick a propeller that fits with the requirements or a specific new propeller can be designed. Since the vehicle has fairly specific requirements given the fact that the propellers need to be rotors as well, a first design has been made. This was done using the validated JavaProp programme. This programme is based on the theory of Design of optimum Propeller. [46] The theory uses a combination of momentum and circulation calculations and then optimises for the lowest energy loss and therefore highest efficiency. This program only requires very few inputs which were perfect for this stage of the design. Using the number of blades, RPM, diameter, spinner diameter, horizontal velocity, required power, and aerofoil, the program designs a propeller that is optimal for the use case. For the aerofoil, the Clark Y was chosen since it is a commonly used aerofoil about which a lot of information can be found.

The output of the programme includes but is not limited to, the geometry of the propeller, the aerodynamic coefficients, thrust available, and a predictive flow field. The approach to the propeller design was to design a propeller that is efficient in cruise but can deliver the required power for hover. As has been explained before, the decision was made to maximise the propeller diameter. This was done by the following calculation:

$$d_{\text{propeller}} = \frac{\text{wingspan} - \text{width}_{\text{fuselage}} - \text{clearance}}{2} \tag{10.10}$$

It was then rounded down to decimetres. This way there is a little extra margin to accommodate for manufacturing or placement issues. The clearance used is 2.54 cm which is in accordance with the clearance requirements [15]. Using this diameter of 2.6 m and the original inputs from the cruise stage the propeller design can be made. Then, by modifying the geometry and iterating with the power calculations explained below, the final propeller design can be made. The geometry of one of the three propeller blades can be seen in Figure 10.2. Additionally, the values for twist, chord, and thickness along the radius of the blade are shown in Table 10.3. Note that the parameters are not displayed at r/R is 0 because at that point there would be a spinner and no blade.

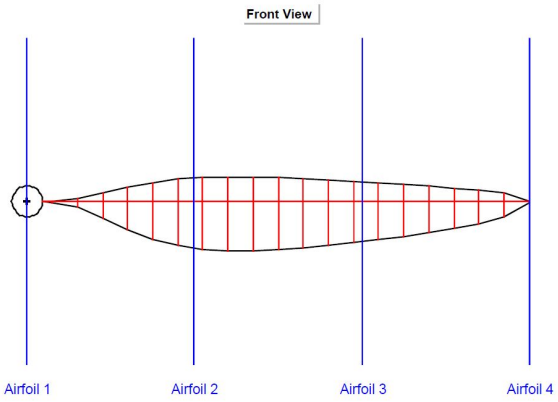

Figure 10.2: Geometry of one propeller blade

Table 10.3: 3 Bladed Propeller Geometry

r/R [-]	β [°]	c [mm]	t [mm]
0.0500	79.1	18.0	2.2
0.1000	69.0	68.3	8.3
0.1500	60.2	129.3	15.7
0.2000	52.7	180.0	21.9
0.2500	46.5	212.8	25.9
0.3000	41.3	229.2	27.9
0.3500	36.9	233.7	28.4
0.4000	33.3	230.3	28.0
0.4500	30.3	222.2	27.0
0.5000	27.7	211.5	25.7

r/R [-]	β [°]	c [mm]	t [mm]
0.5500	25.5	199.1	24.2
0.6000	23.6	186.0	22.6
0.6500	22.0	172.4	21.0
0.7000	20.5	158.2	19.2
0.7500	19.3	143.5	17.4
0.8000	18.1	127.8	15.5
0.8500	17.1	110.3	13.4
0.9000	16.2	90.0	10.9
0.9500	15.4	63.6	7.7
1.0000	14.6	3.2	0.4

Mass and cost of the propeller From a weight and sustainability perspective, a composite propeller would be the best fit with the current design. Therefore a study into composite propeller manufacturers was performed and one suitable manufacturer was chosen such that a mass estimation could be made. Based on their biggest propeller and taking into account a margin of 1.25 % the propeller mass can be estimated to be 10 kg per propeller. Regarding the cost, the biggest propeller costs around 700 euros, therefore it was estimated that these propellers will cost around 1000 euros. [3]

10.4.4. Power Curves

Once the parameters of the propeller had been established, power curves could be constructed. This was done to gain more insight into the different powers required throughout the mission. A separation for this is made between the VTOL configuration and the cruise configuration.

Vertical Flight Configuration The power required is a summation of the induced power, the parasite power and the profile power. To start off, the parasite power is the power required to overcome the drag of the body and wing. It was calculated with the drag coefficients and reference areas that were estimated in Chapter 7 and Chapter 8. Note, that it was assumed that the interference drag was negligible. [47]

$$P_P = \frac{1}{2}\rho V^3 (C_{D_{wing}} S_{wing} + C_{D_{body}} S_{body}) \tag{10.11}$$

In this equation P_P is the parasite power in W, ρ is the density in kg/m^3, which is 1.07393, the C_D is the drag coefficient and S is the reference areas in m^2. The drag coefficients are 0.03 and 0.2 for the wing and the body respectively. The value for the wing has been estimated in Chapter 7 and the value for the body was set as a goal to design the fuselage shape for. The reference areas are 0.74 and 3.34 for the body and wing respectively. Again these values have been established in Chapter 7 and Chapter 8.

Next to that, the profile power is the power required to rotate the blades through the air. This power can be calculated with Equation 10.12 and Equation 10.13. [42]

$$P_0 = 2C_{P_0}\rho A_{disc} V_{tip}^3 \tag{10.12}$$

$$C_{P_0} = \frac{\sigma C_d}{8} \cdot (1 + 4.6\mu^2) = \frac{NcC_d}{\pi R 8} \cdot (1 + 4.6\mu^2) \tag{10.13}$$

In this equation P_0 is the profile power in W, ρ is the density in kg/m^3, which is 1.07393, the C_{P_0} is the profile power coefficient and A_{disc} is the disk area in m^2, which is 5.309. The V_{tip} is the tip speed, which is 248 m/s. The solidity (σ) is calculated with the number of blades (N), the average chord (c) of the blades and the radius (R) of the blades. These values are 3 blades, 0.142m and 1.3m respectively. The C_d is the

[3] https://shop.mejzlik.eu/all-products/ [visited on 15/01/2021

average drag coefficient of the blades, which is 0.015 and lastly, the advance ratio can be calculated with Equation 10.6.

Lastly, the induced power is defined as the power required to overcome the induced drag of the blades. It can be calculated according to Equation 10.14 and Equation 10.15. [42] [48]

$$P_i = \frac{(W f_{vd})^{\frac{3}{2}} K_h}{\sqrt{2\rho A_{disc}}} \tag{10.14}$$

$$\frac{V}{U_h} = \frac{V}{\sqrt{\frac{W f_{vd}}{2\rho A_{disc}}}} = \sqrt{\frac{1}{K_h^2} - K_h^2} \tag{10.15}$$

Here P_i is the induced power in W, K_h is the induced velocity, W the weight in N, which is 3482.55 and the f_{vd} the download factor to account for the download of the vertical drag, this value can be estimated to be 1.03 [48]. Again ρ is the density in kg/m^3, which is 1.07393 and A_{disc} is the disk area in m^2, which is 5.309. V is the velocity in m/s and U_h is the induced rotor inflow velocity in m/s.

The results for this can be represented in a graph with the powers as a function of the forward velocity, see Figure 10.3.

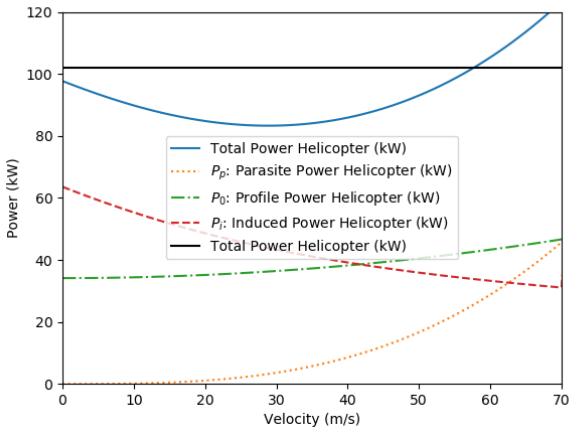

Figure 10.3: Power curve for the vertical flight configuration

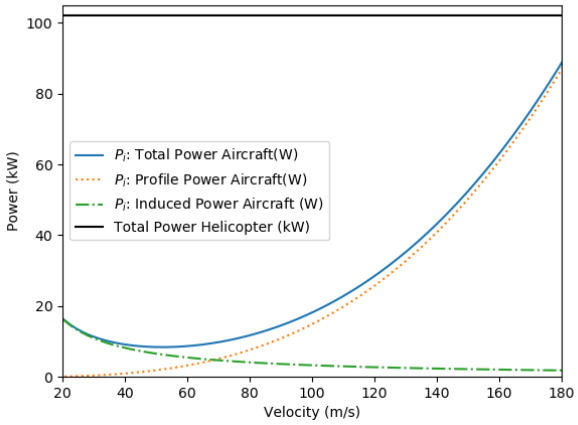

Figure 10.4: Power curve for the horizontal flight configuration

Horizontal Flight Configuration In horizontal flight, a distinction can be made between the parasite power and the induced power.

The parasite power is the power required to overcome the drag as a result of the shape of the vehicle and the skin friction. It can be calculated with Equation 10.16.

In this equation P_P is the parasite power in W, ρ is the density in kg/m^3, which is 1.07393, the C_{D_0} is the zero-lift drag coefficient, which has been estimated to be 0.044 in Chapter 7 and S is the reference areas in m^2m which is 3.34 m^2. Lastly, V is the forward velocity in m/s

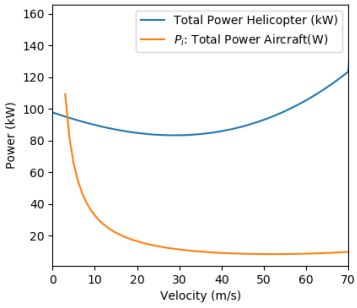

Figure 10.5: The power curves for the total powers of the horizontal and vertical flight

$$P_P = \frac{1}{2}\rho S C_{D_0} V^3 \tag{10.16}$$

$$P_i = \frac{W^2}{\frac{1}{2}\rho V S \pi e AR} \tag{10.17}$$

The induced power is the power required as a result of the vortices at the tip of the wing. It is calculated with Equation 10.17. In this equation P_i is the induced power in W, the weight (W) is 3482.55N, ρ is the density in kg/m^3, which is 1.07393, and S is the reference areas in m^2m which is 3.34 m^2. The Oswald factor (e) and the aspect ratio (AR) have been decided to be 0.78 and 10.4 in Chapter 7. Lastly, V is the forward velocity in m/s. The summation of the powers can be seen in Figure 10.4.

A combination of the total power for the helicopter configuration and aircraft configuration can be seen in Figure 10.5. It is clear that more power is required for the hovering flight already from a low forward speed. Therefore, the transition is entered from a minimal forward speed to quickly convert to horizontal flight with the aircraft configuration. It was clear from the sensitivity analysis that the design has to be optimised for forward flight. However, due to the fact that the curves are separated heavily, it might be interesting to calculate the effects on the weight if the design was adjusted to perform better in hover as well.

Transition One of the greatest challenges for a tilt-wing is the transition phase, during which stall can lead to an exponential increase in required power. It was estimated from a control perspective that the transition time is 15 seconds. One of the advantages of this transition time is that according to McCormic and Miller (1957), the power required in transition never exceeds the power required in hover. [36] Therefore, on a mission of either 2 times 28 minutes or 75 minutes, the influence on the total energy is limited. For the calculation of the total power required, the transition has to be further analysed. Which is considered outside of the scope of this project. [41]

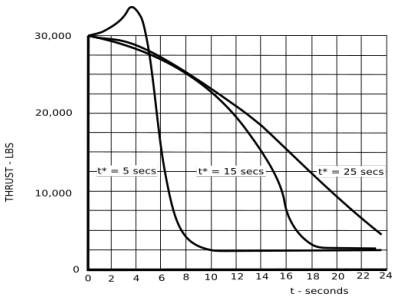

Figure 10.6: Relation between transition time and power

10.4.5. Thrust of the Propeller

Hover performance It was decided to apply the blade element theory to investigate if the propeller can provide sufficient thrust in hover. This theory relates to the forces and moments generated by the motion of the rotor through the air. The forces of a section of the blade are defined by the lift and drag coefficients. To get the total force, these parameters were integrated over the whole radius of the blade. The theory assumes a high aspect ratio for the propeller and a low disk loading.[42] The thrust coefficient can be calculated with Equation 10.18

$$C_T = \int_0^1 \frac{\sigma C_l R^2}{2} dR \tag{10.18}$$

In this equation, C_T is the thrust coefficient, σ the solidity that was calculated in Equation 10.13. R is the blade radius in m and lastly, C_l the lift coefficient of the blade. This parameter changes along the chord as indicated in Table 10.3.

Integrating these values over the radius of the blade gives the thrust coefficient. From which the total thrust can be calculated with Equation 10.19:

$$T_R = 2C_T A_{disc} V_{tip}^2 \tag{10.19}$$

$$T_R = W f_{vd} \tag{10.20}$$

In this equation, T_R is the thrust in N, C_T the thrust coefficient, A_{disc} the disc area in m^2, which is 5.309. Lastly, V_{tip} is the tip speed (248 m/s).

The thrust that can be delivered by the propeller can be found to be 3682.7 N. This is more than the required thrust that was estimated with Equation 10.20. Therefore, the propeller design is able to deliver the required thrust, with the RPMs that can be delivered by the engine.

With thrust in N, which is 3587N, weight (W) is 3482.55N and the download factor which is 1.03. [48]

10.4.6. Engine Design

The design of the UAV consisted of two main engines, one on each wing, and an auxiliary engine on the tail for stability. These engines were sized separately.

Main Engines As stated previously, the design of an engine is out of the scope of this project. Rather an existing engine is chosen for the UAV. Once the requirements for the engine had been well established, an engine could be picked. Mainly, the peak power, continuous power and torque required were needed to make a selection of an engine. With these values in mind, the lightest and most efficient (T/W) was chosen.

In the range of the power required for this UAV, two brushless engines seemed most suitable. It was decided to favour a brushless motor over a brushed motor, because of its higher efficiency and lower noise. [4] The properties of the engines are depicted in Table 10.4.

Table 10.4: Parameters of the Plettenberg and Saluqi engines

Engines	Saluqi P20S4	Plettenberg Nova 30
Mass (kg)	17	6.5
Torque max (Nm)	120	80
Rpm max (1/min)	2400	7000
Power max	60	30
Power continuous	40	-

Although the thrust over weight of the Plettenberg is higher, a very high RPM is required to achieve this. As a result, it performs less than the Saluqi engine. Therefore, it was decided to use the Saluqi for the main engines of the vehicle. Moreover, Saluqi provides a twin-engine option. As a result of this, for a single-engine failure, the power delivered is halved and a safe landing can be accommodated.

Auxiliary Engine When the vehicle is in VTOL configuration, the main engines create a pitch up moment around the centre of mass, since the thrust line is in front of the cg, as shown in Figure 10.7. Therefore a reaction moment is necessary to ensure longitudinal stability and control. It has been decided that a smaller "auxiliary" engine placed in the tail structure would be an adequate solution to balance the aircraft and provide pitch control (see Chapter 9). Furthermore, when performing moment equilibrium (Figure 10.7), the auxiliary engine needs to generate lift to counteract the moment of the main engines, much like a seesaw.

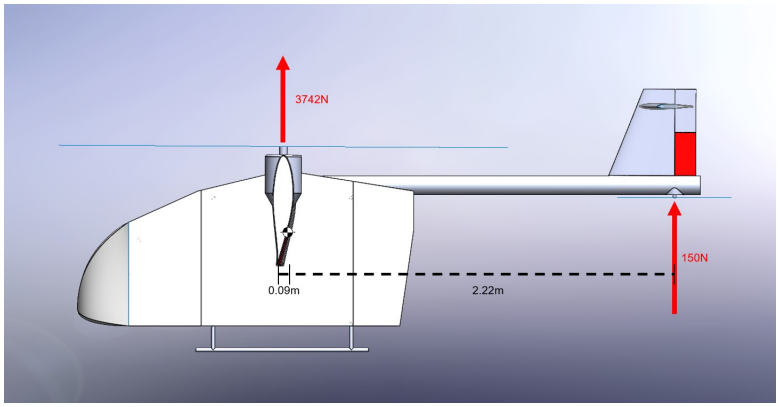

Figure 10.7: Longitudinal moments diagram

A simple calculation reveals how much thrust such an engine should be capable of providing. By taking the maximum thrust generated by both engines (3742N) in the vertical position, and taking the distance from the thrust line to the centre of gravity (0.09m in front), the total moment to be counteracted is known to be 340Nm. This auxiliary engine is desired to be as far away from the centre of mass to increase its moment arm, and therefore, it is placed at 2.22m from the centre of mass, or 0.15m from the edge of the tail, which results in a thrust requirement of 150N. To satisfy this requirement, commercially-available electric engines were compared and it was decided to make use of the Plettenberg Terminator 30-8 6kW engine with the Menz S 26x10" propeller, capable of generating 170N of thrust and weighing around a kilogram (without propeller and electrical cabling). See Figure 10.7 for a force schematic.

10.5. Verification and Validation

During the constructing of the design tools, the tools were continuously verified. This was done to ensure that the data outputted was correct. The following methods have been used:

[4] https://eltra-trade.com/blog/brushless-vs-brushed-motor#bldc-advantages-and-disadvantages [visited on 15/01/2021]

- Unit tests were performed on the separate equations of the power curves.
- The function used to perform the integration of the blade element theory was checked by comparing results to hand calculations.
- The intersection for the induced power factor was checked by comparing outputted values with a graph that can be used to estimate the induced power factor.
- Power curves were compared to reference curves, to investigate if the shape was correct.
- The power curves are in the same order of magnitude as they were in the previous calculations.
- Separate python files were used so the integration of multiple methods could be checked
- JavaProp is a pre-verified and validated program
- The internal complexity of the codes is low and therefore verification by unit and integration tests was sufficient.

In the future validation can be performed. The system described before is best validated by performing tests on the thrust delivered and the power required of the propeller. This has to be done with a prototype and is therefore out of the scope of this report.

10.6. Sustainability Analysis

The sustainability analysis of the power and propulsion subsystem consists of three main points of interest: Emissions, Materials, and Noise. These items are discussed in following paragraphs.

10.6.1. Emissions

As became clear after the Midterm [2], an electric vehicle is most promising and can be seen as future proof. Not only because there are still a lot of developments to be made in the near future regarding battery density, electric engines and the full system, but also because the emissions of hazardous fumes and gases are zero when functioning nominally. Since the vehicle works on lithium-ion batteries and the engine is directly powered by those batteries, combustion is never present and no CO_2 is excreted. With respect to the emissions associated with the mission, naturally, emissions are produced during the production of engines, propellers and batteries. Also, for some missions, it might be impossible to use the planned solar plant and a generator could solve the issue in short term. These emissions should be considered when thinking about sustainability.

10.6.2. Materials

Another part of the sustainability analysis for the power and propulsion subsystem is the use of materials. By choosing an off the shelf engine that is mainly made of aluminium increases the ease of recycling. On the other hand, using composite propellers increases the environmental footprint. The main reason for choosing these propellers is that the weight is less leading to a lower maximum take-off weight and therefore less required batteries that also impact the sustainability. As has been explained in Section 10.4 the propeller manufacturing would most likely involve specific and detailed testing and validation before the actual manufacturing to ensure the capabilities. Additional testing would be performed after manufacturing to guarantee the proper functioning of the propeller. This way the least amount of propellers need to be manufactured and the footprint on sustainability is minimal.

10.6.3. Noise

Noise estimations were performed based on the noise review methods of the California Jet propulsion laboratory. [49] This analysis uses the RPM, propeller diameter, flight conditions, and distance to the propeller as inputs to find the noise. From these steps, an overall sound pressure level of 123 dB right below the vehicle at 150 m is found. This level is quite high for a vehicle this size but the efficiency of the propellers is inversely related to this number. Therefore, decreasing the noise would decrease efficiency. One benefit of the noise level is that during landing, birds or wild animals are warned without extra warning sounds that would add extra weight to the vehicle. The noise estimation has not only been performed at the 150m vertical distance. At 25 meters distance, the noise level is 137.5 dB and at 500m the noise level is 110.5 dB. These estimations are above or around the pain threshold and therefore, this would need to be addressed in future design.

10.7. Flight Performance

At this point, the power and propulsion characteristic of the UAV has been well established. Therefore, the quantified performance of the design can be addressed. Note that some performance elements have been mentioned already, namely climb performance, noise characteristics, emissions and the mass and power needs. Consequently, this section only presents the maximum speed that can be achieved, as well as the maximum range and the longest time that can be flown.

10.7.1. Maximum Speed

The maximum speed that the aircraft can fly is the speed at which the power required equals the maximum continuous power available times the efficiency as stated by Equation 10.21. [50]

$$P_a \eta_p = P_r = \frac{1}{2}\rho S C_{D_0} V^3 + \frac{W^2}{\frac{1}{2}\rho V S \pi e AR} \tag{10.21}$$

The parameters indicated are: W is weight (3482.55N), ρ is the density (1.07393 kg/m^3), S the reference area (3.34 m^2), C_{D_0} is the zero-lift drag coefficient (0.044), e the Oswald Factor (0.78) and AR the aspect ratio (10.4). Solving the equation shows that the maximum speed is 163 m/s. The UAV is never be able to fly at this speed, because the structure and the propellers fail before this speed is reached.

10.7.2. Maximum Range

The vehicle is able to fly for the longest distance at the speed which results in the lowest drag. This velocity can be calculated with Equation 10.22. The energy left after the vertical take-off is at least 26800 Wh. The maximum range is calculated with Equation 10.23. The velocity for the maximum range is therefore 42.8 m/s and the range 333.3 km. [51]

$$V = \sqrt{\frac{2W}{\rho S}\sqrt{\frac{1}{\pi e AR C_{D_0}}}} \tag{10.22}$$

$$Range = \frac{E_{batt}}{D} = \frac{E_{batt}}{\frac{1}{2}\rho S C_{D_0} V^2 + \frac{W^2}{\frac{1}{2}\rho V^2 S \pi e AR}} \tag{10.23}$$

10.7.3. Maximum Endurance

For maximum endurance, the vehicle has the fly at the speed that results in the minimum power required, see Equation 10.24. With the parameters described before, the maximum endurance can be calculated to be 2.16hrs. [51]

$$V = \sqrt{\frac{2W}{\rho S}\sqrt{\frac{1}{3\pi e AR C_{D_0}}}} \tag{10.24}$$

$$Endurance = \frac{E_{batt}}{P_r} \tag{10.25}$$

10.8. Future Recommendations

During the design of the power and propulsion subsystem emphasise was placed on the calculations of the mass of the vehicle and the engine and propeller sizing. As a result of this, some areas could have received more attention and would have to be discussed more extensively during a hypothetical future design phase. Firstly, it is crucial to do a thorough analysis of the power required during the transition of the vehicle. The importance of power during this phase has been highlighted. However, due to time constraints, it has not been investigated thoroughly. Next to that, the propeller design can be further optimised for the given flight conditions and more specifically designed to lower the noise of the vehicle. Moreover, the aero-elastic effects of a tilt-wing have to be further investigated. With regards to this, it would be wise to investigate the propeller vibrations that can occur as a result of its own natural frequency, and the coupled natural frequency with the wing. Next to that, the sensitivity of the design to changes in the energy density of the battery was very clear. Therefore, it could be enlightening to investigate the effect of this on the final design with a sensitivity analysis. Similarly, the change of structural components also appeared to have a significant influence on the design, this influence has to be further evaluated as well. Lastly, a manufacturing plan must be created for all components and technical drawings must be drafted together with the bill of materials.

11
Hardware and Software

In the past, the only means to control an aircraft was a human, sitting in the cockpit, controlling the aircraft through a physical connection to the control actuators. With time came the availability of highly accurate electronic computing and sensing devices. These are interconnected with the use of software to model the physical aircraft and its controls. This chapter will discuss the electronic components (Section 11.1) and their software interactions (Section 11.3) for an autonomous vehicle, the Healios, driven by coded control programs (Section 11.2).

11.1. Wiring and Data Handling Diagrams

Most unmanned aircraft have a list of mutual components. All of these are readily available as COTS (commercial off-the-shelf) components. COTS allows for a modular design which can be upgraded or replaced easily. Computers and sensors are selected rather than developed since this will have a definite decrease in development time of the control hardware. The design of these hardware components is out of scope for this project as it would require a separate, dedicated project on just the hardware components. A supplier for all avionics has been selected, namely Curtiss-Wright defence solutions.[1] This supplier has sufficient experience in the field of aerospace. All its avionics are catalogued such that an appropriate system can be mixed and matched to the customer's specific needs.

Since these are all high-grade military components, the smallest computer motherboard was chosen: a 3U VPX. Where 3U denotes the PCB's (printed circuit board) standard size and VPX denotes a bus bridging capable board such that multiple protocols can be used for communication. Apart from the computers, the system will need a multitude of other hardware to detect, store and communicate its states to an operator or between processes. At this point in the detailed design, statistical relationships to estimate relationships for avionics is not sufficient. A concrete selection has to be made to have information to continue the design. Voltages have to be known to figure out what the main voltages are for the voltage converter. Volumes have to be known to continue internal fuselage design. The website of Curtiss-Wright contains a depiction of a drone with all its necessary hardware. This was a starting point to find an appropriate selection of avionics. Selections will be made based on complementary operating systems and communication protocols as well as processing power. A graphical representation is given after the explanation of each component. If in future work, one or more components do not operate as intended, it is swapped for another.

Mission Computer Curtiss-Wright VPX3-133, it contains a 64-bit 1.8GHz processor and supports up to 8GB of DDR3 memory. The mission computer is the most critical component of the unmanned aircraft. It functions as the 'brain' of the vehicle. It will acquire all information from sensors and actuators and compute the necessary values to pass to the flight controller. It will also be connected to the graphical processor, enabling machine vision for application such as object detection and avoidance. The 'brain' also has a need to communicate its state to the GCS (ground control station). Therefore the mission computer will also be connected to a radio and antenna combination allowing for telemetry transfer and manual override by a human operator.

Flight Controller Curtiss-Wright VPX3-1707, a 16 core 64-bit 2.2GHz processor board with up to 32GB of DDR4 memory. It can be seen as the vehicle's lymphatic system. This computer takes in the necessary information from the flight computer, which can consist of the system's actual states and desired states to estimate the appropriate control inputs or interrupt commands in the case of object detection. New estimated system states are relayed back to the mission computer whereas necessary control inputs are sent to the actuators and motors. The flight controller will need a firmware that is appropriate for every flight

[1] https://www.curtisswrightds.com/ [visited on 18/01/2021]

situation. Those flight situations include take-off, landing, cruise, hover, flight with one or more engines inoperable. The point being, this computer will need to run all the time in tandem with the mission computer such that appropriate flight situations are detected and executed.

Graphics Processor Curtiss-Wright VPX3-4924, containing an NVIDIA Tesla Pascal P6 chip with 2048 CUDA cores and 16GB of GDDR5 memory. This computer is capable of 6.2 TFLOPS (terra floating-point operations per second). This board takes in the output of the cameras in the form of a set of matrices. These matrices, structured per colour band, represent the picture from the camera with a value of 0 for low-intensity levels and 255 for high-intensity levels.

Transponder Sagetech MXS [2]. Which is a mode S transponder for unmanned aircraft. It includes a 1090MHz ADS-B communication link. Aviation authorities require all air traffic that flies in and out of controlled airspace to be monitored. The transponder is a means to report the aircraft's position and altitude to air traffic control.

Optical Sensor Hub Controp M-STAMP [3]. It is a miniature stabilised camera system. Three axis rotation and stabilisation is provided by gimbals. This will be the UA's primary visual system. The cameras included are an infrared IR x4 continuous optical zoom and a CCD (charged coupled device) camera chip with x10 continuous optical zoom and is stabilised with a damping gimbal system. Its resolution will allow seeing targets from up to 2.5km away. Firstly a more bulky hub which could see up to 10km was chosen. But, the M-STAMP was chosen later in an attempt to decrease weight in all departments. The chosen hub's weight is just 1/10th of what is was previously.

Air Data Computer Curtiss-Wright ESCADU. This small computer does some pre-processing of the data from the dynamic and static pressure sensors. It will provide flight data to the mission computer: static pressure, pressure altitude, barometric corrected altitude, vertical speed, impact pressure, total pressure, indicated airspeed, computed airspeed, Mach number, total air temperature, static air temperature, true airspeed and maximum allowable airspeed.

Air Traffic Detection UAV FLARM [4]. The flarm system will alert the operator and the system itself if another vehicle with FLARM installed is in the vicinity. This system is used as an extra precaution. When something is wrong or simply no connection is possible with air traffic control and the vision system has not picked up any objects there is still a way to sense other aircraft.

Appropriate sensors for flight control are chosen based on Jay Gundlach's book on designing unmanned aircraft [52].

INS-GPS Advanced Navigation Certus Eva [5]. The INS (inertial navigation system) consists of accelerometer (measure 3D accelerations) and gyroscopes (measure Euler angles). Due to disturbances (e.g. turbulence), small electronic measurement devices such as accelerometers and gyroscopes build up an error related to sensor drift. This is precisely when the GPS (global positioning system) comes into play to correct this drift. It gives us the vehicle's geographic location directly as well as altitude. The Certus Eva receives the newest Galileo along with older GPS systems for a highly accurate result. A magnetic compass is also included for the system to estimate wind direction and absolute heading.

Above Ground Level (AGL) Sensor Sick DS35-B15221 [6]. This is a laser sensor that has a minimum measurement distance of 200mm. The AGL sensor is used in take-off and especially landing since the altitude measurement based on pressure sensors and GPS can still have insufficient accuracy of its altitude outputs.

[2] https://sagetech.com/ [visited on 18/12/2020]
[3] https://www.controp.com/ [visited on 18/12/2020]
[4] https://flarm.com/ [visited on 18/12/2020]
[5] https://www.advancednavigation.com/ [visited on 18/12/2020]
[6] https://www.sick.com [visited on 18/12/2020]

The more accurate the ground position estimate, the more accurate the vehicle's estimate of its landing position is.

Lighting During night operations, whenever or if that is necessary. The aircraft must be capable to maintain a safe flying distance from other aircraft. That is why red anti-collision (Thiesen-electronics ACL4 [7]) and positional lights (Thiesen-electronics EPTA-NG) will be installed according to their appropriate conventions. These lights will be situated at the aircraft's wingtips, top, belly and tail. They all have a FLARM interface. This means that the lights are able to flash brighter once an aircraft is detected. These lights are synchronised using the appropriate device from Thiesen-electronics such that the flashing will not overlap.

Actuator Actuation is necessary at different locations. For flight control: ESCs (electronic speed controller), engines and control surface actuators are necessary to control the aircraft in all flight conditions. Whereas the payload and wing actuators move the payload and the wing respectively. It should be mentioned that the wing actuator should include an internal braking mechanism, such that the locking mechanism carries the load when applying thrust rather than the actuation mechanism itself.

Removed Components As mentioned in the optical sensor hub paragraph. At the beginning of the detailed design phase, the team was facing a difficult challenge of continuously increasing weight. That is why some components that were originally included in the design, now are omitted due to their weight. The casing for the primary computers (mission, flight and graphical) of 5.85kg and the flight recorder of 3.85kg. The flight recorder would have functioned as a so-called black box. Flight data would be recorded and stored for later retrieval in case of a crash. Since the UA will not carry any humans and will not directly put human lives at risk and data logging can also be done on a less protected storage device, it was omitted. The casing would have protected the primary computers from any bit corruption due to electromagnetic interference and kept the computers cool. It was assumed over-designed for the team's purposes and therefore omitted to be replaced with a lighter purpose-built casing.

Electrical Properties Now that all the hardware components necessary to control the vehicle have been presented, each component needs to be inspected to group them according to their operating voltages and communication protocol. These properties are presented in Table 11.1. The reason why this is done is that the goal of the electrical analysis is to keep the cable length to a minimum such that no extra unnecessary weight is introduced.

The data transfer protocols which are used include UART, RS232, RS422 and PCIe. Since no UART port is present on the primary computers, but other types of serial connections are. The UART connections (maximum 9.6 kbps [8]) are converted to RS232 so they can all be connected to the same bus. This leaves several RS232 connections (maximum 19.2 kbps [9]), one RS422 connection for the optical hub (maximum 10 kbps [10]), one PCIe connection for the graphical processor (maximum 8 Gbps [11]). Input voltage for the voltage converter is dependent on the voltage of the battery. Since the battery voltage is dependent on the voltage required for the main engines, its voltage will equal 100V. Most function with 12V or 18V. Thus, 2 step-down converters are necessary to supply all components with electrical power.

In Table 11.1, some prices have been roughly estimated and can not be assumed to give us accurate results. The optical sensor hub's price is determined on the fact that prices range from 5k euros to 5M euros and it is part of the 5 lower range sensors. Cable length has been determined by looking at the 2D length between connection points and multiplying that length by a factor of 1.5.

[7] https://www.thiesen-electronics.com [visited on 18/12/2020]
[8] https://learn.sparkfun.com/tutorials/serial-communication/all [visited on 18/12/2020]
[9] https://www.lammertbies.nl/comm/info/nl-rs-232-specs [visited on 18/12/2020]
[10] http://www.rs485.com/rs485spec.html [visited on 18/12/2020]
[11] https://www.trentonsystems.com/blog/pcie-gen4-vs-gen3-slots-speeds [visited on 18/12/2020]

Wiring & Data Flow Diagram

Legend			
	A = phase A B = phase B C = phase C	black: ground red: + current grey: data	D1 = Universal Asynchronous Rx - Tx (UART) D2 = RS232 D3 = RS422 PCIe = Peripheral Component Interconnect Express

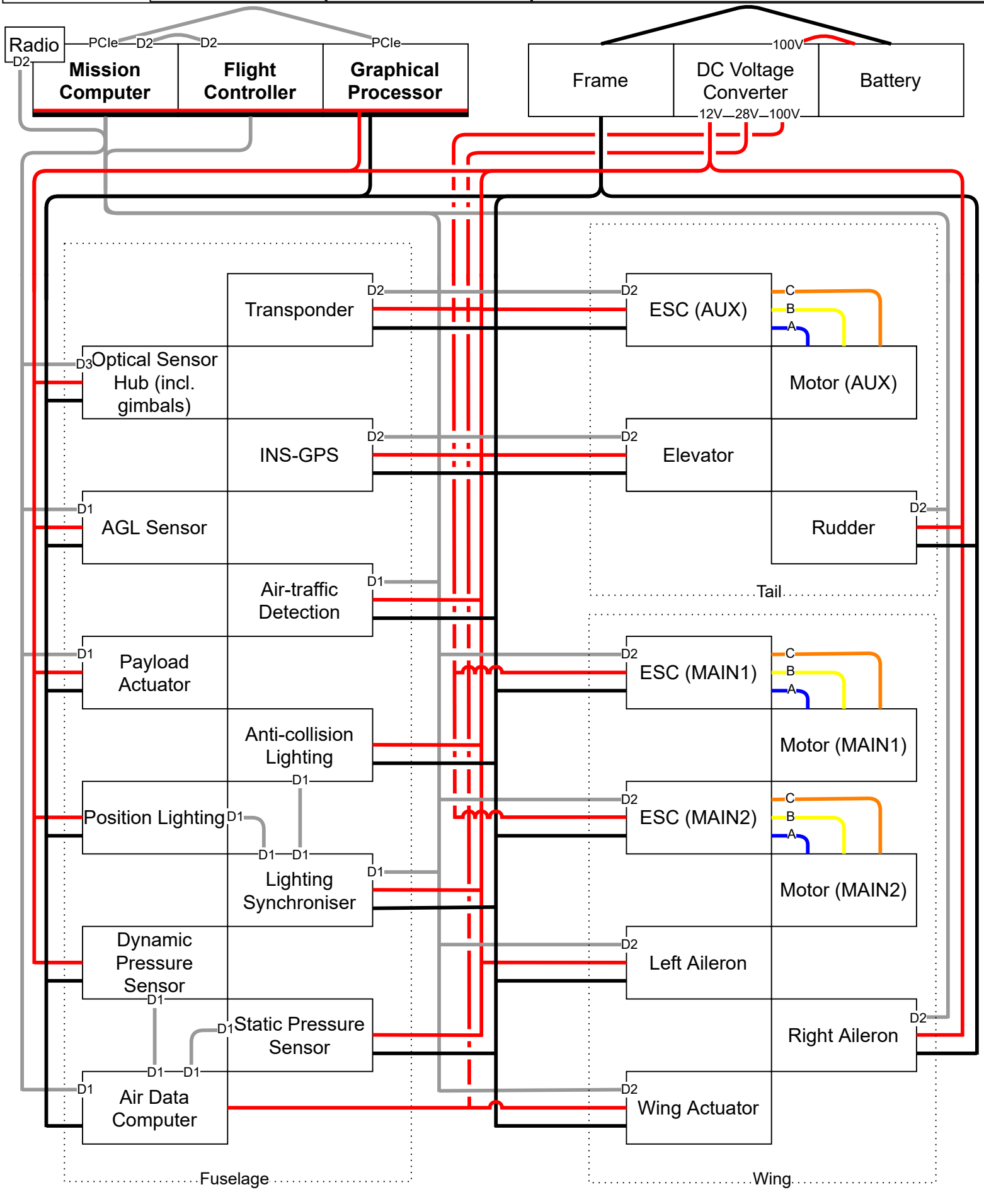

Table 11.1: Onboard Electrical Components

Component	Power [W]	Voltage [V]	Protocol [-]	Weight [kg]	Cost [eur]
INS + GPS	2.64	9-36	Eth, CAN, RS232, RS422, GPIO	0.300	11726
AGL Laser	1.70	12-30	Profibus	0.065	551.5976
Transponder	10.00	14-28	Eth, RS232, RS422	0.180	1230
Pitot-static probe	30.00	9-32	UART	0.095	90
Air-trafic etection	0.20	4-15	UART	0.012	699
Flight controller	60.00	12	Eth, RS232, RS422, PCIe	0.500	8282
Mission computer	35.00	5	Eth, RS232, RS422, PCIe	0.467	6806
Graphics processor	90.00	12	PCIe	0.800	14596
Air data computer	15.00	28	ARINC 429	1.300	13120
E.S.C.	33,000.00	63 - 120	CAN, RS232, RS422	1.180	2041.8
Static pressure sensor	negligible	-	UART		2.52
Anti-collision lights (red)	10.00	10-17	UART	0.086	324.72
Position lights	20.00	10-17	UART	0.076	439
Light sync device	-	10-17	UART	0.024	85.9
Optical sensor hub	-	-	RS422	1.300	25000
Actuator payload	7.80	12	UART	0.086	115.99
Voltage Transformer	4,000.00	-	-	5.600	100
Main Actuator	7,000.00	-	-	21.000	300
Power cabling (main engines)	-	-	-	4.710	3.42
Power cabling (other)	-	-	-	0.550	2
Data cabling	-	-	-	0.850	2
TOTAL	**44,282.34**			**39.181**	**60517.94**

11.2. Flight planning and Obstacle Avoidance

For the UAV to be autonomous, it needs an onboard computer that calculates the path the vehicle must follow to arrive at its destination safely. The output of the path panning computer is the waypoints which are inputs to the control system. Path planning is the task of finding the optimal sequence of configurations (waypoints) that move the vehicle from the source to its destination [53]. Optimal paths do not only entail the shortest path but also paths that avoid known obstacles or paths that improve mission characteristics, such as flying in a region with beneficial weather. In order to combine these characteristics, the flight path planning framework must have an environment in which no-fly zones, known obstacles, weather forecasts, and population density maps are modelled [54].

In order for the UAV to know the optimal route, it must have an environment in which data about its surroundings is available. When data of its surroundings is obtained, these can be modelled in a cost map. Each point on the map returns a cost for the UAV to be at that location, areas inside obstacles and no-fly zones have an infinite cost (Figure 11.1), since the vehicle should never fly in these areas. Locations with unfavourable weather conditions or high population densities have high costs since it is preferable that the UAV avoids these areas (Figure 11.2). The cost maps for the different influences are superimposed to create a combined cost map which represents the environment the UAV is flying in. The task that remains for flight planning, is to find the route to the destination with the lowest cost. There are various algorithms that determine the optimal path from the cost map, an example is A* [55].

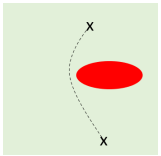

Figure 11.1: Cost Map of Static Obstacle

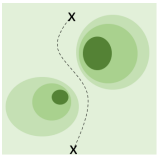

Figure 11.2: Cost Map of Population Density

Throughout the flight, the flight path constantly needs to be re-planned and updated. This needs to happen since the UAV might not exactly follow the flight path. This can happen if the state estimation has errors, or because the response of the drone might have some delay. For these reasons, the path needs to be updated at a high rate such that the optimal path from its new position is known. Other reasons re-planning might

have to occur for is for a change in the weather forecast, which could influence the optimal path trajectory. Therefore, throughout the flight, the path planning will be updated at a high frequency such that the UAV always knows its optimal path [54].

Obstacle Avoidance The distinction between flight planning and object avoidance is that flight planning is something that can be done before the UAV moves. Contrarily, obstacle avoidance is something that is done as the UAV moves. This implies a time constraint to process the information of the surroundings and to perform the avoidance manoeuvre. In the case that an obstacle is detected, the flight path plan will be overridden, once the obstacle has been cleared, a new flight path is generated from its new position [56]. The obstacle avoidance gathers information about its close surroundings with a 360-degree rotatable camera, and infrared camera. The information is processed to determine the position and trajectory (in case of a bird) of the incoming obstacle. The UAV also has a FLARM which alerts the UAV of potential aircraft collisions.

When landing the cameras will be pointed downward, using the gimbals, to see if the landing area is satisfactory. If an obstacle is detected, the landing procedure is aborted and the flight path planning generates a new landing location in the proximity. If no nearby landing location is found, the UAV heads back to its starting point.

11.3. Software, Communication and Autonomy

The main software will consist of four components (see Figure 11.3):

- The kernel, the piece of software which is closest to the hardware of the SBC (single board computer). It translates the command inputs from the user in understandable machine code that the SBC understands.
- The OS (operating system), the interaction layer between the user and the kernel. The OS allows the user to input commands in the form of code. Pre-written scripts can be loaded in from memory by the OS. These scripts will be compiled into a program that fulfils all necessary functions.
- The program, a collection of in house coded scripts that allow the vehicle to communicate, sense, guide itself and operate over the whole mission flight profile.
- Drivers, they are small pieces of software similar to a kernel. Only it provides for the communication between the program running on the OS and its peripherals. Drivers allow the program to ask a sensor to give its value of the current measurement without knowing the sensor's language. Other peripherals in need of a driver are the actuators and the ESCs [12].

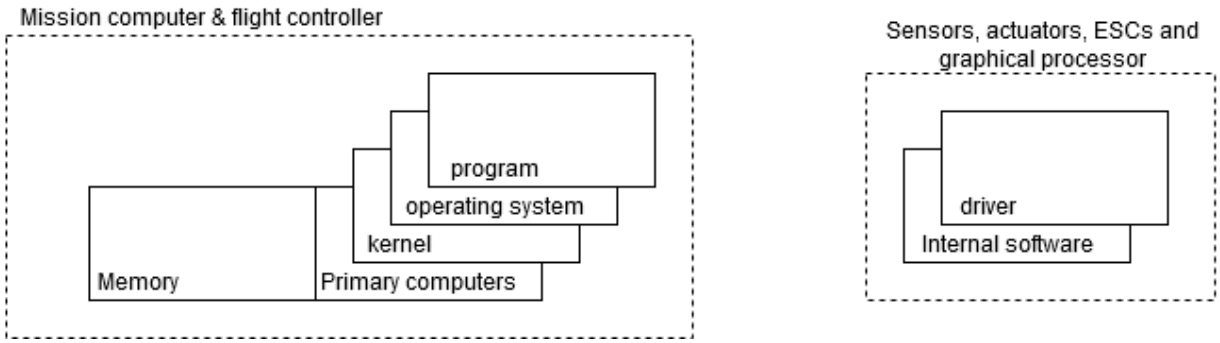

Figure 11.3: Graphical representation of software

To improve the development time of the UAS, most of the software should be open source. The more open source software is picked, analysed and possibly adjusted for use on the vehicle, the less development is necessary to complete the aircraft. In that regard, open-source software has a lot in common with COTS. Unfortunately, the OS and the kernel are the only pieces of software that do not have to be significantly adjusted for the OS. Some options are considered for the software and argumentation is given on why one would be better for the system design than the other.

[12] https://docs.microsoft.com/en-us/windows-hardware/drivers/gettingstarted/what-is-a-driver- [visited on 18/12/2020]

The two main competitors that the main computer supports are Linux and LynxOS [13]. They are both UNIX based systems. Linux is a general use operating system which is completely open-source and s, whereas LynxOS has a cost. On the other hand, LynxOS offers security out of the box. They have proven to be a successful and secure system for major players in aviation. As they are both UNIX based, they both have the advantage of having a huge amount of contributors. Software packages such as ROS (Robot Operating System) are readily available and can be calibrated to give excellent results for the UA. To keep the cost down it is decided to use Linux as an initial tool for program development, believing that all the program code is usable in LynxOS without modification or porting. Before initial production, the OS can later be switched from Linux to LynxOS to decrease possible in-flight hijack risks if necessary. Linux comes with a compatible kernel. Linux is used for the OS of the flight controller and the mission controller. The graphical processor will be defined as a peripheral.

In order to certify the aircraft for safety critical A scenarios under software requirements stated by DO-178B, LynxOS has to be used [14]. This OS provides complete documentation for the OS code, requirement traceability and test results. DO-178B denotes a software standard that must be complied with in order to meet certification requirements.

In nominal operations, non-emergency situations, the script in the program related to path planning will generate data coordinates corresponding to a 3D position that is desired to continue along the flight path. This data will be combined with the primary flight sensors depicted in the fuselage component group, being the INS-GPS and output of the air data computer. The INS-GPS unit receives encoded RF (radio-frequency) signals from multiple satellites. It then combines its geographic data with its accelerations and Euler angles. Once all this data is gathered, the current state is computed, logged and sent to the flight controller. The flight controller as discussed earlier in this chapter accepts information from the vehicle's current and desired states from the flight computer, selects an appropriate controller based on the flight condition and computes a control response for the ESCs and actuators. This control response is logged and send off. The actuators and engines perform their assigned tasks, the new states are captured by the flight primary sensors and the process begins all over again until the interrupt command is given to shut off the system after mission completion. The transponder receives its pressure altitude from the mission computer and sends that to ATC (Air Traffic Control). Non-nominal operations always go paired with one or multiple interrupts to the main loop that is running the nominal operations.

In the case of landing, some minor adjustments are made to the nominal case. Before landing at a remote unprepared location, the UA needs to determine a safe landing zone and approach trajectory by means of an algorithm based on machine vision. Most likely this algorithm will be neural network-based. While the UA is loitering above the remote landing location, the optical sensor hub catches the image and sends the image matrices to the mission computer. The mission computer runs the algorithm with the help of the graphical processor. A map is constructed indicating topology and favourable approach corridors. The mission computer decides on an appropriate spot for landing and an approach flight trajectory. The Air data computer information related to AGL altitude is replaced by the reading of the AGL sensor after transition when above the picked landing spot (<10m AGL). This allows the aircraft to sense the ground up till a minimum of 200mm. At this point, the mission computer will assume that the vehicle is on the ground. An interrupt is send to the ESCs to stop the flow of power to the engines. The propellers will be despun which allows for a smooth touchdown. Such an interrupt is commonly known as disarming the engines and can also be done for payload handling operations to keep the vehicle ready to arm and fly off once the payload is loaded/unloaded and it is safe to takeoff. When landing on a prepared landing spot, the same procedure can be used and stored for further reference as to skip the loitering phase.

For take-off, the engines are armed at the appropriate time, the first coordinate set for the flight controller is set for an AGL altitude of above the minimum accuracy of the AGL sensor (200mm) and the current AGL altitude is assumed to be zero. That way the vehicle will take off and the AGL sensor can be effective before continuing to the next location. For the rest of this procedure, everything is the same as in a landing case, but in reverse.

[13] https://www.lynx.com/ [visited on 18/12/2020]
[14] https://www.embedded.com/lynuxworks-tailors-lynxos-for-do-178b/

12
Operations and Logistics

As described in Chapter 3, the main function of Project Healios is to provide autonomous VTOL delivery of medical supplies to remote locations affected by natural disasters. Now that the design of the UAV has been presented in Chapters 4 to 5, it is necessary to investigate the operations and logistics that must be put in place to support the vehicle during its missions. That is the objective of this chapter.

To that end, it is first necessary to describe the different use cases of the vehicle. This is done in Section 12.1. Then, a description of the equipment and infrastructure needed at the base from where the UAV will be deployed is given in Section 12.3. Thereafter, a complete overview of the operations and logistics is presented in the form of a flow diagram in Section 12.4. Lastly, the sustainability of the bases is discussed in Section 12.5.

12.1. Use Cases

The reason why different use cases must be identified is due to the complex nature of the project's goal. Delivering medical supplies to remote areas is a very broad goal that could encompass many activities. Furthermore, depending on the context of the vehicle's operations (i.e. where the vehicle is operating, the time constraints imposed by the customer, etc...) the necessary operations could differ significantly. Although this versatility is an advantage of the Healios system, it is necessary to study these different use cases from an operational point of view.

Two distinct use cases have been identified for the vehicle. The first type of use case is the one where an immediate response is needed, such as after a natural disaster like a tsunami or an earthquake. The second type deals with long-term responses where an immediate response is not needed, and more elaborate operations and logistics can be planned in advance. Both of these types of use cases are discussed hereinafter, and examples of how Project Healios could be used in such situations are provided.

12.1.1. Immediate Response

This use case deals with situations in which a natural disaster affects a specific region of the world suddenly, such as a tsunami or an earthquake. In those situations, a quick response is vital. Areas affected by such natural disasters would suffer from: severely comprised infrastructure; a rapid increase in demand of medical supplies; difficult or impossible communication by traditional methods such as roads, and power outages for extended periods of time.

One can imagine that in such situations it is not viable to construct an entire base for the operations of the UAV, since that would be extremely time consuming and would defeat the purpose of providing medical supplies during such emergency situations. Therefore, in this use case, it would be necessary to establish mobile bases. Such bases would be made up of a mobile truck which carries the vehicle in addition to the necessary equipment to support its operation. Each base would only be able to support the operation of a single UAV. A detailed description of such a base is provided in Section 12.3.

The operational concept for this first use case would be to quickly deploy as many mobile bases as necessary depending on the specific demands imposed by the customer, each of them allowing one UAV to operate. The mobile bases would allow the operator to get as close as possible to the affected area. How close one can get will depend on the specific magnitude of the disaster, but as long as the mobile base can be securely placed within 50 km of the end-user location, the UAV can then be deployed and reach the end customers.

It is worth noting that depending on the magnitude of the natural disaster, setting up a stationary base for long-term response could be possible while the mobile bases are operating. In those cases, mobile bases would take care of providing the much-needed emergency relief immediately after the incident, while a stationary base would then provide further support to the affected area during the weeks, months, or even

years after the incident. Refer to subsection 12.1.2 for a more detailed description of the long-term response use case.

In summary, the advantage of using a mobile base for immediate emergency response is clear: it can be deployed quickly to the affected area, and once the UAV is deployed, the mobile base is free to move if necessary. This is particularly useful in emergency situations since the affected area might change rapidly. As an example, consider the area affected by a tsunami. The area most affected by the floods following the tsunami might change over the days following the incident. Thus, it might be beneficial to have a system where the deployment point of the UAV can change between mission over the time-span of days or even hours. This flexibility and its quick response time are the main advantages of the mobile bases, which form the backbone of the response of Project Healios to use cases that require an immediate response.

The effectiveness of Project Healios for immediate response is briefly explored in subsection 12.2.1 with a case study focused on the 2011 earthquake and consequent tsunami that affected the Pacific coast of Japan.

12.1.2. Long-Term Response

The second use case is that of long-term response. This refers to situations in which Project Healios is used as a tool to solve bottlenecks in the supply chain of medical payloads due to reasons *other than* a natural disaster. Examples of this are remote locations that are difficult to access, areas with poorly developed infrastructure, areas where the supply chain of medical supplies is not optimised, and/or developing countries where the healthcare system might be unable to cope with the demand for medical supplies (for instance because of a lack of funding or development). In most cases, a combination of these reasons, amongst others, will results in certain communities not having access to much needed medical supplies.

The operational concept is radically different than that for the immediate response use case. In this case, there is no natural disaster, but the problem is just as important. Project Healios could coordinate with local governments to establish a long-term base that can support the operations of many drones (in the order of 5-10). This would improve the flexibility, effectiveness, and response time of the medical supply chain by connecting remote inaccessible areas with local hospitals in a quick and reliable way.

In an ideal case Project Healios would perform its operations while the local government tries to fix the underlying issues that created the bottleneck in the first place. In this case Project Healios would not only try to mitigate the problem in the short and medium-term, but it would also cooperate with authorities to hopefully eradicate the problem altogether. This might not always be possible or it may take a long time. In either case, Project Healios could formulate a detailed plan to determine how to tackle the specific problems that affect a particular region.

The project would span over many months and potentially years. Firstly, a detailed project plan would be established in coordination with local governments to determine exactly what problems would be tackled and how. Detailed goals would be formulated and deadlines put into place. A stationary base would then be built, which would support the operation of many drones. The necessary equipment and infrastructure of that base is discussed in Section 12.3.

Of course, this stationary base could work in tandem with the mobile bases described in the previous section. One can imagine having a stationary base serving as a central hub, with several mobile bases in the vicinity depending on the coverage that needs to be provided and the specifics of the project.

The effectiveness of Project Healios for long-term responses will be briefly discussed using a case study, presented in subsection 12.2.2. In this case, the case study focuses on Rwanda and the difficulties that the country faces in terms of delivering medical supplies to remote rural areas.

12.2. Case Studies

This section presents two brief case studies to demonstrate the potential of Project Healios. The first case study focuses on an immediate response scenario caused by a natural disaster in Japan. The second, on a long-term response scenario due to a bottleneck in the medical supply chain of Rwanda. In both cases, the effectiveness of Project Healios is demonstrated by showing that with a relatively small number of bases (ei-

ther mobile or stationary), Project Healios can cover large areas affected by these difficulties in transporting critical medical supplies.

12.2.1. Case Study A — Immediate Response in Japan

The earthquake and consequent tsunami that struck the Tōhoku region of Japan in 2011 was the costliest natural disaster in history, with an estimated economic cost of US$235 billion [1]. More importantly, it left more than 15000 dead, 6000 injured, and 2500 missing people [57]. The earthquake was the most powerful in Japan's history, and the 4th most powerful ever recorded in history [2]. Reports show that in 2015, 4 years after the incident, more than 230000 people could still not move to their residence due to the necessary relocations and the extent of the damage to existing infrastructure [57].

The most affected prefectures in Japan were those of Miyagi, Iwate, and Fukushima. In particular, this short case study focuses on the Miyagi prefecture, where waves of up to 40 meters in height were recorded, reaching up to 10 km inland [3]. The goal is to investigate how effective of a solution Project Healios could have been at providing an immediate response for emergency relief following the tsunami. Figure 12.1 shows a map of the Miyagi prefecture. Red dots indicate the main cities along the coastline which were severely affected by the tsunami. The blue dots represent the proposed locations for the mobile bases. The circles represent the 50 km range of the UAV for delivery missions. The figure shows that with only 3 mobile bases, the UAV could cover the entire coastline of Miyagi.

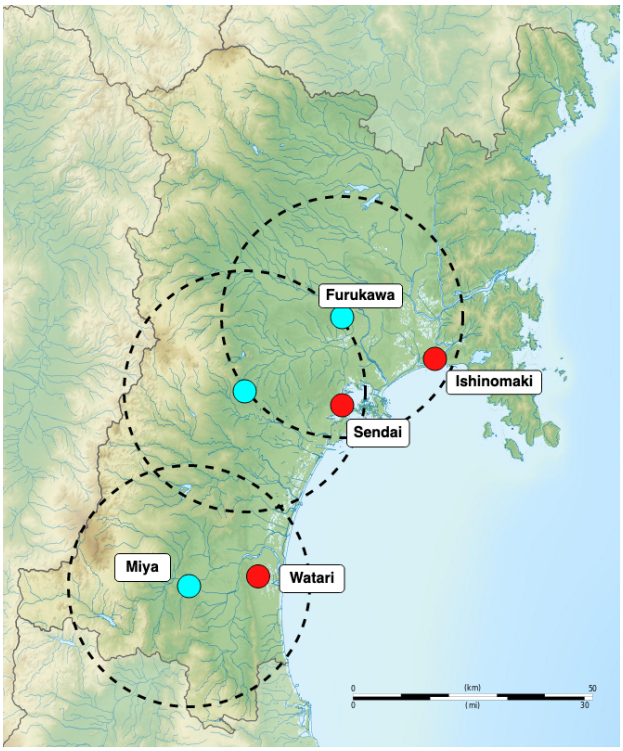

Figure 12.1: Proposed coverage of the Miyagi prefecture by Project Healios

Note that the aim of this case study is to show the potential of Project Healios, but the details of the project's implementation for any particular emergency scenario would need further investigation. For example, the specific locations of the bases could change. There is a multitude of methods that can be used to optimise the locations of the mobile bases for any particular response scenario. In particular, references [58, 59] propose two different probabilistic methods that can be used to optimise the location of emergency vehicles for disaster relief. These methods rely on cost functions to prioritise which areas need the most help and depend on information such as the actual demand for the service and the location of the nearest hospitals capable of providing the medical supplies, amongst others. Performing such a detailed analysis of the base locations is deemed to be beyond the scope of the present work.

Nevertheless, the location of the bases shown in Figure 12.1 proves to be effective for two reasons. Firstly, the combined range of the three bases provides coverage for the entire target area, namely the coastline of the Miyagi prefecture. Secondly, the two northernmost bases are within reach of one another. This allows for communication between those bases, allowing transport of payloads between bases in case one of them were to become inoperative and had to be relocated. In addition, if the 200km radius of a logistics mission is used (which is acceptable for travel between bases), then all three bases are reachable from any of the other bases.

Lastly, two of the three bases are located in big cities (the southern one in Miya, and the northern on in

[1] https://www.latimes.com/business/la-fgw-japan-quake-world-bank-20110322-story.html [visited on 14/01/2021]
[2] https://www.theguardian.com/world/2011/mar/13/japan-tsunami-earthquake-power-cuts [visited on 14/01/2021]
[3] https://www.bbc.com/news/world-asia-pacific-12709598 [visited on 14/01/2021]

Furukawa). This allows for medical supplies to be provided rapidly from hospitals located in the city and its surroundings. The last base is placed on the semi-mountainous region near Sendai, the largest city in the region.

12.2.2. Case Study B — Long Term Response in Rwanda

Rwanda is a prime example of a country where autonomous long-term solutions like Project Healios could make a huge difference in the availability of much needed medical supplies to rural areas. As is the case in many African countries the problem is not the lack of healthcare solutions, but rather the difficulty in accessing those solutions for a large part of the population. Rwanda suffers from a severe lack in road infrastructure which makes it extremely difficult to reach some of the more remote areas of the country [4].

The country has a mostly rural population with over 80% of its residents living in rural areas [60], most of which are difficult to access due to the aforementioned lack of functional road infrastructure. Furthermore Rwanda suffers from problems related to diseases like HIV/AIDS and malaria, which affect a significant part of the population [5]. In recent years the government of Rwanda has made great strides to improve the quality of its healthcare system, making it one of their top priorities for their '2020 Vision' programme [61]. These efforts have paid off, with Rwanda's universal healthcare system being one of the best in the African continent [62]. Although Rwanda has a functioning and capable healthcare system, the underlying problem is the poor infrastructure which leaves remote rural areas even more isolated by preventing them from accessing critical medical supplies.

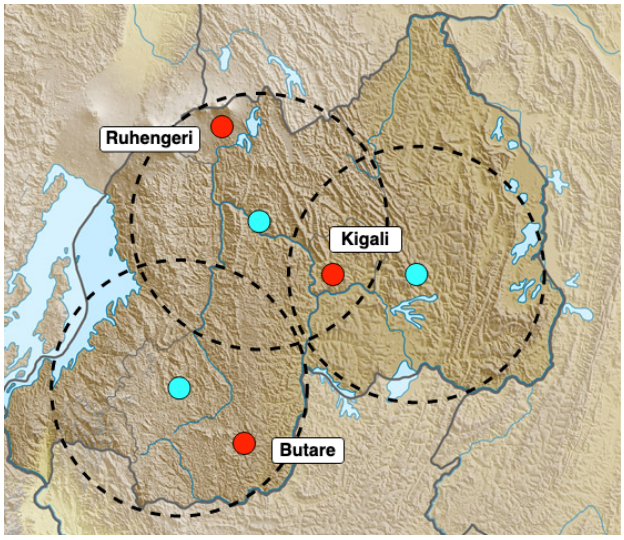

Figure 12.2: Proposed coverage of Rwanda by Project Healios

The reference [63] presents an analysis of the geographical coverage and accessibility of the primary health care network in Rwanda, particularly focused on the Western region of the country. The authors quantified the degree of geographical accessibility using three methods (walking, walking and cycling, and walking and public transport). They concluded that "regardless of which travel scenario is used, the majority of the population in the Western Province does not have access to the existing primary health facility network" [63]. The information presented thus far demonstrates that the source of the problem is not the lack of healthcare solutions, but rather the difficulty in bringing those solutions quickly and reliably to those who need it most.

Project Healios provides an attractive solution to help the Rwandan government improve the health of its citizens by establishing a long-term presence in the country. By developing bases that connect some of the biggest hospitals in the country's rural areas, the efficiency and reliability of the supply chain of vital supplies can be greatly increased. These supplies could include blood kits (both for transfusions and for testing diseases like HIV), vaccines, malaria drugs, and antibiotics.

Figure 12.2 shows the proposed coverage of Rwanda by Project Healios. The red dots indicate three major cities in Rwanda: Kigali is the capital city, where a variety of hospitals (including the biggest in the country) are located; Butare is a city in the southern region of Rwanda which has the second-largest hospital in the country, and Ruhengeri is a city in the northern region which has a large regional hospital [6].

[4] https://medium.com/thebeammagazine/how-do-you-get-medical-supplies-delivered-to-remote%2Dafrican-communities-800270c48fd7 [visited on 14/01/2021]

[5] https://web.archive.org/web/20151208111222/http://hir.harvard.edu/health-equity-in-rwanda/ [visited on 14/01/2021]

[6] https://fortuneofafrica.com/rwanda/hospitals-in-rwanda/ [visited on 14/01/2021]

The blue dots represent the proposed locations of the stationary bases. The circles represent an area with a radius of 50 km from the centre of the bases, equivalent to the range of the UAV for a delivery mission. It can be seen from Figure 12.2 that three stationary bases are capable of providing coverage to almost the entirety of Rwanda. The bases were selected so that (a) the bases cover as much area as possible and (b) at least two bases provide coverage over the capital city of Kigali since it is assumed that it can provide the majority of the needed medical supplies. The addition of a fourth base would yield complete coverage of the entire country and it would also improve the interconnection between bases.

In summary, it can be seen that Project Healios can also provide an effective solution for the long-term use case by providing quick and reliable transportation of medical payloads and therefore improving the effectiveness and geographic reach of the primary health facility network in Rwanda.

12.3. Base Description

In order to develop a vehicle which can fly autonomously, and deliver payload; there must be a base, a supporting infrastructure to house and maintain the vehicles, as well as charging the vehicles. Thus, it is important to consider where these bases will be built; and how many of them will be built. The aim is to first establish bases in a pilot location, where it will mainly operate for the distribution of medical supplies in remote areas. However, as the size of the project grows; we must ensure that the mission can also be scaled to accommodate a larger demand. Thus starting from the pilot location, more bases will be built in strategic locations; to minimise the number of bases required to cover the maximum amount of land. Sections 12.3.1 and 12.3.2 will describe in more detail what the mobile and stationary bases consist of.

12.3.1. Mobile Base

As the service which the system must provide is inherently linked with emergencies, it is essential, that considerations to the scenarios where the urgent distribution of supplies outside the covered area have been made. Thus, for this reason, the service will also accommodate for the construction and transportation of mobile bases which can be transported via a truck to the proximity of the disaster for urgent disaster relief. An example of a mobile base configuration is given in Figure 12.3 and 12.4 (figures are to scale). The truck would transport the UAV, a diesel generator to charge the UAV, two operators to move the base as necessary and operate the UAV, a small computer that could serve as a flight control centre to communicate with the vehicle, and the medical payloads to be supplied to the end-user. When operating the mobile base, the UAV would land at a safe distance from the truck, the charging cables would then be brought to the drone to charge it. To fit the UAV inside the truck the wing and propellers must be disassembled and then re-assembled once the truck arrives on site. As can be seen in Figure 12.3, the wing itself would remain one piece for structural reasons. A similar set up could be achieved with the use of shipping containers. The generator, medical supplies, and the UAV would be stored inside the shipping container, consequently a truck would bring the shipping containers to a desired site.

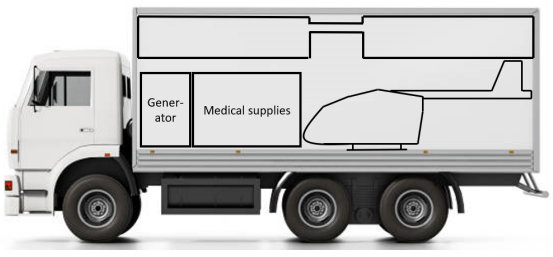

Figure 12.3: Mobile base side view

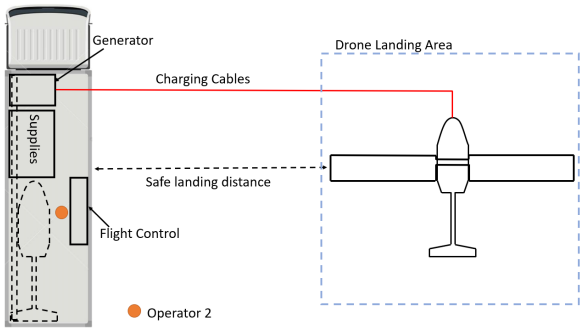

Figure 12.4: Mobile base top view

12.3.2. Stationary base

Figure 12.5 presents a sketch of the fixed base layout and the necessary equipment needed to support the mission. The base is composed of a warehouse where supplies and equipment can be delivered, and prepared for delivery. A hangar area is dedicated to the maintenance of the vehicles. The base is powered by

a solar farm which provides enough energy to charge the UAVs and power the base. The base would be operated by 5 people, 2 to control the drones, 2 maintenance/logistics employees, and one manager. In Figure 12.5, the base shows 5 landing pads for UAVs, however, the number of UAVs that can be operated from this base (with 5 workers) may range between 5 and 10.

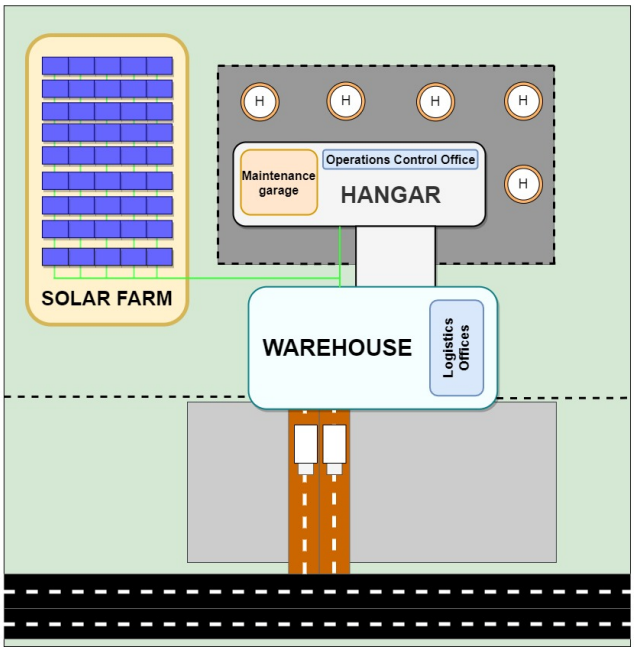

Figure 12.5: Stationary Base Concept

12.4. Operational Flow Diagram

After discussing the use cases of the vehicle (Section 12.1) and describing what the required ground infrastructure would be for each case (Section 12.3), a complete overview of the operations of the Healios system can be provided.

This is done through the use of an operational flow diagram. It visually represents all of the activities performed by the *system* during any given mission. In particular, it highlights the connections between the vehicle and the ground infrastructure, demonstrating how they communicate with one another during the mission.

The operational flow diagram is presented on a separate page at the end of this chapter. It is divided into four phases: planning & communication, pre-flight operations, in-flight operations, and post-flight operations. These are briefly explained in the following paragraphs, paying particular attention to how the activities within each phase would differ depending on the type of mission (immediate vs. long-term response).

Planning and Communication: First, contact from the customer who can either request or send a delivery is established. A delivery request entails the UAV delivering a package from the base to a location. In the case of a long-term response scenario, the delivery can be planned in advance, the inventory can be inspected upon arrival, categorised, and stored at the warehouse ready to be loaded onto the vehicle. The payload is then taken by a payload handling system which takes the supplies from the warehouse to the hangar at the base where the corresponding vehicle is located. In the case of an immediate response scenario, it is assumed that the payload has already been provided in advance by the responsible authorities. Thus, the required amount is selected from the inventory and it is loaded onto the mobile base. The vehicle is also loaded onto the base and the mobile base is deployed to the affected area.

Pre-flight Operations: This phase begins with the flight planning and preliminary ground operations. In the case of a long-term response, the flight plan is shared with air traffic control (ATC), which may accept, reject, or modify that flight plan. In the case of an immediate response the flight plan is generated from the mobile base and the operator directly oversees the operations of the vehicle during flight, relaying information to the responsible ATC authorities if necessary. The vehicle is then prepared for take-off by performing the necessary start-up procedures and system checks.

In-flight Operations: The UAV starts its engines, takes off, and climbs to the transition altitude. The vehicle might have to hover out of ground effect depending on the mission (logistics vs. delivery). The vehicle then undergoes the transition procedure and enters its cruise configuration. After a climbing procedure to the required altitude, the vehicle accelerates to its cruise speed and starts to continuously relay data to the base operators (mobile or stationary). When near the landing site, the UAS scans the landing site for landing and performs the necessary landing procedures. Once landed, the payload is deployed and the UAV takes-off and flies back to a base (for a delivery mission) or it is simply returned to the hangar for post-flight operations (for a logistics mission).

Post-flight Operations: After arrival the UAV is inspected, cleaned, and plugged in to recharge. Maintenance may be performed depending on the use case (long-term vs. immediate response) and other factors such as vehicle availability and demand. The frequency of the maintenance operations can occur every flight (simple visual checks) and/or periodically (detailed inspections after a certain amount of flight hours)

12.5. Sustainability Analysis

Sustainability has been an important criterion throughout the design of the UAV, therefore it is important that it is also analysed for the bases themselves. The sustainability of the two bases will be qualitatively analysed regarding environmental, social, and economic sustainability.

The permanent base has a low environmental impact mainly due to the solar farm that powers the base. The largest environmental impact is the construction of the base itself. Regarding social sustainability, the base has a beneficial impact in its local area, due to the local jobs it can provide to nearby communities. On top of that, it also provides high benefits to the nearby communities by improving the local healthcare system, thus directly improving the quality of life of everyone in the operational area of the UAV. Lastly, comparing the base to a helicopter and helipad, it can be deduced that the base is also economically sustainable, mainly due to the much lower operational cost of the UAV compared to helicopters.

The mobile base is less environmentally sustainable compared to the permanent base due to the diesel generator it uses to recharge the UAVs. The impact of transporting the drone by truck is considered to be minimal since the truck will be stationary the majority of the time. In general, compared to a helicopter, the environmental impact remains low. The mobile base contributes to social sustainability by providing crucial aid in emergency situations such as natural disasters. The aid it provides in these situations is extremely valuable since it is supplied to the least accessible victims, which are often the most affected by the disaster. Lastly, the mobile base is economically sustainable due to the fact that it is less costly than comparable alternatives such as helicopters. It is more expensive than ground vehicles, however, it compensates this by providing higher social value by helping victims faster, which was found to be the most important factor during emergency management (see Chapter 2).

Summarising, the operation of the UAV in the described use cases is sustainable on all three fronts. The permanent base is more environmentally friendly and also more economically sustainable in the long term compared to the mobile base. From this discussion, it can be said that the UAV and its operations would also be more sustainable than comparable alternatives, however further numerical analysis of operations at these bases would provide more concrete evidence of this.

Future Recommendations

Throughout this chapter the emphasis was placed on the operations and logistics description for the use of the system (UAV and base). Is worth noting that in future stages of the design, particular attention should also be placed into the logistics and operations necessary to certify, manufacture, and assemble the UAV and bases.

In addition, more onsite research should be undertaken to gain a better understanding of the demand for Project Healios. This could be used to estimate the reach of the system in a particular location (i.e. the amount of people that could be provided with medical supplies per day per base).

Lastly, more research should be undertaken to determine if other types of payloads (other than medical supplies) are of interest to be delivered by the UAVs. This could expand the market for the UAV, making its operations more versatile and increasing the profits generated by Project Healios.

General overview

Ground movement and communication → Pre-flight operations → In-flight operations → Post-flight operations

Iterate continuously to maximise vehicle flight time

Legend

Sample block #1 — *Sequential tasks* → Sample block #2 → Sample block #3 (*Parallel tasks (AND tasks)*) → Sample block #4 → OR → Sample block #5 (*OR tasks*) / Sample block #6

Iteration/loop: Sample block #2 → Sample block #1

Construct flight plan

Gather delivery coordinates and input into flightplanning software → Generate preliminary flight plan → Check weather conditions and expected traffic density → Coordinate with authorities (U-space) → Iterate/ adapt flight plan → Load flightpath onto vehicle → Generate final flight plan

Establish contact with customer

Receive order request → Review customer information → Review payload and order information → Confirm/reject order

Confirm/reject order → *Planned delivery (long-term response)*

Confirm/reject order → *Emergency delivery (immediate reponse)*

In-house payload handling

Planned delivery (long-term response) → Wait for delivery of supplies → Inspect receive payload (mass, volume, content) → Categorize, make inventory, and store payload in warehouse

Emergency delivery (immediate reponse) → Check availability of supplies → Select and reserve supply batches from warehouse

Take Off

Vertical climb to transition altitude ← Lift-off ← Set engines & control surface to take-off mode ← Check for obstacles & debris

Transition

Activate control surfaces for transition → Activate actuators and rotate wing → Climb to cruise altitude → Accelerate to Vc

Pre-flight vehicle operations

Initialise vehicle software system → Perform autonomous pre-flight diagnostics (battery status, control system) → Perform wing actuator check → Standby for take-off confirmation

Perform once-over visual check (propellers, structure, landing gear, sensors) → Clear helipad → Startup engines and warmup → Perform control surfaces check (rigged controls)

Pre-flight ground operations

Assign vehicle → Transport payload batch(es) to hangar → Load payload → Taxi vehicle to helipad

Cruise

Gather telemetry → Obstacle avoidance reports; Autonomous Flight Data; Position status; Battery Level; Engine Status → Relay data to U-Space AND/OR Control Center

Continuously relay data

Taxiing and unloading

Remove and store payload (when applicable) → Return vehicle to hangar

Vehicle inspection

Perform once-over visual check (propellers, structure, landing gear, sensors) → Decide if unplanned maintenance is required, if not proceed to charging → OR → Take vehicle to garage for maintenance / Recharge vehicle (plug-in to HVDC system or swap batteries)

Maintenance and cleaning

Perform periodic cleaning and maintenance of stand-by vehicles

Perform periodic cleaning and maintenance of base equipment

Return to base

Shutdown engines and enter standby ← Perform nominal landing procedures at base ← Repeat cruise procedures ← Repeat transition procedures ← Repeat take-off procedures

Approach

Begin approach procedure → Perform holding pattern around landing site; Scan → Determine feasibility of landing → OR → Proceed / Consider relocating landing site

Relocate and begin new approach

Landing

Countinuously scan landing area and process data

Turn on landing lights → Start vertical landing → Reach decision altitude (go vs. no-go) → OR → Abort Landing → Communicate with base / Payload Deployment (landing method still TBD) → Confirm Delivery → Communicate with end user

13
Road to Certification

To get certified for the intended category and purpose, it is important to know at this point of the project whether requirements are fulfilled and risks are being mitigated. Therefore this chapter consists of the requirement compliance matrix and risk assessments. Both the general risk assessment as the strategic operations risk assessment will be displayed and explained.

13.1. Compliance Matrix

The vehicle shall be able to satisfy requirements set by the stakeholders, to complete the mission successfully. These requirements are listed in Table 13.1. The design of the vehicle has been guided by the constraints placed by these requirements, as reflected in the table. Unfortunately, a few requirements (noted below) were not possible to comply with due to insufficient resources during the detailed design phase, or because the requirement was not applicable to the current vehicle's configuration. In any case, the team recommends serious time investments into the compliance of these requirements in a hypothetical future design phase.

Table 13.1: Requirement Compliance Matrix

ID	REQUIREMENT	COMPLY	NOTE
OP-CER-UAS-01	The limits for mass and centre of gravity that provide for the safe operation of the UA shall be determined.	Yes	
OP-CER-UAS-02	The condition of the UA at the time of determining its mass and centre of gravity shall be well defined and easily repeatable.	Yes	
OP-CER-UAS-03	The boundaries of the approved flight envelope within which safe flight, under normal, abnormal and emergency conditions shall be determined.	Yes	
OP-CER-UAS-04	There shall be a means to prevent exceeding the approved flight envelope.	Yes	
OP-CER-UAS-05	The demonstrated flight envelope shall contain a safety margin agreed by the competent authority.	Yes	
OP-CER-UAS-06	Performance data shall account for losses due to atmospheric conditions, cooling needs, installation, downwash considerations, and other demands on power sources.	Yes	
OP-CER-UAS-07	The UA minimum safe speed or the minimum steady flight speed for each flight configuration and phase of flight shall be determined.	Yes	
OP-CER-UAS-08	The minimum safe speed determination shall account for the most adverse conditions for each flight configuration within the approved flight envelope.	Yes	
OP-CER-UAS-09	The UA minimum power required for take-off shall be determined.	Yes	
OP-CER-UAS-10	If the most critical flight phase is other than take-off, the UA minimum power for this flight phase shall be determined.	Yes	
OP-CER-UAS-11	Minimum climb performance at critical combinations of mass, altitude, and ambient temperature within the operating limitations shall be determined.	Yes	
OP-CER-UAS-12	The rate of descent performance in normal operation at critical combinations of mass, altitude, and ambient temperature within the operating limitations shall be determined.	Yes	
OP-CER-UAS-13	The rate of descent performance after a critical loss of propulsion at critical combinations of mass, altitude, and ambient temperature within the operating limitations shall be determined.	Yes	
OP-CER-UAS-15	The approach and landing speeds, configurations, and procedures, which allows for landing within the determined landing area consistently and without causing damage or injury shall be determined for ambient temperatures at critical combinations of mass and altitude within the operating limits.	Yes	
OP-CER-UAS-16	The approach and landing speeds, configurations, and procedures, which allows for a safe transition to the banked landing conditions accounting for the minimum safe speed shall be determined for ambient temperatures at critical combinations of mass and altitude within the operating limits.	Yes	
OP-CER-UAS-17	The UA shall be controllable and manoeuvrable, within the demonstrated flight envelope at all loading conditions for which certification is requested.	Yes	
OP-CER-UAS-18	The UA shall be controllable and manoeuvrable, within the demonstrated flight envelope during all phases of flight, including ground phases.	Yes	
OP-CER-UAS-19	The UA shall be controllable and manoeuvrable, within the demonstrated flight envelope during configuration changes.	Yes	
OP-CER-UAS-20	The UA shall be controllable and manoeuvrable, within the demonstrated flight envelope considering all related effects such as sensor inaccuracy, computational errors, and delay.	Yes	
OP-CER-UAS-21	The UA shall be controllable and manoeuvrable, within the demonstrated flight envelope in all degraded operating modes of the flight control systems.	Yes	
OP-CER-UAS-22	The UA shall not exhibit any unrecoverable divergent stability characteristic in all phases of flight, including ground phases.	Yes	
OP-CER-UAS-23	Each part of the UA shall be free from vibration and buffeting that could adversely affect subsystems within the approved flight envelope.	Yes	
OP-CER-UAS-25	The MTOM of the UA shall not exceed 3715kg.	Yes	
OP-CER-UAS-26	The UA shall not transport humans in any way.	Yes	
OP-CER-UAS-27	The UAS shall only be certified based on deterministic systems.	Yes	
OP-CER-UAS-28	The limitations of the operation within which safe flight, under normal and emergency conditions is conducted shall be defined.	Yes	
OP-CER-UAS-29	In defining the limitations of the operation within which safe flight, under normal and emergency conditions, environmental conditions shall be considered.	Yes	
OP-CER-UAS-30	There shall be a means to prevent exceeding the operating limitations.	Yes	
OP-CER-CI-01	The Remote Pilot Station shall be adequate to support the command and control of the UA by the remote crew for the intended operations.	Yes	
OP-CER-CI-02	The Remote Pilot Station and its installed equipment shall be qualified against the RPS environmental conditions expected for the intended operation.	Yes	
OP-CER-CI-03	The remote pilot station arrangement and its equipment shall allow the remote crew to perform their duties without excessive concentration, skill, alertness, or fatigue.	Yes	
OP-CER-CI-04	All flight, navigation, surveillance, and powerplant controls and displays shall be designed so that a qualified remote crew can monitor and perform defined tasks associated with the intended functions of systems and equipment.	Yes	
OP-CER-CI-05	The system and equipment design shall minimise remote crew errors, which could result in additional hazards.	Yes	
OP-CER-CI-06	Physical security requirements shall be considered.	Yes	
OP-CER-CI-20	Structural failures due to foreseeable causes of strength degradation on the UA, which could result in loss of control over the UA or extended periods of operation with reduced safety margins, shall be developed and implemented.	Yes	
OP-MI-UAS-01	The UA shall be able to take off vertically.	Yes	
OP-MI-UAS-02	The UAS shall be able to confirm if the landing site is clear and safe for landing operations.	Yes	
OP-MI-UAS-03	The UA shall be able to return to launch site carrying maximum payload during local delivery misson.	Yes	
OP-MI-UAS-04	The UAS shall be capable of executing the LDM and LM without any reconfiguration.	Yes	
OP-MI-UAS-06	The UA shall be certified to operate over rural and medium density suburban populations.	Yes	
OP-MI-UAS-07	The UA shall operate in flight conditions consistent with visual flight rules operation, both day and night.	Yes	
OP-MI-UAS-08	For the Local Delivery Mission, the UA shall not be refuelled or recharged at the delivery site.	Yes	
OP-MI-UAS-10	The payload shall be autonomously released from the UA.	Yes	

Table 13.1 continued from previous page

ID	REQUIREMENT	COMPL	NOTE
OP-MI-UAS-11	The UA shall be able to anchor the payload container.	Yes	
OP-MI-UAS-13	Ground infrastructure features shall accomodate operation of the UAS.	Yes	
OP-MI-PER-01	The system shall be able to carry at most 50kg payload for the LDM and LM.	Yes	
OP-MI-PER-02	The maximum range shall be 200km carrying maximum payload.	Yes	
OP-MI-PER-03	The UA planform shall be less than or equal to 6.1m x 6.1m.	Yes	
OP-MI-PER-04	Mission-Performance	Yes	
OP-MI-PER-05	The UA shall be able to carry a payload with dimensions 70cmx70cmx70cm	Yes	
OP-MI-PER-06	The UA shall be abble to carry a payload with dimensions 140cmx50cmx50cm	Yes	
OP-MI-PER-07	The block time of the UA for the LDM shall not exceed 28 minutes.	Yes	
OP-MI-PER-08	The block time of the UA for the LM shall not exceed 75 minutes.	Yes	
OP-MI-PER-09	The UA shall be designed for a cruise altitude of 150m above ground level.	Yes	
OP-MI-PER-10	The maximum operational altitude shall not exceed 1350m above sea level.	Yes	
OP-MI-CON-01	The UA shall have the capability to perform the LDM and LM autonomously.	Yes	
OP-MI-CON-02	The UA shall avoid obstacles in its flight path.	Yes	
OP-MI-CON-03	The UA shall avoid obstacles in the vicinity of the delivery site.	Yes	
FU-SYS-01	Equipment and systems shall be designed and installed so that they perform their intended function throughout the operating and environmental limits for which the UAS is certified.	Yes	
FU-SYS-02	Each item of installed equipment shall be installed according to limitations specified for that equipment.	Yes	
FU-SYS-03	Engine-driven accessories essential to safe operation shall be distributed among all engines.	Yes	
FU-SYS-04	The equipment and systems considered separately and in relation to other systems, shall be designed and installed such that each catastrophic failure condition is extremely improbable.	Yes	
FU-SYS-05	The equipment and systems considered separately and in relation to other systems, shall be designed and installed such that each hazardous failure condition is condition is extremely remote.	Yes	
FU-SYS-06	The equipment and systems considered separately and in relation to other systems, shall be designed and installed such that each major failure condition is remote.	Yes	
FU-SYS-07	UAS equipment, systems and networks, considered separately and in relation to other systems, shall be protected from intentional unauthorised electronic interactions that may result in catastrophic effects on the safety of the UAS.	Yes	
FU-SYS-08	Protection from cyber crime shall be ensured by showing that the security risks have been identified, assessed and mitigated as necessary.	Yes	
FU-SYS-09	The on-board generation, storage, distribution and supply of power to each system shall be designed and installed to supply the power required for operation of connected loads during all approved operating conditions.	Yes	
FU-SYS-10	The on-board generation, storage, distribution and supply of power to each system shall be designed and installed to ensure no single failure or malfunction will prevent the system from supplying the essential loads required for continued safe flight and landing or emergency recovery.	Yes	
FU-SYS-11	The on-board generation, storage, distribution and supply of power to each system shall be designed and installed to have enough capacity, if the primary source fails, to supply essential loads, including non-continuous essential loads for the time needed to complete the function, required for safe flight and landing or emergency recovery.	Yes	
FU-SYS-12	The UA flight control system shall comprise of sensors, actuators, computers and all those elements of the UAS, necessary to control the attitude, speed, trajectory and 3-dimensional position of the UA and to ensure the UA remains within the approved flight envelope, the intended flight path and within all spatial limitations in all flight phases.	Yes	
FU-SYS-13	If the approved flight envelope, the intended flight path or the spatial limitations can no longer be ensured, a means to transmit this information to the surrounding aviation system shall be available.	Yes	
FU-SYS-14	Any position lights and anti-collision lights, if required by operational rules, shall have the intensities, flash rate, colours, fields of coverage, position and other characteristics to provide sufficient time for another aircraft to avoid a collision.	Yes	
FU-SYS-15	Any position lights, if required by operational rules, shall include a red light on the port side of the UA, a green light on the starboard side of the UA spaced laterally as far as practical and a white light facing aft as far aft of the UA as practicable.	Yes	
FU-SYS-16	Taxi and landing lights or any other equivalent means, if required, shall be designed and installed so they provide sufficient guidance for the intended operations.	Yes	
FU-SYS-17	Pressurised systems shall withstand appropriate proof and burst pressures.	Yes	
FU-SYS-18	Equipment containing high-energy rotating parts shall be designed or installed such that, in the event they fail: they are safely contained, or they cannot damage other systems or subsystems.	Yes	
FU-SYS-19	If recording is required by the operational rules, the system shall ensure accurate and intelligible recording, safeguarding and locating of the required data, also in conditions encountered during emergencies, crash, water immersion or fire.	Yes	
FU-SYS-20	The UAS shall have the capability to perform Emergency Procedures and operational rules, to prevent fatal injuries to people on the ground.	Yes	
FU-SYS-21	The UAS shall have the capability to perform Emergency Procedures and operational rules, to prevent fatal injuries to people in the air.	Yes	
FU-SYS-22	The UAS shall have the capability to perform emergency procedures and operational rules, to prevent damage to critical infrastructure.	Yes	
FU-SYS-23	Where the safe operation of the UAS requires command, control and communication functionality, the UA shall initiate adequate contingency procedures following a command, control or communication function loss or a degraded status which no longer ensures safe operation of the UA by the crew.	Yes	
FU-SYS-25	There shall be a means to transmit to the surrounding aviation system the relevant information about the UA contingency procedures.	Yes	
FU-PPI-1	The UA powerplant installation shall include each component that is necessary for propulsion, affects propulsion safety, or provides auxiliary power to the UA.	Yes	
FU-PPI-3	The powerplant design shall account for all likely operating conditions, including foreign object threats.	Yes	
FU-PPI-4	The powerplant design shall account for sufficient clearance of moving parts to other UA parts and their surroundings.	Yes	
FU-PPI-5	The powerplant design shall account for likely hazards in operation, including hazards to ground personnel.	Yes	
FU-PPI-8	The powerplant design shall account for hazardous accumulations of fluids, vapours or gases.	Yes	
FU-PPI-9	Power or thrust control systems shall be designed so no unsafe condition will result during normal operation of the system.	Yes	
FU-PPI-10	Any single failure or likely combination of failures of a power or thrust control system shall not prevent continued safe flight and landing of the UA.	Yes	
FU-PPI-11	The system shall provide a means for the Flight Control System or the remote crew to override the automatic function.	Yes	
FU-PPI-13	A likely failure of any system component or accessory will not shall not prevent continued safe flight and landing.	Yes	
FU-PPI-14	If continued safe flight and landing cannot be ensured, an emergency recovery shall be initiated.	Yes	
FU-PPI-15	A likely failure of any system component or accessory shall not require immediate action by the remote crew for continued operation of any remaining powerplant system.	Yes	
FU-PPI-17	The installed powerplant shall operate without any hazardous characteristics during normal and emergency operation within the range of operation limitations for the UA and powerplant installation.	Yes	
FU-PPI-18	The design shall allow in flight shutdown of any powerplant or groups of powerplants if required by continued safe flight.	Yes	
FU-PPI-19	The design shall allow in flight restart of any powerplant if required by continued safe flight.	Yes	
FU-PPI-20	For powerplant containing rotating parts, if continued powerplant rotation after a powerplant shutdown would cause a hazardous event , means shall be provided that the powerplant stops rotating.	Yes	
FU-PPI-21	For VTOL UA certified with autorotation capability, autorotation shall be demonstrated.	Yes	
FU-PPI-22	Each system shall be designed to provide independence between multiple energy storage and supply systems so that a failure of any one component in one system will not result in the loss of energy storage or supply of another system.	Yes	
FU-PPI-24	Each system shall provide energy to the powerplant installation with adequate margins to ensure safe functioning under all permitted and likely operating conditions, and accounting for likely component failures.	Yes	
FU-PPI-25	Each system shall provide uninterrupted supply of that energy when the system is correctly operated, accounting for likely energy fluctuations.	Yes	
FU-PPI-26	Each system shall provide a means to safely remove or isolate the energy stored within the system.	Yes	
FU-PPI-27	Each system shall be designed to retain the energy under all likely operating conditions.	Yes	
FU-PPI-28	Each system shall prevent hazardous contamination of the energy supplied to each powerplant installation.	Yes	
FU-PPI-29	Each storage system shall withstand the loads under likely operating conditions without failure, accounting for installation.	Yes	
FU-PPI-31	Each storage system shall provide energy for Emergency Recovery if needed.	Yes	
FU-PPI-32	Each storage system shall be capable of jettisoning energy safely if this functionality is provided.	No	
FU-PPI-36	Likely errors during ground handling of the UA shall not lead to a hazardous loss of stored energy.	Yes	
FU-PPI-37	Powerplant installation support systems shall be designed for the operating conditions applicable to the location of installation.	Yes	
FU-PPI-38	System function and characteristics that have an effect on the powerplant installation system performance shall be established.	Yes	
FU-PPI-39	Ingestion of likely foreign objects that would be hazardous to the engine shall be prevented.	Yes	
FU-PPI-40	Any likely single failures of powerplant installation support systems that result in a critical loss of thrust shall be mitigated.	Yes	
FU-PPI-41	The powerplant installation and its support systems shall be designed to mitigate catastrophic events due to fire or overheat in operation so that an emergency recovery can be performed.	Yes	
FU-PPI-48	Information shall be established on any additional information necessary for the safe operation of the UA.	Yes	
FU-STR-01	The structural design envelope shall be determined, which describes the range and limits of UA design and operating parameters.	Yes	
FU-STR-02	The system structural design and operating parameters shall account for structural design speeds.	Yes	
FU-STR-03	The system structural design and operating parameters shall account for flight and ground load conditions to be expected in service.	Yes	

Table 13.1 continued from previous page

ID	REQUIREMENT	COMPL	NOTE
FU-STR-04	The system structural design and operating parameters shall account for mass variations and distributions over the applicable mass and centre of gravity envelope, within the operating limitations .	Yes	
FU-STR-05	The system structural design and operating parameters shall account for loads in response to all designed control inputs.	Yes	
FU-STR-06	The system structural design and operating parameters shall account for rotors/fans/propellers rpm ranges for power-on and power-off.	Yes	
FU-STR-07	The system structural design and operating parameters shall account for rotational speed ratios between powerplant and each connected rotating component.	Yes	
FU-STR-08	The system structural design and operating parameters shall account for the redistribution of loads if deflections under load would significantly change the distribution of external or internal loads.	Yes	
FU-STR-09	For UA equipped with systems that affect structural performance, either directly or as a result of failure or malfunction, the influence and failure conditions of these systems shall be accounted for.	Yes	
FU-STR-10	The structural internal and external design loads at all critical combinations of parameters, at and within the boundaries of the structural design envelope shall be determined.	Yes	
FU-STR-11	The flight load conditions shall be determined, to ensure critical flight loads are established for symmetrical and asymmetrical loading from all combinations of speeds and load factors at and within the boundaries of the maneuver and gust envelope.	Yes	
FU-STR-12	The flight load conditions shall be determined, to ensure vibration, including air resonance, and buffeting does not result in structural damage up to the maximum design speed.	No	Insufficient Resources
FU-STR-13	The flight load conditions shall be determined, to ensure flight loads resulting from a failure of an UA system, such as component, engine, rotor or propeller, are determined.	Yes	
FU-STR-14	The structural design loads resulting from taxi, take-off, launch, landing, handling and transportation conditions on the applicable surfaces in normal and adverse attitudes, configurations and conditions shall be determined.	Yes	
FU-STR-15	The UA shall have no dangerous tendency to develop ground resonance in normal conditions.	No	Insufficient Resources
FU-STR-16	The loads acting upon all relevant structural components shall be determined in response to the interaction of systems and structures.	Yes	
FU-STR-17	The loads acting upon all relevant structural components shall be determined in response to the structural design loads.	Yes	
FU-STR-18	The loads acting upon all relevant structural components shall be determined in response to the flight load conditions.	Yes	
FU-STR-19	The loads acting upon all relevant structural components shall be determined in response to the ground and water load conditions.	No	Insufficient Resources
FU-STR-20	The loads acting upon all relevant structural components shall be determined in response to the powerplant.	Yes	
FU-STR-21	The loads acting upon all relevant structural components shall be determined in response to the drive system.	Yes	
FU-STR-22	Pressurised compartments shall be designed to withstand the differential pressure loads corresponding to the maximum relief valve setting multiplied by a factor of 1.33, without considering other loads.	N/A	
FU-STR-23	The structural design loads acting on rotor assemblies, considering loads resulting from flight and ground conditions, as well as limit input torque at any rotational speed shall be determined.	Yes	
FU-STR-24	The limit loads, which are equal to the structural design loads shall be determined.	Yes	
FU-STR-25	The ultimate loads, which are equal to the limit loads multiplied by a 1.5 factor of safety shall be determined.	Yes	
FU-STR-26	The structure shall support limit loads without interference with the safe operation of the UA.	Yes	
FU-STR-27	The structure shall support limit loads without detrimental permanent deformation.	Yes	
FU-STR-28	The structure shall support limit loads without ultimate loads without failure.	Yes	
FU-STR-29	The system shall implement maintenance inspections or other maintenance procedures to prevent structural failures due to foreseeable causes of strength degradation, which could result in fatal injuries, or extended periods of operation with reduced safety margins.	Yes	
FU-STR-32	For UA with pressurised compartments, the UA shall be capable of continued safe flight and landing or emergency recovery following a sudden release of pressure in any pressurised compartment, as a consequence of any probable cause.	N/A	
FU-STR-33	For UA with pressurised compartments, the maintenance procedures shall be capable of detecting damage to the pressurised compartment structure before the damage could result in rapid decompression or in a structural failure that would result in a catastrophic event.	N/A	
FU-STR-34	The UA shall be designed to minimise hazards to the UA due to structural damage caused by high-energy fragments from an uncontained engine or rotating-machinery failure.	Yes	
FU-STR-35	The UA shall be free from flutter, control reversal, and divergence at all speeds within and sufficiently beyond the structural design envelope.	No	Insufficient Resources
FU-STR-36	The UA shall be free from flutter, control reversal, and divergence for any configuration and condition of operation.	No	Insufficient Resources
FU-STR-37	The UA shall be free from flutter, control reversal, and divergence accounting for critical degrees of freedom.	No	Insufficient Resources
FU-STR-38	The UA shall be free from flutter, control reversal, and divergence accounting for any critical failures or malfunctions.	No	Insufficient Resources
FU-STR-39	Tolerances for all quantities that affect flutter shall be accounted for.	No	Insufficient Resources
FU-STR-40	Each part, article, and assembly shall be designed for the expected operating conditions of the UA.	Yes	
FU-STR-41	Design data shall adequately define the part, article, or assembly configuration, its design features, and any materials and processes used	Yes	
FU-STR-42	The suitability of each design detail and part having an important bearing on safety in operations shall be determined.	Yes	
FU-STR-43	The flight control system shall be free from jamming, excessive friction, obstruction and or excessive deflection when the UA is subjected to expected limit air loads.	Yes	
FU-STR-44	Doors, access panels and canopies shall be protected against inadvertent opening in flight, unless shown to create no hazard, when opened in flight.	Yes	
FU-STR-45	If the type design includes critical parts, a critical parts list shall be established.	No	
FU-STR-48	Each part of the UA, shall have adequate provisions for ventilation and drainage.	N/A	
FU-STR-49	For each part that requires maintenance, preventive maintenance, or servicing, a means into the UA design to allow such actions to be accomplished shall be incorporated.	Yes	
FU-STR-50	There shall be enough clearance between movable or rotating parts (such as propellers or rotor blades) and other parts of the structure to prevent the movable or rotating parts from striking any part of the structure during any operating condition including emergency recovery.	Yes	
FU-STR-54	Design values that ensure material strength with probabilities that account for the criticality of the structural element shall be selected.	Yes	
FU-STR-65	Each cargo compartment shall be designed for its maximum loading and for the critical load distributions at the maximum load factors corresponding to the flight and ground load conditions.	Yes	
FU-STR-66	Each cargo compartment shall have a means to prevent the contents of the compartment from becoming a hazard by impacting or shifting.	Yes	
FU-STR-67	Each cargo compartment shall protect controls, wiring, lines, equipment, or accessories whose damage or failure would prevent continued safe flight and landing or its emergency recovery capability.	Yes	
SUS-SOC-REL-1	The UA shall be controllable and manoeuvrable, within the demonstrated flight envelope with a reversible flight control system failure.	Yes	
SUS-SOC-REL-2	The UA shall be controllable and manoeuvrable, within the demonstrated flight envelope with a propulsion system failure.	Yes	
SUS-SOC-REL-3	In a non-catastrophic failure scenario the UA shall be capable of continued safe flight for 15 minutes.	Yes	
SUS-SOC-REL-4	In a non-catastrophic failure scenario the UA shall be capable to perform safe landing without damage to the UAS	Yes	
SUS-SOC-REL-6	Fail-safe design practices shall be conducted under the reference advisory circular C25.1309-1A for the US Federal Aviation Administration.	Yes	
SUS-SOC-DaC-2	Trim systems, if installed, shall be designed to protect against inadvertent, incorrect, or abrupt trim operation	N/A	
SUS-SOC-DaC-3	The take-off and landing device shall be designed to provide stable support and control to the UA during ground operation.	Yes	
SUS-SOC-DaC-4	The take-off and landing device shall be designed to account for likely system failures and likely operation environment (including anticipated limitation exceedances and Emergency Procedures)	Yes	
SUS-SOC-DaC-5	The UA shall be designed to absorb the kinetic energy for the landing performance and in the normal and adverse loading conditions.	No	
SUS-SOC-DaC-6	There shall be a positive means to keep the landing devices in the landing position.	N/A	
SUS-SOC-DaC-7	There shall be an alternative means available to bring the landing devices in the landing position when a non-deployed system position would be a hazard	N/A	
SUS-SOC-DaC-9	The UA shall be designed to minimise the risk of fire.	Yes	
SUS-SOC-DaC-12	Terminals, equipment, and electrical cables used during Emergency Procedures shall be fire-resistant or safely shielded.	Yes	
SUS-SOC-DaC-13	Where the emergency procedure foresees a forced landing or a controlled crash the UA shall be designed with sufficient self-containment features to minimize the risks resulting from possible debris, fire or explosions extending beyond the forced landing or controlled crash area.	Yes	
SUS-SOC-DaC-15	Non-essential systems and equipment, whose functioning is not required to comply with type certification requirements, airspace requirements or operational rules, shall be installed and have design characteristics to ensure no hazardous or catastrophic events occur, under any foreseeable operating condition for which the UAS is certified.	Yes	
SUS-SOC-DaC-19	Any additional information necessary for the safe operation of the UA shall be defined.	Yes	
SUS-SOC-DaC-20	The UA external cargo load attaching means, and corresponding carrying device system to be used for external cargo applications, shall withstand the loads associated with the maximum mass and critical configurations of external cargo for which certification is requested, with adequate safety margins.	N/A	
SUS-SOC-DaC-21	The external cargo loads shall be shown to be transportable and, if required, releasable throughout the approved external cargo l envelope without hazard for the UAS or people during normal and emergency conditions.	N/A	
SUS-SOC-DaC-23	The applicant shall comply with CS-UAS by using an authority accepted Airworthiness Design Standard (ADS).	Yes	

13.2. Risk Assessment

An important step on the way to certification is a risk assessment. As this step has been a recurring activity throughout the Design Synthesis Exercise the same method has been followed during the detailed design. In addition to the risk identification and risk mitigation regarding the process, finances, design and operations risks a new category has been created, namely project risks. This category incorporates the risks that might occur between the finalisation of the DSE and the implementation of the vehicle. Adding this extra category ensures risks are identified and mitigated across all aspects of the design. In addition to this general risk assessment, a Strategic Operations Risk Assessment (SORA) is required for certification. This SORA will be conducted and displayed after the general risk assessment.

13.2.1. General Risk Assessment

The general risk assessment is the overarching risk identification and mitigation. It considers risks on the system base instead of subsystem base and, in addition to the technical risks, it considers non-technical risks. The method of identifying and assessing risks can be explained as follows: In different categories, multiple different actions or events can occur that pose a risk to the design or mission. These events are devised throughout the project and altered along the way depending on different circumstances and changes. They are based on personal experience, comparable or preceding projects and common expectations. After identification of these risks, a risk level can be assigned. This is done by assigning each risk with a level of likelihood and consequence. These levels are explained below

Likelihood
1 - The likelihood of the event occurring is negligible
2 - The event is unlikely to occur
3 - There is a fair chance the event will occur
4 - The event will most likely occur
5 - It is more likely the event will occur than not

Consequence
1 - The consequence of the event is negligible
2 - There is a consequence but it is not severe
3 - The consequence of the event leads to required actions
4 - There is a high consequence to the occurrence leading to extra work or substantial changes
5 - The consequence of the occurrence is disastrous and might lead to fatalities or cancellation

Using these levels of likelihood and consequence, risk levels can be assigned ranging between negligible risk (NR), low risk (LR), medium risk (MR), high risk (HR), and extreme risk (ER). These risk levels belong to the following sums of likelihood and consequence levels:

2 Negligible 3-4 Low 5-6 Medium 7-8 High 9-10 Extreme

These risks can then be mitigated by defining preventive and corrective actions that will either decrease the likelihood of occurrence or the consequence caused by any of the risks. Taking into account these risk-specific mitigations. The new likelihood and consequence levels can be assigned and a new risk level follows from these combinations. To visualise the effectivity of mitigation, the risks can be shown in a risk map. These risk maps are displayed at the end of this chapter in Table 13.3 and Table 13.4. Before this conclusion, the devised risks are displayed with their specific levels and mitigations in Table 13.2.

Table 13.2: Risk assessment

ID	Safety item or hazard	LH/C	RL	Worst consequence	Mitigation	NLH/C	NRL	Resp
F1	Stock-market crash	2/3	MR	Cancellation of project	PA: Financial buffer, CA: Re-focus acquisition	2/2	LR	AS
F2	Price rise for required products	3/3	MR	Scarceness/project termination	PA: Financial planning, CA: Revise material selection	3/2	MR	AS
F3	Competitor stealing investors	2/3	MR	Cancellation of project	PA: Minimise conservatism, CA: Re-focus promotion	1/3	LR	All
F4	Expenditure due to inexperience	3/3	MR	Waste of time and resources	PA: Logical task allocation, CA: Reassigning resources	2/2	LR	All
P1	Work lost due to technical issues	4/3	HR	Overwork	PA: Making back-ups of all work, CA: -	4/2	MR	All
P2	Misalignment in subsystems	3/4	HR	More reiterations and time lost	PA: Clear N2 chart and plan, CA: Revising subsystems	2/3	MR	MF, BS

P3	Feedback requiring change	4/4	HR	Overwork	PA: Clear communication, CA: Applying feedback	4/2	MR	All
D1	Infeasible concept	3/4	HR	Revision of concept	PA: Thorough trade-off, CA: Rethinking concept	2/3	MR	All
D2	Calculation and design errors	4/3	HR	Faults in design and extra reiteration	PA: Verification and Validation with built in checks, CA: Recalculation	3/2	MR	All
D3	Neglection of external inputs	2/4	MR	Inability to operate during extreme conditions	PA: Extensive requirement identification, CA: Re-designing subsystems	1/3	LR	JR, BS, DW, MF
D4	Misalignment between design and operations	2/4	MR	Unfeasible design	PA: Extensive requirement identification, CA: Revising requirements and demands	1/3	LR	JR, BS, DW, MF
D5	Design does not uphold standards	2/5	HR	Certification impossible	PA: Extensive requirement identification and risk management, CA: Revising the design	1/4	MR	JS, BS, DW, MF, YH
D6	Issues causing delay in other subsystems	3/3	MR	Delay and less time to iterate and improve	PA: Issuing a detailed planning, CA: Re-allocation of resources	2/2	LR	PG
D7	Feedback requiring adjustments	4/3	HR	Unplanned revision	PA: Clear communication with tutor, coaches and TA, CA: Make required changes	3/2	MR	All
D8	Unexpected technological advancements	5/3	HR	Outdated or too futuristic design	PA: Extensive research into current technologies and possibilities, CA: Adjusting design if necessary/possible	4/2	MR	All
D9	Lack of robustness	3/3	MR	Operations failure	PA: Designing for redundancies and fail safes, CA: Revision of subsystems	2/3	MR	All
D10	Missing subsystem design	2/4	MR	Overwork and integration issues	PA: Complete N2 chart, CA: Re-allocate resources	2/3	MR	JR, MF, BS
D11	Unsolvable complexity issues	3/4	HR	Infeasible concept	PA: Thorough literature study and trade-off, CA: Find alternatives	2/3	MR	All
D12	Inability to meet constraints	3/4	HR	Infeasible concept	PA: Preliminary sizing and thorough trade-off, CA: Revising concept and subsystems	2/3	MR	All
OD1	Collision	3/5	HR	Destruction of vehicle and fatalities	PA: Extensive iteration of control subsystem, CA: -	2/5	HR	AM, PG, MF
OD2	Loss of subsystem	3/4	HR	Vehicle mission compromised	PA: Built in safety margins and extensive verification and validation, CA: -	3/3	MR	All
OD3	Severe weather and disruptive climatic events disrupt operations	3/4	HR	Inability to perform mission	PA: Adjusting design to specified requirements, CA: -	2/4	MR	All
OD4	Take-off and landing issues	3/4	HR	Destruction of infrastructure, vehicle and fatalities	PA: Iteration and verification and validation of system, CA: -	2/3	MR	All
OD5	Piloting errors	2/4	MR	Destruction of vehicle and fatalities	PA: Research into piloting possibilities with fitting design, CA: -	2/3	MR	As, CC

OD6	Corrosion or fatigue problems	2/4	MR	Short lifetime and high cost	PA: Materials trade-off and LCA, CA: -	2/3	MR	AM, BS, DW
OD7	Destruction to surroundings	3/5	HR	Destruction of infrastructure, vehicle and fatalities	PA: Designing redundancies and thorough V&V approach, CA: reprogramming/redesigning	2/5	HR	All
OD8	Ground crew endangerment	3/4	HR	Physical injuries and fatalities	PA: Establishing clear guidelines and design for safety, CA: Increase safety measures and reschool users	2/4	MR	All
OD9	Operations out of design envelope	2/4	MR	System failure	PA: Design with safety margins and clear programming, CA: -	2/3	MR	All
OD10	Sustainability risk	3/3	HR	Contributing to environmental decay and loss of investors	PA: Thorough sustainability approach, CA: Redesign (sub)systems	2/2	LR	All
OD11	Payload endangerment*	3/5	HR	Destruction or loss of payload	PA: Thorough design of payload handling system with safety margins, CA: -	3/4	HR	BS, DW, DL
OD12	Inability to locate drop-off site	3/5	HR	Inability to complete mission	PA: Detailed design of control and communication systems. CA: Redesign/reprogram subsystems	2/4	MR	AM. PG, MF
OD13	Unavailability of resources on landing site	3/5	HR	Inabillity to complete mission or return	PA: Design detailed operations plan, CA: Relocating resources	2/4	MR	CC, AS
PR1	Unability to get certified	3/5	HR	Failure to meet goal	PA: Risk analysis and well developed design, CA: Redesign of vehicle	2/4	MR	All
PR2	Exceeding of time	3/4	HR	Delay in employment	PA: Create detailed project planning and Gantt chart, CA: -	2/4	MR	JR, BS, PG
PR3	Discovery of mistakes	5/3	HR	Delay and extra resources	PA: accurate reporting and V&V, CA: Redesign (sub)systems	4/2	MR	All
PR4	Difficulties manufacturing	3/3	MR	Delay or redesign	PA: Design with manufacturing in mind, CA: Redesign parts and switch materials	2/2	LR	All

* This risk also takes into account criminal activities or destruction of the vehicle by bystanders with bad intentions.

Table 13.3: Risk map (before mitigation)

Likelihood	Consequence 1	2	3	4	5
1					
2				OD5, OD6, OD9	
3			OD10	OD2, OD3, OD4, OD8, PR2, PR4	OD1, OD7, OD11, OD12, OD13, PR1
4					
5			PR3		

Table 13.4: Risk map after mitigation

Likelihood	Consequence 1	2	3	4	5
1					
2		OD10, PR4	OD4, OD5, OD6, OD9	OD3, OD8, OD12, OD13, PR1, PR2, PR3	OD1, OD7
3			OD2	OD11	
4			PR3		
5					

Risk maps are used to quickly highlight critical risks. For the purpose of clarity, only the scenarios that were added with respect to the Midterm Report [2] are shown in the risk map in Table 13.3 (before mitigation) and Table 13.4 (after mitigation), the other scenarios are not displayed in the risk map but their risk levels

and accompanying colours are shown in the table. Moreover, scenarios that had not yet been assigned a risk level are displayed in the map.

13.2.2. Strategic Operations Risk Assessment

One of the main requirements to get certified by the Joint Authorities for Rulemaking of Unmanned Systems (JARUS) is to perform the Strategic Operations Risk Assessment (SORA). This assessment consists of 10 steps that need to be done, which will be displayed below. The method has been previously explained in the Baseline Report, therefore the execution is short and concise. [4]

1. **ConOps Description**
   The ConOps Description that is used for the SORA can be found in Chapter 12.
2. **Determination of the intrinsic UAS Ground Risk**
   The intrinsic UAS Ground Risk Class (GRC) is related to the risk of a person being hit by the UAS. It is related to the maximum characteristic dimensions and intended operations. Healios falls in the category: Max 8m wingspan/rotor diameter/maximum dimension, flying in a (sparsely) populated area Beyond Visual Line of Sight. The value for this category is a GRC of 8. For the UAS to be certified, a GRC of 7 or less is required. Therefore mitigations are required to reduce the GRC.
3. **Final GRC Determination**
   The GRC can be decreased by mitigating risks. These mitigations all deal with the safety of surrounding people. This can include mitigations during design like: The propellers are never completely forward at ground level, but always under an angle. The UAS will fly over the least populated areas between the hub and destination. Safety protocols for handling the UAS will be developed at later stages. Taking into account these mitigations the GRC can be decreased to 6 or 7 which falls within the requirements for certification in the specific category.
4. **Determination of the initial Air Risk Class (ARC)**
   Using the decision tree in the SORA document, the ARC can be found to be either B or C depending in the specifics of the mission. This depends on whether the airspace is over urban or rural areas which can differ between missions.
5. **Determination of residual ARC**
   If the initial ARC is too high for the condition in the local Operational Volume the ARC can be reduced. Given the lack of a highly detailed operational volume, this step is not performed and the ARC is assumed to be C.
6. **Tactical Mitigation Performance Requirement (TMPR) and Robustness Levels.**
   Tactical mitigations are applied to mitigate the residual risk of collision mid-air. Based on the ARC of C Medium TMPR and Robustness are required. These include systems for object avoidance and emergency processes that would be designed in the future.
7. **Specific Assurance and Integrity Levels (SAIL) determination**
   SAIL drives required activities based on the GRC and ARC. Based on the table in the SORA the SAIL of Healios is V-VI.
8. **Identification of Operational Safety Objectives**
   Using this SAIL parameter, the required robustness of the Operational Safety Objectives can be found. For the SAIL of V-VI, all OSO require a robustness of medium to high. These 24 OSO relate to technical issues with the UAS, deterioration of external systems supporting UAS operation, human error, and adverse operating conditions. This means that well-developed protocols need to be in place and have to be designed in the future.
9. **Adjacent area/Airspace considerations**
   These considerations take into account the chance of loss of control and pose safety requirements: No probable failure of the UAS or supporting system shall lead to operation outside of the operational volume. The probability of leaving the operational volume shall be less than $10^{-}4$/FH. Software and airborne electronic hardware whose development error(s) could directly lead to operations outside of the ground risk buffer shall be developed to an industry-standard or methodology recognised as adequate by the competent. Since off the shelf avionics will be used, these requirements have been or will be covered.
10. **Safety Portfolio**
    In future steps of the project, a comprehensive safety portfolio needs to be developed and updated in order to apply for certification.

14

Sustainable Development Strategy

Sustainability is a crucial part of the project's design, as Healios is to set an example of how to develop UAV technology for medical distribution that can be socially friendly, environmentally responsible, and economically viable [2]. Furthermore, sustainability has been implemented in all the design efforts made during the project; by decreasing the UAV's drag in order to reduce the power consumption during flight (Section 7.8), choosing materials with a high recycle fraction where possible (Section 8.6), designing a control system that offers redundancy and minimises the risk of injuring people, makes the UAV fly efficiently, and reduces the hardware footprint (Section 9.11), while utilising an electric propulsion system that minimises emissions and noise (Section 10.6). Furthermore, the design of the permanent operational bases minimises the environmental impact by using solar farms to recharge the batteries when possible, provides jobs for the local communities while improving the local healthcare system, and reduces the cost when compared against helicopter bases.The movable bases allow for flexible emergency responses (Section 12.5), thus improving the social sustainability of project Healios.
Now that these design efforts have been made, this section analyses how project Healios contributes to sustainability(Section 14.1), while also performing a Life Cycle Assessment (LCA) to calculate the project's footprint (Section 14.2). From this LCA, the end of life phase is also analysed (Section 14.3)(and coordinated with the cost analysis). Finally, future design recommendations are indicated with the information gathered from the LCA in order to further improve Healios' sustainability (Section 14.4).

14.1. Contributing to Sustainability

Project Healios contributes to sustainability in several ways. This section investigates the social, economic, and environmental impact Healios can have once it is deployed.

Between 1995 and 2015, weather-related disasters *"claimed over 606,000 lives and left 4.1 billion people injured, homeless, and/or in need of emergency assistance"*[64]. Having an effective response to natural disasters is thus crucial. Healios contributes to generating this effective response, as the UAV can be used to deliver emergency payloads in situations where the affected area is not accessible by land or is too dangerous for manned air systems. Furthermore, Healios can provide a faster response service when compared to ground-based services, as it cruises at over 180 km/h, and can be more versatile than planes (as it has VTOL capabilities) as well as landing on smaller areas when compared to helicopters. Additionally, Healios can work alongside trucks, helicopters and other emergency response devices to provide a flexible and effective response to different emergency situations (i.e helicopters could be used to evacuate people or carry heavy payloads while Healios deploys medications, or in some situations, Healios can provide medication before the land-based units arrive at the required location).

Furthermore, it is important to understand the public acceptance of civil drones, as it is perceived that drones can be an issue primarily in regards to crime and misuse, violation of privacy, liability and insurance, as well as transport safety, [65]. However, from a study made by [65] 49% of the population has a positive attitude towards civil drones, whereas 43% has a negative attitude and 8 % are undecided with regards to the use of civil drones. Nevertheless, if the UAV is used primarily for functions of rescue and protection, public acceptance is high, even for drone overflight [65]. Thus, since Healios is primarily used for emergency situations, it will potentially have a positive public acceptance.

Additionally, Project Healios can provide a long term cost-effective solution regarding emergency response systems once the project reaches economies of scale. Drones can provide a cheaper solution when compared to trucks, as shown in Figure 14.1 and Figure 14.2 [64]. In this way Healios may contribute to the future economic sustainability of the emergency relief sector, and lead the way for other drones to enter this sector as well as creating new jobs, thus helping with the overall economic sustainability of the sector.

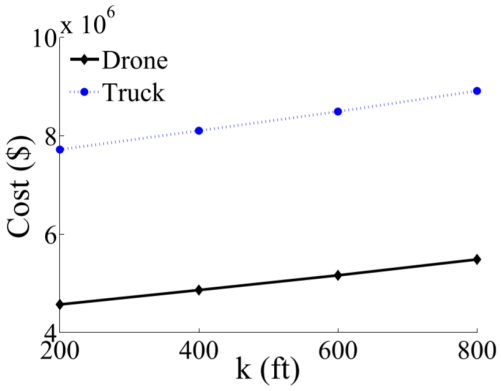

Figure 14.1: Cost of emergency payload delivery vs altitude [64]

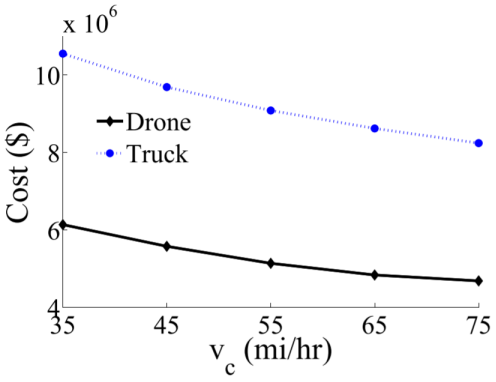

Figure 14.2: Cost of emergency payload delivery vs cruise speed [64]

Moreover, Healios positively contributes to improving the environmental sustainability of the emergency response sector. When compared to trucks Healios can help reduce the CO2 footprint by as much as 23,000 kg (see Section 14.2).

14.2. Life Cycle Assessment

From a sustainability standpoint, it is important to understand how the choices made during the design of the UAV affect the environment. This can then allow refining these design choices in future iterations of the design to further minimise the environmental impact of Healios.

In order to estimate the environmental impact of one UAV, a LCA is done to calculate the energy consumption and CO2 emissions required for primary producing, processing, operating and recycling (if possible) the different materials used in the UAV vehicle. This is mainly done by using the EduPack 2020 software database in regards to the different materials that constitute the UAV, while the battery LCA is calculated from the study *"Analysis of the climate impact of lithium-ion batteries and how to measure it"* from the *Circular Energy Storage* [66]. Figure 14.3 shows the different parts of the LCA.

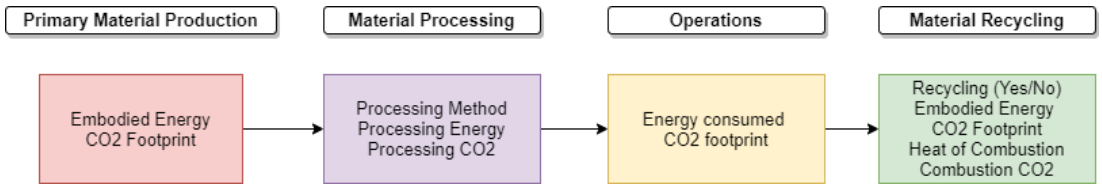

Figure 14.3: LCA calculation process

Additionally, when calculating the operations' energy usage and CO2 emissions, the UAV is assumed to be in service for a total duration of 10 years, flying 450 hours per year (300 missions) (see Chapter 2). Also, all the missions performed are assumed to fly to logistic centres 200 km away, as this is the most demanding mission in terms of energy needed. Furthermore, it is assumed that one set of batteries is used for the 10 years operational duration.

Since the embedded CO2 emissions and energy consumption of the battery can vary significantly (between 39 up to 196 CO2e/kWh)[66], a conservative estimate for the pack production footprint (assuming 73 CO2e/kWh and 990 MJ/kWh) is used to account for the operational footprint of the batteries.

Furthermore, when performing the LCA, the parts that constitute the UAV have been split into two main branches: structural components, and power and propulsion components. This is done to help identify which subsystems of the drone are more demanding in terms of sustainability, and to generate future design decisions to reduce the UAV's footprint (see Section 14.4). In addition, for each of these parts, the appropriate manufacturing technique is applied to calculate the material processing characteristics.

Regarding the structural components, the only off-the-shelf component is the wing actuator, which is modelled as being mainly composed by Aluminium. Furthermore, the materials used are Al7075 and GFRP. All this is shown in Table 14.1:

Table 14.1: Structural components used for LCA

Feature	Parts	Materials used	Material Mass [kg]	Production Method
Wing				
	Spar	Al7075	28.86	Extrusion
	Skin	Al7075	13.6	Roll forming
	Ribs	Al7075	4.8	Coarse machining
	Stiffeners	Al7075	7.74	Extrusion
Tail				
	Tail arm	Al7075	5	Extrusion
	Vertical tail	Al7075	3	Coarse machining
	Horizontal Tail	Al7075	4	Coarse machining
Frame				
	Truss	Al7075	6.5	Extrusion+welding
	Fairing	GFRP	5	Resin transfer molding
	Wing actuator	Al7075	21	Coarse machining

Regarding the propulsion components, the rotor blades are made out of CFRP, while the motors, which are off-the-shelf, are modelled as being made out of Aluminum (if more accuracy is needed in this regard, the engines could be broken down into several components and their respective materials, however as a first order LCA, this model is considered to be of sufficient accuracy). This is shown in Table 14.2:

Table 14.2: Propulsion components used for LCA

Feature	Parts	Materials used	Material Mass [kg]	Primary material production
Engines				
	Blades	CFRP	10	Filament winding
	Engine	Al7075-T6	40	Coarse machining
	Engine aux	Al7075-T6	1.5	Coarse machining
Li-Ion Batteries			134.8	

Then, the energy consumption and CO2 emissions of the different materials as given by EduPack 2020 are shown in Tables 14.3 to 14.5. Notice that the batteries are analysed according to [66], where a cradle to gate energy consumption of 990 MJ/KWh and emissions of 140 kg CO2/KWh is used.

Table 14.3: Al7075 energy consumption and CO2 emissions

	Primary Material Production	Extrusion	Roll Forming	Coarse Machining	Recycling
Energy [MJ/kg]	206	19.8	10	1.98	35.5
CO2 [kg/kg]	13.7	1.48	0.752	0.149	2.79

Table 14.4: CFRP energy consumption and CO2 emissions

	Primary Material Production	Filament Winding	Combust for Energy Recovery
Energy [MJ/kg]	723	2.84	32.9
CO2 [kg/kg]	50.5	0.227	3.33

Table 14.5: GFRP energy consumption and CO2 emissions

	Primary Material Production	Resin Transfer Molding	Combust for Energy Recovery
Energy [MJ/kg]	110	13.4	12.6
CO2 [kg/kg]	6.49	1.08	1.02

Furthermore, the calculated LCA results are shown in Table 14.6. These are calculated by multiplying the respective specific energy and CO2 emissions by the corresponding material masses, or in the case of the battery, by the KWh energy needed to perform a mission to logistics centres. This gives a total energy consumption footprint of over 97,000 MJ and roughly 7,000 kgs of CO2 (see Table 14.6). When compared to cars, Healios reduces the CO2 footprint by 23,528 kg when compared to internal combustion engine cars, and 12,327 kg when compared to electric cars [67]. Since this value is heavily dependent on the embedded footprint used (which is 73 kg CO2e/kWh), a sensitivity analysis has been done in this regard, changing the embedded footprint from 39 kg CO2e/kWh up to 196 kg CO2e/kWh (which are the bounds stated in [66]). Thus, as a best case scenario, Healios reduces its footprint by 25,410 Kg vs ICEV, and 14,209 kg vs EV, and as a worst case scenario, by 16,721 kg vs ICEV, and 5,521 kg vs EV.

Table 14.6: LCA emissions and energy consumption for the different components

	Wing	Tail	Frame	Propulsion	Batteries	Total
Energy consumption [MJ/kg]	14152.7	3010.9	7491.5	17691.8	54787.5	97135.4
CO2 emissions [kg/kg]	972.1	206.3	509.2	1231.1	4039.9	6959.5

14.3. End of Life

Regarding the approach to the End of Life of the UAV, first, the components of the UAV are inspected and reused when possible (structural components such as the frame or the wing components can be implemented into new UAVs or be used as backups if the fatigue levels are acceptable), this way both the UAV unit cost and footprint are reduced. Furthermore, as specified in Chapter 16, the components of the UAV that can not be reused are outsourced to companies that recycle them. Additionally, most of the structural and propulsion components of the drone are made out of Aluminium (see Tables 14.1 and 14.2) which has a high recycle fraction (50 % or more in the current supply, as stated in EduPack 2020). Regarding the CFRP and GFRP, during the LCA it is assumed that the materials can't be recycled and can only be used for energy recovery. However, this was done to give a conservative estimate of the footprint of these materials, as the companies to which these polymers are outsourced can recycle up to 30 percent [68]. Finally, the battery pack recycle fraction is assumed to be 15% for the LCA (which is the worst-case scenario [66]) in order to have a conservative estimate, however, the company to which the battery pack is outsourced can recycle up to 80% of the battery pack [69]. Thus the UAV materials are either recycled or reused, and the only waste generated comes from the parts that can not be fully recycled, which are mainly the rotor blades, fuselage fairing, and the battery pack.

14.4. Future Design Recommendations

In order to improve the sustainability of the vehicle, several measures can be taken. Regarding environmental sustainability, the LCA is used to assess which components of the UAV produce a larger footprint. This is shown in Table 14.7, where it is observed that the batteries are responsible for almost 60% of the UAV's footprint. Thus in future design iterations or UAV modifications, batteries with more sustainable characteristics should be used, when possible. Furthermore, the components made out of CFRP or GFRP could be changed by materials composed of natural fibres. Regarding the economic sustainability of the project, expensive components such as some parts of the control hardware or the main motors could be produced in house once the volume of drones produced is sufficient, thus also using economies of scale. Furthermore, social sustainability can be improved by making continuous updates in the control software regarding safety awareness, as well as to further reduce the noise of the vehicle. Lastly, the bases deployed should employ people that live in the region, to ensure that Healios positively contributes to the populations where it operates.

Table 14.7: Percentage of total LCA emissions and energy consumption for the different components

	Wing	**Tail**	**Frame**	**Propulsion**	**Batteries**	**Total**
% Energy Consumption	14.570	3.100	7.712	18.214	56.403	100
% CO2 emissions	13.967	2.965	7.316	17.689	58.048	100

15
Resource Allocation and Budget Breakdown

When designing any type of vehicle, it is important to keep an overview of the budgets assigned to each system. This can be seen as a requirement setting a limit to each system allowing for all systems to work together as predicted. An estimation is made before the detailed design phase and a more accurate budget has been found. The resources available also have to be allocated effectively to each system. Doing this before the detailed design phase ensures that each system has the necessary available resources in order to most effectively deliver its part of the vehicle design. A first estimate has been delivered in [4]. The actual budget breakdown and resources allocation will be presented following the detailed design phase. Comparing the estimated budgets and allocated resources with the actual values gives an overview of how accurate the predictions have been and understand if and where there have been unexpected factors affecting these.

15.1. Budget Breakdown

In this section, the previously estimated budgets will be compared to the ones which can be computed at this stage of the design process. All first estimates for the different budgets were taken from [4]. The current estimates are more accurate and computed per subsystem.

- **Financial Budget:** A first estimate of the financial budget of the entire UAV was based on statistics and looked at the vehicle as a whole. As stated before, the cost can be estimated for different subsystem characteristic designs and is computed in detail in Chapter 16. The total control and electronics come from Table 11.1. The price of each component is taken based on information available to the open public and shown in Table 15.1, it is a more accurate estimation than made in [4] but the prices may and will vary when contact is established with the provider.

Table 15.1: Cost budget estimation comparison

Subsystem	Initial Cost Estimation [€]	Actual Estimated Cost [€]	Offset [€/%]
Control System	-	60517.94	-
Propulsion (engines + batteries)	-	44500	-
Production	-	93492	-
UNIT COST	574 000 / 112.6	270 000	(-) 304 000

  The total unit cost has been clearly overestimated in [4]. Following some more accurate estimation, the cost is estimated to be less than half, meaning that a great enough margin has been taken into account at the beginning, which has a positive effect on the cost-efficiency of the UAV. A lower cost increases the affordability and the feasibility of the production process. The current estimation is also conservative, as some costs related to on-board hardware components are taken directly from the sellers, without any long-term contract allowing for significant discounts. These costs are expected vary in our favour. The previous contingency factor, when compared to the current value, was 1.12. This factor should converge to 0 as we approach the actual value and this should be at least halved at each iteration, leading to a factor of 0.56.
- **Mass Budget:** The mass estimation for the different systems is presented here and compared. The different masses are the power system mass (see Section 10.4) , control system mass (taken from Table 11.1) and the structural mass. From this table it can be seen that the propulsion weight has clearly been overestimated, leading to scepticism about the feasibility of an electrical UAV design. Further research has proven otherwise. This is positive in the sense that the MTOW was set to a maximum value which has not been overshot while being less than 30% off. The propulsion masses have been computed using material densities and weight ratios based on very similar engines/batteries (Chapter 10). Note that the MTOW in the table below does not correspond to the sum of the previous components as it was calculated with statistical methods without a propulsion system.

Table 15.2: Mass budget estimation comparison

Subsystem	Initial Mass Estimation [kg]	Actual Estimated Mass [kg]	Offset [kg/%]
Control System	8.8	40.00	31.20
Structures	65.3	92.00	26.70
Wing	-	55	
Fuselage	-	12	
Tail	-	7	
Others	-	18	
Propulsion	782.65	186.3	(-) 596.35
Engines	76.65	40	(-)36.65
Batteries	706	134.82	(-)571.18
MTOW	**500**	**355.00 (+/- 30)**	**(-)145.00 / 77.75**

- **Power Budget:** Similarly to the mass estimation, the power budget was estimated for different systems which are: control and sensors (including cameras as well), the propulsion system and the total power (sum of both). These two budgets are compared and shown in Table 15.3:

Table 15.3: Power budget estimation comparison

Subsystem	Initial Power Estimation [kW]	Actual Estimated Power [kW]	Offset [kW]
Control System	0.6	11.28	10.68
Propulsion	169.45	126	(-)43.45
TOTAL	170.05	137.28	(-)32.77/23.87

The power needed during the most power expensive mission does not exceed the first estimation of 170 and therefore it has a positive influence on the drone design. Having less power required leads to smaller engines and thus smaller weight, bringing the design into a beneficial snowball effect.

The first stage estimations were fairly conservative and allowed for large errors, therefore, none of the estimated values have been overshot. A viable upper limit was set and reduced with this second estimation while maintaining a reasonable margin. In further design, the budgets would become more and more specific and thus converge to more precise values. It is desired that at the next iteration the contingency factors become at least half of the current ones.

15.2. Resource Allocation

In order to optimise the allocation of the available resources during this design process, several factors have been taken into account and different tools were used. The resources available come in different forms:

Manpower: This resource was the most critical as a task division had to be made which can lead to great time gain and improved quality of work if managed correctly. As mentioned in [2] and [1], team members were allocated to the different technical and non-technical subgroups depending on the expected workload, the skills, and preferences of each member. Constant communication amongst the subgroups allowed for the appointed members to change when needed in order to improve the work distribution.
Computing Power: Within each technical group, different software was used such as CATIA, ANSYS and EDUPACK. Research in the most suitable software to be used was made and the aforementioned ones were chosen. Making use of these programs allowed for an efficient use of the time available to the team. Programming language Python was also used for calculations needed within iterative processes, allowing, again, for great time gains.
Working Time: An important constraint for this design process was the time available, that is why allocating the right amount of time to each deliverable is of importance. In order set specific time slots and to keep an overview of the progress of the design process, tools such as a Gantt Chart (see Chapter 17) were used, as well as Clockify [1].

This resource allocation has been discussed and set within the team based on group decisions. Communication was a key point to maintain the optimum allocation of resources and discuss any need for change.

[1] https://clockify.me/

16
Cost Breakdown Structure

Although changes in these costs are common during the system's life cycle, it is still required to make initial assumptions early in the design phase. Changes are then usually estimated through a sensitivity analysis. As these costs are composed of several activities, they are to be organised hierarchically in the Cost Breakdown Structure. The aim of this chapter is to estimate the cost of these categories, and using them, to determine a unit cost for the UAV.

16.1. Method

Complex systems, such as the design in question, consists of the following cost categories[70]:

- Research and development
- Manufacturing and construction
- Operation and support
- Decommissioning and disposal

Jiuping Xu , and Lei Xu proposes the reference depicted on Figure 16.2:

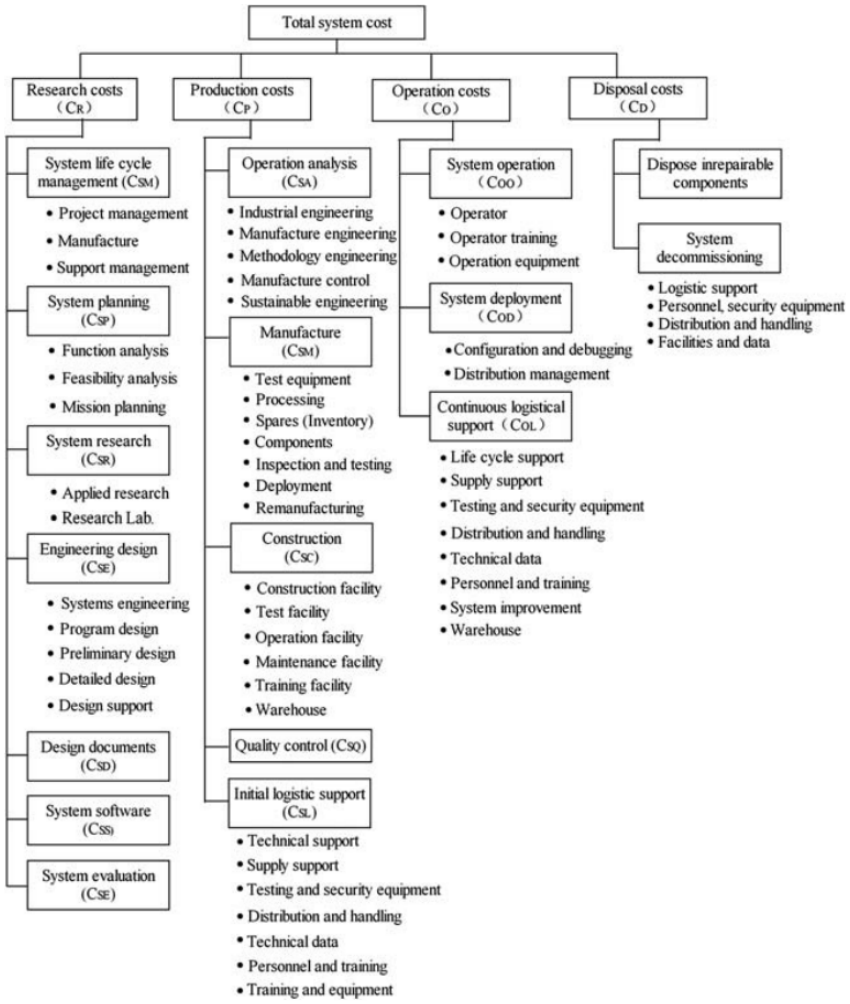

Figure 16.1: Cost Breakdown Structure Reference[70]

A CBS shall have the following properties:

1. The system's life-cycle cost shall be determined at the highest level in Figure 16.2.
2. The cost classification in CBS should be defined such that every reader must have a common understanding of what is included in the defined cost categories.

In the following sub-sections, the high-level categories are discussed, followed by the construction of the CBS.

16.2. Cost Estimations

16.2.1. Research Costs Estimation

The Design Synthesis Exercise consists of 9 weeks of work of 10 students which with the 8-hour workdays and 5 days workweeks equals 3,600 hours of work. The average cost of an engineering employee in the Netherlands is 42 euros an hour[1]. The DSE exercise includes the System planning, System research and Engineering Design, Design documents, and the System life cycle management blocks of Figure 16.2.

The costs of individual components are based on the hour allocation of the DSE exercise. These are summarised in Table 16.1.

Excluded blocks from the DSE are System software and System evaluation.

The System software block includes two major parts in this project:

- The software used for the design of the system.
- The software developed for the use of the system.

Two paid software packages are used for the design of the system: DS Dassault Solidworks package, including structural and flow simulation, and MATLAB. This package's cost based on sources[2] from the industry is approximated per user to be 4,000 euros one-time fee, and additional subscription fee of 1,000 euros per year. Based on the DSE exercise experience, 3 licenses are required for the system design, which equates to a one-time fee of 12,000 euros and a yearly cost of 3 000 euros. For MATLAB licenses 3 are used, which costs 800 euros annually, totalling a yearly fee of 2,400 euros. [3] These costs are added to Table 16.1.

It is assumed that the software required for using the system (ground station) is developed and maintained in house, which requires an additional employee. The estimated number of hours for developing such software is 320 hours, costing 13,440 euros. This input is again added to Table 16.1.

The system evaluation consists of the validation of the designed system and certification. Since the system requirements for this design are also based on the certification requirements, a valid design proves a design that can obtain certification. Validation of the system is a process that confirms that the designed and the built product both comply with all the stated requirements. The easiest methods to perform validation is inspection and demonstration, and the more complex methods are analysis and testing. During the design, 197 system and sub-system requirements were set in eight different categories. The requirements can be further put into two classifications based on the validation methods: Non-destructive tests possible, destructive tests required.

For non-destructive tests, a built prototype is to be used, and for destructive tests, the required systems are prepared. Therefore, the cost of non-destructive tests are based upon the cost on the hours required from the certification agencies, and for the destructive tests, the construction of the tested components is added. It is assumed that each category's testing takes one day, and for the cost of the certification agency, consulting hour costs are calculated. For destructive testing, the cost of the preparation is also added.

The total costs for the Research costs are summarised in Table 16.1. As design challenges are partly unknown at this point of the design, the estimated cost is very optimistic.

[1] https://octagon.nl/the-true-costs-of-paying-your-own-employees/
[2] https://www.alignex.com/
[3] https://nl.mathworks.com/pricing-licensing.html

Table 16.1: Research costs summary

Name	Hours	Cost in euro	Name	Hours	Cost in euro
System life cycle management	**320**	**€13 440**	**Design Documents**	**780**	**€20 160**
Project planning and scheduling	173	€7 296	Project planning	80	€3 360
Organizational framework	58	€2 432	Baseline report	160	€6 720
Financial analysis	24	€1 024	Mid-term report	240	€10 080
Business operation planning	64	€2 688	Detailed design report	300	€12 600
System Planning	320	**€13 440**	**System Software**	**-**	**€54 840**
Mission Planning	28	€1 189	DS Dassault Solidworks	-	€15 000
Literature study	79	€3 330	Matlab	-	€2 400
Requirement identification	212	€8 920	Control software	320	€13 440
System research	**960**	**€40 320**	**System evaulatiuon**	**-**	**€72 000**
Concept Generation	583	€24 493	Destructive testing	-	€24 000
Trade-off	24	€1 249	Non-destructive testing	-	€248 000
Engineering Design	**1300**	**€54 600**	**Further R&D**	4500	**€189 000**
Power and Propulsion subsystem	316	€13 272	**Further Engineering Costs**	**30%**	**€193 800**
Control and Stability subsystem	337	€14 181			
Aerodynamics subsystem	295	€12 409			
Structures subsystem	295	€12 409			
Electrical subsystem	113	€4 786			
Total				-	**€840 200**

16.2.2. Production Costs Estimation

Research costs related to the production of the UAV are related to the development costs of this phase. These activities are further explained in Chapter 17. The summary is presented in Table 16.2:

Table 16.2: Research costs for production

Name	**Hours**	**Cost in euro**
Production Design	400	€16 800
Quality Control	160	€6 720
Total	-	**€23 520**

Table 16.3: Production cost of components

Component	**Material Cost**	**Production Method**	**Produced Cost**
Spar+aileron	€114	Extrusion	136.8
Skin	€54	Roll forming	€64.8
Ribs	€19	Coarse machining	€57
Stiffeners	€301	Extrusion	€361.2
Tail arm	€20	Extrusion	€24
Vertical tail	€12	Coarse machining	€36
Horizontal Tail	€16	Coarse machining	€48
Truss+landing gear	€26	Extrusion and welding	€78
Fairing	€166	Layup	€498
Wing actuator	€83	Coarse machining	€249
Blades	€310	Filament winding	€930
Engine mount	€158	Coarse machining	€474
AUX engine mount	€6	Coarse machining	€18
Total			**2974.8**

The complete manufacturing process is planned to be outsourced. Therefore, the production cost can be split into two major components: cost of off the shelf components & materials, and the cost of construction and assembly of such components.

The total cost of the off the shelf components are 60,517 euros. The total material cost for aluminium components is 523 euros and for composites components 476 euros. The cost of the production for these components is based on the manufacturing method. For extrusion and roll forming 120% of the material cost is used for the produced form, while for coarse machining and other methods 300 % is used. These results are summarised in Table 16.3.

The assembly assumes that companies charge 150 euros per hour, and the assembly takes 3 work weeks, costing 18,000 euros. The cost of the engines is 12,000 euros and the battery costs and approximate 32 500 euros. This brings the total production costs of about **126,000 euros** per UAV and a one time 23,520 euros research cost for production.

16.2.3. Operation Costs Estimation

The operation costs consist of the costs to support customers and their UAV's. This team will be made up of 5 people, one manager, one who organises the manufacturing (which is outsourced), handles the business side, and two customer support employees. If a client wants an additional feature that was not initially designed, an external company would be hired to 'retrofit' the feature to the existing UAV design. These resources sum up to 2080 hours a year, which with a cost of 40 euros per hour equates to €416,000.

16.2.4. Disposal Costs Estimation

The two major components of the Disposal costs are as depicted in Figure 16.2 are due to the disposal of irreparable components during the lifetime of the product, and the cost of system decommissioning at the end of the life.

The most common irreparable elements include: batteries, electrical components, composite elements, and metal elements. Of these components, metal elements are clearly recyclable. There is already an existing infrastructure with a list of companies who take metals for free to recycle them at a profit. For the batteries, the recycling fee is 110 euros for the battery weight of the system.[4] For electrical components, the recycling fee is around 40 cents per kilogram. This results in the total fee of 16 euros.[5] For composite components, the recycling fee is estimated to be 5 euros per kilogram. The total fee based on the components used is 75 euros.[6]

When a system is completely decommissioned, recycling is similar to that of irreparable elements. This would bring the total cost to 201 euros.

16.3. Summarised CBS

Based on the values calculated in the previous sections, the cost breakdown diagram can be constructed, as seen in Figure 16.2.

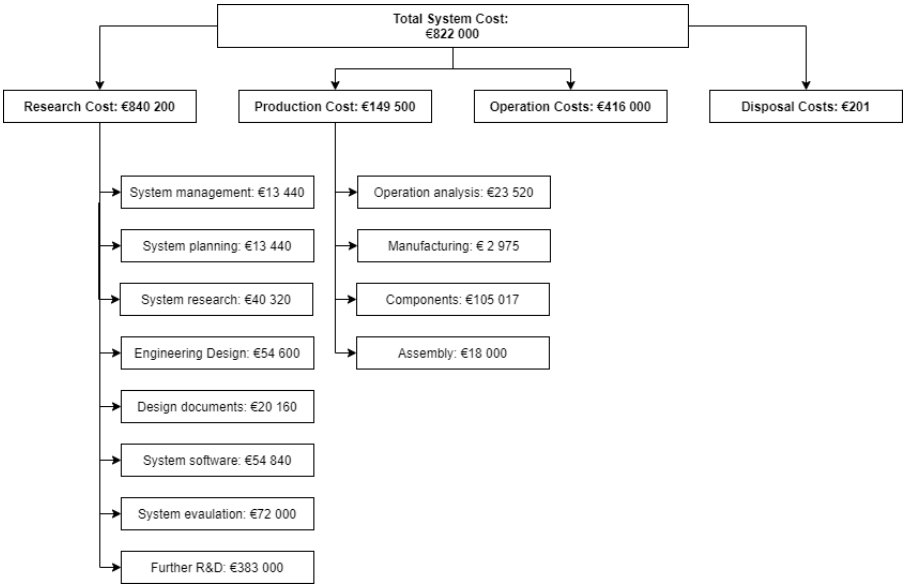

Figure 16.2: Cost Breakdown Structure

[4] https://arn.nl/en/lower-recycling-fee-for-cars-and-car-batteries-starting-from-1-january-2020/

[5] https://info.mayeralloys.com/ewaste-blog/why-is-there-a-recycling-fee-for-electronics#:~:text=The20average20cost20for20recycling,per20pound20of20electronic20waste.

[6] (https://www.researchgate.net/publication/321794490_Environmental_and_cost_analysis_of_carbon_fibre_composites_recycling

16.4. UAV Unit Cost

The UAV cost is based on the cost required to break even with the expenses, or in the best scenario, achieve a profit for the project. Setting the price too high could also result in losses, as selling the product is less likely. The costs considered for the unit cost calculation includes fixed, and reoccurring costs as well. Fixed costs are the upfront research and development cost: 840,200 euros. Reoccurring costs are the production cost of each drone, 126,000 euros, and the yearly operational cost of 416,000 euros. Based on this data, Table 16.4 can constructed which includes the total costs per year and per drone sold:

Table 16.4: Total costs

UAV/ Year	1	2	3	4	5	6	7	8	9	10
Year 1	€1,405,720	€1,531,720	€1,657,720	€1,783,720	€1,909,720	€2,035,720	€2,161,720	€2,287,720	€2,413,720	€2,539,720
Year 2	€1,947,720	€2,199,720	€2,451,720	€2,703,720	€2,955,720	€3,207,720	€3,459,720	€3,711,720	€3,963,720	€4,215,720
Year 3	€2,489,720	€2,867,720	€3,245,720	€3,623,720	€4,001,720	€4,379,720	€4,757,720	€5,135,720	€5,513,720	€5,891,720
Year 4	€3,031,720	€3,535,720	€4,039,720	€4,543,720	€5,047,720	€5,551,720	€6,055,720	€6,559,720	€7,063,720	€7,567,720
Year 5	€3,573,720	€4,203,720	€4,833,720	€5,463,720	€6,093,720	€6,723,720	€7,353,720	€7,983,720	€8,613,720	€9,243,720
Year 6	€4,115,720	€4,871,720	€5,627,720	€6,383,720	€7,139,720	€7,895,720	€8,651,720	€9,407,720	€10,163,720	€10,919,720
Year 7	€4,657,720	€5,539,720	€6,421,720	€7,303,720	€8,185,720	€9,067,720	€9,949,720	€10,831,720	€11,713,720	€12,595,720
Year 8	€5,199,720	€6,207,720	€7,215,720	€8,223,720	€9,231,720	€10,239,720	€11,247,720	€12,255,720	€13,263,720	€14,271,720
Year 9	€5,741,720	€6,875,720	€8,009,720	€9,143,720	€10,277,720	€11,411,720	€12,545,720	€13,679,720	€14,813,720	€15,947,720
Year 10	€6,283,720	€7,543,720	€8,803,720	€10,063,720	€11,323,720	€12,583,720	€13,843,720	€15,103,720	€16,363,720	€17,623,720

By dividing values within these tables with the total number of drones sold, the unit cost to break even can be calculated, as shown in Table 16.5

Table 16.5: Unit Cost to break even

UAV/ Year	1	2	3	4	5	6	7	8	9	10
Year 1	€1,405,720	€765,860	€552,573	€445,930	€381,944	€339,287	€308,817	€285,965	€268,191	€253,972
Year 2	€973,860	€549,930	€408,620	€337,965	€295,572	€267,310	€247,123	€231,983	€220,207	€210,786
Year 3	€829,907	€477,953	€360,636	€301,977	€266,781	€243,318	€226,558	€213,988	€204,212	€196,391
Year 4	€757,930	€441,965	€336,643	€283,983	€252,386	€231,322	€216,276	€204,991	€196,214	€189,193
Year 5	€714,744	€420,372	€322,248	€273,186	€243,749	€224,124	€210,106	€199,593	€191,416	€184,874
Year 6	€685,953	€405,977	€312,651	€265,988	€237,991	€219,326	€205,993	€195,994	€188,217	€181,995
Year 7	€665,389	€395,694	€305,796	€260,847	€233,878	€215,898	€203,056	€193,424	€185,932	€179,939
Year 8	€649,965	€387,983	€300,655	€256,991	€230,793	€213,328	€200,852	€191,496	€184,218	€178,397
Year 9	€637,969	€381,984	€296,656	€253,992	€228,394	€211,328	€199,138	€189,996	€182,885	€177,197
Year 10	€628,372	€377,186	€293,457	€251,593	€226,474	€209,729	€197,767	€188,797	€181,819	€176,237

Based on the average unit cost, the final unit cost is set at 270 000 euros, from which the expected profit can be calculated, displayed in Table 16.6. Here the red cells represent loss and the green cells represent profit:

Table 16.6: Expected profit based on the unit cost of 270 000 euros

UAV/ Year	1	2	3	4	5	6	7	8	9	10
Year 1	€1,135,720	€991,720	€847,720	€703,720	€559,720	€415,720	€271,720	€127,720	€16,280	€160,280
Year 2	€1,407,720	€1,119,720	€831,720	€543,720	€255,720	€32,280	€320,280	€608,280	€896,280	€1,184,280
Year 3	€1,679,720	€1,247,720	€815,720	€383,720	€48,280	€480,280	€912,280	€1,344,280	€1,776,280	€2,208,280
Year 4	€1,951,720	€1,375,720	€799,720	€223,720	€352,280	€928,280	€1,504,280	€2,080,280	€2,656,280	€3,232,280
Year 5	€2,223,720	€1,503,720	€783,720	€63,720	€656,280	€1,376,280	€2,096,280	€2,816,280	€3,536,280	€4,256,280
Year 6	€2,495,720	€1,631,720	€767,720	€96,280	€960,280	€1,824,280	€2,688,280	€3,552,280	€4,416,280	€5,280,280
Year 7	€2,767,720	€1,759,720	€751,720	€256,280	€1,264,280	€2,272,280	€3,280,280	€4,288,280	€5,296,280	€6,304,280
Year 8	€3,039,720	€1,887,720	€735,720	€416,280	€1,568,280	€2,720,280	€3,872,280	€5,024,280	€6,176,280	€7,328,280
Year 9	€3,311,720	€2,015,720	€719,720	€576,280	€1,872,280	€3,168,280	€4,464,280	€5,760,280	€7,056,280	€8,352,280
Year 10	€3,583,720	€2,143,720	€703,720	€736,280	€2,176,280	€3,616,280	€5,056,280	€6,496,280	€7,936,280	€9,376,280

This shows that the first year at least four UAVs have to be sold, followed by a minimum of three in the following year. If that is achieved, it is expected that the following years, the number of sold UAVs would increase, followed by the decline of sales as newer solutions emerge the market. This is represented in Figure 16.3 to Figure 16.5

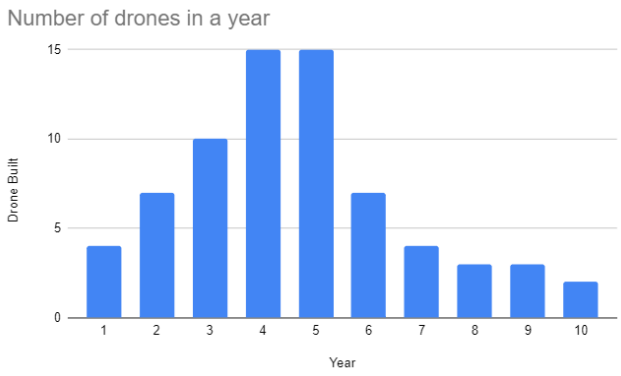

Figure 16.3: Expected sales per year

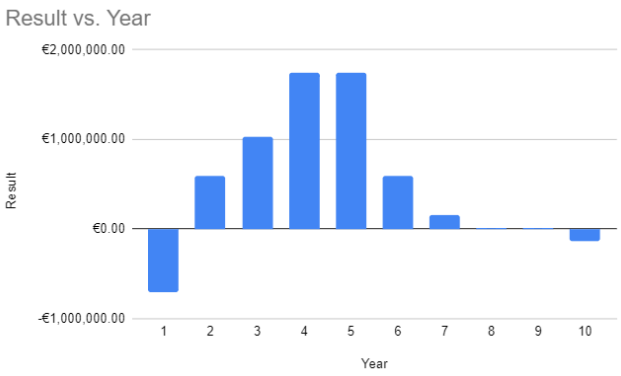

Figure 16.4: Result per year

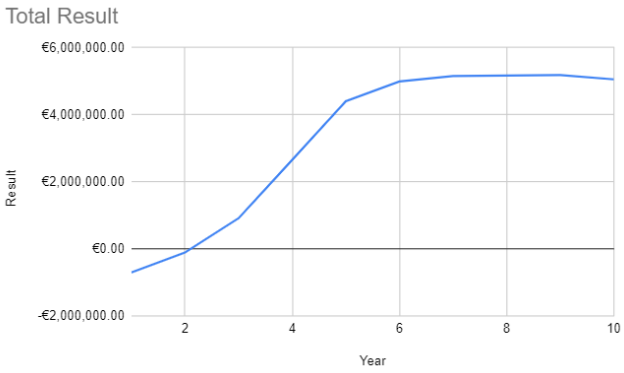

Figure 16.5: Total result over time

This shows that additional development should be considered to keep the UAV in the market once the sales start dropping.

It is also important to mention that the research and development cost is very optimistic in this phase of the design. An increase in the upfront costs would mean that return time would increase, or more drones need to be sold during the first years. Also, the cost of the off-shelf components are assumed to be constant, while it is likely that when a large number of components are ordered, the cost of the individual component decreases by a large amount.

17
Project Planning

The previous chapters have shown progress on the design of the VTOL vehicle. However, multiple phases still have to be completed before the first mission can be performed. This chapter describes the planning to show how the project can be continued. Firstly, the design and development logic is presented, after which these steps are further clarified with a Gantt Chart.

To maximise efficiency, the flow and distribution of the upcoming tasks should be well established. This is presented in a work breakdown structure and work flow diagram. This is in line with activities identified in the cost breakdown presented in Chapter 16. The work breakdown structure and workflow diagram are presented on the next page. Note that no members have been allocated to specific tasks, as currently, the extent of the future planning does not go as in depth as the planning made for the project timeline. Furthermore, in the future planning the following phases can be recognised: the research phase, the production phase, the operational phase and the disposal phase.

Research Phase: A part of this phase has been completed during the Design Synthesis Exercise. However, some parts of the design have been left open. These have been presented in the detailed design. For each subsystem, a future recommendation was written for this exact purpose.

Furthermore, a more accurate software can be developed to model the vehicle in terms of it's structural, aerodynamic, and power performance. Followed by a system evaluation to prepare for certification. Lastly, before manufacturing the certification has to be established.

Production Phase: The research phase is followed by the production phase. The manufacturing of the parts and the assembly will be outsourced and therefore the emphasise during this phase will be on the preparation and checking of the manufacturing.

Operation Phase: The tasks of the operating phase will be performed continuously during the operating life time (OLT) of the UAS. Therefore, it can be seen that no specific hours have been assigned to the operating phase. The tasks of operational phase will consist of tasks related to the sales and providing customer support. These processes have been described more elaborately in Chapter 3, under the name 'Retire vehicle'.

Disposal Phase: Lastly, the vehicle will be deconstructed and disposed. Depending on the materials and manufacturing processes used, parts will either be recycled or disposed entirely. Again these processes have been described more elaborately in Chapter 3.

The work flow diagram and the work breakdown structure are combined into a Gantt chart. This provides a clear overview and can later be used to analyse the process. The Gantt chart is presented on the page after the WBS and WFD. Again the allocated times for the operational phase will be continuous throughout the operational life time and has not yet been determined.

WBS: Post Project

- **PP1. Research Phase**
  - PP1.1 Detailed Design
    - Perform CFD validation — PP1.1.1 — 100 hrs
    - Design payload handling — PP1.1.2 — 150 hrs
    - Establish Control and stability for transition — PP1.1.3 — 150 hrs
    - Update subsystem design — PP1.1.4 — 500 hrs
    - Design subsystem parts — PP1.1.5 — 750 hrs
  - Develop program software — PP1.2 — 320 hrs
  - PP1.3 Preparing certification
    - Finalise SORA — PP1.3.1 — 24 hrs
    - Document design and test results — PP1.3.2 — 200 hrs
    - Destructive testing — PP1.3.3 — 400 hrs
    - Create 'Comprehensive Safety Portfolio' — PP1.3.4 — 24 hrs
    - Apply for certification — PP1.3.5 — 40 hrs
  - PP1.4 certification
    - Certify prototype — PP1.4.1 — 200 hrs
    - Test prototype — PP1.4.2 — 400 hrs
    - Implement evaluation — PP1.4.3 — 600 hrs
    - Iterate — PP1.4.4 — 600 hrs
- **PP2. Production Phase**
  - PP2.1 Production Design
    - Evaluate manufacturability — PP2.1.1 — 160 hrs
    - Choose manufacturing processes — PP2.1.2 — 80 hrs
    - Prepare manufacturing drawing — PP2.1.3 — 160 hrs
  - PP2.2 Manufacturing
    - Oversee production — PP2.2.1 — 80 hrs
    - Perform quality control on system — PP2.2.2 — 80 hrs
- **PP3. Operation Phase**
  - Manage Sales — PP3.1 — O. L. T
  - Support Product Maintenance — PP3.2 — O. L. T
  - Provide technical support — PP3.3 — O. L. T
  - Provide program suppport — PP3.4 — O. L. T
  - Perform design adjustments — PP3.5 — O. L. T
- **PP4. Disposal Phase**
  - Disassemble vehicle — PP4.1 — 40 hrs
  - Recycle compenents if possible — PP4.2 — 40 hrs
  - Dispose of unrecyclable compenents — PP4.3 — 40 hrs

WFD: Post Project

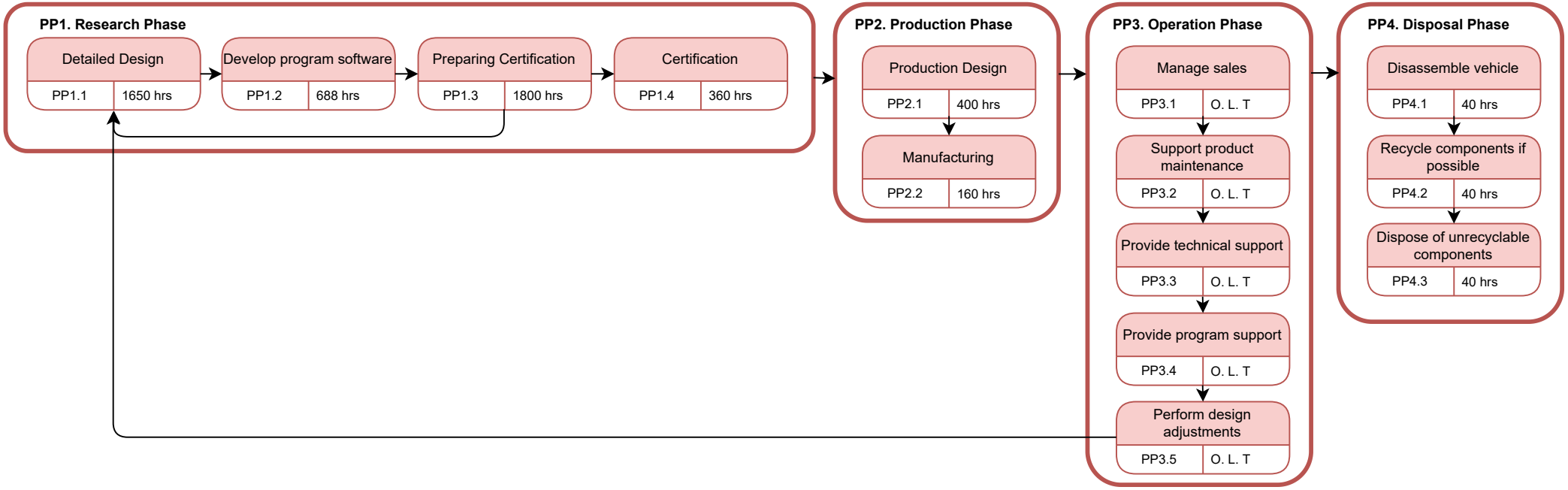

ID	Task Mode	Task Name	Duration	Start	Finish	Predecess	Resource Names	Work	% Complete
0		**Design/Synthesis Exercise 2020**	**1858 hrs**	**11/9/20**	**10/13/21**			**8,111.33 hrs**	**33%**
1		**1. Project Organization**	**40 hrs**	**11/9/20**	**11/13/20**			**242 hrs**	**100%**
32		Project Planning Completed	0 hrs	11/13/20	11/13/20	1		0 hrs	100%
33		**2. Mission Analysis**	**28.07 hrs**	**11/16/20**	**11/19/20**			**148.01 hrs**	**100%**
62		**3. Mission and Design Exploration**	**39.5 hrs**	**11/16/20**	**11/20/20**			**189.6 hrs**	**100%**
86		Baseline Report	0 hrs	11/20/20	11/20/20	33,62		0 hrs	100%
87		**4. Preliminary Design & Trade-Off**	**104 hrs**	**11/23/20**	**12/9/20**			**1,148.72 hrs**	**100%**
128		Mid-term Report	0 hrs	12/9/20	12/9/20	87		0 hrs	100%
129		**5. Detailed design**	**136 hrs**	**12/15/20**	**1/21/21**			**1,165 hrs**	**100%**
202		**PP1. Research Phase**	**1279.33 hrs**	**1/21/21**	**9/1/21**	**129**		**4,458 hrs**	**0%**
203		**PP1.1 Detailed Design**	**450 hrs**	**1/21/21**	**4/9/21**			**1,650 hrs**	**0%**
204		PP1.1.1 Perform CFD validation	50 hrs	1/21/21	1/29/21		A,B	100 hrs	0%
205		PP1.1.2 Design payload handling	75 hrs	1/21/21	2/3/21		C,D	150 hrs	0%
206		PP1.1.3 Establish Control and stability for transition	75 hrs	1/21/21	2/3/21		E,F	150 hrs	0%
207		PP1.1.4 Update subsystem design	250 hrs	2/3/21	3/18/21	204,205,	C,D	500 hrs	0%
208		PP1.1.5 Design subsystem parts	125 hrs	3/18/21	4/9/21	207	A,B,C,D,E,F	750 hrs	0%
209		**PP1.2 Develop program sofware**	8 hrs	1/21/21	1/22/21	129		320 hrs	0%
210		**PP1.3 Preparing certification**	**229.33 hrs**	**4/9/21**	**5/19/21**	**209,203**		**688 hrs**	**0%**
211		PP1.3.1 Finalise SORA	8 hrs	4/9/21	4/12/21		A,B,C	24 hrs	0%
212		PP1.3.2 Document design and test results	66.67 hrs	4/12/21	4/22/21	211	A,B,C	200 hrs	0%
213		PP1.3.3 Destructive testing	133.33 hrs	4/22/21	5/17/21	212	A,B,C	400 hrs	0%
214		PP1.3.4 Create 'Comprehensive Safety Portfolio'	8 hrs	5/17/21	5/18/21	213	A,B,C	24 hrs	0%
215		PP1.3.5 Apply for certification	13.33 hrs	5/18/21	5/19/21	214	A,B,C	40 hrs	0%
216		**PP1.4 certification**	**600 hrs**	**5/19/21**	**9/1/21**	**210**		**1,800 hrs**	**0%**
217		PP1.4.1 Certify prototype	66.67 hrs	5/19/21	6/1/21		A,B,C	200 hrs	0%
218		PP1.4.2 Test prototype	133.33 hrs	6/1/21	6/23/21	217	A,B,C	400 hrs	0%
219		PP1.4.3 Implement evaluation	200 hrs	6/23/21	7/28/21	218	A,B,C	600 hrs	0%
220		PP1.4.4 Iterate	200 hrs	7/28/21	9/1/21	219	A,B,C	600 hrs	0%
221		**PP2. Production Phase**	**186.67 hrs**	**9/1/21**	**10/5/21**	**202**		**560 hrs**	**0%**
222		**PP2.1 Production Design**	**133.33 hrs**	**9/1/21**	**9/24/21**			**400 hrs**	**0%**
223		PP2.1.1 Evaluate manufacturability	53.33 hrs	9/1/21	9/10/21		A,B,C	160 hrs	0%
224		PP2.1.2 Choose manufacturing processes	26.67 hrs	9/10/21	9/15/21	223	A,B,C	80 hrs	0%
225		PP2.1.3 Prepare manufacturing drawing	53.33 hrs	9/15/21	9/24/21	224	A,B,C	160 hrs	0%
226		**PP2.2 Manufacturing**	**53.33 hrs**	**9/24/21**	**10/5/21**			**160 hrs**	**0%**
227		PP2.2.1 Oversee production	26.67 hrs	9/24/21	9/29/21	222	A,B,C	80 hrs	0%
228		PP2.2.2 Perform quality control on system	26.67 hrs	9/29/21	10/5/21	227	A,B,C	80 hrs	0%
229		**PP3. Operation Phase**	**8 hrs**	**10/5/21**	**10/6/21**	**221**		**80 hrs**	**0%**
230		**PP3.1 Manage Sales**	8 hrs	10/5/21	10/6/21		G,H	16 hrs	0%
231		**PP3.2 Support Product Maintenance**	8 hrs	10/5/21	10/6/21		G,H	16 hrs	0%
232		**PP3.3 Provide technical support**	8 hrs	10/5/21	10/6/21		G,H	16 hrs	0%
233		**PP3.4 Provide program suppport**	8 hrs	10/5/21	10/6/21		G,H	16 hrs	0%
234		**PP3.5 Perform design adjustments**	8 hrs	10/5/21	10/6/21		G,H	16 hrs	0%
235		**PP4. Disposal Phase**	**40 hrs**	**10/6/21**	**10/13/21**	**229**		**120 hrs**	**0%**
236		**PP4.1 Disassemble vehicle**	13.33 hrs	10/6/21	10/7/21		A,B,C	40 hrs	0%
237		**PP4.2 Recycle compenents if possible**	13.33 hrs	10/7/21	10/11/21	236	A,B,C	40 hrs	0%
238		**PP4.3 Dispose of unrecyclable compenents**	13.33 hrs	10/11/21	10/13/21	237	A,B,C	40 hrs	0%

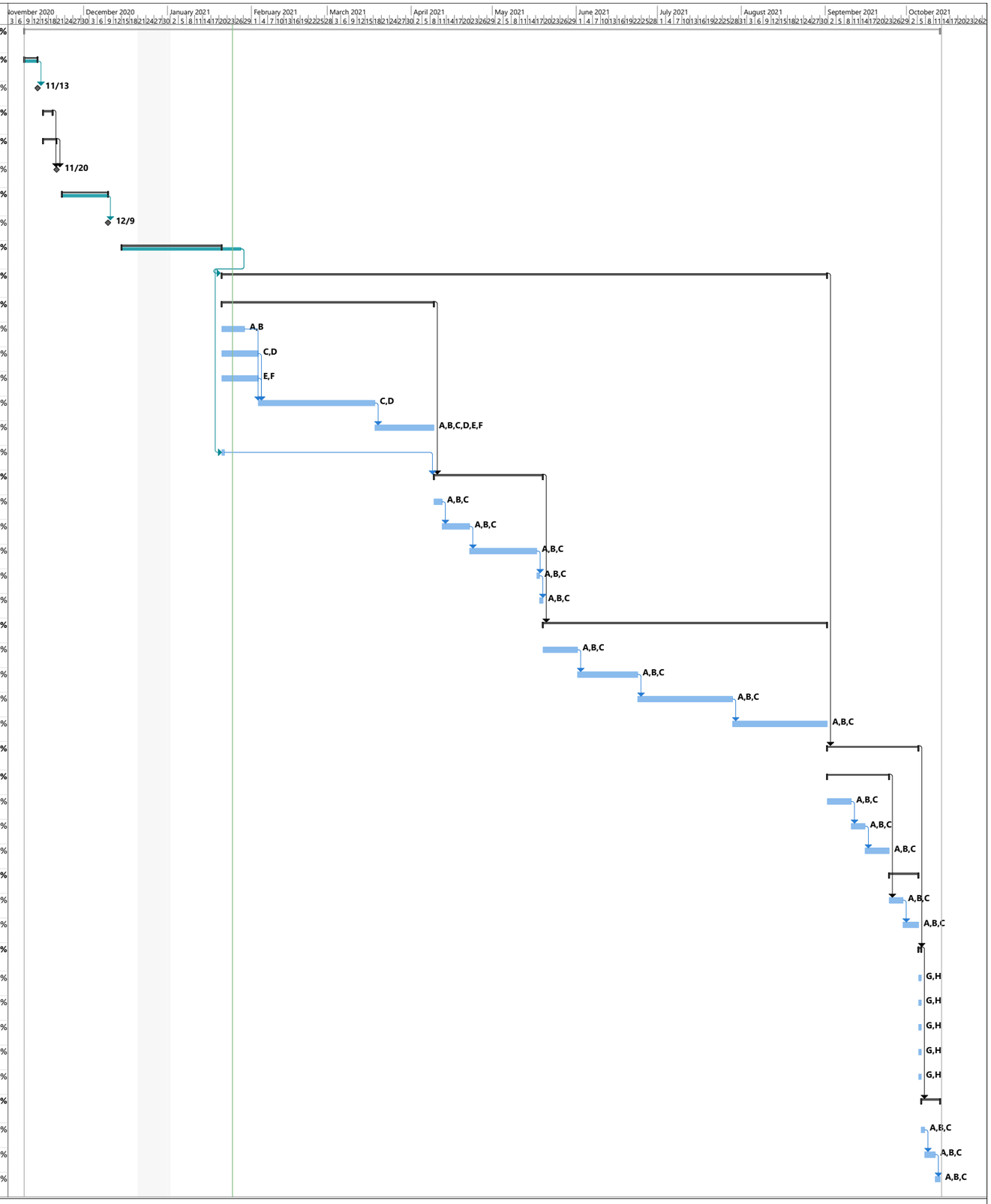

Project: Design/Synthesis Exerc
Date: 1/25/21

Task | Split | Milestone | Summary | Project Summary | Inactive Task | Inactive Milestone | Inactive Summary | Manual Task | Duration-only | Manual Summary Rollup | Manual Summary | Start-only | Finish-only | External Tasks | External Milestone | Deadline | Progress | Manual Progress

18 Conclusion

Infrastructural and technological bottlenecks exist in the supply chain of high-priority medical equipment worldwide. This is particularly critical in remote areas which are partially or completely disconnected from traditional healthcare networks due to poorly developed or non-existent infrastructure. The problems introduced by these hindrances are accentuated during natural disasters such as the ongoing COVID-19 pandemic, making it difficult to provide emergency relief to certain areas of the world.

In light of these issues, the present work has demonstrated the feasibility of VTOL tilt-wing vehicles as a competitive solution capable of delivering medical or other high-value supplies quickly and effectively to those who need it most. The Healios UAV is an autonomous, tilt-wing, fully-electric aircraft that combines the long range performance of traditional aircraft designs with the versatility of VTOL operations. The vehicle is capable of delivering 50 kg of medical supplies to end-users as far as 50 km, and to logistic centres as far as 200 km.

The detailed design phase represents the continuation of the design process, by bringing the system into being. Based on the foundations of the preliminary design, the detailed design went down to the sub-system level and its interactions. The sub-systems design include the propulsion, the aerodynamic, the structures, and control sub-system.

To design such systems, a concurrent approach was selected, as it minimised the time required for the design of each sub-system. After each sub-system group defined the required inputs and outputs for their design, multiple iterations were completed, providing a flow of data between departments. These iterations were all performed in the search of a design point, where all subsystems converge to a solution. The results of this report, present this design point.

The resulting design point reflects a system that is capable of fulfilling the system requirements that are confirmable at this point of the design.

In the future, further design iterations would be advised to be performed. In particular, optimisation of the aerodynamic design of the vehicle would be vital. Furthermore, the possibility of reducing the weight of the wing through the use of composite materials should be explored. Scale models should be built and wind-tunnel experiments performed, providing valuable data that could be used to validate and refine the used methods in addition to performing a more accurate analysis of the stability and controllability characteristics of the vehicle. The interactions between the propeller and the main structural elements should be studied in more detail, paying particular attention to the vibrations and potential interference between these elements. Lastly, resources should be invested in the development of the necessary software to support the vehicle's operations.

Notwithstanding these considerations, the Healios UAV presents itself as an attractive, sustainable, cost-effective, reliable and achievable solution that could make a real impact in the effective delivery of medical supplies to remote areas and to those in need of emergency relief. The results found in the present work demonstrate the potential of this concept and indicate that further research could yield valuable results in the near future.

Bibliography

[1] Chung, C., Firlefyn, M. V. M., Martínez, P. G., Hinssen, Y. M., Ruiz, D. L., de Oñate, A. M., Rademaker, J. T. E., Simonelli, A., Szekeres, B., and van Wagensveld, D., "Project Plan (Design Synthesis Exercise) — Group 3," Tech. rep. 1, TU Delft Aerospace Engineering, Delft, The Netherlands, 2020.

[2] Chung, C., Firlefyn, M. V. M., González Martínez, P., Hinssen, Y. M., Ruiz, D. L., de Oñate, A. M., Rademaker, J. T. E., Simonelli, A., Szekeres, B., and van Wagensveld, D., "Midterm Report (Design Synthesis Exercise) - Group 3," Tech. rep. 3, TU Delft Aerospace Engineering, Delft, The Netherlands, 2020.

[3] Adrianopoli, C., *Decision Making in Emergency Management*, Butterworth-Heinemann Inc., Boston, 2019.

[4] Chung, C., Firlefyn, M. V. M., González Martínez, P., Hinssen, Y. M., Ruiz, D. L., de Oñate, A. M., Rademaker, J. T. E., Simonelli, A., Szekeres, B., and van Wagensveld, D., "Baseline Report (Design Synthesis Exercise) - Group 3," Tech. rep. 2, TU Delft Aerospace Engineering, Delft, The Netherlands, 2020.

[5] Coppola, D., *Introduction to international disaster management*, Butterworth Heinemann, Boston, 2007.

[6] World Economic Forum, *The Next Economic Growth Engine, Scaling Fourth Industrial Revolution Technologies in Production*, Jan. 2018.

[7] Euchi, J., "Do Drones Have a Realistic Place in a Pandemic Fight for Delivering Medical Supplies in Healthcare Systems problems?," *Chinese Journal of Aeronautics*, Jun. 2020, p. 10.

[8] Vertical Flight Society, *38th Annual Student Design Competition (2020-2021) Request for Proposal (RFP) — Unmanned Vertical Lift for Medical Equipment Distribution*, Sep. 2020.

[9] FAA, *Helicopter Performance*, Aviation Supplies Academics, Inc., 2019.

[10] JARUS, "JARUS CS-UAS Recommendations for Certification Specification for Unmanned Aircraft Systems," Tech. rep. 1, EUROCONTROL, Brussels, Sep. 2019.

[11] Hamann, R., and van Tooren, M., *Systems Engineering and Technical Management Techniques part II*, TU Delft Aerospace Engineering, Delft, The Netherlands, 1st ed., Jan. 2006.

[12] Debbabi, M., Hassane, F., Jarraya, Y., Soeanu, A., and Alawneh, L., *Verification and Validation in Systems Engineering: Assessing UML/SysML Design Models*, 1st ed., Springer-Verlag, Berlin, 2010.

[13] Mili, A., and Tchier, F., *Software Testing: Concepts and Operations*, 1st ed., Wiley, Hoboken, NJ, USA, Jul. 2015.

[14] van der Wal, W., *AE3212-II -Simulation, Verification and Validation*, TU Delft Aerospace Engineering, Delft, The Netherlands, 2020, (unpublished).

[15] Sadraey, M. H., *Aircraft Design. A Systems Engineering Approach*, Wiley, 2013.

[16] Anderson, J. D., *Fundamentals of Aerodynamics*, McGraw-Hill Education, 2017.

[17] Saengphet, W., and Thumthae, C., "Conceptual Design of Fixed Wing-VTOL UAV for AED transport" *The 7th TSME International Conference on Mechanical Engineering*, Chiang Mai, Thailand, Dec. 2016, p. 13.

[18] Stuper, J., "Effect of propeller slipstream on wing and tail" , 1938.

[19] Vecchia, P., Malgieri, D., Nicolosi, F., and De Marco, A., "Numerical analysis of propeller effects on wing aerodynamic: tip mounted and distributed propulsion" *Transportation Research Procedia*, Vol. 29, 01 2018, pp. 106–115.

[20] Zhang, F., Khalid, M., Syms, G., and Ball, N., "Numerical Investigation of Propeller Effects on the Aurora Aircrafts" , 01 2010.

[21] Anderson, J., *Introduction to Flight*, eighth ed., McGraw-Hill, 2016.

[22] Megson, T., "Chapter 1 - Basic elasticity" *Aircraft Structures for Engineering Students (Sixth Edition)*, edited by Megson, T., sixth edition ed., Butterworth-Heinemann, 2017.

[23] Rotter, J. M., Sadowski, A. J., and Chen, L., "Nonlinear stability of thin elastic cylinders of different length under global bending" *International Journal of Solids and Structures*, Vol. 51, No. 15, 2014, pp. 2826 – 2839.

[24] Melkert, J., and Rans, C., *AE2135-I Structural Analysis & Design: Buckling*, Delft, The Netherlands, 2018.

[25] Mulder, J., van Staveren, W., van der Vaart, J., de Weerdt, E., de Visser, C., in 't Veld, A., and Mooij, E., *Flight Dynamics — Lecture Notes AE3202*, Mar. 2013.

[26] Hong, S., Jeong, J., Kim, S., Suk, J., and Jung, J. I., "Longitudinal Flight Dynamics of a Single Tilt-wing Unmanned Aerial Vehicle," *IFAC Proceedings Volumes*, Vol. 46, No. 19, 2013, pp. 60–65. 19th IFAC Symposium on Automatic Control in Aerospace.

[27] Binz, F., Islam, T., and Moormann, D., "Attitude Control of Tiltwing Aircraft using a Wing-fixed Coordinate System and Incremental Nonlinear Dynamic Inversion," *International Journal of Micro Air Vehicles*, Vol. 11, Jan. 2019, p. 12.

[28] Drela, M., and Youngren, H., *XFOIL 6.9 User Primer*, MIT, Cambridge MA, USA, 6th ed., dec 2001.

[29] Chambers, J. R., and Grafton, S. B., "Calculation of the Dynamic Longitudinal Stability of a Tilt-wing V/STOL Aircraft and Correlation with Model Flight tests," Tech. rep. Nasa tn d-4344, National Aeronautics and Space Administration — Langley Research Center, Feb. 1968.

[30] Chambers, J. R., and Grafton, S. B., "Investigation of Lateral-directional Dynamic Stability of a Tilt-wing V/STOL Transport," Tech. rep. Nasa tn d-5637, National Aeronautics and Space Administration — Langley Research Center, Feb. 1970.

[31] Elsayed, A., Hafez, A., Ouda, A., Ahmed, H., and Abd-Elkader, H., "Design of Longitudinal Motion Controller of a Small Unmanned Aerial Vehicle," *I.J. Intelligent Systems and Applications*, 2015.

[32] Stevens, B., *Aircraft control and simulation : dynamics, controls design, and autonomous systems*, Wiley, 2015.

[33] Casau, P., Cabecinhas, D., and Silvestre, C., "Transition Control for a fixed-wing Vertical Take-Off and Landing Aircraft*," *IFAC Proceedings Volumes*, Vol. 44, No. 1, 2011, pp. 7250–7255. 18th IFAC World Congress.

[34] Fay, C. B., "A Cursory Analysis of the VTOL Tilt-wing Performance and Control Problems," *Annals of the New York Academy of Sciences*, Vol. 107, 12 1963, pp. 102–146.

[35] Chen, G., Ma, D., Jia, Y., Xia, X., and He, C., "Comprehensive Optimization of the Unmanned Tilt-Wing Cargo Aircraft With Distributed Propulsors," *IEEE Access*, Vol. 8, Jul. 2020, pp. 137867–137883.

[36] Junior, B. W. M., and Mallen, J., "Design Considerations for Tilt-wing Type VTOL Aircraft," *Third Annual Western Forum of the American Helicopter Society*, Oct. 1956.

[37] Chen, G., Ma, D., Jia, Y., Xia, X., and He, C., "Comprehensive Optimization of the Unmanned Tilt-Wing Cargo Aircraft with Distributed Propulsors," *IEEE Access*, Vol. 8, 2020, pp. 137867–137883.

[38] Lu, K., Liu, C., Li, C., and Chen, R., "Flight Dynamics Modeling and Dynamic Stability Analysis of Tilt-Rotor Aircraft," *International Journal of Aerospace Engineering*, Vol. 2019, Aug. 2019, pp. 1–15.

[39] Ferguson, K., Thomson, D., and Glasgow, T., "A Flight Dynamics Investigation of Compound Helicopter Configurations," Douglas AZ, USA, 05 2013.

[40] Hobbs, A., "Limitations of the See-And-Avoid principle," Tech. rep. 1, Bureau of Air Safety Investigation, April 2009.

[41] McCormick, B. W., and Mallen, J., "Design Considerations for Tilt-Wing Type VTOL Aircraft," *Vertol Aircraft Corporation*, 1957.

[42] Johnson, W., *Helicopter Theory*, 1st ed., Dover Publications, New York, 1994.

[43] McKinney, M. O., Kirby, R. H., and Newsom, W. A., "Aerodynamic Factors to be Considered in the Design of Tilt-Wing V/STOL Airplanes," Tech. rep. 1, NASA Langley Research Center, Hampton VA, USA, 1963.

[44] Kamal, A. M., and Ramirez-Serrano, A., "Design Methodology for Hybrid (VTOL + Fixed Wing) Unmanned Aerial Vehicles," *Aeronautics and Aerospace Open Access Journal*, Vol. 2, No. 3, Jun. 2018, pp. 165–176.

[45] Wakefield, B. I., and Dubuque, C., "Exceeding Tire Speed Rating During Takeoff" *Boeing Aero magazine*, Apr. 2009, pp. 15–19.

[46] Adkins, C. N., and Liebeck, R. H., "Design of Optimum Propellers," *Journal of Propulsion and Power Access*, Vol. 10, No. 5, Sep. 1994, pp. 676–682.

[47] Gur, O., Mason, W. H., and Schetz, J. A., "Full-Configuration Drag Estimation," *Journal of Aircraft*, Vol. 47, No. 4, 2010.

[48] Schwartzberg, M. A., "Rotor Induced Power," *Army Aviation Systems Command*, 1975.

[49] Marte, J. E., and Kurtz, D. W., "A review of Aerodynamic Noise From Propellers, Rotors, and Lift Fans," Tech. rep. 31-1462, Jet Propulsion Laboratory, California Institute of Technology, Pasadena, CA, USA, 1970.

[50] Melkert, J. A., *AE1110 – I Introduction to Aerospace Engineering I: Horizontal Flight*, Delft, The Netherlands, 2020.

[51] Traub, L. W., "Range and Endurance Estimates for Battery-Powered Aircraft," *Journal of Aircraft*, Vol. 48, No. 2, 2011.

[52] Gundlach, J., *Designing Unmanned Aircraft Systems: A Comprehensive Approach*, AIAA education series, 1st ed., American Institute of Aeronautics & Astronautics, Reston, VA, USA, 2014.

[53] Fu, Z., Yu, J., Xie, G., Chen, Y., and Mao, Y., "A Heuristic Evolutionary Algorithm of UAV Path Planning," *Wireless Communications and Mobile Computing*, Vol. 2018, 2018, pp. 1–11.

[54] Babel, L., "Flight Path Planning for Unmanned Aerial Vehicles with Landmark-based Visual Navigation," *Robotics and Autonomous Systems*, Vol. 62, Feb. 2014, pp. 142–150.

[55] Dechter, R., and Pearl, J., "Generalized Best-first Search Strategies and the Optimality of A∗," *Journal of the ACM*, Vol. 32, No. 3, Jul. 1985, pp. 505–536.

[56] Cameron, S., "Obstacle Avoidance and Path Planning," *Industrial Robot: An International Journal*, Vol. 21, No. 5, Oct. 1994, pp. 9–14.

[57] National Police Agency of Japan — Emergency Disaster Countermeasures Headquarter, "Police Countermeasures and Damage Situation associated with 2011 Tohoku district - off the Pacific Ocean Earthquake," *National Police Agency of Japan*, Dec. 2020.

[58] Mete, H. O., and Zabinsky, Z. B., "Stochastic Optimization of Medical Supply Location and Distribution in Disaster Management," *International Journal of Production Economics*, Vol. 126, No. 1, Jul. 2010, pp. 76–84.

[59] Beraldi, P., and Bruni, M., "A probabilistic Model Applied to Emergency Service Vehicle Location," *European Journal of Operational Research*, Vol. 196, No. 1, Jul. 2009, pp. 323–331.

[60] World Bank, "Rural Population (% of total population) - Rwanda," Tech. rep. 1, The World Bank IBRD, 2018.

[61] World Health Organisation (WHO), "Official Development Assistance (ODA) for health to Rwanda," Tech. rep. 1, WHO, 2012.

[62] Chemouni, B., "The Political Path to Universal Health Coverage: Power, Ideas and Community-based Health Insurance in Rwanda," *World Development*, Vol. 106, Jun. 2018, pp. 87–98.

[63] Munoz, U. H., and Källestål, C., "Geographical Accessibility and Spatial Coverage Modeling of the Primary Health Care Network in the Western Province of Rwanda," *International Journal of Health Geographics*, Vol. 11, No. 1, 2012, p. 40.

[64] Chowdhury, S., Emelogu, A., Marufuzzaman, M., Nurre, S. G., and Bian, L., "Drones for Disaster Response and Relief Operations: A Continuous Approximation Model," *International Journal of Production Economics*, Vol. 188, Jun. 2017, pp. 167–184.

[65] Eißfeldt, H., Vogelpohl, V., Stolz, M., Papenfuß, A., Biella, M., Belz, J., and Kügler, D., "The Acceptance of Civil Drones in Germany," *CEAS Aeronautical Journal*, Vol. 11, No. 3, Apr. 2020, pp. 665–676.

[66] Melin, H. E., "Analysis of the Climate Impact of Lithium-ion Batteries and How to Measure it," Tech. rep. 1, Circular Energy Storage, Jul. 2019.

[67] Pero, F. D., Delogu, M., and Pierini, M., "Life Cycle Assessment in the Automotive Sector: a Comparative Case Study of Internal Combustion Engine (ICE) and Electric Car," *Procedia Structural Integrity*, Vol. 12, 2018, pp. 521–537.

[68] Zhang, J., Chevali, V. S., Wang, H., and Wang, C.-H., "Current status of carbon fibre and carbon fibre composites recycling" *Composites Part B: Engineering*, Vol. 193, 2020, p. 108053.

[69] Burkert, A., "Effective recycling of electric-vehicle batteries" *MTZ worldwide*, Vol. 79, 09 2018, pp. 8–13.

[70] Xu, J., and Xu, L., *Integrated System Health Management Perspectives on Systems Engineering Techniques*, Elsevier Science and Technology, 2017.